"THE PROBABILITY OF DETECTING AND TRACKING RADAR TARGETS IN CLUTTER AT LOW GRAZING ANGLES"

BY

R W HADDOW OBE, AFM, MSc CEng MIERE MRAeS

A DOCTORAL THESIS

Submitted in partial fulfilment of the requirements

for the award of

Doctor of Philosophy of the Loughborough University of Technology

30 September 1982

CERTIFICATE OF ORIGINALITY

This is to certify that I am responsible for the work submitted in this thesis, that the original work is my own except as specified in acknowledgements or in footnotes, and that neither the thesis nor the original work contained therein has been submitted to this or any other institution for a higher degree.

"It is probably safe to say that clutter will never be understood completely because there are so many variables to control ...."

TOMLINSON

CONTENTS

PREFACE

This report was compiled as a part-time study during the author's appointment as Guided Weapon Specialist at the Department of Air Warfare at Royal Air Force College Cranwell. Although sponsored by the Ministry of Defence the results and opinions are those of the author and should not be taken as official.

ACKNOWLEDGEMENT

Gratitude is expressed to Dr J E Hudson and to Professor J W R Griffiths for the opportunity and assistance in pursuing the research.

Thanks are also due to Mr J S Nicholson of the RAF College Mathematics Department and especially to Mr D Clarke Trenchard Hall Librarian, whose efforts even exceeded the considerable resources of MIT in uncovering associated literature.

Assistance received from the Royal Armament Research and Development, Royal Signals and Radar, and Admiralty Surface Weapons Establishments, Hunting Engineering and particularly British Aerospace Dynamics is most gratefully acknowledged; as is the financial sponsorship of the Ministry of Defence.

Finally the time-consuming survey and data tabulation effort alone could not have been completed as a part-time task without the support of an understanding family - who have somehow withstood five such tasks in a decade - interspersed with an ever increasing external lecturing commitment at home and abroad.

ABSTRACT

Modern military acquisition and tracking radars are required to operate against aircraft and missiles specifically designed to have minimal radar cross section (RCS) and which fly at very low level to take maximum advantage of terrain screening.

A model for predicting system performance is necessary for a range of terrain types in varying precipitation and seasonal cultural conditions. While the main degradation is from surface clutter and denial of sightline due to terrain and other local obstructions, several other factors such as multipath propagation, deliberate jamming and even operator performance contribute to the total model. The possibility that some radars may track obscured targets, however briefly, by using the diffraction path, is of particular interest.

Although this report critically examines each of the contributory factors in order to select optimum values for inclusion in an overall computer prediction model; a new surface clutter model is specifically developed for sloped terrain using actual clutter measurements. The model is validated by comparison with an extensive survey of worldwide clutter results from both published and unpublished sources.

Certain constraints have been necessary to restrict the study to a manageable size, while meeting the requirements of the sponsors. Attention is therefore focussed upon performance prediction for typical mobile tracking radar systems designed for operation against small RCS low level targets flying overland.

INDEX (TO PART I)

Page

CHAPTER 10 - TERRAIN SLOPE CLUTTER WITH AND WITHOUT TREE COVER

CHAPTER 11 - RADAR PERFORMANCE ASSESSMENT MODEL

CHAPTER 12 - SUMMARY OF RESEARCH AND RECOMMENDATIONS

GLOSSARY OF TERMS AND SYMBOLS

Chapter 1

τ	Radar pulse width (pulse duration) secs.
GRAZING ANGLE =	The angle between the local horizon at the target and the radar beam direction.

Chapter 2

λ	Radar wavelength (m).
d, R	Distance or range to target (m).
h_1	Height of radar transmitter (m).
r_e	Earth's radius (km).
h_2	Height of Target (m).

4/3 Earth's Radius = 8494.7 Km (4587 nmls).

Chapter 3

f	Radar Transmitter frequency (Hz).
D	Particle diameter (cm).
ρ	Density of water.
v	Optical visibility (feet).
M	Liquid water content of cloud or fog ($g.m^{-3}$)
α	Atmospheric Attenuation Coefficient.
R	Range (target, obstacle or rain) (m).
m	Complex refractive index (water).
D	Diameter of rain drop.
ζ	Radar reflectivity of rain ($m^3.m^{-3}$).
Z	Rain reflectivity factor.
p	Precipitation rate ($mm.hr^{-1}$).
θ_A	Aerial 3dB Beamwidth, Azimuth (deg).
θ_E	Aerial 3dB Beamwidth, Elevation (deg).
ϕ_A, ϕ_E	Angular departure from beam axis in Azimuth or Elevation (rads).
σ_R	Beam rain filled echoing area (m^2).
K	Windshear coefficient ($m\ sec^{-1}.m^{-1}$).
C	Speed of light ($m.s^{-1}$).
S	Spectrum of wind velocity.
fd	Doppler frequency (Hz).
fw	Doppler freq at mean wind velocity (Hz).
sd	Standard deviation.
n	Rainfall frequency per 10 years.
t	Rainfall duration (hours).
Λ	Total rainfall in time t (inches).

Chapter 4

σ_m	Median RCS $m^2.m^{-1}$ (or average where shown).
μ	Spatial mean value of m.
A(t)	)
R(t)	) Amplitude, Range and Phase components
$\phi(t)$	)
β	$2\pi/\lambda$
τ	Radar pulse duration.
a_k	Lumped amplitude term

m	Average σ_o.
ψ	Grazing Angle (without terrain slope).
γ	
c	Weibull shape parameter.
a	Weibull slope parameter.
A, B, C, D, K, A_n, n, γ_t, m, c; R_l, R_h, f	Model constants (subscripted as necessary).
F_s	Spherical earth shadow factor.
ψ^1	Actual surface grazing angle.
Δh	rms height of surface irregularities.
θ_A	Radar beamwidth.
r_e	4/3 earths radius.
v	Detector output voltage.
V_t	False alarm threshold.
P_{fa}	Probability of False Alarm.
P_d	Probability of detection.
N_f	No of radar operating frequencies.
T_r, C_r	Target and clutter received power.
I	Integration improvement factor.
C_m	Median Clutter Power.

Chapter 5

V	Wind Velocity (knots).
V_o	Wind Velocity (ms^{-1}).
β	Azimuth angle relative to beamwidth.
θ_2	2-way half power beamwidth (rads).
σ_s	Chaff RCS per dipole.
Σ_o	Chaff volume reflectivity density ($m^2.m^{-3}$).
N	No of chaff dipoles.
E	Chaff Dispersal efficiency.
p(f)	Clutter power spectrum as a function of frequency.

Chapter 6

Standard symbols are listed with equations (1-13).

σ_{AV}	Average target RCS (m^2).
σ	Quoted target RCS (m^2).
L_o/λ	Characteristic target length.
$\Delta\theta/\Delta t$	Rate of change of target aspect.

Chapter 7

E_S, E_I, E_O	Scattered and incident intensity from target.
α	Diffraction angle.
v	Dimensionless Fresnel-Kirchoff parameter.
A(v)	Diffraction loss rate.
r(m)	Fresnel zone radius.
a_m	Diffraction loss.
a_o	Free space loss.

R	Range beyond diffraction ridge.
R_c	Radius of curvature of diffracting edge.
R^1	First Fresnel zone radius.
P_{tgt}	Power at target.
α	Curvature factor.

Chapter 8

a_o, a	Earth's radius 6370 Km, effective earth's radius.
N	Refractivity.
N_s	Refractivity at earths surface.

(Remaining symbols dimensioned on diagrams).

Chapter 9

E_i	Incident radiation. E_t Transmitted Radiation
E_d	Directly backscattered radiation.
ρ	Surface reflection coefficient.
R_D, R_I	Direct and indirect path lengths.
Δ_R	Path length difference (m).
$\Delta\phi$	Phase difference between paths (rads).
F	Pattern Propagation Factor.
F_t	Tracker loop bandwidth (Hz).
ε	Elevation error (rads).
V	Target velocity ($m.s^{-1}$).
σ_ϕ	rms elevation tracking error.
θ_E,E	Radar elevation beamwidth, target elevation angle.
θ_r	Specular reflection angle.
G_s	Main to sidelobe gain (power) ratio.
P_r	Signal power received via multipath.
σ_{tgt}	Target RCS (m^2).

(Remaining symbols dimensioned on diagrams).

Chapter 10

h_t	Average height terrain clutter patch (m).
h_{t_x}	Height of radar aerial.

(Remaining symbols dimensioned on diagrams).

Chapter 11

P_{DET}	Probability: Detection.
P_{TL}	: of obtaining minumum track length.
P_{MX}	: of missile success.
P_{OE}	: of operator (efficiency) performance.
P_R	: of system availability (Readiness).

Annex A and Appendix 1 to Annex A

m	Weibull shape parameter (replaced by b).
λ	Weibull scale parameter (replaced by c).
x	Signal level.
(n)	Gamma function.
N	Echo amplitude level.
P	Echo amplitude level.
m^2	Ratio of constant power to random power.
s	Standard deviation.
μ	Median value of x.
x	Normally distributed variable.
Y	Lognormally distributed variable.
Y_m	Median value of Y.

Annex B

S_R	Received echo from target (watts).
P_T	Peak transmitted power (watts).
G	Peak Aerial Gain.
σ	Radar cross section (RCS) of target (m^2).
R	Range to target (m).
A_e	Effective aerial capture area (m^2).
λ	Radar wavelength (m).
L	Combined system losses.
τ	Radar pulsewidth (sec).
θ_A	Aerial azimuth 3dB beamwidth (deg).
γ	Grazing angle characteristic.
σ^o	Scattering RCS pwer unit area (m^2)
θ	Grazing angle (defined at Chap 1) (deg).
θ_E	Aerial elevation 3dB beamwidth (deg).
Δh	Height difference due to surface
ρs	Specular reflection.
ρS	Smith Factor

Annex C

E	= Electronic field at receiver (target) from unit source.
S_1C	= Fresnel integrals of argument.
θ	= Diffraction angle.
ν	$= \theta\sqrt{do/\lambda}$
k	$= 2\pi/\lambda$
d_o	$= 2d_1d_2/d$ (distances annotated on diagrams in Chapter 7).

Annex E

ε	Linear tracking error (m).
q_s^2	Power ratio of direct and indirect signal.
α	Tracking error for target.
α_o	Displacement of peak of aerial beam relative to equal signal line.
$\Delta\alpha$	Angular distance between real and image target.
S_1	Required signal.
S_2	Interfering signal (multipath).

G_S	Specular power gain ratio.

(Remaining symbols specified in Annex text or in diagrams).

ρoi	Fresnel reflection coefficient for element i
ρos	Fresnel reflection coefficient for specular reflection.
T	Tracking condition.
$\bar{T}$	Non tracking condition.
q	1- probability of success.
V_t	Threshold voltage.
N	Number of signals integrated.

Annex F and Appendix 1 to Annex F

A_1 to A_9	Terrain spot heights in 3 x 3 grouping.
a to f	Terrain slope, aspect and convexity coefficients.
$\hat{r}$, $\hat{n}$, λ, μ, γ, l, m, n	Direction cosine designation.

(All other symbols listed in text or on diagrams).

ψ	Actual terrain/radar energy grazing angle.
θ	Mean terrain gradient.
s	Observable (in shadowed) slope.

Annex G

V_m	Velocity of missile ($m.s^{-1}$).
P_E	Probability of detection becoming an engagement.
P_{fa}	Probability of false alarm.
P_b	Probability of detection during a single transmitter burst of pulses.
D_f	Diffraction enhancement factor.
P_s	Probability of sightline falling on target.
E_f	ECM effectiveness factors.

CHAPTER 1

THE NATURE OF RADAR CLUTTER

INTRODUCTION

1. This report considers radar performance prediction when operating at low grazing angles with the horizon - such that radar beam illumination of the ground inevitably occurs, resulting in unwanted clutter echoes. These clutter signals diminish the probability, or even totally prevent the radar from detecting the wanted signal from aircraft and missiles.

2. Minimisation of interference effects, based on a knowledge of the expected clutter, is possible to a certain degree at the radar design stage. However, it is also necessary to be able to assess the probability of detecting and tracking a target of given radar cross section (RCS) for an existing radar when the target is at very low altitude over variable terrain, or water. Probability of overall success clearly depends upon the likelihood of encountering competing clutter, the time for which such clutter persists before the target moves to a more advantageous position (where the target signal overrides the clutter signal) and the reaction time of the associated command and control or missile system which is to make use of the target tracking data. Hence a statistical analysis is necessary which takes into account the very large numbers of variables involved. (Annex A).

3. To make a complete assessment for a particular radar type and location it is first necessary to analyse the terrain profile to obtain sightline data to the target. Secondly to investigate the corresponding surface characteristics beneath the target, and finally to assess degradation of signals due to volume clutter including cloud, rain, snow etc and the

effects of deliberate clutter such as chaff (electronic countermeasures). Several techniques are used to reduce clutter effects but even these may have only minimal effect in the scenario in question. A general selection of parameters to minimise clutter are set out at Table 1 below:

	EFFECTIVE AGAINST				
PARAMETERS	GROUND CLUTTER	WEATHER CLUTTER	CHAFF (ECM)	SEA CLUTTER	ANGELS
LOW RF		X			
NARROW AE BW	X	X		X	X
SHORT PULSE (RESOLUTION CELL)	X	X		X	X
STC				X	X
MTI	X	(X)	X	(X)	
LOG RX/FTC	X	X		X	
CIRCULAR POLARISATION		X	(X)	X	
FREQ DIVERSITY/ AGILITY		X	(X)	X	

Table 1 - Clutter Reduction Techniques

Notes: 1. X Effective in limiting clutter

2. (X) Effective in some cases

FORMS OF CLUTTER

4. In differentiating between surface-distributed and volume-distributed clutter the situation can be initially described by geometry, detailed at Annex B. In particular it is seen that the illuminated surface area

and volume vary with range and pulse duration, as well as with the radar aerial depression angle. The existence of clutter returns overland from long ranges is significantly dependent upon the height of the scanned terrain, since hills at short range will often shadow any possible signal returns (see Fig 1b) from targets further away. However, this shadowing effect may be limited in azimuth and will therefore depend critically upon line of sight terrain screening as the radar aerial is incrementally scanned in azimuth. On the contrary, measurements taken at sea will be more or less uniformly distributed over the surface. Here the surface clutter echo strength will be directly related to the area of the resolution cell, in contrast to ground clutter which varies from place to place within the cell, and is not therefore proportional to the resolution cell size (Warden {1} and Riley {2}). It is however convenient to use the echoing area per resolution cell (σ_o) as a standard; explained at p 4-82. This allows direct comparison with the target echoing area in studies of the probability of detection. At sea, multipath signal phenomena (see Fig 1a) are quite probable, whereas this effect is possible overland, but far less likely.

RESEARCH PARAMETERS

5. Detection predictions are required for radars having the typical parameters listed below. Monostatic radars are the main interest, although some bistatic work has been done (mainly in the USA) and this may be referred to, where applicable. The following main characteristics are adhered to throughout the study:

a. Radar Wavelength < 3 cm (10 GHz up to 18 GHz)

b. Pencil or Fan aerial beams, with sharp beamwidths and mounted on masts up to 30 m high.

c. Small radar resolution cells (15 ns < τ < 2μs).

d. Small target radar cross section (0.05 m^2 minimum).

e. Tracking type radars, as distinct from surveillance radars.

CLUTTER VARIABLES

6. Variables contributing to the complex overall extent of clutter in any particular radar system include:

a. Topographical Features

1. Terrain Type - Snow, Desert, Forest, Urban, Water etc.

2. Seasonal Variations - Defoliation, surface water content, surface motion.

3. Terrain Profile - Hills, undulating, flat etc.

b. Radar Characteristics

1. Resolution cell size - dependent on pulse duration (PD) and radiated beamwidth (BW).

2. Radio Frequency (RF), polarisation of transmit and receive aerials and distribution of radiation.

3. Aerial induced fluctuations.

4. Grazing angle of radar beam with surface, also known

as 'depression' or 'incidence' angle. (But see later definitions).

c. Atmospheric and Propagation Effects

1. Diffraction, Reflection and Refraction, including multipath.

2. Air temperature, water vapour absorption.

3. Rain/precipitation, chaff attenuation and backscatter.

CLUTTER STATISTICAL DISTRIBUTIONS

7. Weibull, Ricean, Rayleigh and Gaussian statistical distributions are used in clutter research and although stated in the main text, since some are uncommon, they are detailed at Annex A. Spatial and temporal characteristics of the variables at para 6 above are summarized at table 2 and each is investigated fully in the following chapters. (except sea clutter).

RELIABILITY AND REPEATABILITY OF CLUTTER MEASUREMENTS AND ASSESSMENTS

8. Despite the considerable number of clutter research programmes over many years it is unfortunate that few have used identical test parameters, particularly in relation to those areas critical to this study. Probabilities obtained even day to day have varied significantly and a large number of research workers have reported that the available database may be inadequate at present for conclusive and repeatable relationships to be stated. While there are considerable shortcomings in most clutter models, worse still there appears to be no standardised approach discernable in the many papers read during this study.

TABLE 2 CLUTTER MODELLING PARAMETERS

CLUTTER TYPE	INPUT PARAMETERS	MODELLING DESCRIPTION
RAIN BACKSCATTER	Rainfall Rate, Type, Rain Frequency, Radar Frequency (RF).	Spatial distribution of Reflectivity Spectrum and Probability of occurence.
CHAFF BACKSCATTER	Amount and Type, Dissemination Mode, RF.	Spatial and Temporal distribution of Reflectivity, Spectrum.
SEA BACKSCATTER	Sea State, Incidence Angle, RF and radar polarisation.	Reflectivity (average) and Clutter Signal distribution.
LAND BACKSCATTER	Land type, Incidence Angle, RF, Pulse length.	Distribution of reflectivity Spectrum of motion.
REFLECTIONS/MULTIPATH	Geometry, RF, Surface Roughness, Polarisation	Coherent propagation loss. Diffuse scattering intensity.
ATMOSPHERIC/RAIN ATTENUATION	RF, Range, Rain Rate, Type and Frequency, Atmospheric Characteristics.	Propagation loss. Attenuation rates.
REFRACTION AND DIFFRACTION	Geometry, RF.	Propagation losses, path patterns.
JAMMING	Type.	Modulation, Signal ratios and thresholds.

9. Recently, Allan { 3 } in particular, surveyed a number of clutter prediction papers and found both anomalies and inadequacy of data; concluding that "a completely general analytical method is probably an impossibility". The added complications of terrain screening, chaff or atmospheric propogation effects were outside the scope of Allan's paper, as with many other research studies. On consideration it was felt necessary to include all these factors in a more comprehensive study. Meanwhile, it was discovered (by chance) that an ongoing study at MIT (USA) has similar terms of research, hence the author and Dr Briggs { 4 } have been able to exchange information on clutter research reports. Despite the wide resources of MIT in producing a world-wide clutter bibliography of some 300 items, the author's investigations at Cranwell have resulted in the addition of another 70 to 80 reports to the MIT list. (at PART II)

REVIEW OF CLUTTER RESEARCH

10. In preparation for the construction of a model, a comprehensive review of radar clutter and associated literature was a time consuming initial requirement. However, with respect to the radar parameters required for this study, the search revealed that many reports used parameters very widely dispersed from those of interest. Nevertheless several hundred papers were filtered for information.

11. Extensive descriptions of clutter are given in several standard texts { 5, 6, 7 }. However, they are usually intended for the radar student requiring a general grasp of the problem and they invariably avoid the difficulty of assessing practical system performance. That there is a serious lack of data and that researchers, for their own specific purposes, have embarked on measurement programmes with a range of

different averaging criteria - even though ostensibly repeating research done by others - all serves to cast doubt on the integrity of conclusions drawn from comparison studies. Hence, published sets of results for (apparently) the same test conditions may not correlate and it is clear that the phenomenon of surface clutter in radar receivers remains poorly understood and poorly predictable.

12. During the study, discussions and correspondence with MIT (USA), RSRE (Malvern) and UK Industry has proved rewarding. It is clear that the respective Departments of Defence have a particular interest at present in this topic, but both now realise the enormity of the task if all unknowns in the clutter parameter matrix are to be found. The use of the best published research is therefore essential, since no organisation could afford to undertake the vast range of measurements necessary to build a complete picture from the beginning. On the other hand, confidence in a model will only be acheived if a spread of repeatable results is identified, and with the shortage of data, certain assumptions and judgements based upon sound reasoning must be used if any sort of useable algorithm is to be attempted. It is found that research papers fall, in general, into 3 main types:

a. Short radar range, scientifically orientated reflectivity experiments, specifically radiated narrow-beam energy against small but highly homogeneous clutter patches eg snow, crops, concrete or regular vegetations. Usually the radiating and receiving aerials are stationary.

b. Intermediate range measurements using large clutter patches, trees, fields, etc, again using narrow beamwidths, and often exploring stationary single resolution cells.

c. Surveillance radar measurements, usually involving 360° azimuth coverage with clutter sources varying from flat to rough terrain and containing both diffuse scatterers such as crops, weeds etc and point scatterers of the isolated type such as pylons, and water towers.

13. Since a complete clutter detection model should embrace all possible variables which degrade the radar performance it is appropriate at this point to differentiate between the amplitude, phase and other fluctuations leading to the clutter statistics received as signals from outside the receiver, and including all the effects mentioned so far including RF spectrum and frequency agility effects; contrasted with the characteristics of the clutter signal processing circuits which are inside the radar. Published reports often attempt modelling while accounting for several variables but ignore others pertinent to the circumstances of a practical scenario. For example a seaborne radar model would not normally need to account for sightline screening since, unlike on land, the only screening at sea is the longer range horizon limiting. On land there is the infinite variability of the terrain to contend with and so the modelling task becomes daunting; and even worse if the model is to cover both sea and land mixed. Investigations have shown that the simple categorisation of landscape into broad types is not suitable, and it has been well established that detailed categorisation is necessary. Indeed it is possible that reliable radar prediction under all conditions may be denied until clutter descriptions become more elaborate.

14. The Canadian Soil Survey Committee adopted a hierarchical classification scheme in 1976 { 8 } which allocates 10 first level classes (eg undulating, rolling, level etc); second level modifiers (eg eroded) and other levels specifying coverage slope, local relief and so on. Any type of terrain can be described by the system. The USA also have a land use and cover

classification system. However a truly comprehensive scheme would necessitate a means of describing, for example, the natural, cultural and man-made vertical obstructions which tend to cluster along roads and field edges; and seasonal effects. United Kindom and European terrain data bases are also considered in the investigations at Chapter 4.

PROBLEM AREAS

15. The foregoing paragraphs generally highlight the shortcomings in the raw material to insert into a clutter model. Coupling this with the lack of a widely applicable analysis method, one approach would be to use homogeneous clutter, using perhaps 8 or 10 surface classifications and to assume the entire resolution cell "footprint" contains one type of scatterer. An extreme alternative would involve detailed mathematical representation of the reflectivity of every scatterer within the cell, taking for example, in the limit, grass-blades to be dipoles with associated phase and amplitude behaviour. After investigations a method is developed (and justified in later chapters) as the most reasonable practical approach, given the limitations described above.

16. Chaff and Electronic Jamming. **One aspect, so far not expanded** upon, is the use of deliberate radar clutter to reduce the probability of detection, ie the dispersion of "chaff" within the resolution cell by military targets or the radiation of interfering or misleading (deception) signals. In both cases a serious degradation of radar performance may result in tracking disturbance or break-lock on a target of interest.

17. Electronic jamming may not emanate from the target being tracked but from another source which is giving countermeasures support, ie a 'stand-off' jamming aircraft. These emissions may enter the tracking radar through the main beam or sidelobes. Chaff interference is also considered and it is of interest that statistically chaff and rain backscatter characteristics are similar.

18. <u>Diffraction and Terrain Slope</u>. Surface obstacle diffraction and clutter from sloped terrain are of particular importance to the prediction of performance of low grazing angle tracking radars. Since few practical measurements have been published on these topics, they seemed to be worthwhile areas for detailed study.

MINIMUM AIMS OF THE STUDY

19. As a minimum the author sets out, it is believed uniquely, to summarize in one document:

a. A reasonably detailed method of assessing the performance to be expected from a tracking radar and associated missile system when deployed on a pre-surveyed site, by computer modelling.

b. A simpler method of performance prediction for a system deployed anywhere within a geographical area where terrain data may be available only in general form and where radar performance data is perhaps limited.

In both cases either the specific radar and relevant system parameters are known or can be varied to observe the effects, for example, with and without interference.

BIBLIOGRAPHY

20. It should be stated that the bibliography, because of the nature of the study, is unusually extensive for a report of this type. Items listed are not all cross-referenced in the main text but it is considered necessary to include the entire reading list for completeness as a new consolidated clutter reference. Readers will find a proportion of the bibliography repeated in the MIT list (4) as mentioned at para 9 above.

DEFINITION

21. For the purpose of this study 'clutter' is generally taken to mean all effects which impede or degrade detection and hence tracking. It maybe caused by the type or condition of the surface, hindrance or disturbance of propagation due to volume clutter, atmospheric effects, or by jamming or target manoeuvre.

ORIGINAL RESEARCH

22. It has already been mentioned that a single prediction document is probably unique. To achieve the aims at para 19 above, each of the contributory factors to tracking radar performance (relevant to the radar characteristics described at para 5) have been examined in detail:

a. To select the best method of representing terrain data for prediction purposes.

b. To select the best model to describe clutter in all it's forms with particular emphasis on those aspects where measurements or results are scarce or of doubtful value.

As a result, indeed as expected, surface clutter modelling proved to be the weakest link in the overall prediction model. To overcome this shortcoming, first an extensive survey of existing measurements was made to bring all known models together for comparison. But, most importantly, a new model is developed from raw radar measurements and critically compared with the existing real or interpolated models.

PRESENTATION

23. Perhaps unusually, so that the report should meet the requirements of the sponsors as an easily readable reference for both the scientific and non-scientific reader, results, reasoning and models are stated in the appropriate chapter with a summary at each chapter end. Expanded detail is in the Annexures; hence the original research on the new clutter model over sloped terrain is detailed at Annex F, with the resulting model contrasted with others in the clutter chapter (Chap 4). All aspects are brought together at Chapter 11, for the overall performance prediction model, with detailed examples at Annexures G and H.

FIG 1

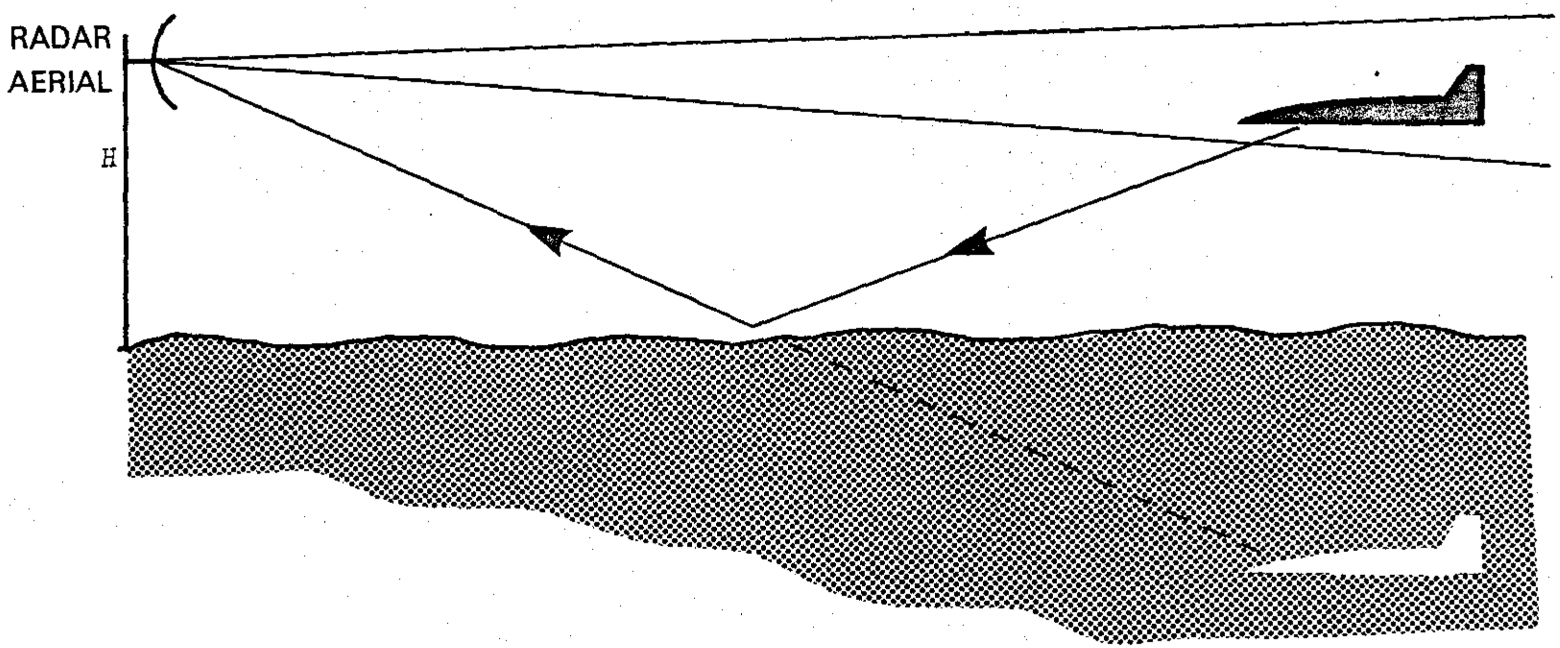

FIG 1a MULTIPATH

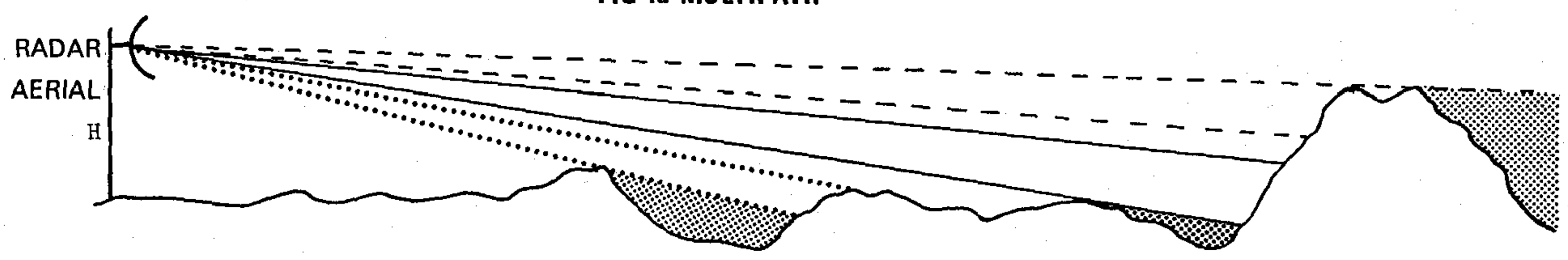

FIG 1b SHADOWING

CHAPTER 2

TERRAIN MODELLING

INTRODUCTION

1. Chapter 1 considered the various sources of radar clutter in general, however, a more precise examination of the system geometry pertaining to ground clutter is necessary for the planning of a meaningful terrain model. With the exception of those occasions where obstacle diffraction occurs (thus possibly allowing radar tracking when a direct optical sight line does not exist), a sight line from the radar aerial to the target is normally essential. Radar aerial and target heights and positions are used in a simple geometrical calculation in conjunction with terrain, building and obstacle data to check for sight-line blockage.

2. It is also necessary to consider Earth's curvature, refraction and reflection effects, hence the terrain model is built up in several stages. Diffraction effects are complex and they are considered separately at Chapter 7

EARTH'S SURFACE MODEL

3. The purpose of the surface model is to determine:

   a. Unobstructed Surface Sight Lines. Using contour heights from Ordinance Survey maps, it is possible to test for the existence, or otherwise, of a tracking sight line between any 2 points at any altitude on the terrain. Accurate terrain data is thus a basic requirement for the geographical area in which the radar is to operate. Manual production of this type of data base is tedious, but several agencies have produced terrain data which is suitable for clutter studies. Terrain data base methods are outlined in paras 16-19 below.

b. Surface Obstructions. Super-position of a surface culture and obstacle array upon the terrain array and which describes the mean height of all surface obstacles and types of reflecting surface, enables blocked sight lines to be identified and reflectivity to be accurately modelled.

c. Tracking Times. Low level target tracking may be periodically interrupted by terrain or obstacle screening. The time elapsing from a sight line being first established until the sight line ceases to exist (as the target again becomes obscured), may be critical in the case of missile fire control systems or aircraft on a landing approach. Tracking times are, of course, a function of aircraft velocity as well as obstructions. (Also see Annex E).

d. Clutter Levels. Undulations in terrain may present a situation where a target can be seen but the underlying ground or obstacles are in shadows and hence clutter returns in the main beam are not possible, (examples of this are noted later). Clutter may be received by side lobes (if the side lobe suppression is poor) from terrain not in the resolution cell currently being searched.

SIGHT-LINE

4. Given the radar aerial height and site position within the terrain array, together with the target height, track, and the position as it enters the array, the sight lines are calculated and then clutter criteria is applied. Radar cross section modelling of the target itself is of course necessary for signal comparison purposes and the signal from the target should itself fluctuate realistically to allow for glint (scintillation). If weather degradation is to be included, the attenuation due to precipitation can also be applied. The typical effects of weather on radar are considered at Chapter 3. Other assumptions made for the model are:

a. Initially the targets will fly straight lines and constant altitude and would not be planned, for example, to take deliberate advantage of terrain screening.

b. Ground tracks can transit across the terrain in any direction, including passing overhead the radar.

c. No wind drift is incorporated and hence the attitude aspect of the target with respect to the ground radar station would be predictable within the limits of the scintillation required.

d. Radial ground tracks, with a subsequent period when targets are within the radar's minimum tracking range are simulated.

e. When RCS is modelled on a crossing target maximum signal value is assigned when the target is at a tangent to the radar normal.

f. When RCS is modelled on an approaching target RCS is modelled to fluctuate statistically about a mean.

TERRAIN SPOT HEIGHTS

5. Terrain matrix array spacing of 500 metres was used initially for the Malvern area, by interpolating, as necessary, between contours. 250 metre and 125 metre matrix spacing is also available for areas of UK and Germany. A maximum useful radar tracking range of 25 km is assumed against a low level target flying at altitudes between 30 metres and 150 metres (clearance above ground level (agl)). A 50m matrix spacing was used for slope studies.

EARTH'S CURVATURE AND INTER-VISIBILITY

6. Earth's curvature is a basic limitation in considering inter-visibility at significant ranges over the earth's surface. Approximating the Earth's radius as 6400 km, there is a finite distance within which 2 points are inter-visible depending on their height. A general description follows which ignores refraction but gives an approximation of the range of values used in the model. Refraction is considered separately at Chapter 8, where r_e is replaced by kr_e, $(k \simeq 4/3)$; with the resulting extension of the radar horizon.

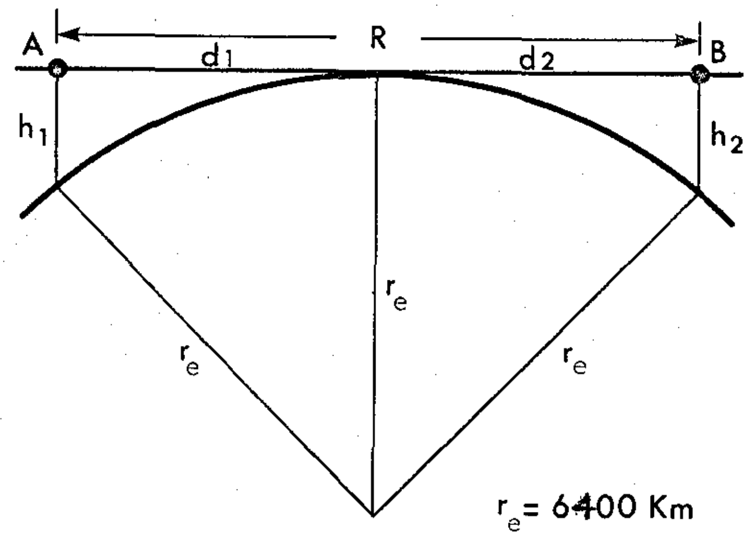

7. Point A can just see point B using a tangential sight line. Maximum range $R = d_1 + d_2$, where $d_1 = \sqrt{(h_1 + r_e)^2 - r_e^2}$ and $d_2 = \sqrt{(h_2 + r_e)^2 - r_e^2}$

If h is negligible in both cases compared with the earth's radius r, then

$$R = \sqrt{2r_eh_1} + \sqrt{2r_eh_2}$$

$$= \sqrt{2 \times 6400 \times 10^3}(\sqrt{h_1} + \sqrt{h_2})$$

$$\simeq 3.6 (\sqrt{h_1} + \sqrt{h_2}) \text{ km}$$

Example unobstructed maximum sight line ranges are given below at Table 1 . Targets and radars at various altitudes are assumed to be over a "smooth earth" and with no refraction or diffraction,

Radar Aerial Ht (m)	Target Ht (m)	Maximum Unobstructed Sight Line (km)
5	30	27.76
5	60	35.93
10	30	31.10
10	60	39.26
30	30	39. 4
60	60	47. 6

TABLE 1
MAXIMUM UNOBSTRUCTED SIGHT LINE RANGES
FOR GIVEN RADAR AND TARGET HEIGHTS

corrections, using the simplified method above:

GRAZING ANGLES

8. Table 2 gives approximated grazing angles to the surface (assuming the target to be at ground level) for various aerial heights at fixed ranges. (See figure 1). Bracketed figures are for the 4/3 earth correction, which is necessary for the more exact results required in subsequent chapters.

Aerial Ht (m)	Grazing Angle for Target Horizon Range (Degrees)		
	5 km	10 km	15 km
5	0.05 (0.04)	0.03 (0.02)	0.01 (-)
15	0.17 (0.15)	0.08 (0.05)	0.05 (-)
20	0.22 (0.21)	0.11 (0.08)	0.07 (0.02)
30	0.34 (0.32)	0.17 (0.14)	0.11 (0.06)

TABLE 2
GRAZING ANGLE FOR TARGETS AT FIXED RANGES FOR GIVEN RADAR AERIAL MAST HEIGHTS

EFFECT OF AERIAL BEAMWIDTHS

9. Table 3 gives the approximate range to the surface when grazing at low angles for a spread of typical 3dB beamwidths. (See figure 2).

Vert 3dB BEAMWIDTH (Deg)	TARGET RANGE km FOR AERIAL HEIGHT (m)			
	30	20	15	5
0.2	17.18 km	11.46 km	8.59 km	2.86 km
0.4	8.59 km	5.73 km	4.30 km	1.43 km
0.6	5.73 km	3.82 km	2.86 km	0.95 km
0.8	4.28 km	2.86 km	2.15 km	0.71 km
1.0	3.43 km	2.29 km	1.72 km	0.57 km

TABLE 3
RANGE TO SURFACE FOR 3dB BEAMWIDTHS AND GIVEN AERIAL MAST HEIGHTS

10. If a radar is designed for tracking rather than surveillance, it's vertical beamwidth is narrow, hence targets tracked at the higher angles enable the radar to be well clear of the ground clutter. As target altitudes are reduced eventually the beam will collect ground clutter. For tracking radars a 'rule of thumb' for radars at ground level, is to assume the radar beam is well clear of ground clutter if the difference in elevation between the target and the ground is > 0.7 times the vertical beamwidth. For example a tracking radar with a 1^{o}elevation beamwidth and target at 100 metres altitude will be free of clutter if the target is closer than 8 km; but at 30 metres altitude the target must be at range 2.4 km or closer. The geometry is shown at figure 3.

RESOLUTION CELLS

11. The simulation model calculates the cell size and associated surface area, "footprint" taking into account the diverging radar beam.

Pulse Width	Resolution Cell Length (m)
13 ns	1.95
15 ns	2.25
20 ns	3.00
40 ns	6.00
200 ns (0.2μs)	30.00

TABLE 4
RESOLUTION CELL LENGTH FOR GIVEN PULSE WIDTHS

CLUTTER REFLECTORS WITHIN RESOLUTION CELLS

12. Within each resolution cell the reflecting surface type can be determined from the obstacle matrix (see para 3b above). This is achieved by adding a terrain identifying factor into the terrain data and extracting this value each time to assess the surface clutter reflectivity likely to occur. A scale of identifiers is used as follows; with typical median backscatter values (for $\lambda = 3cm$):

1 Swamp/Marsh. (−40dB)

2 Discrete (prominent isolated reflectors)

3 Water (Landlocked) (−60dB)

4 Grassland/Cropped fields (−35dB)

5 Buildings (continuous) (−23dB)

6 Buildings (scattered) (−30dB)

7 Forest/Trees (−30dB)

A roughness factor and hence reflectivity (backscatter) value is then allocated, so that clutter versus target signal levels can be studied. (Using more precise models at Chap 4 paras 22-34).

13. <u>Homogeneity of Terrain Within a Cell</u>. It is seen that the spatial distribution of scatterers within a resolution cell will significantly alter the received backscatter. This problem is necessarily addressed again at Chapter 4, as it is of prime importance in the determination of a statistical clutter distribution. From the purely geometrical viewpoint the area of the surface 'footprint' can be calculated from the resolution cell length and diverging aerial beamwidth at the given range. It is however clear that really accurate predictions from modelling will only be possible with an enhanced terrain descriptive system in contrast to the very basic framework shown at para 12. Terrain spot heights will also be required on a finer matrix spacing of 90, 75 or even 30 metres (US National Cartographic Centre Grid).

SLOPE(TILT) OF SURFACE WITHIN RESOLUTION CELL

14. Backscatter is not only dependent upon the resolution cell area, but also to some extent on the aspect or 'tilt' of the cell area or 'facet' to the incident wavefront. The terrain model must calculate the cell area and cell slope to provide the clutter subroutine with information to enable adjustment of the signal/clutter ratio. It is of interest that the clutter and target aspects presented by a particular resolution cell to a radar receiver at a monostatic site are quite different from that in a bistatic system, where the aspect illuminated by the transmitter is not the same as that presented to the receiver; however this is outside the scope of the study.

15. Francois {9} states that the average slope of terrain has only a second order effect on clutter patch locations and terrain masking. Adgie {10} in conversation, states that slope probably has a limited effect on

backscatter. It is clear that little, if any, serious work has been done on the dependence of backscatter on slope for any of the terrain types of interest. As this seemed a fruitful area in which to make some basic research, raw measurements taken at RSRE and BAe have been obtained and correlation runs computed for terrain slope using a prepared terrain data base. The method and results are detailed at Chapter 10, & Annex F, App 1.

TERRAIN DATA BASE

16. Paragraph 3 introduced the concept of a terrain data matrix, and the necessity for an adequate descriptive system for the total surface features was further outlined at Chapter 1. It remains to consolidate the options available in the representation of surface obstacles and to state the reasons for selecting the method used here.

17. In the past many studies used an approach which categorised large areas of terrain and obstacles according to average type - and used statistical descriptions for terrain having like backscatter characteristics. Degradation was then determined over given flight profiles. This approach is not considered adequate (but see Chapter 11 for approximate predictions).

18. Another alternative for representing obstacles, but also rejected, is briefly described here to show its disadvantages. A string of profile co-ordinates is produced to describe the edge profiles of each obstacle. Each obstacle perimeter is therefore represented by a group of points produced by approximating all obstacles into a series of straight lines. Obscuration is then determined by geometric considerations as to whether the intended sightline and obstacle edge lines intersect. An underlying basic culture data base using a matrix or lattice method would still be

necessary, but the storage requirement for obstacles would naturally be a variable quantity for each geographical area, depending on it's constituent surface features. Generation of this type of data is especially tedious since every obstacle must be catergorised by its extremities and assigned an obstacle height and type to be added to the underlying terrain spot heights. Data production is tedious because it is a difficult process to automate.

19. An added complication which may arise with large obstacles when using this method is shown at figure 4. Sightlines are confirmed by checking for obscuration at the obstacle boundaries B1, B2, and special arrangements would be required to ensure the situation at figure 4 did not exist. Theresby {11} states that the "co-ordinate string" method in fact has the potential for a more accurate obstacle representation and indeed Hunting Engineering Ltd have used this approach for models of limited geographical extent. The penalties, apart from the relatively larger volume of data preparation, impinge upon timing overheads, extra software, retrieval, and storage requirements. Theresby {11} estimates a total storage requirement for a 20 km by 20 km area to be 4 times as great as matrix methods of obstacle representation.

SELECTED METHOD

20. Figure 5 shows an example terrain matrix at 500 x 500 metre spacing. Terrain spot heights are known at each intersecting point of the matrix. The figures bracketed represent the various terrain factors (see para 12). Reference to figure 6 shows the same area as fig 5, but with forest areas (F) and built-up areas (B) shown outlined. In allocating terrain factors two anomalies will be seen when the figures are compared. One of the spot values (70) (at the South East Corner) is assigned terrain factor 6, although

it appears outside the B area boundary. This illustrates the difficulty of sharply delineating towns or villages when discrete obstructions tend to cluster, for example, along roads in the suburbs.

21. A second anomaly is in the large forest area to the west where 95 (7) would appear to be the correct value but 95 (4) is used. This situation can arise when a significant open area (clearing), often several hundred square metres in area is surrounded by trees. As a result it is seen that since this particular forest does not embrace any other intersections (with the matrix spacing used X = Y = 500 metres) the forest area would not be represented correctly in the model. Interpolations made for the remainder of the area would be inaccurate since tree height would not be incorporated. Surface objects such as the more specific vertical reflectors eg towers, culture and buildings can therefore only be represented if the matrix is fine. Much data has been produced in the past using old maps in which the contour accuracy may be in doubt, and there is an urgent need to digitise data directly from stereo photos.

INTERVISIBILITY AND SCREENING DIAGRAMS

22. Mobile radar systems unfortunately suffer from target and terrain masking which is site-specific, and although a geometric model, given sufficient data, can predict the positions of probable clutter patches, clutter strength from within a patch is far more difficult to predict (see Chap 4).

23. If the target is assumed to be at zero altitude then clutter patch masking predictions are the same as predictions of target masking at zero altitude (see para 30).

24. Whether the clutter actually prevents detection or causes break-track depends on the clutter strengths, clutter rejection capability of the system and relative radar cross section of the target. Investigations by Briggs and Billingsley [4] have revealed in the past that insufficient data is available to support an accurate low grazing angle model.

25. Clutter Predictions. Francois [9] has researched the sensitivity of clutter prediction using the geometry of aerial and target height. In particular it was found that on examination of some 20 sites, coverage in geometrical prediction was "rarely in good quantatitive agreement with the spherical earth". Further, the radar site must be in good fit; or very near to the best fit plane with the terrain data. Plots showing the sensitivity of coverage to the aerial and target heights typically take the form shown at figure 7. These are clearly site-specific, however it is possible to predict (for the type of terrain prevailing in a general geographic area), a probability that unmask will occur out to a given range for a given target height and radar height. In these assessments an expected percentage of the 360° scan will be denied due to terrain screening.

26. Once a clutter prediction has been made it is further modified in practice by smearing due to the convolution of the clutter within the appropriate resolution cell (see also dependence of clutter on aerial motion - Chapter 5).

27. Actual and geometrically - predicted clutter maps have, on occasion, proved successful and useful, but uncertainties in terrain spot height, data base, culture variations and propagation effects unfortunately tend to degrade results.

INTERVISIBILITY PLOTS

28. Figures 8 and 9 show typical intervisibility plots (using program SLINE.FOR) for two aerial heights. Targets were at 70 metres altitude in both cases. The percentage masking at a given range is plotted at Figure 10. Terrain spot height only was used to produce these results and a far more serious effect follows when the terrain surface culture and obstructions are included. (See also Annex E).

29. A first approach to the production of realistic screening diagrams ignores the effects of microwave radar energy partially penetrating vegetation, diffraction effects, or multipath which causes angular errors. It is assumed that target range-gating will always be used by modern tracking radars, hence only clutter from a range close to that of the target has to be considered. This implies a clutter problem only when the surface beneath an aircraft is illuminated by the radar. Since a sightline may not exist to this area beneath the target due to terrain or obstacle screening, there will be many occasions when clutter cannot be received.

30. A simple way to check those cells in which clutter is obscured is to place the target at zero altitude and test for the existence of a sightline. A "Clutter Visibility" map can be drawn and combined with the terrain screening map to produce an overall map where the clear areas represent positions where the target can be seen but the ground underneath cannot. On flat ground, near to the radar, the ground is likely to be seen, since the probability of a sightline is high. Hence at close ranges the target will be in a clutter region. Readers of the short paper {10} could misinterpret the significance of this situation and it should be noted that paper was produced initially for an optical visibility study. At close target

ranges the radar beam elevation angle is likely to increase, (taking narrow tracking beams clear of the surface clutter), while simultaneously at shorter ranges the returned target signal will be greater due to the shortened two-way transmission path length and will better compete with any remaining noise or clutter.

31. Figures 11 and 12 show typical (max range 30 km) screening diagrams for fairly flat terrain for aircraft at 100 metres altitude and zero (notionally) altitude respectively. The example diagram at Fig 13 {10} indicates where targets can be seen but the co-located clutter cells cannot. It is seen that many (clear) areas exist, particularly in the NE quadrant, where a high probability of successful and uninterrupted detection and tracking will exist. (Fig 13 = Fig 11 + negative of Fig 12)

32. Figures 14 and 15 compare the probabilities of target visibility (for targets at 100 m altitude) and clutter averaging 0m and 10m above terrain spot heights. Adgie's paper naturally assumes the same clutter from all ranges, since from the optical point of view all obstacles are the same. Chapter 4 investigates radar clutter levels in detail. Figure 14 shows the typical trend for fairly flat terrain where the upper curve probability falls almost linearly with range, compared with Fig 15, where hilly terrain cause the corresponding curve to fall rapidly as the closest ground cover to the radar on some azimuths causes the inevitable loss of sightline. The measurements at fig 14 correspond with the plan diagram at fig 11. Two lower curves at figs 14 and 15 representing the combined effects (with and without the 10m tree cover) indicate:

a. As expected the probability of detection is lower in hilly terrain (but not necessarily the probability of obtaining a required crossing track length in the same terrain - See Annex E).

b. Best visibility is at intermediate range (ie the highest probability of target sightline coincident with the lowest probability of clutter beneath the target).

c. The difference in detection probability made by a 10 m coverage of trees is small. The differences are plotted at figure 16 where it can be seen that they are remarkably constant out to about 26km on flat terrain and out to 14-16 km on hilly ground.

It should of course be stressed that results are site dependent, but the trend perhaps indicates that constant height ground cover (ie over large tree covered areas) does not reduce the overall detection probability by as much as was expected, particularly in the intermediate ranges; important for example in surface to air missile tracking scenarios. (See Fig 16).

35. Dependent on the radar type, 2km may be an impractically short range for tracking purposes, since although the minimum range of the radar may be less than 2km, high speed targets at very short range present an extremely high sightline rate which may well exceed the lock-follow rate of the associated tracker control loop.

CHAPTER SUMMARY

36. An earth's surface model has been investigated in order to set up:

a. Sight lines to the target.

b. Corresponding sightline to clutter regions below the target.

Methods of constructing a terrain data base have been examined and the matrix method of spot heights and culture identification system selected for this project. The necessity of allowing for ground footprint resolution cell "tilt" (or slope) has been recognised and some original work has been done on this in a later chapter. The problems of intervisibility have been outlined and shown to be site-specific. Clutter prediction research in the USA has been investigated and this confirms the necessity for fineness of terrain descriptive data to enable a realistic clutter prediction map to be produced. This approach is of course recognised as a means only of identifying the existence of a probable clutter patch in any particular position, and not of the signal nature of the clutter itself; these aspects are examined in detail in Chapter 4.

37. Example intervisibility plots have been used to highlight the difficulty of predicting masking, even in a most arbitrary manner. Particularly sensitive variables in relation to mobile radars will therefore be:

a. The necessity to operate at any time in terrain which varies from hilly to smooth.

b. Nearby obstacles which are fixed (ie poles, pylons etc)which block sectors, but which may not appear on maps.

c. The inability (or inadvisability) of the radar to move to a better position from the clutter viewpoint under battle conditions.

38. Thus it is seen that a realistic assessment of the probability of a radar obtaining a sightline to a target at a given range and altitude when sited at some arbitary position that has not been painstakingly surveyed

is indeed difficult, and this does not yet include the many other factors covered in later chapters concerning the ability of the radar to detect and track the target successfully when the clutter backscatter is competing with the target echo.

39. Computer Program. Details of a terrain sightline computer program are briefly described at Annex D.

40. Observed Track-Lengths. A useful aspect of terrain survey data is the ability to predict, for a given radar position, the unmasked sectors (shown at Figure 10), not in unmasked percentages but as probability of observing given track lengths. This is an important concept since tracking of any consequence can only take place if a sightline exists for a minimum period. Taken a stage further by the author, it is shown that this can be extended to a probability plot for total missile firing opportunities; by taking missile and target speeds and system reaction time into account. This is pursued as a separate part of the study, with an attempt to classify typical areas with deployed radars as 'high' or 'low' risk areas to an aircraft transitting through. (See also Annex E).

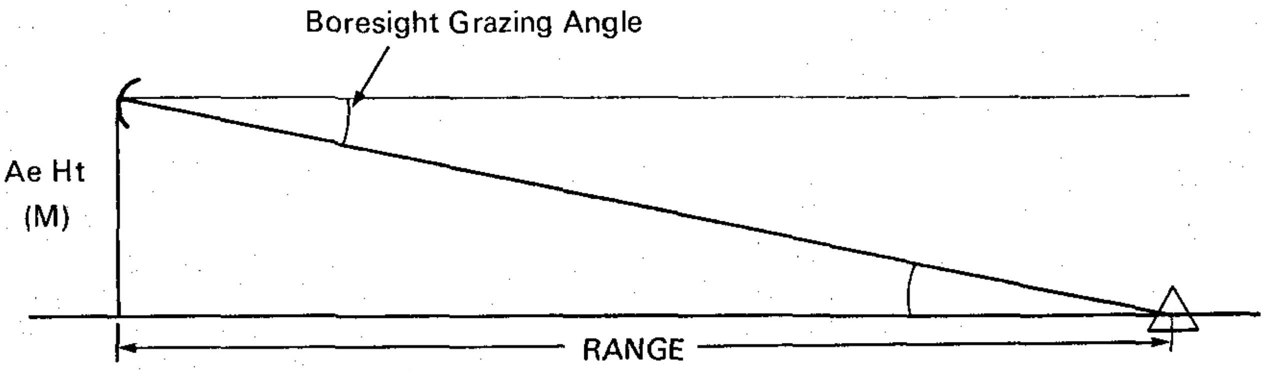

FIG 1 GRAZING ANGLE FOR TARGET ON SURFACE

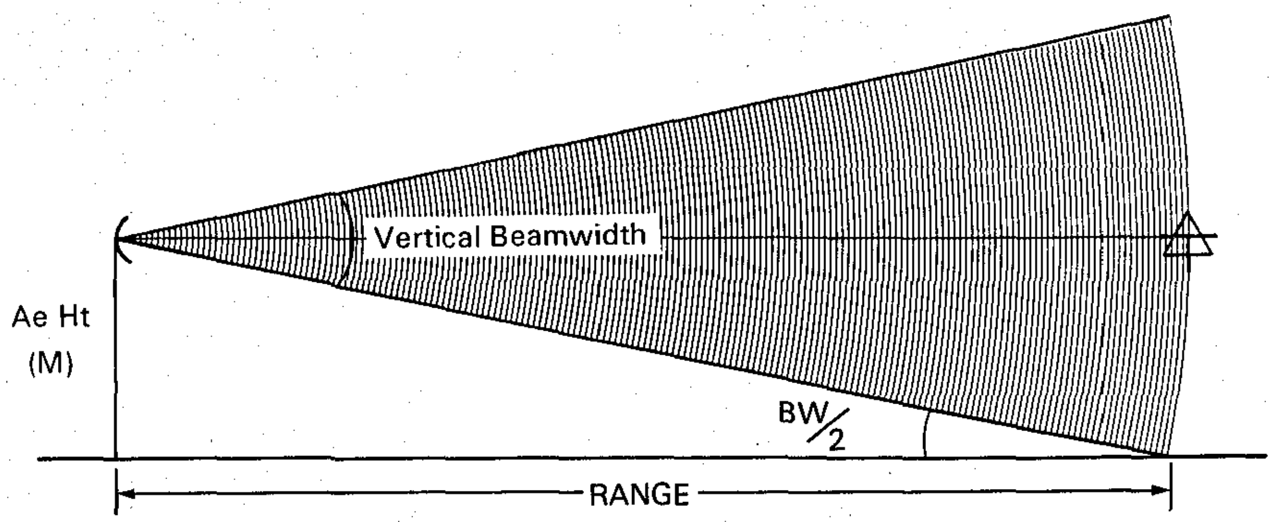

FIG 2 RANGE TO SURFACE FOR GIVEN BW & AE HEIGHT

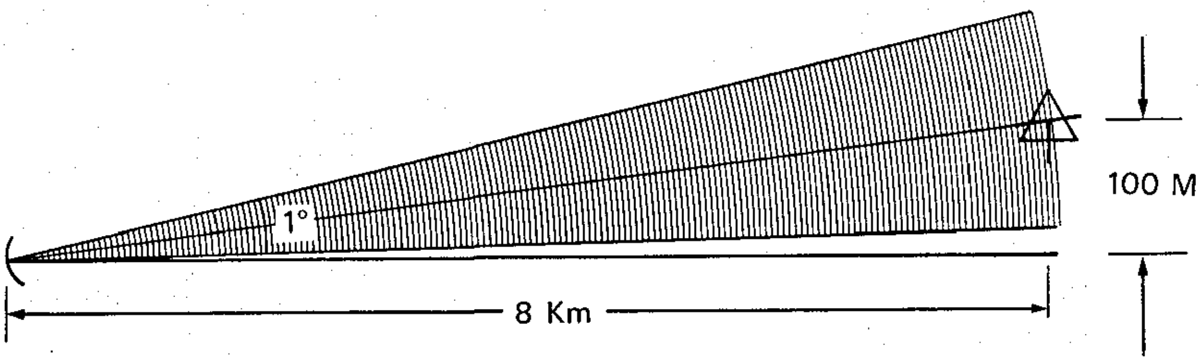

FIG 3 CLUTTER BEAMWIDTH/ANGLE CRITERIA

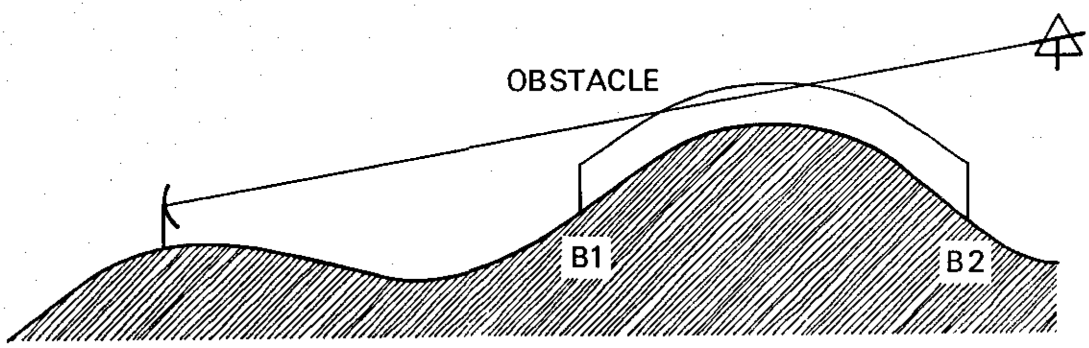

FIG 4 OBSTACLE REPRESENTATION

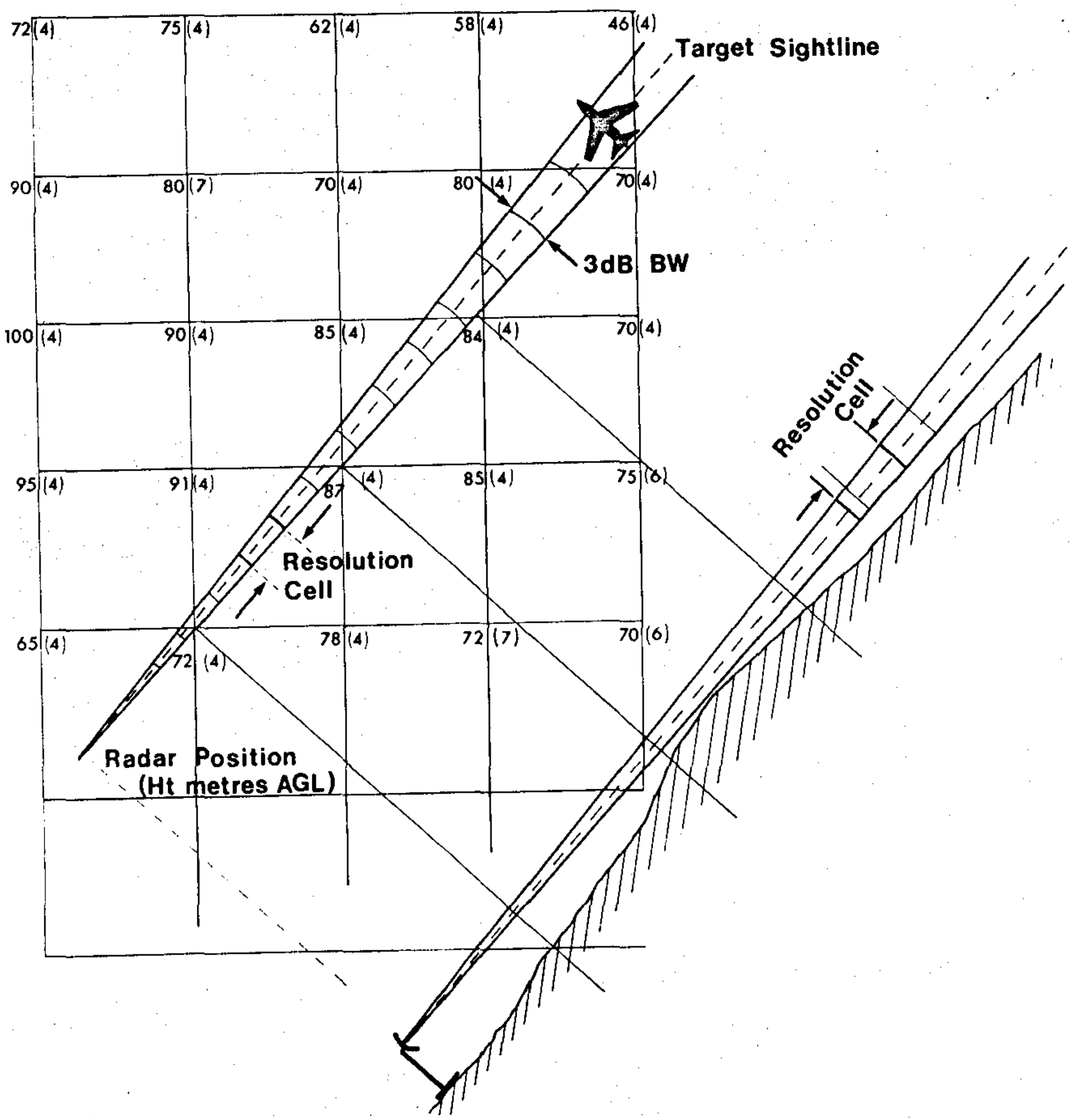

FIG 5 GEOMETRY OF PENCIL BEAM RADAR BACKSCATTER CELLS OVER TERRAIN

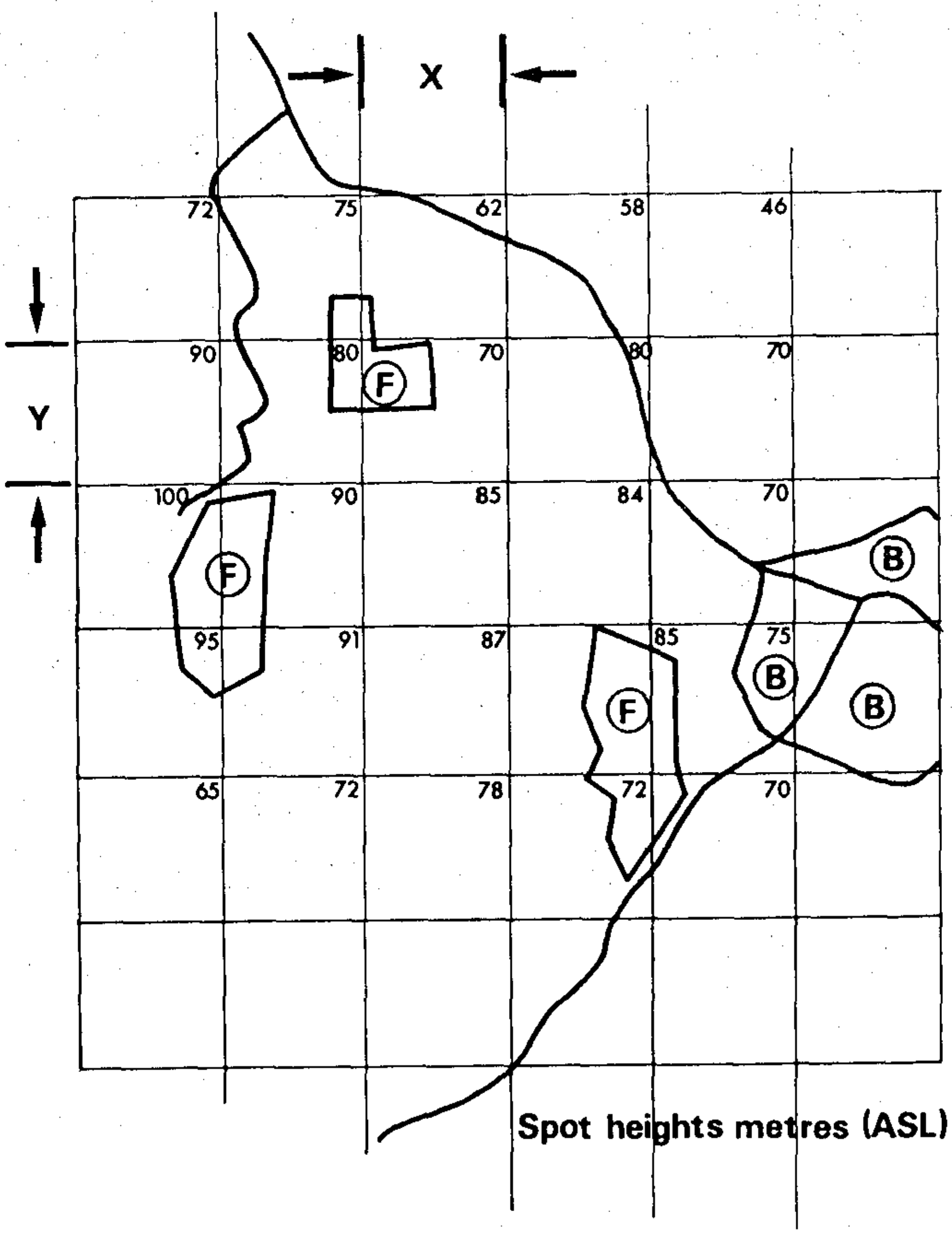

FIG 6 MATRIX FOR TERRAIN DATA BASE

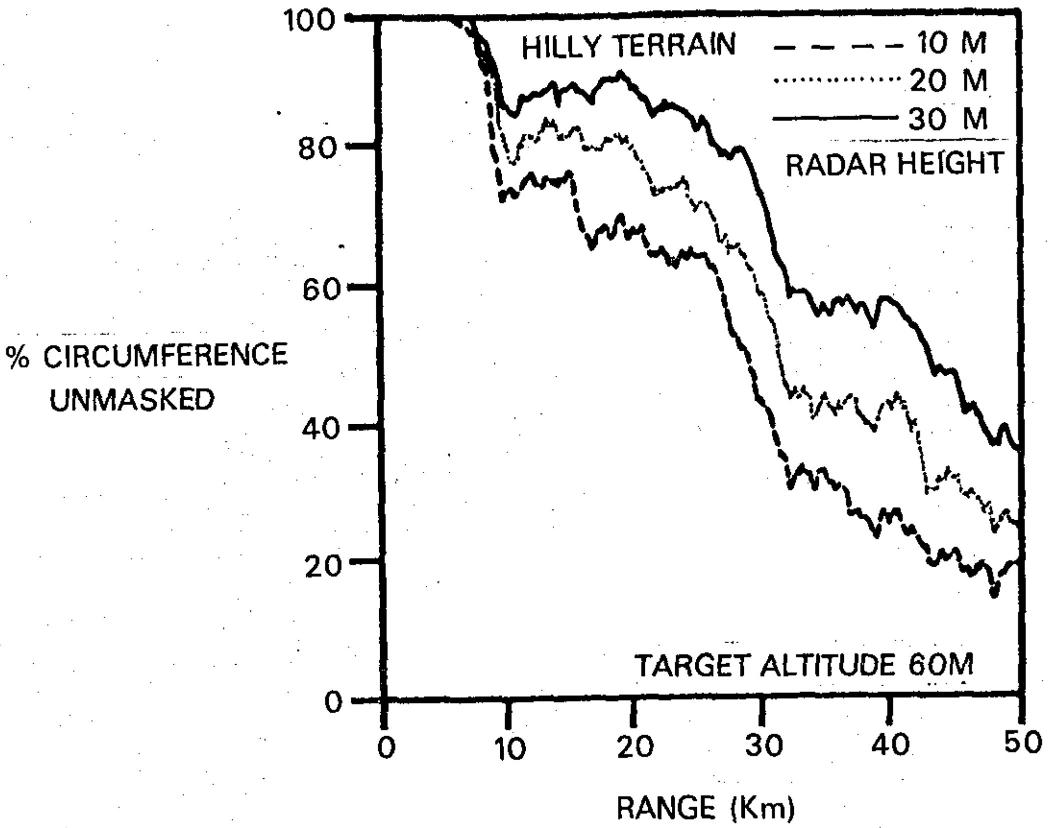

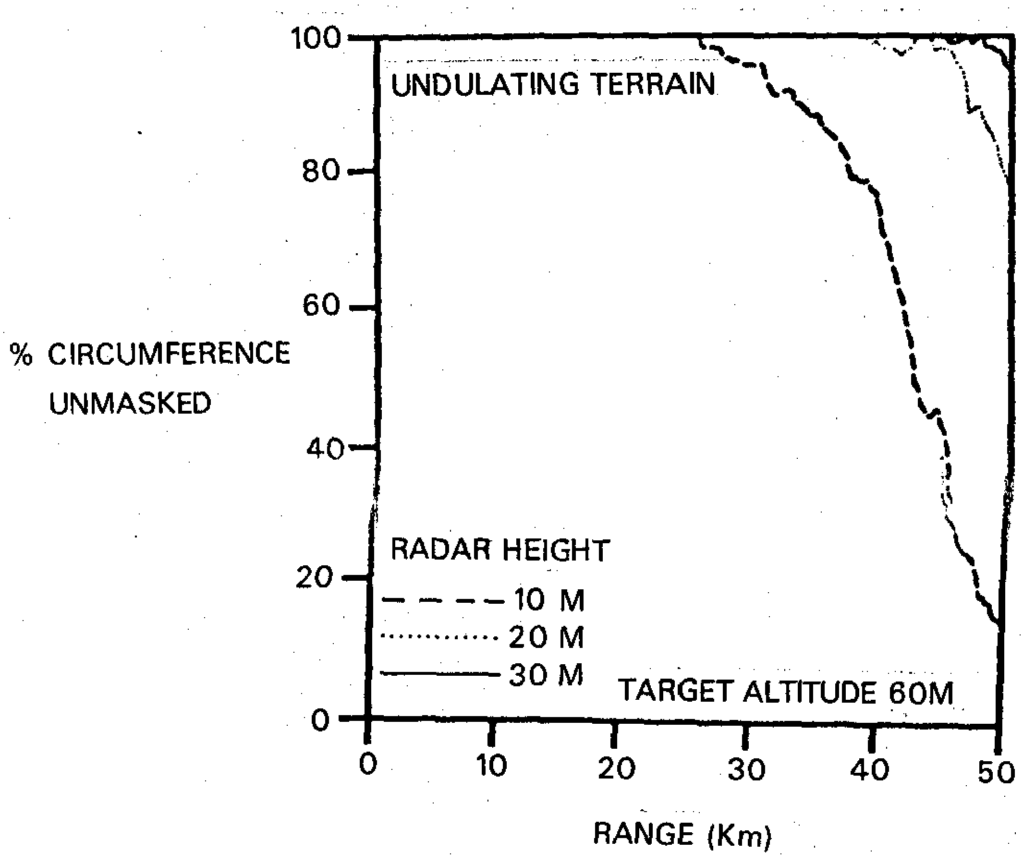

FIG 7 PERCENTAGE CIRCUMFERENCE UNMASKED

FIG 8 INTERVISIBILITY PLOT

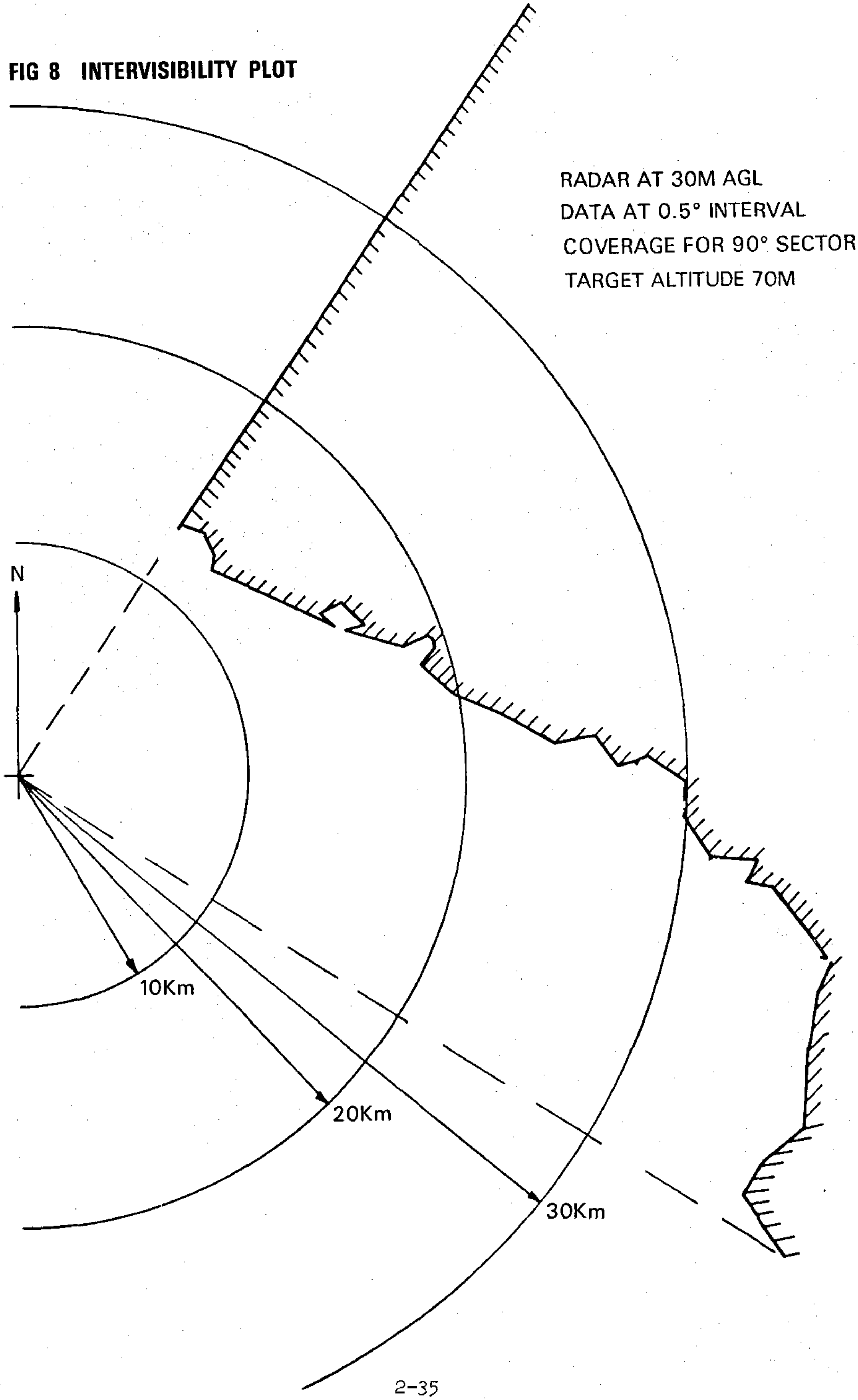

FIG 9 INTERVISIBILITY PLOT

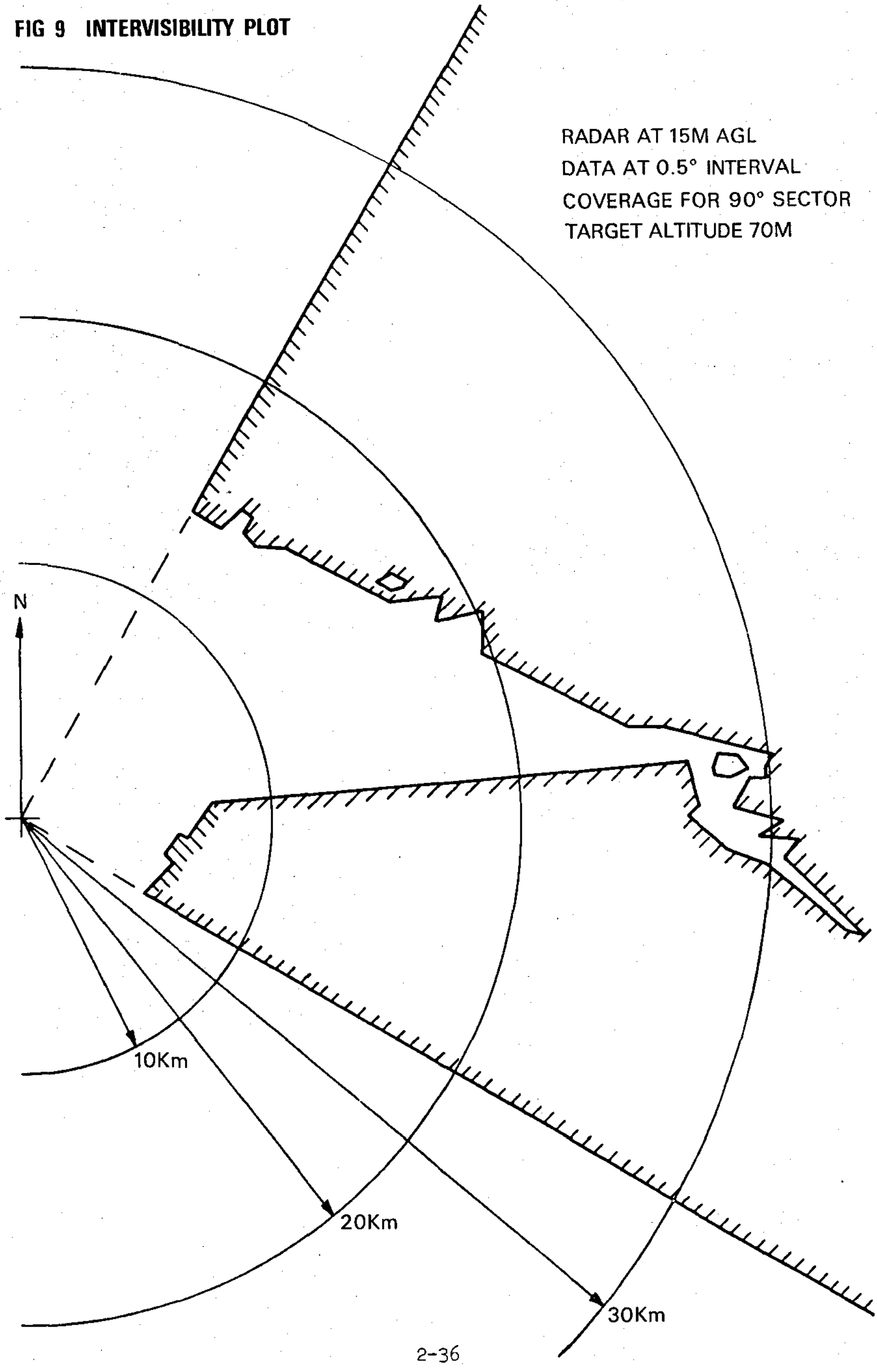

RANGE OUT TO	RADAR AERIAL HEIGHT(M) 15	30
10 Km	15%	0%
20 Km	56%	16%
40 Km	89%	58%

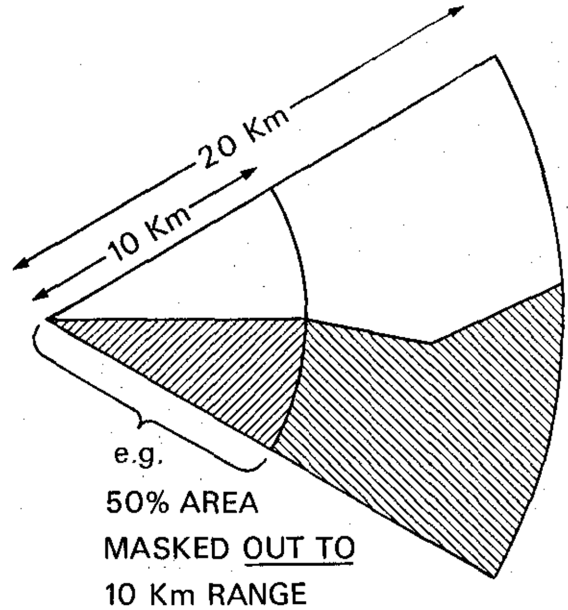

FIG 10(a) PERCENTAGE AREA MASKING OUT TO SPECIFIC RANGES

RANGE AT WHICH MASKED	RADAR AERIAL HEIGHT(M) 15	30
10 Km	42%	0%
20 Km	96%	45%
40 Km	100%	100%

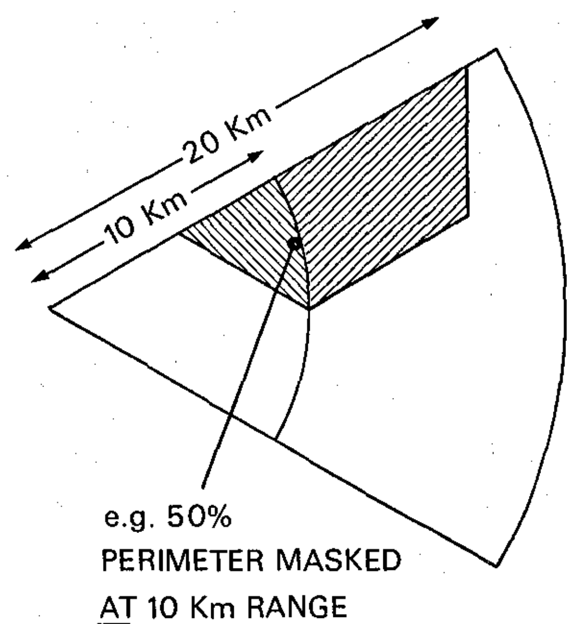

FIG 10(b) PERCENTAGE PERIMETER MASKING AT SPECIFIC RANGES

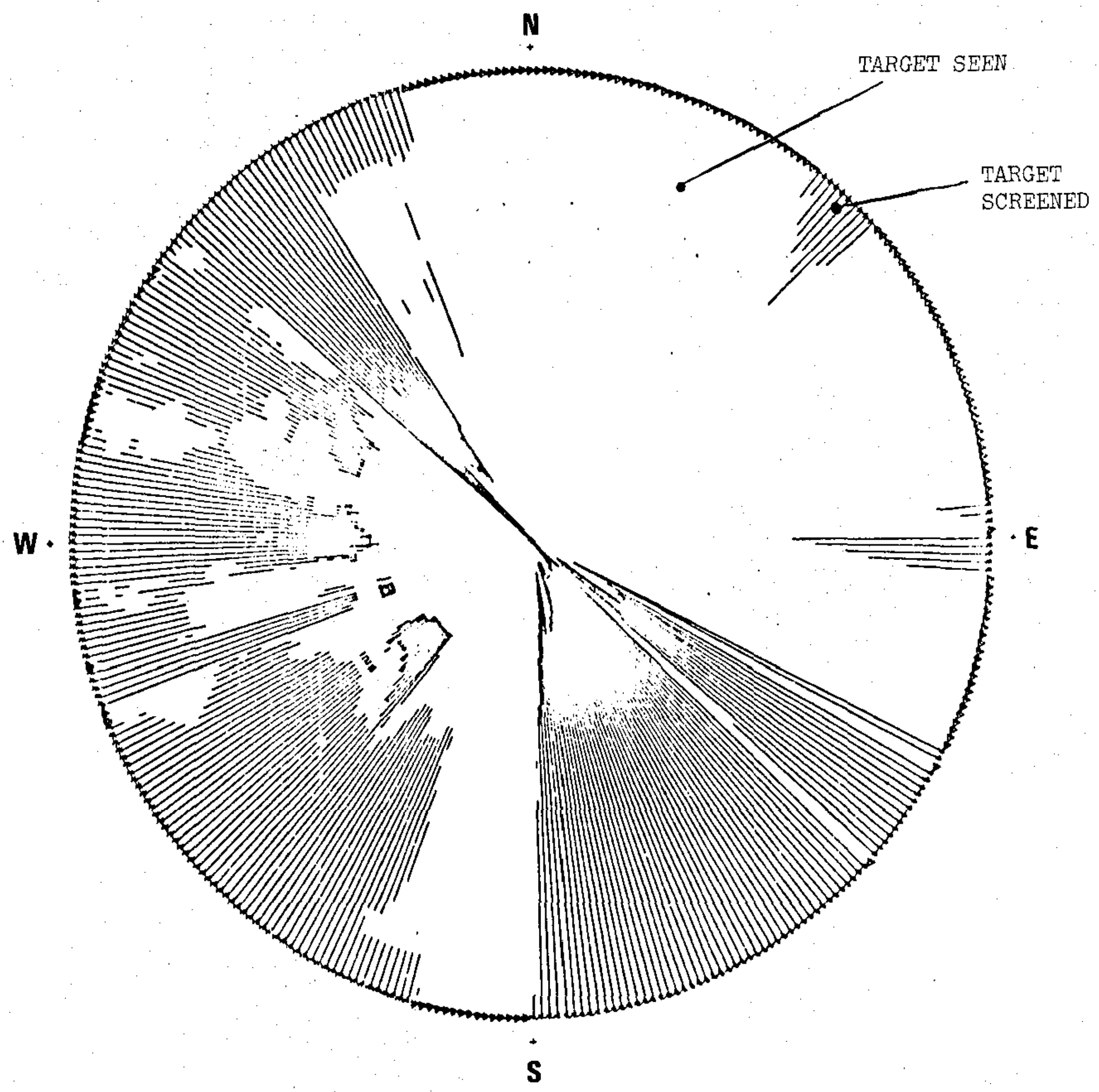

MAXIMUM RANGE 30Km

AIRCRAFT ALTITUDE 100M

RADAR ZERO ALTITUDE

FIG 11 NORMAL SCREENING DIAGRAM

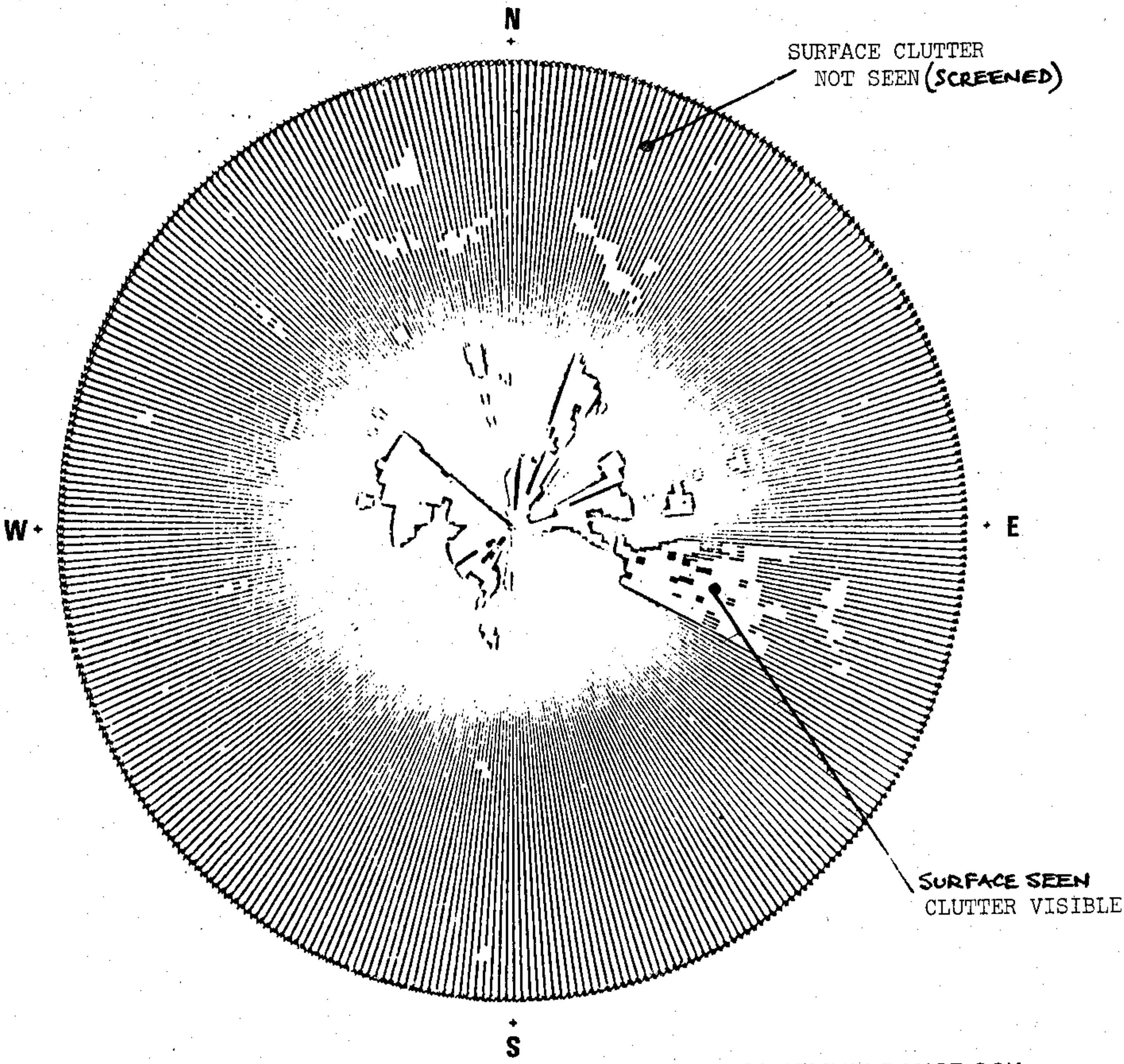

MAXIMUM RANGE 30Km

AIRCRAFT ALTITUDE 0M

RADAR ZERO ALTITUDE

FIG 12 CLUTTER VISIBILITY DIAGRAM

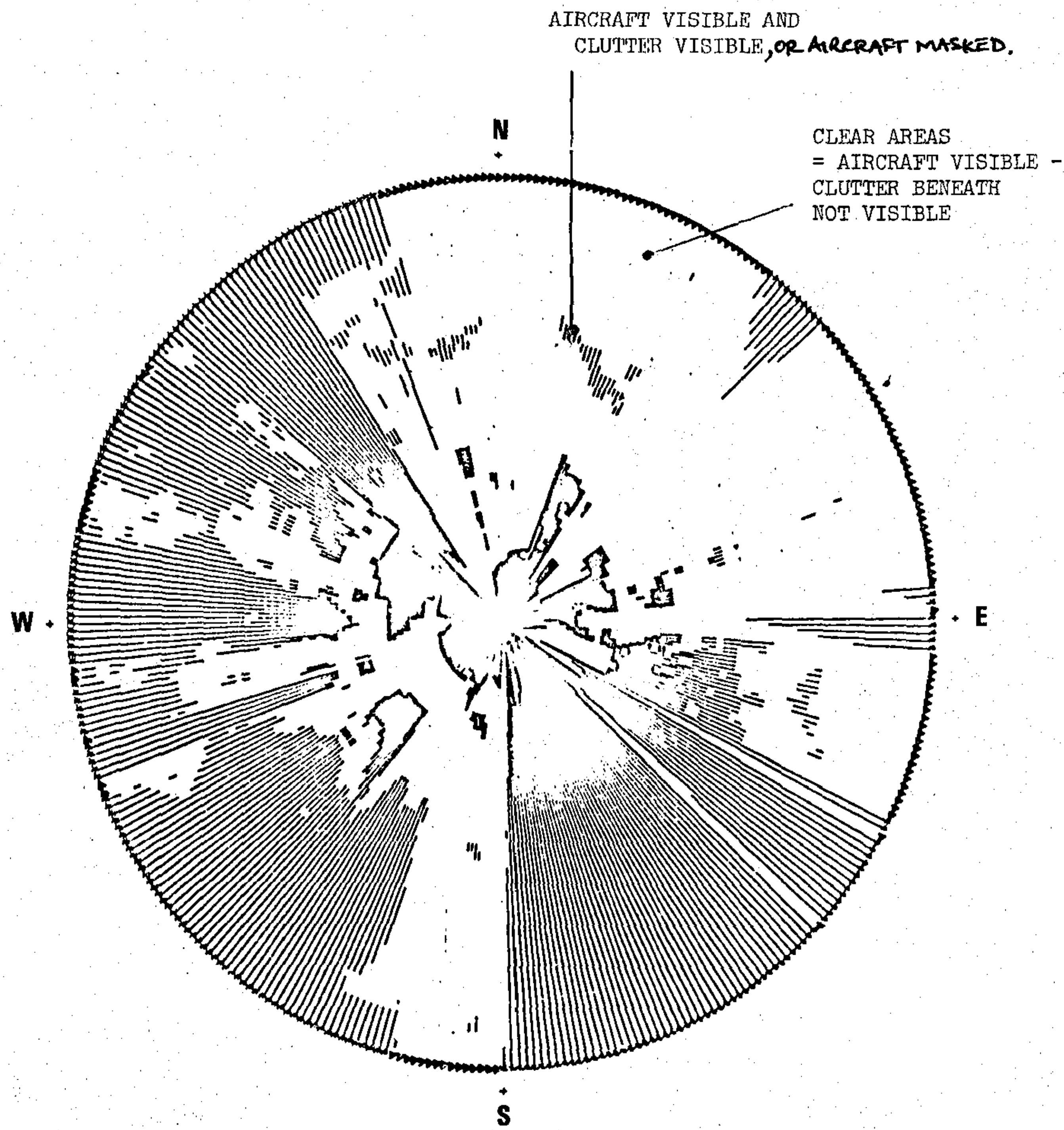

MAXIMUM RANGE 30Km

AIRCRAFT ALTITUDE 100M

RADAR ZERO ALTITUDE

FIG 13 COMBINED SCREENING DIAGRAM

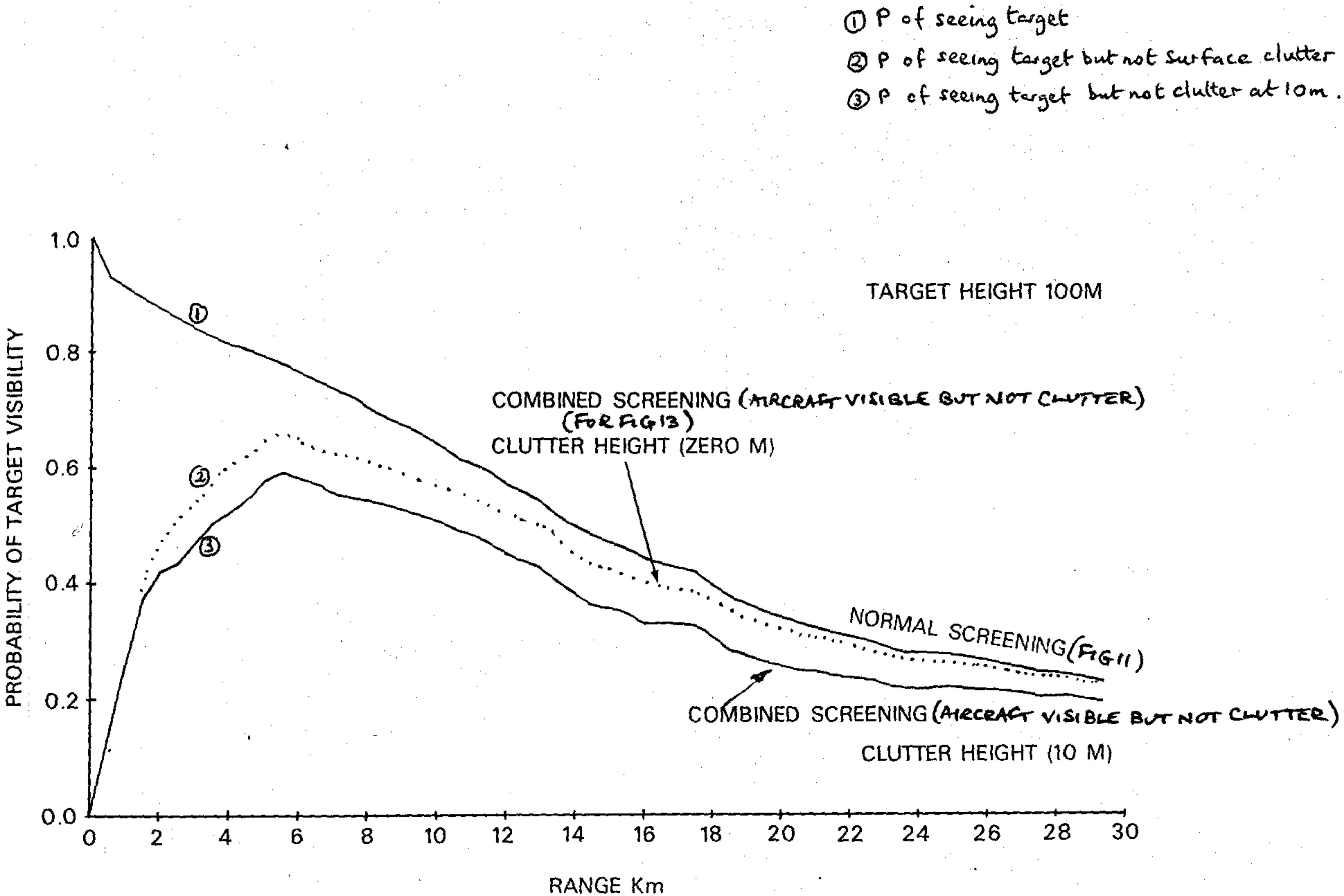

FIG 14 AVERAGE PROBABILITY OF TARGET VISIBILITY (FAIRLY FLAT TERRAIN)

(AFTER ADGIE)

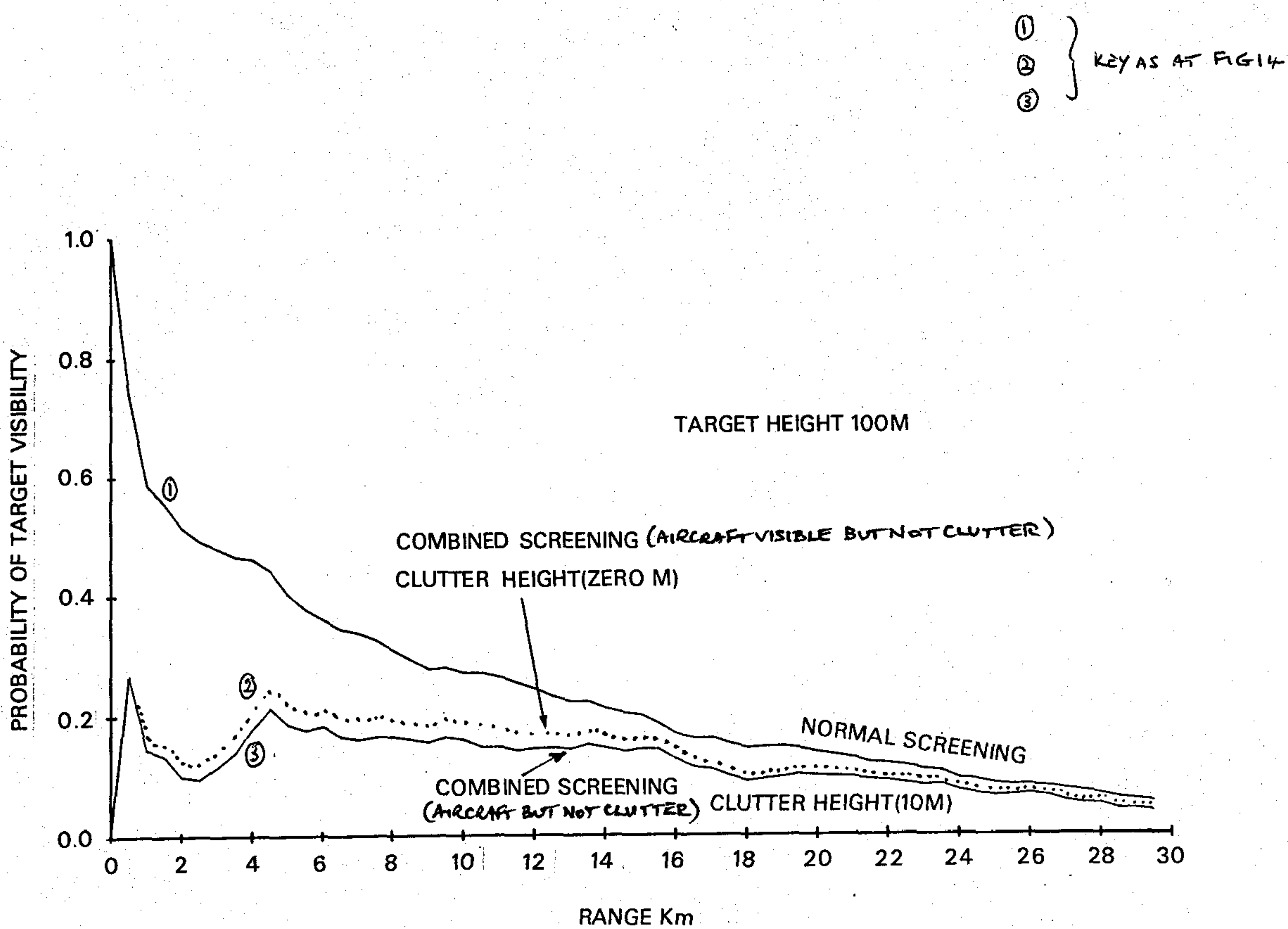

(AFTER ADGIE)

FIG 15 AVERAGE PROBABILITY OF TARGET VISIBILITY (HILLY TERRAIN)

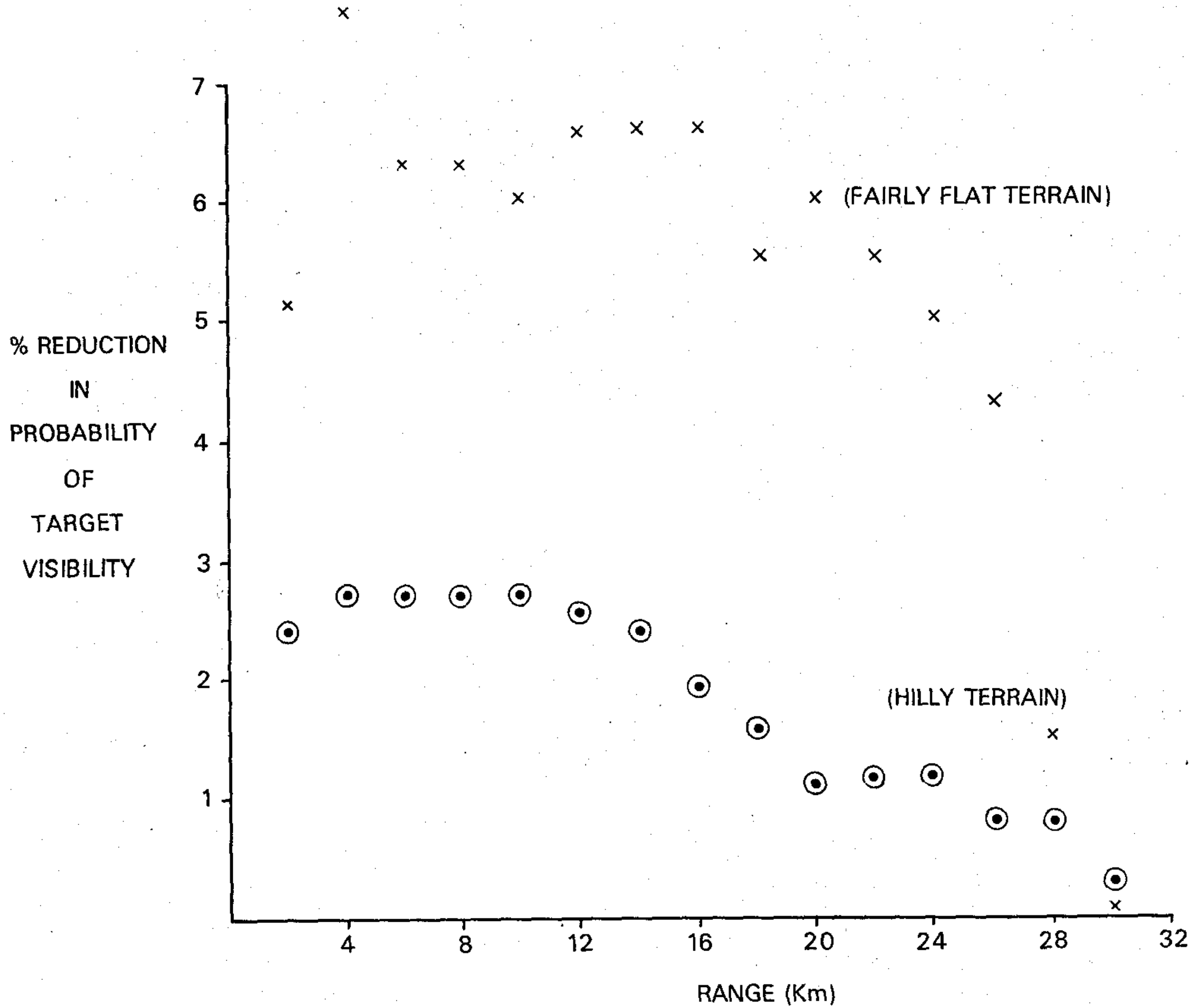

FIG 16 REDUCTION IN SIGHTLINE PROBABILITY DUE TO 10 M GROUND COVER (AFTER ADGIE)

CHAPTER 3

VOLUME CLUTTER - RAIN AND ATMOSPHERIC CLUTTER

GENERAL

1. Attempts are made to detect and track low level military aircraft in almost any conditions of weather, in contrast to civil operations, where airports may be below safe civil operating criteria if the visibility is degraded under conditions of intense rainfall, low cloud or fog.

2. The aim of this chapter is to provide realistic modelling values for rain and atmospheric clutter and to assess the atmospheric constraints on target detection for incorporation into the overall clutter model at chapter 11.

3. Effect of Operating Wavelength. For the purpose of the study the radar frequency is fixed at > 10,000 MHz; but where a choice is to be made for a radar operating in rain the preference would be for lower frequencies unless of course rain is to be deliberately detected for weather avoidance purposes. That the echoing area of rain increases dramatically with frequency is clearly seen from a simple example, by taking the specific echoing area of rain (m^2m^{-3}) for 1 and 3 GHz band radars respectively (with two identical radars 1^o Beamwidth, 1 μ sec pulse length and 50 nml range), would give a ratio of $\approx$ 32 to 1.1 m^2, ie approximately 15 dB extra echoing area in favour of the 10 cm equipment. And for example, a difference of 20 dB (typically - 73 dB and - 53 dB) is found respectively for λ = 3 cm and 9.3 cm in heavy rain at precipitation rate p = 16 $mm.hr^{-1}$. Rain attenuation effects are also important and these are considered first, followed by the reflectivity of rain later in the chapter at para 14.

4. Rain. While the little atmospheric attenuation in good weather is due to gases and water vapour, precipitation in the form of rain, ice, hail or snow can significantly increase signal attenuation. Values can be calculated using Mie {12} theory and is given in graphical form for a range of values in Skolnik P543/544 (note graphical error in Skolnik Fig 12.12).

5. For 3 cm radars calculated values are found to be different than those summarised by Nathanson {13} p 197 see figure 1, who presents measurements by a number of researchers, mostly at frequencies above 10 GHz (3 cm), and arrives at a mean curve which is fitted by the equation:

$$\text{Log } A = 1.85 \text{ Log } (f \times 10^{-9}) - 3.0 \quad \text{------------------------------} (1)$$

Where A = 2 way atten dB.Km^{-1} mm.hr^{-1} f = frequency Hz

Both sets of values are summarised at Table 1 below (for 10 GHz). Hayes uses $0.00919p^{1.16}$ and $1{\cdot}6p^{0.64}$ dB.Km^{-1} for 9.4 GHz and 94 GHz respectively {54}.

Rainfall rate (p) mm.hr^{-1}	TWO-WAY ATTENUATION dB.Km^{-1}			
	10 GHz Mie	10 GHz Nathanson	9.4 GHz Hayes	94 GHz Hayes
0.25 (Drizzle)	0.008	0.016	0.002	0.65
1.0 (Light Rain)	0.04	0.063	0.009	1.6
4.0 (Moderate Rain)	0.16	0.25	0.046	3.88
16 (Heavy Rain)	1.2	1.0	0.229	9.4
40	4.0	-	-	-
64 (Excessive)	-	4.0	-	-

TABLE 1 - Rain Attenuation of Radar Signals

6. <u>Attenuation Modelling Values</u>. Specific values for attenuation and reflectivity for rain and cloud for use in the overall model are considered in the summary to this chapter at para 37.

7. <u>Cloud and Fog</u>. Water droplets are small compared with λ, and summing over $1m^3$ the Rayleigh approximation is used {14}.

$$\text{Attn } (dB.km^{-1}) = 0.434 \left| \frac{\pi^2}{\lambda} \quad (\Sigma D^3) \text{ Im } (-K) \right| \qquad (2)$$

D = Particle Diameter (cm)

Im(-K) = Imaginary part of -K (0.0247 for λ = 3.2 cm), the dielectric dependent factor.

re-writing (2)

$$\text{Attn } (dB.km^{-1}) = 0.434 \frac{6\pi}{\lambda} \quad \frac{M\text{Im}}{\rho} \quad (-K) \qquad (3)$$

M = Liquid water content ($g.m^{-3}$)

ρ = Density of water (taken as unity)

λ = Wavelength (cm)

8. Since it has been shown empirically that at λ = 3 cm, Im varies as λ^{-1}, eqn (3) can be approximated within 5% to be:

$$\text{Attn } (dB.km^{-1}) = \frac{0.438M}{\lambda^2} \qquad (4)$$

Together with $\overline{M} = 1660\bar{v}^{-1.43}$, where $\bar{v}$ = optical visibility (feet) and $\overline{M}$ = average moisture content ($g.m^{-3}$) the one way attenuation curve at figure 2 is produced at 18°C. (Two way attenuation variation with RF is shown at Fig 3.)

9. It is seen that one way attenuation values at $\lambda = 3$ cm spread from about 0.10 $db.km^{-1}$ for heavy fog to 0.001 $dB.km^{-1}$ for light fog. These values decrease by more than a factor of 3 as the temperature varies over the range $0^{o}C$ to $40^{o}C$.

10. Figure 3a. presents two atmospheric attenuations curves interpolated for the radar parameters for this study, from which it is seen that within the low ranges and low grazing angles limits, there is an almost linear relationship. These were calculated from the US Central Radio Propogation Laboratory exponential reference atmosphere for refraction and the International Civil Aviation Organisation (ICAO) standard atmosphere for pressure - temperature values. The atmosphere is assumed to be regular and the one way attenuation factor (F) is given by:

$$F = e^{-\alpha R} \quad \text{or} \quad e^{-2\alpha R} \quad \text{(for two-way)} \quad \text{--------------------} \quad (5)$$

α = attenuation coefficient

R = target range

$$\alpha = \frac{\text{one-way attenuation loss}}{\text{range}} \quad \text{--------------------} \quad (6)$$

11. Attenuation coefficients for a 10 GHz (3 cm) radar with 0^{o} and 0.5^{o} elevation angles have been calculated at intervals from figure 3, and graphed at figure 4a (1). It is seen that the curve of the attenuation coefficients is not linear with range. Using a constant value for the attenuation coefficient introduces an error that can be significant for high frequency radars at low grazing angles. Table 2 gives the one way attenuation losses for 10 GHz at 0.5^{o} grazing angle. Fig 3b (from an alternative source) confirms the 10 GHz 0^{o} and 0.5^{o} spot values.

Range (nml)	5	10	15	20	25	30	35	40	45	50
Loss dB Per nml	0.0250	0.0241	0.0230	0.0225	0.0220	0.0217	0.0214	0.0212	0.0208	0.0205

TABLE 2 - ONE WAY ATTEN, LOSSES 10 GHz AND 0.5° ANGLE

12. To determine the attenuation coefficient a natural logarithm curve fitting technique was used with eqn (7) as the regression equation. Regression coefficients are α, and α_2.

$$\alpha = \alpha_1 + \alpha_2 \;\mathrm{Log}_e\, R \text{ ------------------------------ } (7)$$

changing to attenuation loss from Fig 4.

$$R\,\alpha = R\,\alpha_1 + R\,\alpha_2\,\mathrm{Log}_e\, R \text{ ---------------------- } (8)$$

$$L = L_1 + L_2\,\mathrm{Log}_e R \text{ ---------------------------- } (9)$$

L = attn loss for range R at 0.5° = $0.0283 - 0.001972\,\mathrm{Log}_e\, R$ (See figure 4a(2))

13. The theoretical values are plotted at figure 5 using eqn (9) and compared with the values from figure 3. Conclusions as to the most reasonable values to use in the model are at para 37 below.

ASSESSMENT OF RAIN REFLECTIVITY

14. Rain. The second effect of precipitation produces backscatter, or clutter. Surveillance radars are designed to detect targets in rainfall up to 15 $\mathrm{mm.hr}^{-1}$. Heavier rainfall is the exception and normally only occurs for a small percentage of the time and it's spatial extent is usually limited. Modification to the basic radar equation is necessary to take account of the reflectivity of rain. When viewed with linear polarisation the echoing area of a single raindrop whose diameter is very small compared with λ, is given by {15} p 38, as:

$$\sigma_i = \frac{\pi^5}{\lambda^4} \left| \frac{m^2 - 1}{m^2 + 2} \right|^2 d^6 \quad \text{———} \quad (m^2) \quad \text{———} \quad (10)$$

m = complex refractive index of water

d = diameter of raindrop

15. Up to a frequency of 10 GHz (3 cm) the raindrop size assumption holds but beyond 10 GHz in heavy rain the Mie scattering theory is required. Using a figure of 0.93 for λ = 3.2 cm {18}, for $\left|\frac{m^2 - 1}{m^2 + 2}\right|^2$, the radar reflectivity σ_v is the echoing area of unit volume of rain:

$$\sigma_v = (0.93)\, \frac{\pi^5}{\lambda^4}\, \Sigma d^6 \quad \text{———} \quad (m^3.m^{-3}) \quad \text{———} \quad (11)$$

Quantity Σd^6 is the reflectivity factor, normally denoted Z, and the relationship between precipitation rate p ($mm.hr^{-1}$) and Z is taken {18} and {16} to be ($mm^6.m^{-3}$):

(a) Stratiform rain $Z = 200p^{1.6}$

(b) Orgraphic rain $Z = 31p^{1.71}$

(c) Thunderstorm rain $Z = 486p^{1.37}$

16. Nathanson {13} p200 and Barton {17} p105 quote the value for stratiform rain as the most representative, and so this value is used here. Taking the value Z and changing units in eqn (11):

$$\sigma_v = 0.93\, \frac{\pi^5}{\lambda^4}\, (200 \times 10^{-18})\, p^{1.6}\ m^2.m^{-3} \quad \text{———} \quad (12)$$

for λ in metres and f in Hz:

$$\sigma_v = 5.69 \times 10^{-14} \frac{p^{1.6}}{\lambda^4} \quad \text{or} \quad 7.05 \times 10^{-48} p^{1.6} f^4 \quad \text{———} (m^2m^{-3}) \text{———} \quad (13)$$

In terms of dB relative to $1m^2$

$$10 \log \sigma_v = -471.5 + 16 \log_{10} p + 40 \log_{10} f \qquad (14)$$

Hence for λ = 3·2cm the reflectivity in dB relative to $1m^2$ is at Table 3.

Rainfall Rate	1 $mm.hr^{-1}$	4 $mm.hr^{-1}$	16 $mm.hr^{-1}$	64 $mm.hr^{-1}$
dB	-72.6	-63	-53.4	-43.7

Table 3 Radar Reflectivity for λ = 3·2cm for Rain

17. According to Battan {19} p 100 it has been shown that on the average the calculated rain echo will be 1.4 dB greater than the measured value but it is not usual to make any allowance for this. Figure 6 shows radar reflectivity of rain for given radar frequency and precipitation rate, however variation in drop size causes minor variations regardless of rate.

ECHOING AREA OF RADAR PENCIL BEAM FILLED WITH RAIN

18. Since this study is concerned solely with monostatic pencil beam tracking radar performance(which are often mobile), it is assumed that the radar uses the same beam for both transmit and receive. It must also be assumed that the precipitation rate is uniform within the radar resolution cell. If the resolution cell is completely filled (worst case radar condition), and the polar diagram in both planes is rectangular, a first approximation of the echoing area of the rain in the beam is given by:

$$\sigma_R = \sigma_v \frac{\pi}{4} \theta_A \theta_E \left(\frac{\pi}{180}\right)^2 R^2 \frac{c\tau}{2} \qquad (m^2) \qquad (15)$$

θ_A = azimuth 3dB beamwidth (deg)

θ_E = elevation 3dB beamwidth (deg)

R = range of rain (metres)

19. A more exact result would be obtained by taking into account the variation in aerial gain over the beam cross section. If the polar diagram is assumed Gaussian in both planes the azimuth polar diagram power pattern is:

$$\exp \left| -\tfrac{1}{2} \left(\frac{1.665\theta_a}{\theta_A}\right)^2 \right| \text{ ------------------------------ } (16)$$

and, the two-way pattern in terms of power is:

$$\exp \left| -\tfrac{1}{2} \left(\frac{3.33\theta_a}{\theta_A}\right)^2 \right| \text{ ------------------------------ } (17)$$

θ_a = Angular departure in azimuth from the beam axis (radians)
& below θ_e = " " " elevation " " " " "

20. Considering now a horizontal slice of beam with this pattern, of width $d\phi$ and a maximum value of power:

$$P_{(slice)} = Pd\phi \int_{-\infty}^{+\infty} \exp \left| -\tfrac{1}{2} \left(\frac{3.33\theta_a}{\theta_A}\right)^2 \right| d\theta \text{ ---------- } (18)$$

$$= Pd\phi \left| \frac{\sqrt{2\pi}}{3.33} \right| \theta_A = 0.7527\theta_A\, Pd\phi \text{ -------------- } (19)$$

Also, $P = \exp \left| -\tfrac{1}{2} \left(\frac{3.33\theta_e}{\theta_E}\right)^2 \right|$ ------------------------------ (20)

$$\text{Total Power} = 0.7527\ \theta_A \int_{-\infty}^{+\infty} \text{Pd}\ \phi = 0.566\ \theta_A\ \theta_E \quad \text{------------------} \quad (21)$$

Compared with $\frac{\pi}{4}\ \theta_A\ \theta_E$ at eqn (15) above.

21. Beam Echoing Area. With linear polarisation the beam echoing area of the gaussian beam filled with rain is:

$$\sigma_R = (7.05 \times 10^{-48}) p^{1.6} f^{4} (0.5666)\ \theta_A\ \theta_E\ \left(\frac{\pi}{180}\right)^2 R^2 \frac{c\tau}{2} \qquad (m^2) \text{ --- } (22)$$

$$\text{or } \sigma_R = (1.82 \times 10^{-43})\ \theta_A\ \theta_E\ R^2 \tau p^{1.6} f^4 \text{ --------- } (m^2) \text{ --------- } (23)$$

If rain exists between the radar transmitter and the resolution cell, attenuation effects will make the resolution cell rain echoing area appear to be less (see attenuation effects at paras 4 and 5 above).

22. The case where a beam is partially filled with rain {20, 16} is not pursued, since only low level targets are of interest. For radar modelling it is customary to assume {16} that precipitation is constant below some arbitrary ceiling and zero above, hence with a pencil beam at low grazing angles and short range it is reasonable to assume that only rain filled resolution cells are pertinent. For very low angles part of the beam may intercept the ground but the small effect of this is ignored.

23. An exception to this situation would exist if the resolution cell was just below the $0^\circ C$ altitude level, where the so called "bright band" is situated and the reflectivity suddenly increases, because water has a greater reflectivity than snow and so the particles also change size and shape. Battan {19} p 192 gives the increase in the bright band as

12-15 dB above that of snow 500 metres above, while the value of the rain at lower altitudes beneath the bright band may be 6-10 dB lower. Harrold {21} suggests 9 dB and 8 dB respectively. The $0^{o}C$ level may occur at any altitude. It is assumed that there exists an exponential change of reflectivity above the 0^{o} level, and $\sigma_{v} \alpha \exp(-0.6 \times 10^{-6} h^{2})$ ---- (24)
h = height above the freezing level (metres).

POLARISATION EFFECTS

24. If in an ideal situation a perfectly spherical raindrop is illuminated by a circularly polarized wave, the reflected signal will have the opposite hand of polarisation and can be totally rejected on reception. In practice, raindrops are not perfectly spherical and it is not practicable to generate perfectly polarised waves, particularly over the whole of the beam. Rain rejection is not perfect although a significant degree of cancellation can be achieved. Warden {22} gives experimental results averaging 20 dB. Reiss et al {23} using results taken over a year averages 16 dB and this is accepted as a typical figure (cancellation = ratio of return using linear polarisation to the accepted part of the return with circular polarisation).

25. Since raindrops can be regarded as oblate spheroids, optimised elliptical polarisation will give better cancellation than circular. However the optimum cancellation characteristics vary with range and the nature of the precipitation. This point is not pursued for the study in hand. On the average the backscatter for horizontal polarisation is larger than that for vertical polarisation.

26. Assuming the rain moved with the wind {24} pp 205-212, the doppler spectrum arises from the resolved radial component of the wind velocity as it changes across the resolution volume. To this is added a component representing turbulence. The worst cases exist when looking up or down wind. Mean wind velocity and change of velocity with height (wind shear) are the main parameters. Assuming a two-way power pattern, Gaussian beam vertical polar diagram:

$$\text{Power} = \exp\left| -\tfrac{1}{2}\left(\frac{3.33\theta_e}{\theta_E}\right)^2\right| \quad \text{------------------} \quad (25)$$

θ_E = 3dB beamwidth

θ_e = Angular departure in elevation from the beam axis (rads)

27. If it is assumed that wind velocity changes uniformly with height and therefore uniformly with elevation angle, the standard deviation of velocity due to wind shear is {24}:

$$\text{s.d (Vel)} = KR\,\frac{\theta_E}{3.33}\,\frac{\pi}{180} \quad \text{---------- } ms^{-1} \text{ ----------} \quad (26)$$

K = Windshear coefficient $m.sec^{-1}.m^{-1}$

R = Range in metres

$$= (5.24 \times 10^{-3})\ KR\theta_E \qquad m.s^{-1} \quad \text{---------------} \quad (27)$$

28. The turbulent component is assumed to have a standard deviation of $1m.sec^{-1}$. So that the total standard deviation of velocity is:

$$\approx \left\{1 + (2.75 \times 10^{-5})\ (KR\theta_E)^2\right\}^{\frac{1}{2}} \qquad m.s^{-1} \text{ ---------------- } (28)$$

the corresponding standard deviation of the doppler spectrum is thus:

$$f_{sd} = \frac{2f}{c} \left\{1 + (2.75 \times 10^{-5})\ (KR\theta_E)^2\right\}^{\frac{1}{2}} \qquad (Hz) \text{ ---------- } (29)$$

$$= (6.67 \times 10^{-9}) \left\{1 + (2.75 \times 10^{-5})\ (KR\theta_E)^2\right\}^{\frac{1}{2}} f \qquad (Hz) \text{ ------ } (30)$$

where f is the frequency in hertz.

29. This spectrum is Gaussian in shape and centred on the frequency corresponding to the mean wind velocity in the resolution cell and can be written as:

$$S\ (fd) = \exp\left\{-\tfrac{1}{2}\left(\frac{fd - fw}{f_{sd}}\right)^2\right\} \text{ ----------------------- } (31)$$

fd = doppler frequency (Hz)

fw = doppler frequency corresponding to mean wind velocity (Hz)

SHORT TERM FLUCTUATION OF RAIN ECHOES

30. As the rain echo is made up of contributions from a very large number of droplet scatterers the probability distributions of the envelope can be expected to be Rayleigh in characteristic, providing precipitation is constant. Warden {22} has confirmed this experimentally. The rain echo therefore has the same distribution as thermal noise but with a much longer correlation time which can be significant when integration over the beamwidth of a scanning radar is considered. Any improvement in signal detectability as a result of integration will depend on the number of independent samples integrated. For thermal noise this would be equal to the number of pulses integrated, but for rain clutter it can be considerably less.

31. Referring to the doppler spectrum (eqn 31) will result in an auto-correlation function of Gaussian Shape and sd = $\frac{1}{2\pi f_{sd}}$. Assuming a time equal to two standard deviations represents near complete decorrelation. This is typically of the order of 10 millisecs when f_{sd} is near to it's lower limit, and this may be a substantial fraction of, or even exceed, the integration time.

SPATIAL CONSIDERATIONS

32. Nathanson {13} p 217 states that the mean echoing area may change by as much as ± 10 dB over 10 nmls under showery conditions and by as little as ± 1 dB in uniform rain. There is evidence {25} from measurements at Cardington that considerably larger fluctuations can occur; 20 dB in 0.5 km on occasions. Nathanson also stated a fall in spatial correlation to 0.5 in 0.6 to 1.4 nmls in showers, and in 2 to 3 nmls in uniform rain.

33. Frequency Correlation of Rain. Nathanson {13} p 213 shows that a change of frequency by the reciprocal of the pulse length is sufficient to reduce the correlation to near zero.

FREQUENCY AND DURATION OF INTENSE RAINFALL

34. Bilham {26} quotes an empirical formula relating rainfall, its duration and frequency of occurence in the UK.

$$\log n = 0.0952 + \log_{10} t - 3.55 \log_{10} (\Lambda + 1.01) \text{ --------- } (32)$$

n = number of occasions in 10 years

t = duration in hours

Λ = total rainfall in inches in time t

Re-written for p = precipitation rate in mm/hour averaged over time t.

$$\log_{10} n = 0.0952 + \log_{10} t - 3.55 \log_{10} \frac{(pt + 2.54)}{25.4} \quad \text{---------- (33)}$$

This is plotted at figure 7 and relates to rainfall at a point on the ground.

RAIN OVER "SMOOTH EARTH"

35. Extensive small random scatterers over a smooth earth or sea can be considered to be uniformly distributed. With certain combinations of polarisation at low grazing angles (HH/VV) the relative radar cross section of the scatterers is enhanced by the smooth surface. This is shown by Long and Zehner {27} to be as much as 7.8 dB larger at λ = 10 cm over the sea. **It is not clear if this would affect multipath at λ=3cm.** The rain scatterers are assumed to extend at least several interference lobes in altitude above the earth's surface. As the depression (grazing) angle approaches zero specular reflection increases. Work reported upon in this field suggests that the problem is complex and that information is incomplete, no results have been found for λ = 3 cm.

CHAPTER SUMMARY

36. From the foregoing, extensive reading and by contrasting the findings of many reports, a number of main conclusions applicable to the radar parameters required have been selected. These are set out below as the basis for the rain and atmospheric clutter inputs to the overall model at Chapter 11.

37. Selected Values. Using as far as possible practical measurements from the sources quoted and including opinions from unpublished sources:

a. Rain Attenuation. Rain attenuation values used are those from Nathanson shown at Table 1 at para 5. The set of results graphed at figure 1 are considered the most representative and the curves show the important trends as both radar operating frequency and rainfall increase.

b. Cloud/Fog Attenuation. Modelling values for cloud and fog attenuation are relatively small compared with the other sources interfering with radar detection. However this value is included for completeness and under certain conditions cloud or fog attenuation effects may just take the radar system below detection threshold or introduce uncertainty. Values calculated from eqn (9) are used. These are plotted at Figure 5 and also tabulated for several values. Curve fitting for eqn 9 was done by computer program, correlation coefficient 0.996.

c. Rain Reflectivity. Rain reflectivity values at Table 3 are considered suitable.

d. Pencil Beam Rain Echoing Area. Resolution cells within pencil radar beams are always considered to be rain-filled, never partially filled because of the geometry of the situation. Aerial polar diagrams are taken to be Gaussian in power distribution.

e. Polarisation Effects. Figures from Reiss (see para 24) are taken to be statistically sound.

f. Doppler Spectrum of Rain. Total standard deviation of doppler shift due to wind effects are incorporated by using equations (30) and (31).

g. Rain Fluctuation and Spatial Extent. Probability meterological statistics for precipitation frequency, duration, short-term fluctuation and intensity are well documented. The model initially operates without reference to the statistics, by using fixed rain values for each target run.

38. Details of the programs used for signal and statistical analysis are briefly described at Annex D.

39. Anomalous Propagation. Finally, atmospheric conditions might exist to produce 'ducting', allowing the unexpected detection of low level targets at greater ranges than normal. Such conditions cannot be predicted overland with total accuracy; but are probable over water as 'evaporation ducts'. Overland there is a 35% probability of some ducting in Europe. Prediction can be enhanced by using radiosonde data, and by using software such as the Ferranti prediction programs. Ducting is not considered to be of interest for a low level tracking radar since 'ducting' ranges are likely to exceed missile system ranges. Ducting might however allow an off-site search radar to detect the target at greater range and thus direct a tracking radar onto a target at an earlier time.

FIG 1 ATTENUATION IN RAIN FOR PRECIPITATION RATE AND RADAR OPERATING FREQUENCY

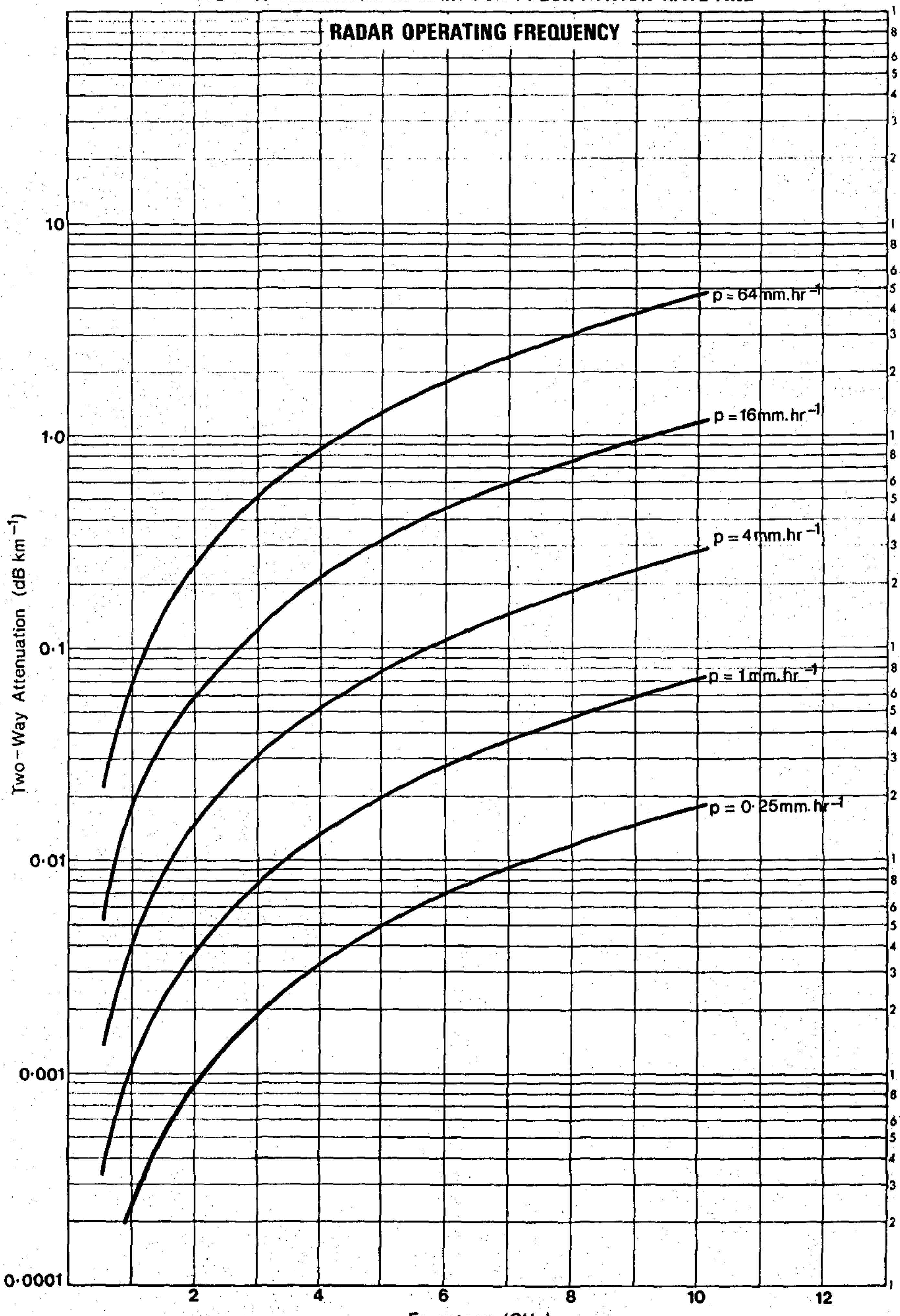

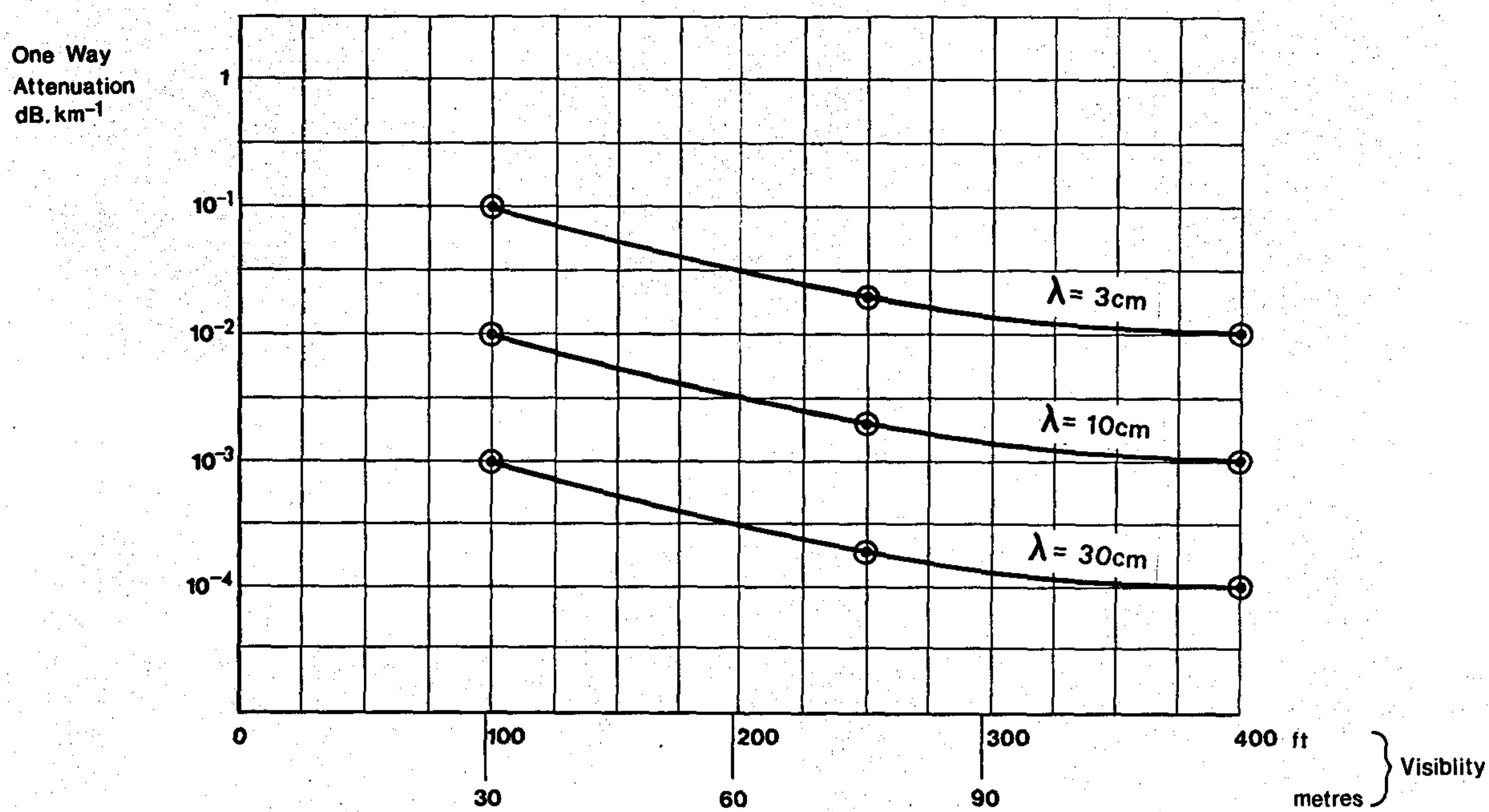

FIG 2 ONE WAY RADAR ATTENUATION IN FOG AT 18°C

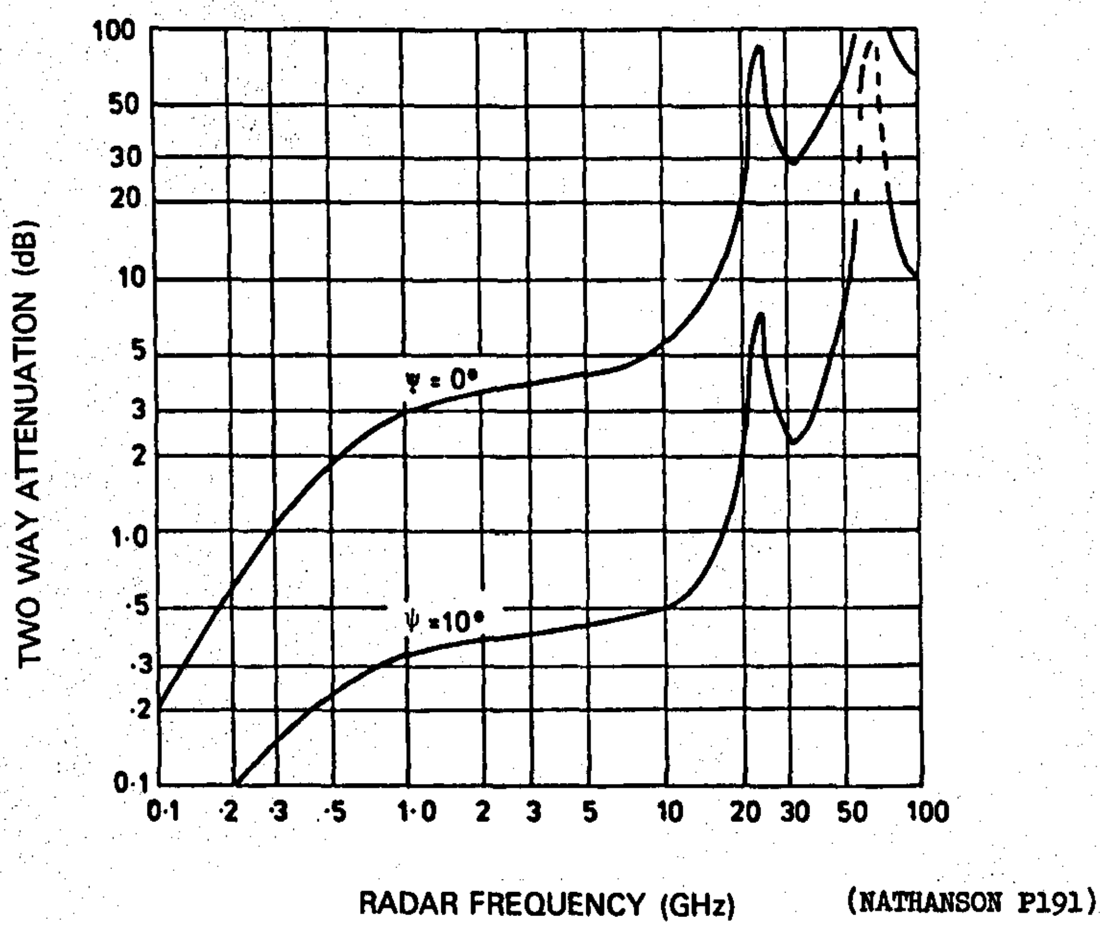

FIG 3 ABSORPTION LOSS vs RADAR CARRIER FREQUENCY FOR DIFFERENT ANGLES OF ANTENNA ELEVATION

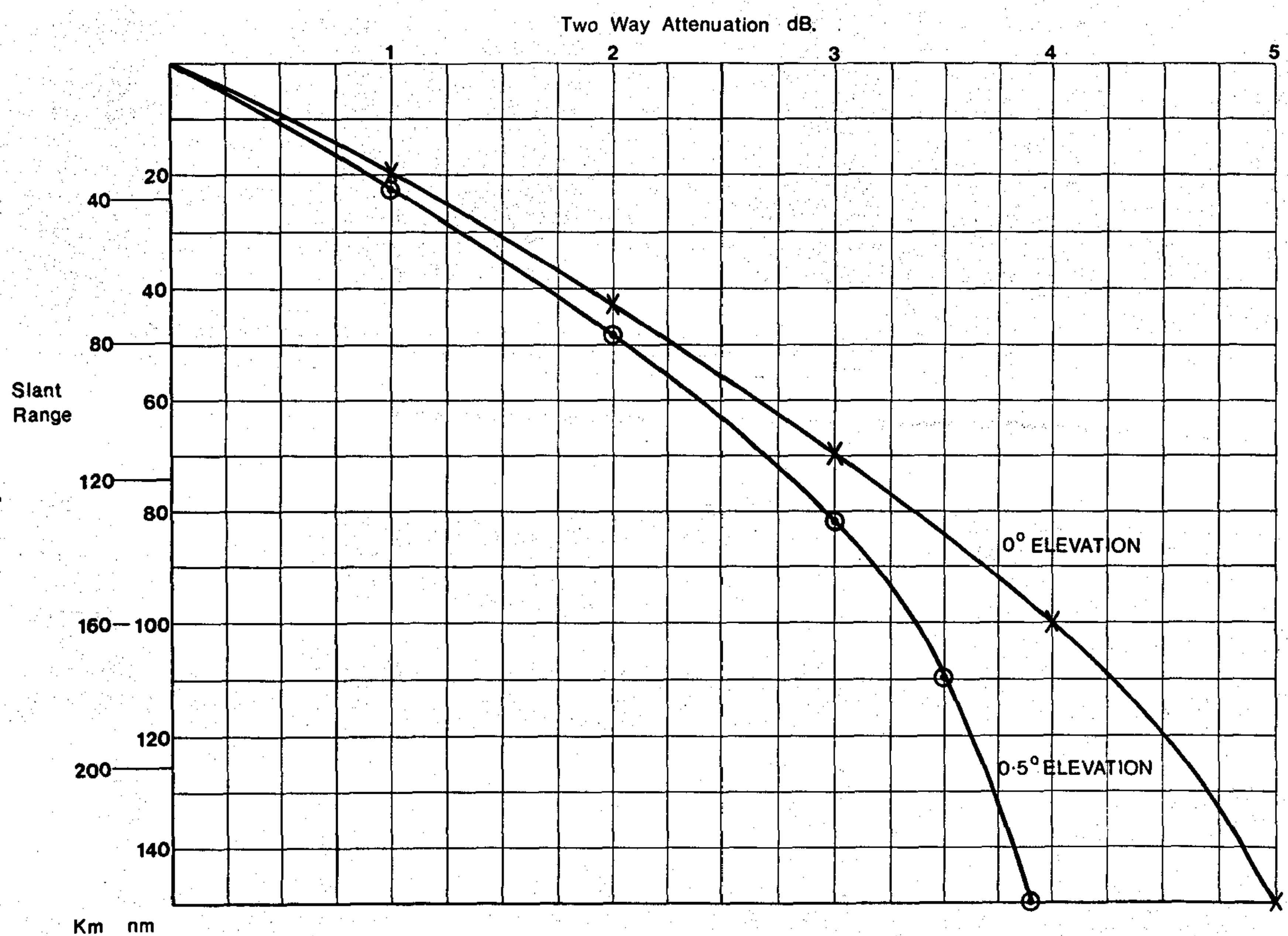

FIG 3a ABSORPTION LOSS AS A FUNCTION OF RADAR RANGE AT 0° AND 0.5° GRAZING ANGLE AT 10 GHz (3cm)

FIG. 3b TWO-WAY ATTENUATION LOSS FOR GIVEN GRAZING ANGLE AT 10GHz

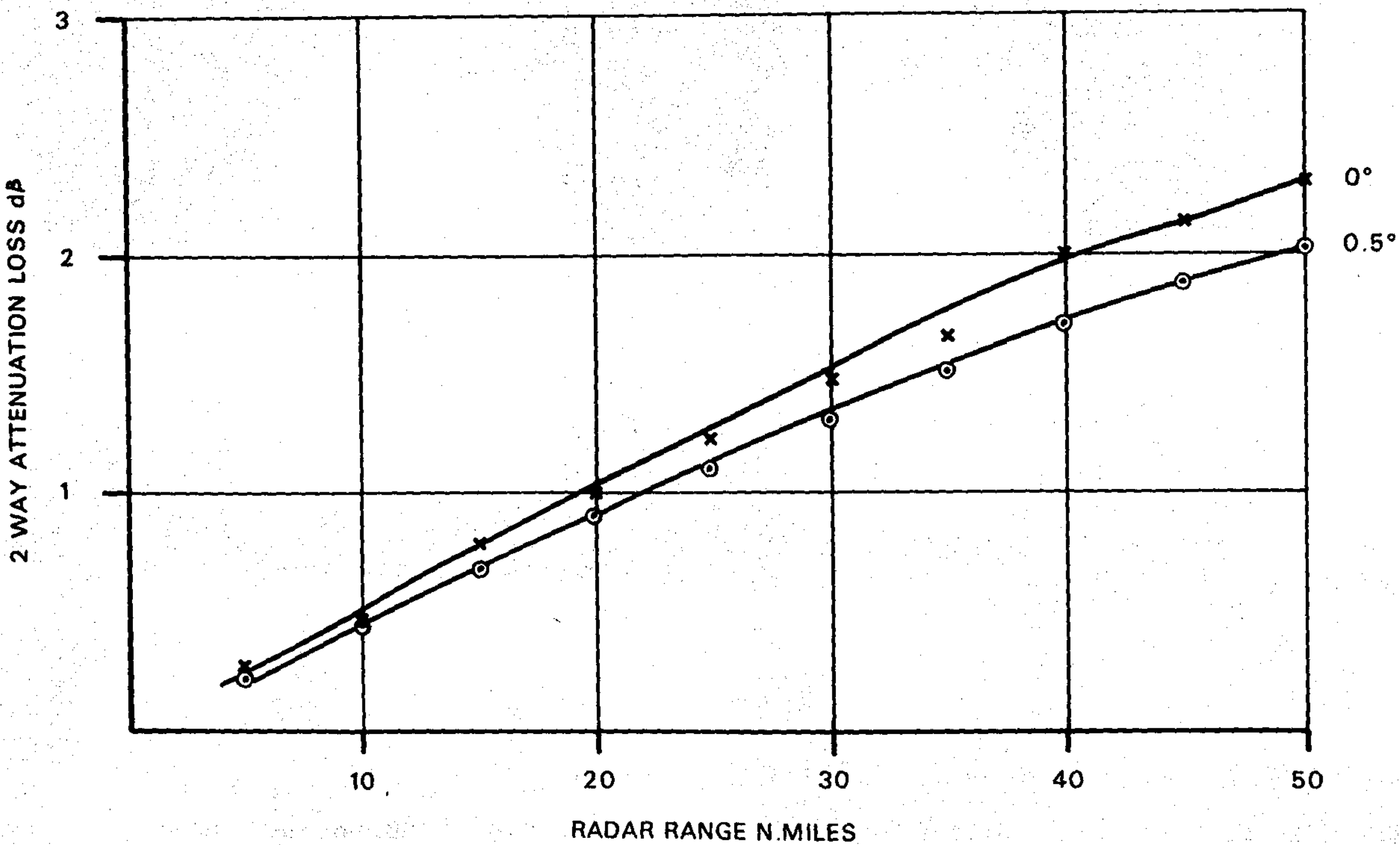

(1)

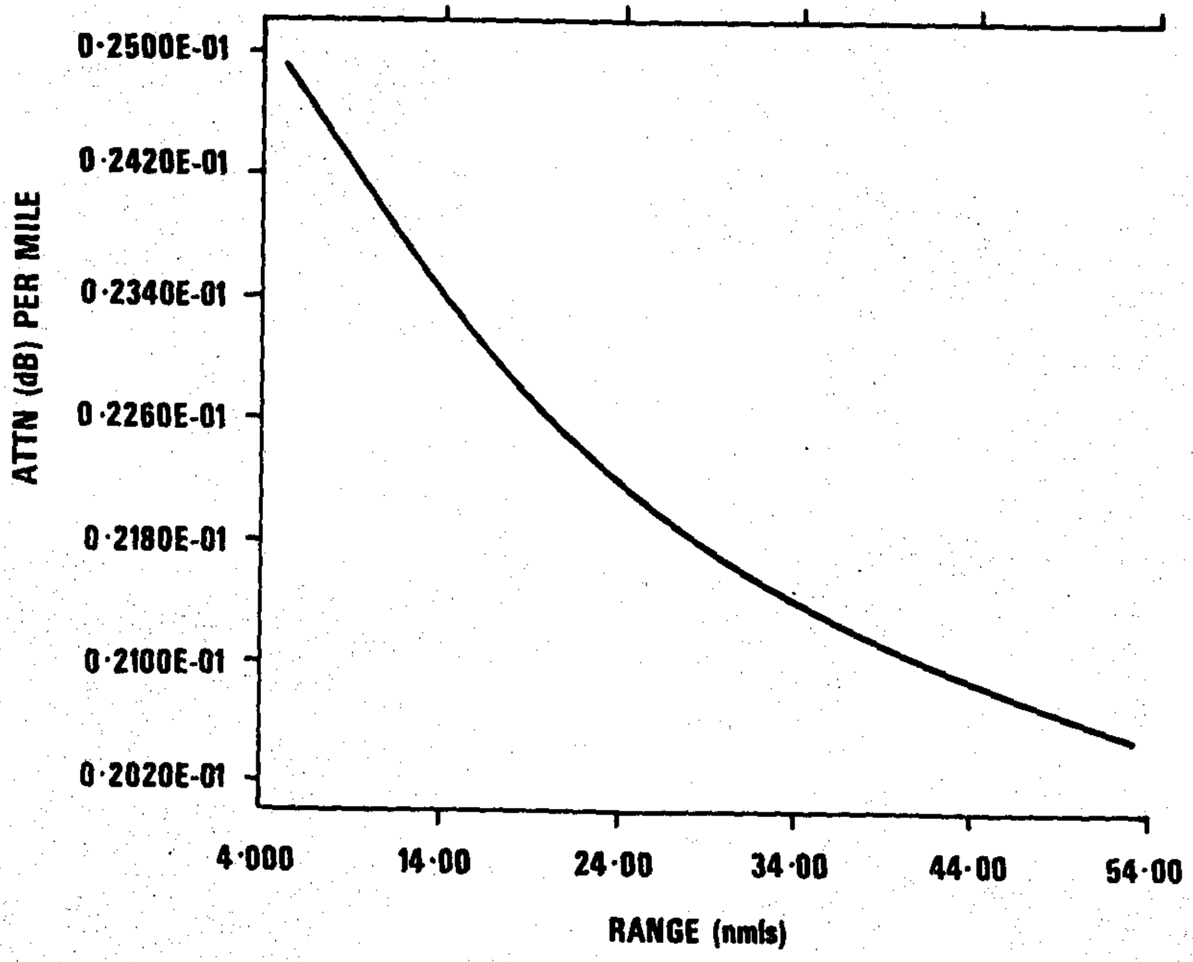

(2)

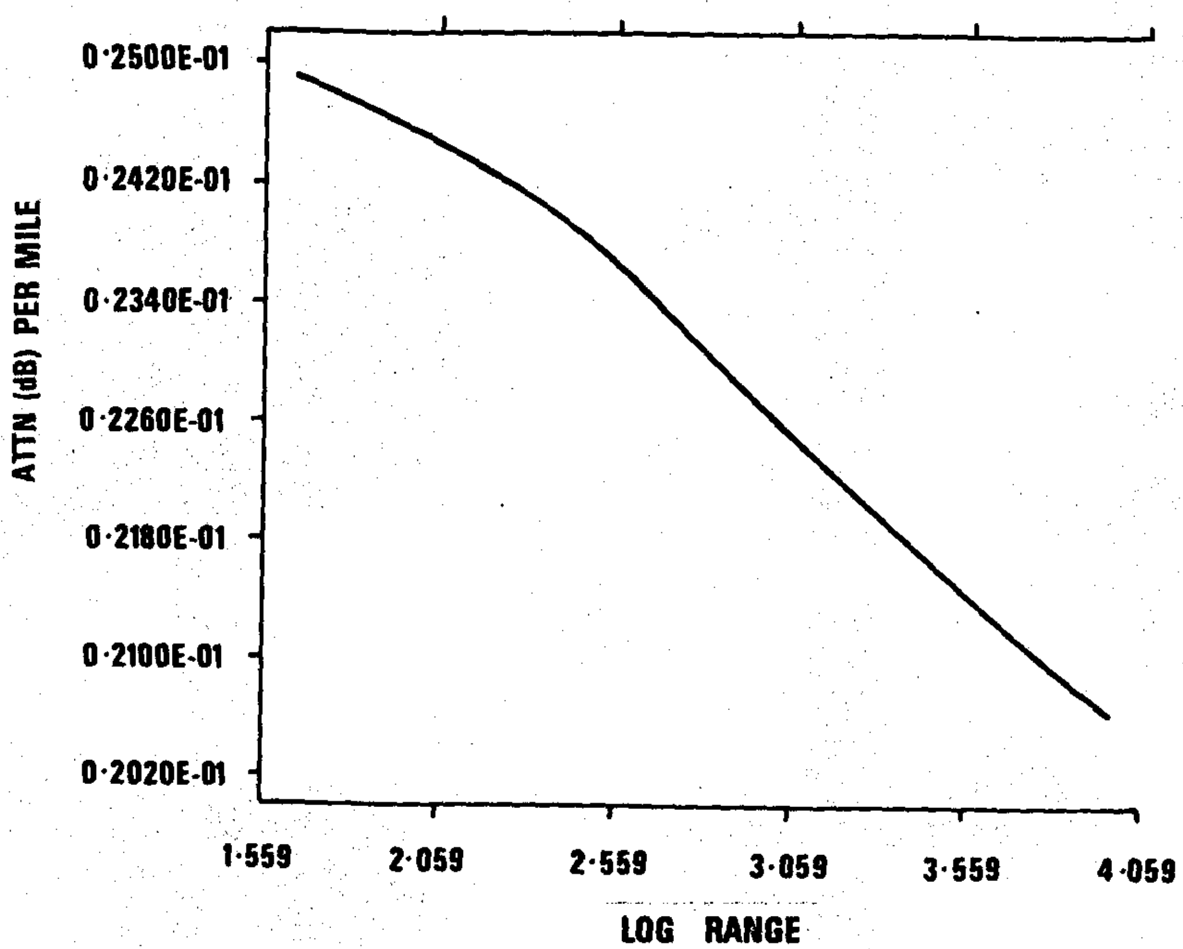

FIG 4a DETERMINATION OF L FOR 0.5° GRAZING ANGLE ($L=0.0283 - 0.001972 \, LOG_e$ RANGE). CORRELATION COEFICIENT 0.96)

(1)

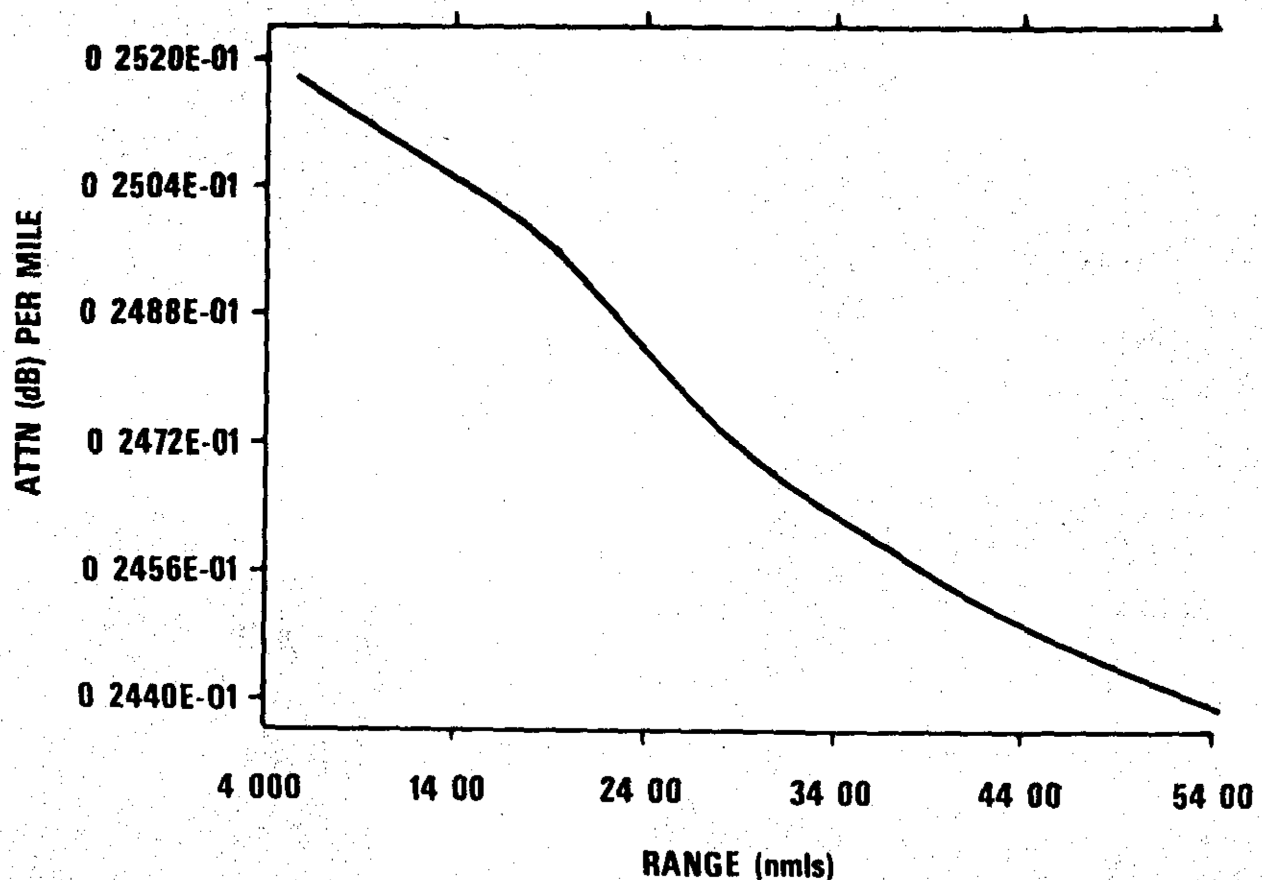

(2)

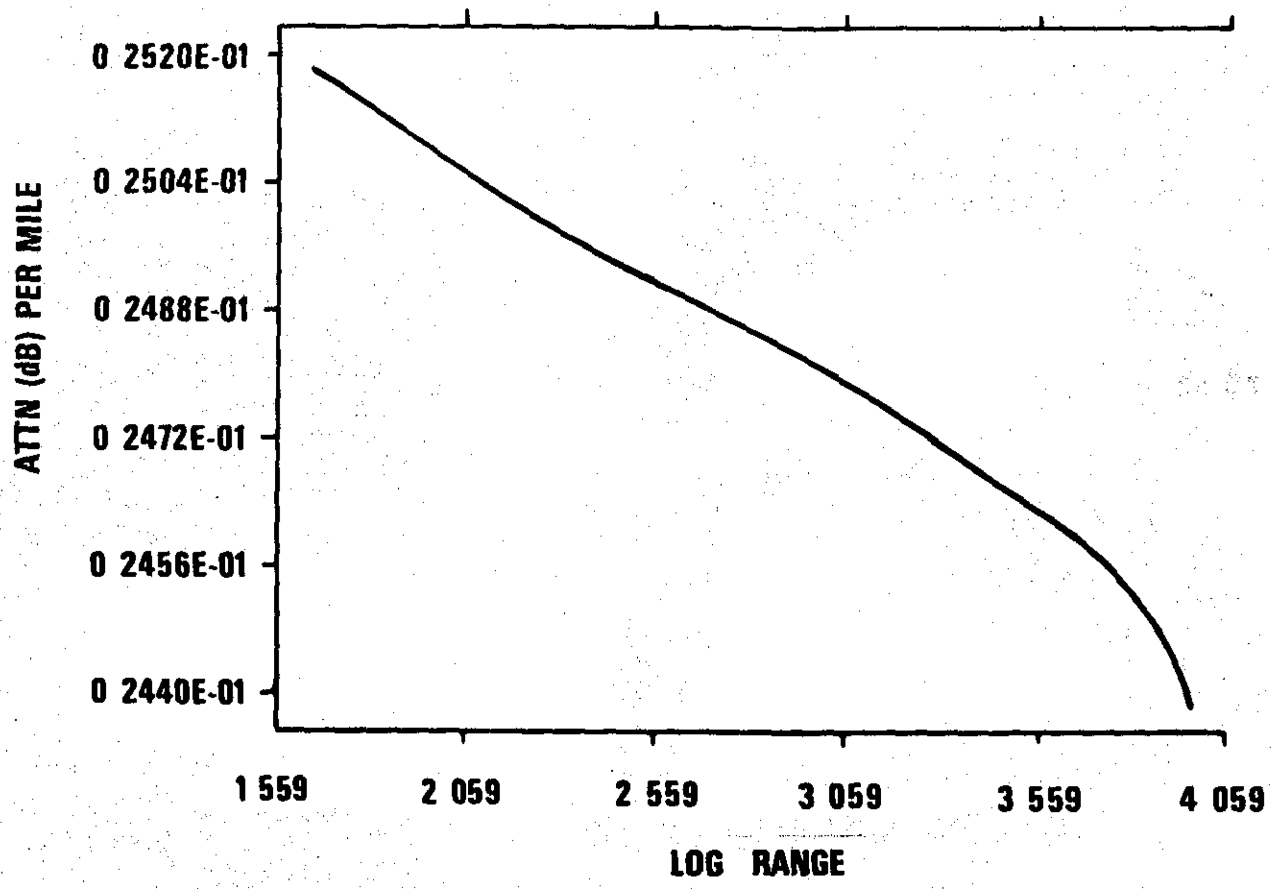

FIG 4b DETERMINATION OF L FOR 0° GRAZING ANGLE ($L = 0.0252 - 0.000018 \ LOG_e$ RANGE). CORRELATION COEFFICIENT 0.98)

FIG.4 COEFFICIENT OF ATTENUATION - GRAZING ANGLE 0.5° AT 10GHz

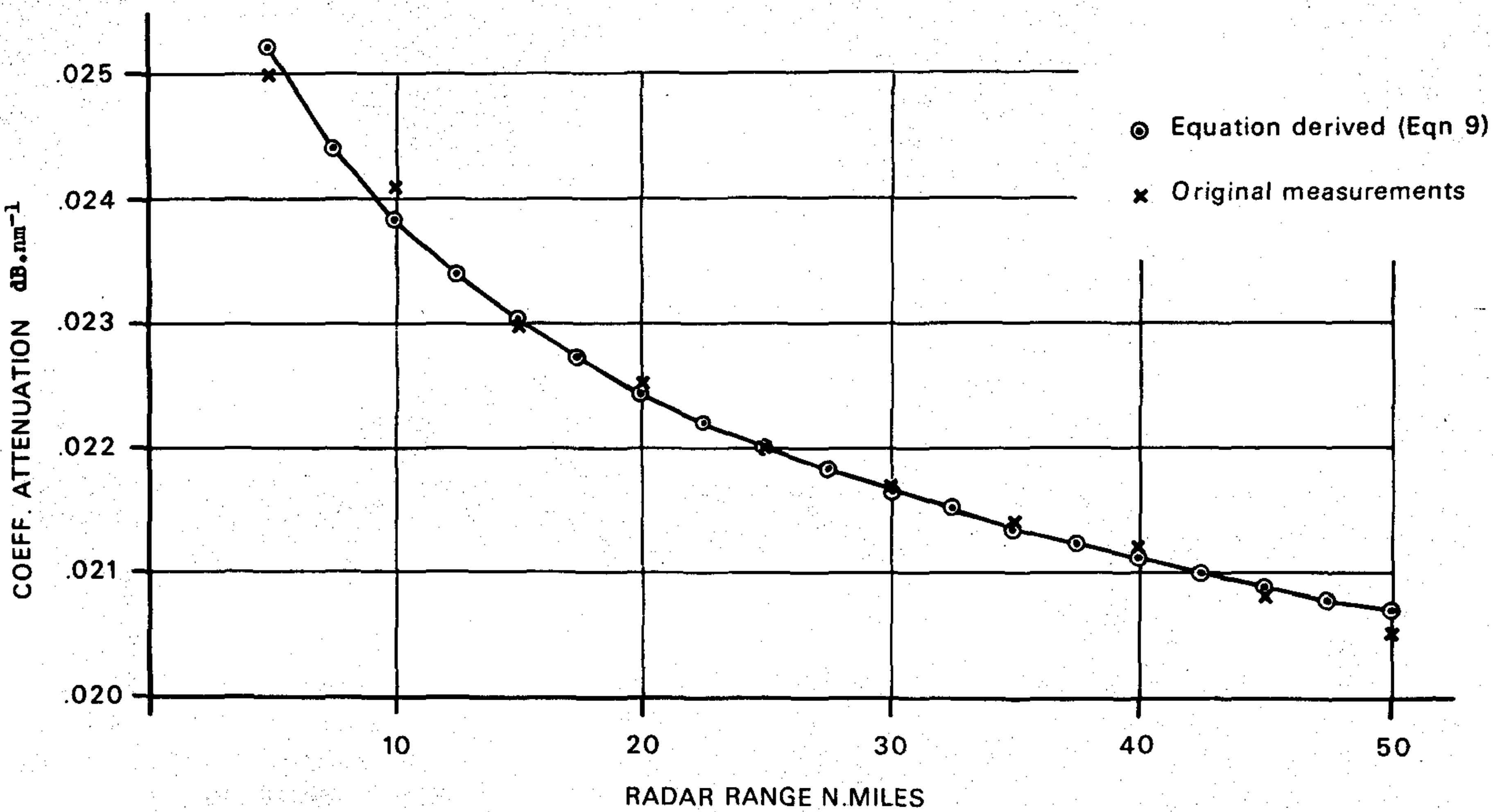

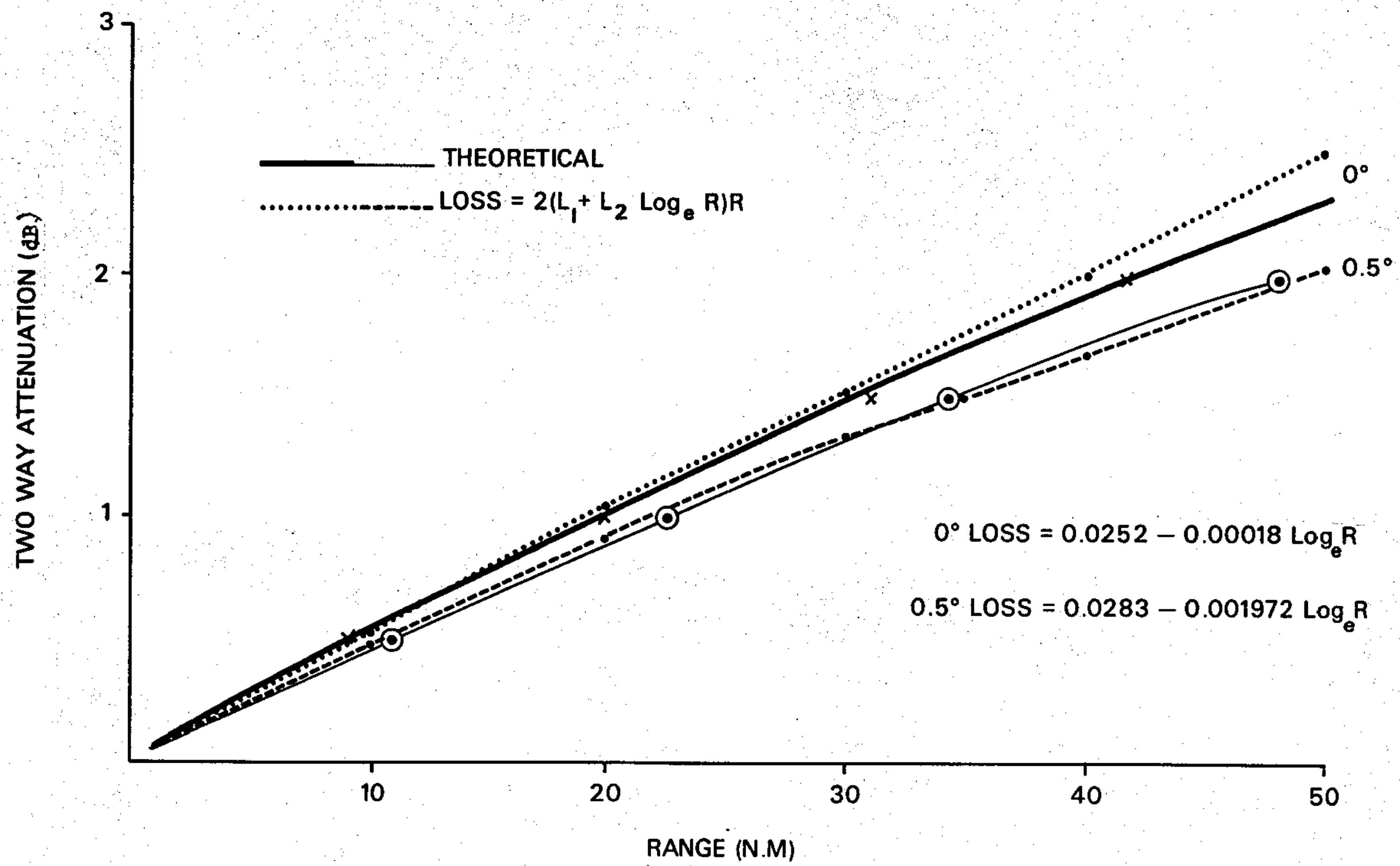

FIG 5 COMPARISON OF THEORETICAL AND ACTUAL VALUES FOR 0° AND 0.5° GRAZING ANGLES

FIG 6 RADAR REFLECTIVITY OF RAIN : σ_v

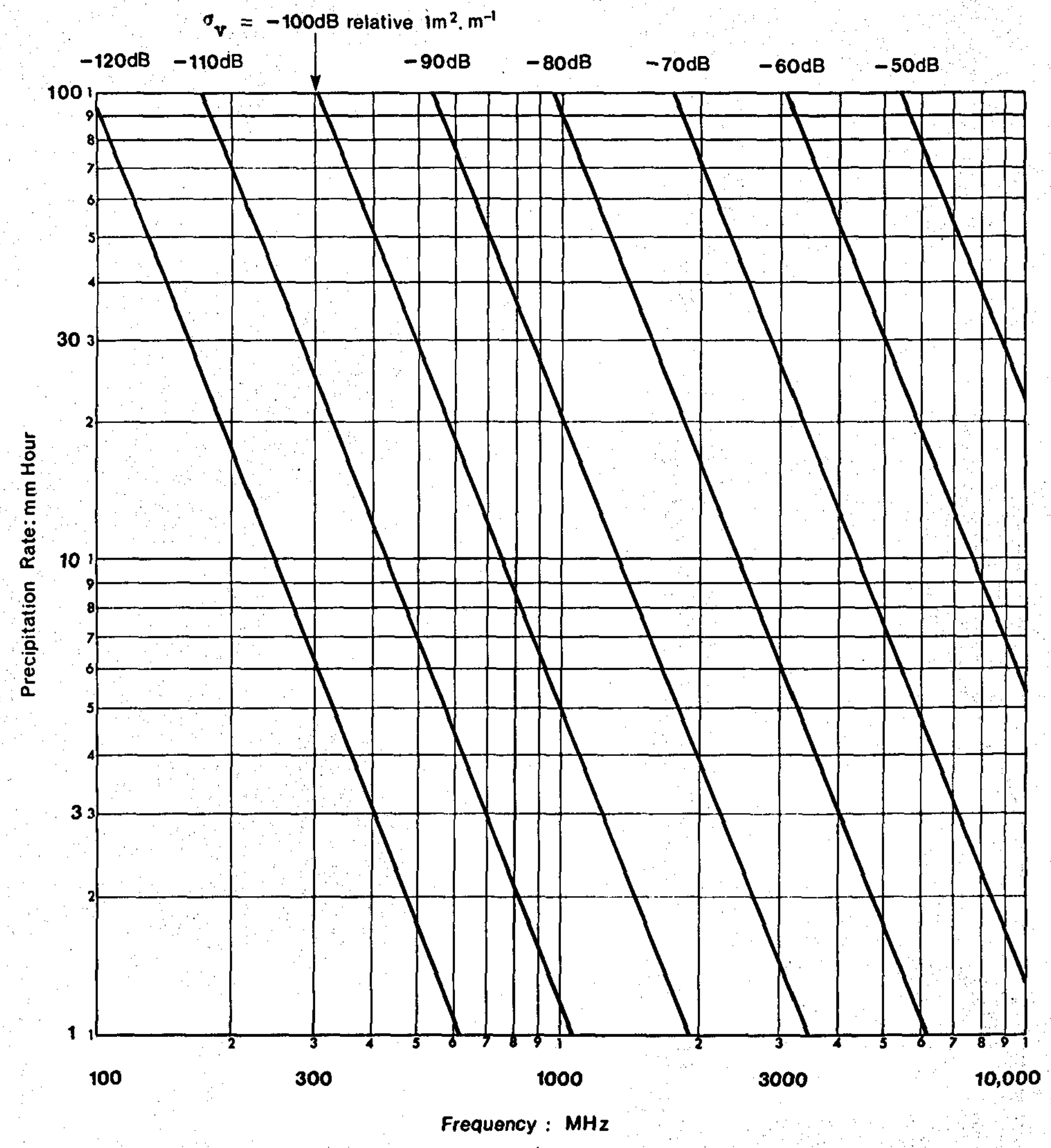

FIG 7 FREQUENCY AND INTENSITY OF RAINFALL IN UK

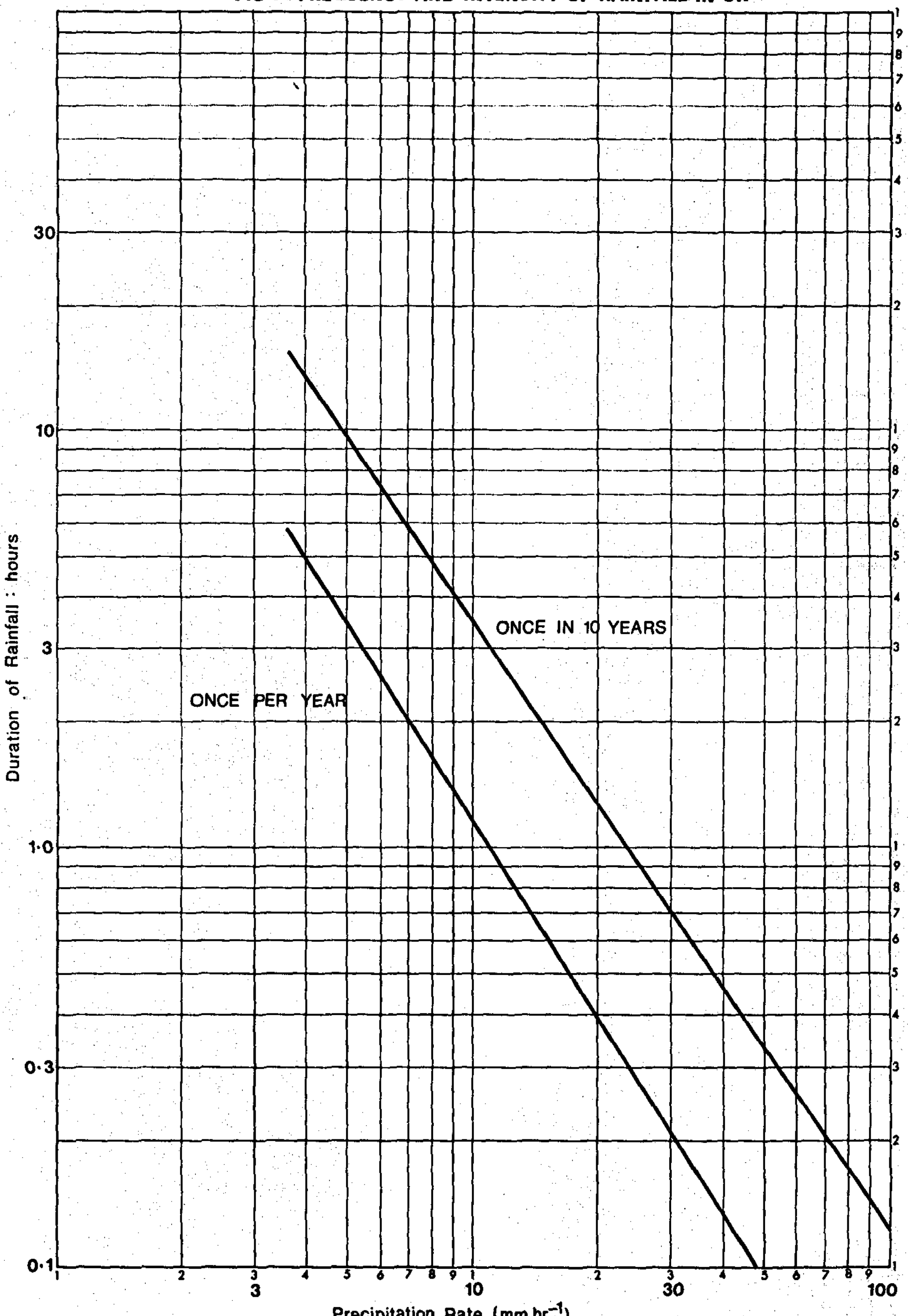

CHAPTER 4

DEPENDENCE OF TERRAIN BACKSCATTER ON RADAR AND SURFACE PARAMETERS

INTRODUCTION

1. Non-uniform scatterers surrounding a radar cannot be easily described by a single coefficient, since the subject of radar energy scatter from terrain is complex. Standard texts often describe surface returns, which produce clutter, in a relatively simple way, but research into terrain response has been the subject of many detailed research reports in past years. It could perhaps be reasonably expected that the multiplicty of measurements taken over some 30 years (although each producing results pertinent to a particular requirement), would nevertheless leave few gaps in the overall knowledge. This is not the case - and so an extensive survey of past surface clutter measurement programmes, and information from other sources has been made and summarised. Many of the clutter measurements made since World War II can be found at {28} {29} {30} {31}.

RESEARCH AIMS

2. In order to assess radar performance with a reasonable degree of confidence, two main aims must be met:

a. A description is required, in mathematical terms, for the expected clutter from any terrain radar resolution cell over which a target is flying, or from which clutter is received (eg sidelobes). The description should account for the clutter dependence of the surface itself, radar grazing angle, resolution cell size, radar frequency, polarisation and spectra; since $\sigma_o = f(\theta, R, \tau, \Psi)$ etc.

b. An assessment of the degrading effect on radar detection, which a specific type of clutter is likely to have on a radar, given the various signal processing options which could be incorporated in the radar, together with its other parameters.

3. Taking 2(a) above, it is suggested that an ideal model should examine the terrain beneath each target resolution cell, by accessing a terrain culture data base for the area overflown. Predetermined reflectivity co-efficients or the reflectivity distribution should be used for the various types of terrain cover, suitably adjusted for the parameters at para 2(a) and further scaled after using local terrain spot heights to calculate slope and aspect angle . With terrain reflectivity as a function of aspect angle it should be possible to finally produce a single value for clutter power to represent the cell under investigation.

4. Initially each contributory clutter factor, in an ideal approach, should be separated from the others, proven experimentally and later made available for recombination with the other detection factors. Separation of the individual dependencies is however extremely difficult in the first place.

5. The observable clutter values have rarely been collected in a useful manner for this purpose; since many researchers have usually collected clutter amplitude, temporal and polarisation characteristics separately but not simultaneously - thus not allowing best correlation to be investigated between the variables. Others have usually ignored terrain slope effects, or radar resolution cell size.

CLUTTER DEPENDENCE

6. Surface clutter characteristics overall can be divided into two categories:

a. Clutter-Processing Dependent. This grouping includes radar signal characteristics, such as amplitude fluctuation statistics, spectrum and frequency agility.

b. Clutter-Backscatter Dependent. Including previously listed parameters, such as grazing angle, RCS terrain type, polarisation, RF and spatial distribution.

7. It is necessary to apportion the probability of detection and false alarm rate (FAR) factors correctly between the two groupings above. A simplified approach is then taken for the purpose of meeting the geometry and target parameters. Detection and FAR probabilities can be obtained from target and clutter fluctuation models - depending upon the effective numbers of statistically independent target clutter samples integrated by a postulated radar signal processing system.

8. Detection probability (high) and FAR (low) thresholds can then be established, based on clutter statistics and the desired FAR. Overall detection probability, above the mean integrated clutter level, can then be computed, based on signal statistics.

STATISTICAL DISTRIBUTIONS

9. Three example statistical distributions {32} are detailed at Annex A:

a. The exponential statistic (Wiebull with exponent parameter = 1) is used when many independent scatterers are within a radar resolution cell.

b. A surface clutter (Ricean) distribution which is used in the case of a single dominant non-fluctuating scatterer (point specular) plus many smaller scatterers in the same resolution cell.

c. The Log-Normal distribution has a longer "tail", is applicable to modelling 'spiky' clutter, and which has also been shown {33}, to give a reasonable description of scattering from randomly orientated shapes which can be represented as plates or cylinders.

DEPENDENCE OF σ_O ON TERRAIN

10. Of the clutter-dependent parameters at para 2(b) above, terrain is the most significant. When observed by pulsed radar at low grazing angles most terrain is non-homogeneous and so a statistical approach is required, since the character of the surface, its slope (see Chapter 10) and consequently the backscatter coefficient, will vary almost from one resolution cell to the next. An overall probability density function (pdf) is required to describe the amplitude distribution. This will provide the probability that a resolution cell selected at random, within the terrain area, will contain clutter with a particular average of clutter power. The model at Chapter 11 will account for those cases where the surface is 'shadowed' using the sightline techniques described at Chapter 2 , and will also indicate if diffraction or refraction could take effect and possibly produce clutter from a cell in 'shadow'.

11. The typical radar resolution cell clutter footprint geometry assumes that any cell will contribute an average clutter value for the particular type of terrain dependent upon grazing angle, slope and the applicable pdf or coefficient of reflectivity.

12. It is seen that the amplitude probability for a single cell does not describe spatial distribution; since each cell is taken independently from within the overall area of radar tracking. Also adjacent cells could be 'shadowed' in hilly terrain, while at other times in a given area there will be extensive regions with the same surface reflectivity

characteristics and slope. Spatial distribution must be necessarily considered whenever a quick (overview) prediction is required for a given area of interest, since backscatter from adjacent cells will often be spatially correlated.

PROBLEMS OF MODELLING THE TERRAIN AMPLITUDE PROBABILITY FUNCTION

13. It has recently {34} been acknowledged that "more comprehensive and carefully controlled backscatter measurement programmes" are necessary at low grazing angles. A preliminary survey in this area by Allan has indicated both disparities and consistencies in an examination of a sample of results from the UK and USA. No attempt is made here to repeat Allan's summaries, but rather to extend his results to include several more sets of measurements which have now become available.

FORMULATION OF STATISTICS

14. It is widely accepted that terrain clutter is the result of 2 basic mechanisms; the individual or specular reflections from strong point reflectors, and a Rayleigh distribution for diffuse clutter. The process can be developed {35} in terms of the statistical properties of the scintillating returns from the elementary point scatterer, with the more complex distribution obtained by superposition of many point scatterers within the radar beam.

15. Type of Terrain. Investigations {36} deduce as a general rule that the type of terrain is identified most markedly in the mean of the Normalised Radar Cross Section (NRCS) and in general clutter is neither Gaussian nor Log-normal. This has been demonstrated by means of a KOLMOGOROV-SMIRNOV test of the cumulative distribution of the NRCS {37}. The return from a point scatterer within the resolution cell will be of the complex form:

$$Y(t) = \frac{A(t)}{R(t)} e^{i\emptyset(t)} e^{-i\omega_o(t)} \qquad \text{------------------(1)}$$

for $0 \leq t \leq T$

$\emptyset = 2\beta R(t)$ is the phase, where $\beta = 2\pi/\lambda$ (propagation factor)

t is the observation time (dependent on aerial beamwidth)

A(t) contains both the amplitude component of the 2-way aerial radiation pattern and the intrinsic amplitude of the scatterer. $R(t) = \sqrt{(R_o^2 + V^2t^2)}$ is the range to the scatterers at the extremities of the beam and R_o is the range along the beam centreline. As the aircraft moves at velocity V this sets the observation time for a given range and beamwidth; for example, if mean R_o = 5 km, V = 300 $m.s^{-1}$ and beamwidth 0.4^o, then t = 0.058 sec. Generally $Vt << R_o$, giving an approximation of the return signal ("scintillating" linear FM signal due to aircraft velocity causing radar resolution cell motion across the point scatterer):

$$Y(t) = \frac{A(t)}{R_o} e^{i(\emptyset_o + Kt^2)} e^{-i\omega_o t} \qquad \text{------------------ (2)}$$

$\emptyset_o = 2\beta R_o$

$K = \beta V^2/R_o$, the scintillation rate

Assuming t>0, then representing terrain clutter as a superposition of many individual scintillating targets:

$$Y(t) = e^{-i\omega_o t} \sum_{k=1}^{n} a_k e^{i\emptyset_k + iK(t - t_k)^2} \qquad \text{---------------(3)}$$

for $0 < t < T$

16. Several assumptions are made above, since in practice, even with the observation time T, with a moving radar aerial the amplitudes and phases and the number of scatterers will be varying. All amplitude effects at (3) are lumped into a_k. Figure 1 shows the general concept of evenly distributed scatterers within a resolution cell.

17. It is normal when following the 'point scatterer' approach to consider fluctuations from a single scatterer, using equation (1) where fluctuations about zero frequency for a linear frequency modulated signal are based upon:

$$Y(t) = A\cos(Kt^2 + \phi) \qquad (4)$$

$$0 \leqslant t \leqslant T$$

It is shown {37} that as $KT^2 \rightarrow \infty$ the spectrum of the scintillating signal tends to a constant, and this is assumed during the observation time. The characteristic function of equation (4) is obtained from:

$$F(\varepsilon) = \int_0^{2X_o} e^{i\varepsilon A\cos\left[(X^2/K) + \phi\right]} p(X)dx \qquad (5)$$

Where $X = Kt$

$$p(X) = \frac{1}{2X_o} = \frac{1}{2KT}$$

18. By manipulation, reversing the order of integration, summation and by changes in variables and, since by definition the pdf is the Fourier transform of the characteristic function then:

$$p(Y) = \begin{cases} \pi^{-1} (A^2 - Y^2)^{-\frac{1}{2}} \sum_{m=o}^{\infty} - ^{(m)} b_m \, Cos(mSin^{-1} \frac{Y}{A} + \frac{m\pi}{2}) & Y<A \\ 0 & Y>A \end{cases} \quad \text{--- (6)}$$

19. From (6) the mean value of the scintillating signal and the convergence of the distribution function are shown at {38 } in some detail. Finally, since in practical terms terrain clutter is the result of many point scatterers within the aerial beam, the mean, variance and other useful descriptive parameters can be obtained so that the statistics of the distribution envelope are evolved. Cumulative distributions at { 39} over city areas clearly show the specular nature of clutter from this type of target, however, one of the difficult areas in this report is the correlation of statistics found by one researcher at a specific location, with those of others at different locations. Much of the early work on the point scatterer formulation of the statistics of terrain clutter was by { 40}, but more recent and extensive work using this technique {41 } invariably recommends the necessity for many more measurements. In general {42 } concluded that the Gaussian distribution applied over homogeneous surfaces such as desert and farmland and lognormal (long tail) distributions would be likely over urban and moutainous areas. Many researchers used smooth surfaces to develop reflectivity models { 43}, however { 44} states that the accompanying theories do not apply directly to the earths vegetation.

SIMULATION OF CLUTTER

20. An alternative approach for the assessment of radar performance in clutter is the use of clutter simulation. However, the simple simulation of clutter as noise alone ignores the need for time, spatial correlation, or of frequency effects. Time correlation could perhaps be introduced in an appropriate way by numerical filtering of the random numbers used to simulate the noise, but frequency and spectral effects are complex. Andre et al {45 } recommends an 'open loop' approach to clutter simulations for basic performance prediction, with a 'closed loop' method preferred for detailed analysis. In the open loop case the sum of the signals from clutter and target signals (from clutter and target signal generators) are fed to the simulated radar receiver. The essential difference for the closed loop solution involves the simulation of a radar transmitter signal which is then processed to obtain signals for target and radar clutter which are mutually coupled to allow signal modification. Finally target and clutter signals are merged for processing by the simulated radar receiver.

21. Considerable effort has also been expended, { 46}, in modelling clutter maps for other purposes, such as flight simulation, where the simulated airborne radar is 'looking down' for targets flying over a clutter-producing surface. In the main such simulations aim to evaluate system reaction to the clutter. Lognormal distributions are often used, and since moving radar platforms are being simulated,

a measure of the rapidity of clutter variation is ideally incorporated. These simulations do not investigate the clutter itself and merely reproduce approximate (but nevertheless representative) visual effects for training purposes. The reader is directed to the reference for further general reading, but the technique cannot realistically contribute to this study.

BACKSCATTER FROM VARIOUS TERRAIN TYPES

22. Although most terrain is composite in character, giving an observed wide dynamic range of land clutter distributions for the differing combinations of woods, fields, rocks, man-made objects and shadowed regions; the following paragraphs briefly consider individual terrain-type reflectivity characteristics, prior to investigations of the dependence of clutter upon the radar parameters τ, RF, polarisation and ψ. Normalised RCS per unit surface area is used throughout:

$$\sigma_o = 10 \, \mathrm{Log}_{10} \, \frac{\text{Effective RCS Area}}{\text{Effective Illuminated Surface Area}} \, (m^2 . \, m^{-2}) \quad -(7)$$

23. Several hundred sets of conditions would be necessary to specify all backscatter, with 8 or 10 different terrain type classifications. Some researchers { 47} have included an extra parameter to account for the practical inconsistencies of σ_o. For example, the large number of small scatterers which under normal circumstances would be labelled 'Rayleigh' in character are found in practice to occur on less than 50% of ocassions { 48}. For the low grazing angles required in this report land backscatter amplitude distributions are often contaminated by shadowing due to trees, hills etc. Taking the extra

problems of backscatter coefficient variations with surface moisture content, and the past measurements taken with fixed and moving radar platforms (ie spatial average v time average), it is seen that uncertainty can easily occur when attempting to survey findings and arrive at a reasonable model.

24. Trees/Forests. Electromagnetic radiation at 10 GHz or above does not significantly penetrate dense areas {49 }. Diffuse returns therefore come predominantly from the upper part of the tree canopy. Raising the aerial above trees and using pencil beam radar reduces clutter only for high flying aircraft { 50}, but gives limited signal to clutter improvement for ultra-low flying aircraft. Aircraft which would otherwise suffer blocked optical sightline may therefore be observed subject to clutter limitations.

25. Researchers in the past {51 } p 221, have investigated backscatter from differing types of tree, ie pine, deciduous, under different moisture conditions and seasons of the year. The average RCS per unit area for trees seems to be about −20dB, with horizontal polarisation exceeding vertical by 1 or 2 dB. Evergreen (pine trees) tend towards a slightly lower RCS per unit area than deciduous (3 dB), using λ=10 GHz {53 }. Clearly those trees which retain their foliage will not vary appreciably in reflectivity with the seasons. From reported data { 54} a survey of amplitude returns from trees, using horizontal polarisation, with log-normal fit is given at equation (8). Contrary to {52} above vertically polarised values were 3 to 4 dB higher.

$$\sigma_o = -15 + 15 \, Log_{10} \frac{\psi}{25} - 8 \, Log_{10} \frac{\lambda}{0.32} \, dB \quad m^2.m^{-2} \quad \text{-------}(8)$$

No other parameters were included, however it is thought that (8) was derived for $\psi < 25^o$, $\leqslant$ 95 GHz. The dependence upon ψ and λ is considered further at paras 47 and 68.

26. Effects of Precipitation. Moisture probably contributes 5 dB extra reflectivity compared with dry trees { 55}; snow and ice cover are separately examined at para 29 below.

27. Urban and City. Significant shadowing can be expected from buildings when operating at low grazing angles, but results must be analysed carefully. For example, Linnells results { 56 } were obtained under conditions where perhaps reduced shadowing is probably because of his radar location on a high tower (30 m). Median back-scatter from urban and city areas at λ = 3 cm are likely to fall between -24-30 dB (below 1 $m^2.m^{-2}$), for very low grazing angles. Katz { 57 }, and others { 58 }, { 59 }, have also produced results for buildings. In general, { 60 } concluded that the log-normal distribution is the best fit for reflectivity from buildings.

28. Flat Farmland and Cultivated Land. Linnell { 61 } also obtained results for farmland; these ranged from -33 dB in March to -21 dB in August, for a spread of values for ψ, discussed below. As expected a maximum σ_o occurred when the area contained fully grown crops. Also confirmed were other previously assumed conditions, such as that of ploughed ground giving a greater value before a rainstorm, since the surface is rougher in texture compared with values after the rain; the dielectric constant of soil being moisture dependent. The reader

is referred to {62 } for detailed information on the variation in average height and reflectivity of farm crops for given ground height above sea level in Germany. Land utilisation for certain crops is predominant in given geographical areas and in N Germany culture data is held to a grid spacing of 150 m (N/S) x 95 m (E/W) in the German Military Geophysical Office Databank.

29. <u>Snow and Ice</u>. In some respects limited data is available concerning clutter directly from ice or snow, especially in those measurements which allow a comparison of the clutter plot from the same terrain both with and without snow cover. Some values obtained with an aerial height of 2 m, RF's at 10, 35 and 94 GHz were made between 0.4 to 1^{o} grazing angle {63 }, but with limitations in range and with the snow overlaying fresh-water ice rather than over trees or soil. Krason and Randig { 64} made reflectivity coefficient measurements at 3 and 10 GHz for Ψ = 0.5 to 4 degrees using common terrain, and with leaves both on and off the trees. AT 9.405 GHz values were consistently shifted by +3 dB due to snow cover.

30. Results obtained using short pulse durations of 0.125, 0.17 and 0.10 μ secs (Hoekstra and Spanogle), together with aerial beamwidths of 1.3, 1.9 and 0.38 degrees, are of particular interest here, since they are appropriate to high performance tracking radars. Unfortunately the 500 to 600 m range is not representative and the results could only be used if they extrapolate satisfactorily to longer ranges. Further at short ranges it is thought possible that the clutter returns may come from beneath the dry snow cover, which varied in depth from 0 to 30 cm. Small amounts of free water in snow can significantly

affect the measured value, which changed due to this effect by about +10 dB in the case of Hoekstra.

31. Temporal Changes. More recently dramatic differences have been observed over short time periods. These may be as much as 10 dB in 30 minutes {65} {66}, and specifically occur when free water freezes, usually - though not exclusively, at night. Transition time is unequal between the two extremes as freezing generally takes longer than thawing. Hayes {67} observes that at least 0.15 m depth of snow is necessary to ensure no reflections from the underlying terrain, and that "calibrated data are insufficient to permit comparison with theoretical calculations".

32. Polarisation in Snow. Polarisation effects under normal conditions are again considered at para 64 below, however it is well established that horizontal aerial polarisation in snow gives approximately 10 dB more than vertical when the snow is dry, but this difference reduces when the snow is wet.

33. Reflectivity Models for Snow. The above comments are included here to show the uncertainty associated with selecting a suitable model, since it is proposed that the underlying snow which receives a proportion of energy (variable with RF), may refract the energy towards the normal; thus allowing backscatter to occur at a higher grazing angle Ψ. In practical terms there will be difficulty,

for example, in predicting the freeze-thaw cycles and possibly sporadic rain on variable-depth snow. It seems probable that a very general statistical clutter value for snow is the best to be hoped for. Other effects noted include evidence of returns from "blown snow" from hill tops {68} getting into sidelobes, and snow in forward scatter (at 35, 95 and 140 GHz) measurements producing as much as 25 dB variation in multipath signals, leading to serious angle tracking errors against horizon targets.

34. Tomlinson {69} obtained backscatter information for space-based radars for seven terrain types, and by regression analysis as a function of RF and ψ obtained analytical models, for snow and other surfaces:

$$\sigma_o = A + B\psi + (C + D\psi) \log f \text{ ------------------------------ } (9)$$

Much larger resolution cells were used than is the case for low level tracking radars, and the applicability of the model calls for caution. However it is seen later that the values produced by this model equate reasonably well with those from other sources. The choice of an absolute value of σ_o to be used for a particular assessment is much more of a problem than the gradient, for example, as the value of ψ changes. Equation (9) above for snow computes with A, B, C and D as -32.97, 0.340, - 1.797 and 0.035 respectively. An 'adjustment factor' of + 2.9dB is applicable.

DEPENDENCE OF σ_o ON τ

35. Results {70} as far back as 1969 indicated that clutter levels, as expected, must be a function of the area of the illuminated clutter patch and therefore dependent on τ and beamwidth. Measurements made at that time with long and short pulses transmitted alternately from the same radar gave differences in clutter levels of about 18 dB.

36. It seems that the effect of τ on clutter lies somewhere between two extremes. On the one hand with a very large number of scatterers, the power returned is proportional to pulse length. But with a very small number of scatterers the probability of <u>any</u> power level being returned is proportional to pulse length. A note on each of these conditions follows, before the results of various research papers and reports are discussed and a suitable model selected.

37. <u>Many Scatterers</u>. As an aerial is moved the short term clutter returns are assumed to be Rayleigh distributed with a mean value which varies slowly to give a lognormal distribution with sd about 20 dB, (ie lognormal running mean with superimposed Rayleigh for the difference between the clutter signal and the running mean). The scatterers are often located in patches so with τ reduced there is some probability that no scatterers are in the reduced resolution cell. It is assumed each large cell (if unshadowed) does contain some clutter.

38. On the average the scatterers in those cells containing them are more densely packed in the smaller cells (to give the same clutter levels). A situation can arise for very small values of τ, where some cells return no power while others may return (since clutter is spatially distributed in patches),

proportionately more. For example if τ is reduced arbitrarily by a factor of 10 and (say) half the new cells contain clutter then:

$$\log p = 0.3 \log \frac{\tau_1}{\tau_2} \qquad (10)$$

p is the probability of the smaller (new) cell containing clutter. τ_1, τ_2 are the short and long values of τ respectively.

$$P = 7 \log \frac{\tau_1}{\tau_2} \text{ dB} \qquad (11)$$

P is the power level returned by the small cell relative to the large cell.

39. Dodsworth {71} proposed a deduction of the effect of a change of pulse length on the probability distribution of clutter. Using a numerical example where $p = 0.5$ and $\frac{\tau_1}{\tau_2} = 0.1$, giving $P = -7$ dB; for the small cell to have an RCS of 0dB (ref $1m^2$), the large cell must have a echoing area of +7 dB, and the probability that this is exceeded is 37%. But $p = 0.5$, hence the probability of the small cell exceeding 0dB is 18.5%. The results are plotted at Figure 2 for 5 ratios of τ_1, τ_2. In modelling clutter {71} chose a lognormal distribution for uniformly reflecting points expressed as a departure from the running mean of the clutter signal, ie the short term clutter component. Using an appropriate number of integrations and by adjustment to the pulse length τ, the sd of the clutter signal increases as pulse length is reduced.

40. If it is assumed that the many clutter points from a large cell are more or less uniform and varying from cell to cell in a lognormal manner, this can be plotted with an arbitrary sd of 25 dB and replotted after τ is reduced by a factor of 10, reducing all echoing areas by 10 dB as shown at figure 3 . If only one echoing point exists within each large resolution cell and the same distribution applies as in the first curve above; and τ is now reduced by a factor of 10, a third curve results with a difference from the first of about 40 dB at the 5% level and 25 dB at the 1% level. This gives the approximate result in para 39 above.

41. Relationship of τ With Wiebull Shape Parameter. **In practice, for a given cell,** ground clutter is not uniform, leading to a non-proportionate change in clutter when a resolution cell is shortened due to shadowing and other effects. Whereas a radar designer may wish to select a set of radar parameters and then find a suitable distribution - typical of the parameters, or alternatively to estimate the distribution change likely when τ alters; performance prediction of existing radar can only be based on the known parameters of the radar. {71}, using the pulse - length - beamwidth product has made empirical estimates of the effect of changing the resolution cell by factor N, on surface clutter distribution. It is established for a range of $\tau \times \theta_A$ of 2.5×10^{-9} to 2.5×10^{-7} radian seconds that a relationship exists between the size τ and the Weibull shape parameter,

42. In practical terms here, with an assumed pulse length $\tau = 0.5\ \mu$ sec and $\theta_A = 2^\circ$, giving $0.0349 \times 0.5 \times 10^{-6}$ radian seconds $= 1.7 \times 10^{-8}$. Given the Wiebull shape parameter relationship:

$$c = 0.192 - 0.0764 \text{ Log } (\theta_A \tau) \qquad \text{------------------- } (12)$$

From which scale parameter b can be obtained. An empirical method of estimating the clutter distribution for other resolution cell sizes is possible. (See also Annex A).

43. The existence of the Weibull distribution as being applicable to land clutter returns was probably first reported by Boothe {72} in 1969. But again, like so many others since he took Linell's results - presumably because they were almost the only ones available at that time which offered a spread of values. It will be shown at para 51 that certain characteristics of Linell's results differ significantly from the majority taken elsewhere - although it must be recognised that this may in part be due to different terrain in Sweden. Also there is a general absence of available measurements from Continental Europe.

44. Boothe's Weibull values, based on Linell's results have been compared by the author here with 11 other sources, now available. Data is listed at Table 1, and correlation computations made between

TABLE 1 DATA FOR WEIBULL INVESTIGATION

		τ (μs)	θ_A (m.rad)	σ_m (dB)	(eqn 12) c (CALC)	b (meas)	
1	RILEY 5 GHz {76}	3.0 1.5 0.9 0.3	33.1 33.1 33.1 33.1	- 43 - 46 - 51 - 51	0.343 0.366 0.382 0.419	2.7 3.6 4.2 4.3	
2	RIGDEN 5.75GHz	0.015	33.1	- 47	0.518	3.0	
3	DODSWORTH {77} 5 GHz	3.5 0.5	8.7 8.7	- 80 (Est) - 80 (Est)	0.382 0.446	7.7 9.0	Estimated σ_m
4	WARDEN et al {78} 5 GHz	5.0 0.5 5.0 0.5	8.7 8.7 8.7 8.7	- 70 (Est) - 70 (Est) - 70 (Est) - 70 (Est)	0.370 0.446 0.370 0.446	6.6 9.5 6.8 5.9	Estimated σ_m
5	DE LOOR et al {79} 10 GHz	0.5	31.4	- 28 - 16 - 14	0.404 0.404 0.404	9.5 7.0 9.5	APR JUL SEP
6	SURADS {80} 10 GHz	0.25	27.9	- 34	0.431	5.7	
7	WARDEN {81} 5 GHz	0.4 12.0 5.0	26.17 8.7 26.17	- 27 - 70 (Est) - 70 (Est)	0.417 0.348 0.333	2.16 - 3.05	Estimated σ_m
8	ERICSON {83}	1.0	57.5	- 25 - 30	0.361 0.361	(not avail)	$\psi = 5^\circ$ $\psi = 0.5^\circ$
9	APL {85} 5 GHz	0.34	34.9	- 40	0.413	3.4	
10	NATHANSON {84} 3 GHz	2.0	26.1	- 46.25	0.364	3.9	
11	APL {85} 8.8 GHz	0.25	20.0	- 52	0.442	3.8	
12	LINELL a {88} 10 GHz b c d	0.17	24.4	- 48 - 46 - 36.4 - 42	0.524 0.524 0.524 0.524	3.3 2.84 3.76 3.95	ψ = 1.25 APR ψ = 1.25 MAY ψ = 0.7 NOV ψ = 0.7 MAR/AUG

NOTE

Selected Data - Serials 1 to 7 rural/farmland

Serials 8-11 (incl) Rural
Serial 12a, 12b rural
Serial 12c, 12d forest
c (calc uses Eqn (12)

θ_A, τ. product and shape parameter c, and between θ_A τ product and σ_m. Few values are still available at λ = 3cm. Detailed results are at Annex A, App 1.

45. Sea Clutter. Observations made in Japan in 1980 {73} relating sea clutter to Weibull, but at λ = 30 cm, were made down to very low values of ψ (0.13 to 0.25^{o}). Sekine et al concluded that a Log Weibull relationship exists, and are currently checking this at λ = 3 cm. Other relevant papers are by Shelerher {74} at about 24 GHz and RSRE {75} at 3 cm - all for sea clutter.

46. In view of the above conclusion in favour of Weibull - which for temporal and small scale fluctuations has implications for CFAR arrangements - it was considered useful here to check some of the measurements taken by Dodsworth and others to see if they also exhibited Weibull for land backscatter. Results of the author's investigations into this are also at Annex A, App 1. False alarm rates are considered later in this chapter at para 85.

DEPENDENCE ON ψ

47. It has been clearly demonstrated {86} that σ_o increases rapidly as near grazing angles are reached, and as expected, σ_o will also be higher at low grazing angles for rougher surfaces. σ_m, the median RCS, is used here for a brief investigation into the dependence of σ on the grazing angle. Many reports use average RCS or γ (see Annex B and para 49 below), caution should be exercised if comparisons are made.

48. While the quantity of measurements is now increasing, principly from space-based observation platforms {87}, these are mostly taken at high grazing angles - usually down to about $\psi = 20^{o}$. It is often difficult and imprecise to extrapolate the low angle significance of these measurements.

49. It is assumed that all targets of interest are in the near grazing zone - in which the use of the conversion $\gamma = \sin \psi/\sigma_o$ is of little use. As ψ reduces, an appreciable rate of change in reflectivity seems to be initiated at values $10^{o} < \psi < 15^{o}$ and unfortunately this corresponds to the lowest value of ψ chosen by the majority of researchers in the past. Extrapolation difficulties can be seen from the general curve at Figure 4. This of course has limited the usable results from which to evolve a model.

50. In Chapter 1, mention was made of the 'slope' or 'aspect angle' of terrain and the scant attention which appears to have been paid to this effect when measurements were taken. Clearly a change in terrain slope implies a change in ψ <u>for the particular resolution cell under investigation</u>. This chapter confines investigations to selecting a model from those measurements already available. It is assumed that the values of ψ are correct and the statistical spread of terrain slope within all the resolution cells scanned did not affect the measured RCS. The author's investigations into slope effects are considered separately at Chapter 10, & Annex F. Appl.

51. Trend of σ_m with ψ. The well documented and widely quoted measurements of Linell {88}, together with as many others available with like (or near like) parameters were plotted by extracting σ_m for variation of ψ. In all cases the results used were for rural, farmland, cultivated terrain and forest/woods. Many results were rejected. A few were interpolated, with care, into the lower values of ψ (eg $15^\circ < \psi < 70^\circ$). The resulting plot at Figure 5 suggests the following conclusions for cultivated terrain:

a. A remarkable number of the curves give similar gradients which average approximately 1.25 dB per degree for $\psi > 3^\circ$. Linell's results give a significantly different gradient.

b. There is a wide spread of absolute values of σ_o. However, it seems reasonable to expect this spread of values, taken in different countries, under variable conditions of moisture, wind, measurement accuracy, calibration differences and instrumentation (monitor losses).

c. The point at which the rate of change of reflectivity becomes more marked is around $\psi = 2^\circ$. Below 2° the slope could be reasonably be approximated by a second straight line with a gradient of approximately 5 dB per degree.

d. Linell's results (figure 5, curve 12) appear to come from a system which is far more sensitive to changes in ψ than the others. It is not clear why this is so, but is may be a direct consequence of the 33 metre aerial height - and that a less shadowed area might provide a greater dynamic range of clutter levels.

52. A further point to consider is that of aerial gain towards a particular clutter patch. Some researchers mention this as part of their calibration process. Others, indeed few have not apparently corrected for this, or for "electrical tilt angle", sidelobe clutter, or variation of gain with range.

53. Forests and Woods. Figure 6, a similar plot for forest and wooded areas, is less explicit. A maximum of 0.5 dB per degree is taken as a reasonable value to use.

SURVEY OF MODELS

54. Incorporation of ψ into a set of model equations together with other parameters has been attempted by several researchers, but again these are often for higher grazing angles such as expected from space and using excessively large dimensions of resolution cell. Models investigated for similarity of results (in regression form) include:

a. $\sigma_o = -20 + 10 \log {}^{\psi}/25 - 15 \log \lambda \ \text{dB}\ m^2.m^{-2}$ --------(13)

where ψ is in degrees, λ in cm.

b. $\sigma_o = -15 + 15 \log {}^{\psi}/25 - 8 \log \frac{\lambda}{0.32} \ \text{dB}\ m^2.m^{-2}$----------(14)

where ψ is in degrees, λ is in metres.

c. $\sigma_o = A + B\theta + Cf \ \text{dB}\ m^2.m^{-2}$ -----------------------------(15)

where $\theta = 90 - \psi$ (deg) f is in GHz.

d. $\sigma_o = -42.36 + 0.52\,\psi + (24.93 - 0.3584)\ \text{Log}\, f\ \text{dB}\ m^2.m^{-2}$--(16)

e. $\sigma_o = A(\psi + C)^B \exp\left[-D/(1 + 0.035_h)\right]$ dB $m^2.m^{-2}$ ------------(17)

where ψ is grazing angle in radians σ_h is RMS surface roughness (cm)

f. $\sigma_o = F_s{}^4\ 2 \times 10^{-6} f \sin\psi$ dB$m^2.m^{-2}$ ------------------------(18)

where F_s = spherical earth shadow factor

f = freq (MHz)

$F_s = 2\ (\pi\ X)^{1.5} \sum_{n=1}^{k} \exp\ (-j A_n X)\ f_n\ (h)$ dB $m^2.m^{-2}$------------(19)

$F_s = 1 - 0.465X$

for x>1
x<1

$X = R(2\pi/\lambda^2 r_e^2)^{1/3}$

Where R = Range (metres)

r_e = 4/3 earth radius

A_n = set of complex constants

n = mode 1, 2 ----- K

K = maximum of 40

$f_n(h)$ = height gain function.

g. $\sigma_o = \sigma_o^1/(1 + R/Rh)^k)$ dB $m^2.m^{-2}$---------------------------- (20)

R = Range to clutter (km)

R_h = Clutter horizon (km)

k = Constant (Value 4-12)

σ_o^1 (typical value as a constant 34dB $m^2.m^{-2}$)

h. $\sigma_o = -C1 + C2 \log (\psi/\psi_o) \; C_3 \; \mathrm{Log} \; (\lambda/\lambda_o) \quad \mathrm{dB\;m^2.m^{-2}}$ --------- (21)

Typical values are:

C1	11.3		$\psi_o = 35^\circ$
C2	26		
C3	8		$\psi_o = 1\mathrm{m}$

j. $\sigma_o = \gamma_t \; f^m \; \mathrm{Sin}^n \; \psi \; \mathrm{dBm^2.m^{-2}}$ ------------------------- (22)

Eqns 21, 22. C_1, C_2, C_3, ψ_o and γ_t are terrain sensitive

Typical values are:

γ_t	2.1
m	$\gtrless$ 0
n	1.8
c	0.008

(see comment on Barton's 'Unified model' at Annex F. App 1. page F1-41)
{234}

55. Equation (13) above is an empirical formula based on statistical information. 10dB extra should be added for foliated trees (dry) and 15 dB for wet trees. {90}. Fig 5 curve 11.

56. Equation (14) above {91} is taken as reasonable for Horizontal polarisation and more accurate at higher RFs than 10GHz. Fig 6 curve 2.

57. Equation (15) is applicable over the range of frequencies 6-17 GHz but to be used with caution at angles of $\psi < 20^{\circ}$ {92}. Moore et al also include a general model with different coefficients. Referring to Figure 5, curve (6), the coefficients used for A, B and C were respectively -7.09, -0.131 and 0.315. While for Figure 6, curve (7) the results of Moore fit over Tomlinsons with negligible difference. Hence curves (3) and (7) are identical; with values of -9.1, -0.12, and 0.25 respectively.

58. Equation (16) contains the coefficients for forest plotted (3) at Figure 6 and is subject to an adjustment factor of +0.91 dB {93}. This equation format is the same for rural terrain (curve (1) at figure 5) but in this case the coefficients for equation (16) change to give:

$$\sigma_o = -23.61 + 0.994\psi + (3.53 + 0.091\psi) \text{ Log } f \text{ ------------ } (23)$$

and the 'adjustment factor' is + 0.79 dB. {94} goes further to discuss snow, desert, terrain and sea, with models for each type. His main objective was to obtain models for space based radars and so detailed measurements at low grazing angles were not required.

59. Equation (17) {95} is the first equation to incorporate RMS surface roughness, presumably to indirectly quantify RF in the model. Plots at Figs 5 and 6 (curves 14, 15 and 8, 9 respectively) use the stated empirical constants for ABC, as 0.079, 1.5 and 0.012 for rural and 0.019, 0.64, 0.002 for forests. There is insufficient data to compute constant D in both cases, although this is stated as 2.3 for soil, sand or rocks.

60. Equation (18), the FTD model {96} is based on generalised site geometry for ψ = 0.17 to 0.05^{o}, but not validated above 2.8 GHz, until present measurements at MIT are completed. Curve 16 at figure 5 shows this result using a K of 3.

61. Equation (20) {97} describes clutter as range dependent remaining constant up to the radar horizon. Beyond Rh the clutter decreases at 10 kdB per decade of range. It is not included on the curves at Figs 5 or 6.

62. Equations (21) and (22). Both developed by Georgia Institute of Technology, are included for completeness but have unfortunately not been validated at low values of ψ and are not included at Fig 5 or 6.

63. From the results examined, replotted and recalculated where necessary to fit the required parameters, it is concluded that the effect of ψ on σ_o is such that the median (σ_m) backscatter increases linearly with ψ in the range approx 0.5^{o} to 10^{o}, but below 0.5^{o} the variance is likely to increase quite markedly. Values selected for the model here are considered at the Chapter Summary.

σ_o DEPENDENCE ON POLARISATION

64. The main cause for polarisation sensitivity of backscatter is multipath reflections, hence polarisation effects are of concern only over relatively smooth surfaces. At λ = 3 cm (or greater RF), and very low values of ψ, the surface is not considered smooth in terms of the Rayleigh Roughness Criterion.

65. Linear Polarisation. For practical purposes, over general terrain a few dB difference may exist between σ_{HH} and σ_{VV} linear polarisations; with horizontal being the higher. This has been well supported with a good spread of measurements over 9 different surfaces at Ohio State University {98}, by Cosgriffe et al, and is reprinted in Barton's textbook {99} pp 165-286 for easy reference. For general terrain it is proposed to neglect small differences at low grazing angles in the model at Chapter 11, and for this reason polarisation was ignored in comparing the effects of ψ and τ from the various sources earlier in this chapter. At the lowest values of ψ, where multipath surfaces exist, a maximum of 10 dB should be applied for horizontal polarisation.

66. Cross and Circular Polarisation. Cross and circular polarisation are of interest here in performance prediction, since these techniques

may be employed to reduce clutter returns compared with the wanted aircraft signals. Few new polarisation results have become available since Allan's recent summary, except Tomlinson {100}, who reinforces earlier findings. The following conclusions apply:

a. For linear (plane) polarisation with cross-polar reception, the backscatter is likely to be up to 10 dB lower in the orthogonal plane than in the parallel plane. For isolated dominant reflectors (eg pylons), this difference may be over 20 dB.

b. At the frequencies in use and low values of ψ, lower than Brewster's angle (20° for earth, 5° to 10° for sea), the sense of circular polarisation is probably not reversed.

67. The reader is cross referred to remarks on polarisation change for raindrop rejection at Chapter 3, and reminded that the RCS of aircraft may be reduced, (typically by 3 to 5 dB), with the same-sense circular polarisation; compared to perhaps 7 dB with crossed linear polarisation. Finally, polarisation effects are usefully considered in the following papers: Ament {101}, Rider {102}, Reiss et al {103}. Gent et al {104}, Brindley {105}, Daley et al {106}, Goodyear {107}, Linell {88 }, Katz and Spetner (for $\psi > 10^{\circ}$) {108}.

σ_o DEPENDENCE ON RF

68. It has previously been stated that backscatter for snow covered terrain is difficult to predict, because of penetration, and it is

here that can be seen an analogous situation in attempting to isolate the effects of RF on backscatter. The dielectric properties of the surface are clearly all-important, since earth, like snow, is penetrated to an extent by microwaves and the actual electromagnetic roughness of the surface may not be visually apparent. Since the dielectric constant of terrain is also a function of λ, that which is seen as 'smooth' by a particular wavelength will be seen as rough by a shorter wavelength. An upwards change in RF therefore implies a change from 'smooth' to 'rough' if the change is such that:

$$\Delta h \sin \psi > \frac{\lambda}{8} \quad \text{--} \quad (24)$$

where Δh = rms height of surface irregularities

ψ = Grazing Angle (after Rayleigh).

69. However, as stated above, microwaves will penetrate the surface (typically 1 to 10 cm {106}) dependent on the conditions - which might vary from one resolution cell to the next - even for the same surface material. And so it is seen that a general tendency can be concluded rather than absolute values. Long {86 } surveyed results in this area and states "the totality of experimental results do not yield agreement". It is probably reasonably to state that the wavelength dependance of σ_o can be expressed generally in terms of λ^{-n} (normally $0<n<1$). Classical interference effects (see Long {86 } pp 219-220) can in principle cause σ_o to vary as fast as λ^{-4} at grazing incidence, but this is for the ideal surface, and is perhaps applicable at sea.

70. It should also be noted that 'roughness', as viewed along the radar beam will depend on ψ, as in equation (24) at para 68. Once again because of the shortage of measurements available at low ψ, reliable data relating σ, f and ψ cannot be used to produce a model of adequate validity. Since this project involves RF's of 10 GHz (or above) it is assumed that all (land) surfaces are 'rough', and indeed this would be the case for measurements used here from all the sources used in earlier paragraphs.

DISTRIBUTION AND CORRELATION OF SPATIAL AND TEMPORAL CLUTTER

71. Distribution. A composite scattering model where the probability density function $P_{(\sigma_o)} = f$ (x. y, t) is considered by {109}, who derive pdf's for use at sea, built-up areas, forest and rural conditions, measurements show time variations to be exponentially distributed. If the required value is $P_{t(\sigma_o)}$ then:

$$P_{\sigma_o} = \int_{-\infty}^{\infty} P_t\ (\sigma|m)\ P_s(m)\ dm \qquad (25)$$

m is the average σ_o, taking into account local terrain slope in the resolution cell. If the surface is flat (facet tilt zero - see Chapter 10), $P_s(m) = d(m - \mu)$.
This is to be expected at sea with many independent scatterers. On flat land if a log normal distribution is assumed then:

$$P(\sigma_o) = \frac{10}{\sqrt{2\pi}\ \log_e 10 s\sigma_o} \exp\left[-\frac{100}{2s^2}\ (\log\sigma_o - \log\sigma_{om})^2\right]$$

$$\text{with median } \sigma_{om} = \mu\exp\left[-\tfrac{1}{2}\left(\frac{\log_e 10}{10}\right)^2\ s^2\right]$$

$$P_t\ (\sigma_o | m) = \left\{ \frac{1}{m} \exp\left(- \frac{\sigma_o}{m} \right) \right\} \sigma_o \geq 0 \quad \text{------------} \quad (26)$$

$$= \left\{ 0 \right\} \sigma_o < 0 \quad \text{------------} \quad (27)$$

$$\underset{(sea)}{P(\sigma_o)} = P_t\ (\sigma_o | \mu) \quad \left\{ \frac{1}{\mu} \exp\left(\frac{-\sigma_o}{\mu} \right) \right\} \sigma_o \geq 0 \quad \text{------------} \quad (28)$$

$$\left\{ 0 \right\} \sigma_o < 0 \quad \text{------------} \quad (29)$$

$P_s(m)$ is the spatial variation pdf

μ is the spatial mean value of m

72. Correlation. The few published data on spatial correlation of land clutter are usually concerned with scanning (rotating) search radars. Results may not be applicable at all times to the pencil beam tracking radars under investigation here. With a circular scanning pattern the clutter components change continuously since clutter elements are regularly entering and leaving the illuminated surface footprint. For a narrow beam tracking radar this would occur most markedly for crossing target flown past at a velocity and range to produce a high sightline rate; reaching a peak rate at the tangential point. Radially or near radically approaching or receding targets could cause less effect.

73. In areas where large single man made objects occur, giving predominant specular returns, the probability of spatial correlation is less likely between adjacent resolution cells, but in normal terrain or forest, spatial correlation is likely to be higher, providing adjacent

cells are similarly tilted to the incident surface illumination. Seek Igloo {110} confirms distributions tending towards log-normal as sampled terrain becomes more homogeneous, although other recent research has shown a distribution falling somewhere between log-normal and contaminated normal. Earlier work by Dodsworth {111} isolated 'fast' and 'slow' components as the radar aerial scans the clutter surface. 'Fast' components are found to fluctuate with the median value equal to the running mean, while 'slow' conponents reflect the majority features of the terrain and are regarded as the running mean.

74. Strong clutter tends to occur in patches, giving good spatial correlation, sloped terrain giving the strongest values. For a pre-surveyed radar site position a terrain data base of the type proposed in Chapter 2 can indicate with fair accuracy the likelihood of positions of clutter patches. At the shorter (millimetric) wavelengths a good indication can be gained from large scale ordinance survey or more particularly vertical photographs of the area.

75. Since clutter is not evenly distributed in practice and it has been shown experimentally (see paras 38 to 40 above) that a change in resolution cell size does not bring about a proportional change in clutter, it is clear that as the radar beam scans with a fixed resolution cell size, (set by τ and θ_A) the loss or gain of surface reflectors for part of the resolution cell, due to aerial rotation, will increase or reduce the number of clutter producing elements in the cell and have a temporary effect as though actual resolution cell size is changing. With very large resolution cells (not usually applicable to the tracking radars), they become more likely to contain partly man-made and partly natural reflectors. In a mobile battle situation

there is some reason to suppose a higher probability that man-made objects will appear in tracker resolution cells since many vehicles are likely to be dispersed in the same area. However this will be dependent on local terrain screening conditions for a ground based radar. If a log-normal distribution is assumed, this will strictly only be applicable to a fraction of the resolution cells in an area (since many are shadowed), or for only parts of cells - if the cells are large. This approach is confirmed at {112} where the cell values aggregated would produce a threshold which is applied to every cell.

76. Spatial Clutter Decorrelation. Autocorrelation factors derived for RF changes (frequency agility) have been researched at {113} where it is proposed that the autocorrelation function of clutter may be periodic, with increasing pulse to pulse RF change. Conditions will be expected to vary with τ and the number of dominant scatterers in the resolution cell, although {114} found that decorrelation times of clutter were not appreciably affected by changes in τ. Autocorrelation lengths investigated by Tomlinson {115} over several terrain types show almost like variations in autocorrelation coefficient irrespective of terrain type at ranges greater than approximately 4 km.

CLUTTER PATCH LENGTH STATISTICS

77. It will be shown in succeeding chapters that the factors affecting an overall effectiveness prediction model for a given tracking radar located at a known geographical position are closely related. No single aspect can be taken in isolation without considering the others. Although this report first attempts to separate these factors for more detailed examination before bringing

them finally together as a complete model, it is difficult to ignore the closely related topic of 'probability of obtaining a given track length' at this early point in the report. The importance of observable track length can be seen from Annex E, but the overall requirement for a certain system must include the probability of maintaining signal detection above the set threshold for the duration of the observable track length. Taking this a stage further, it concerns the probability of maintaining track under these conditions. Probability of holding radar track, loosing track or gaining a new track is also considered at Annex E.

78. Spatial clutter statistics can be presented in various ways:

a. Probability of clutter exceeding a given track length.

b. Probability of clutter patch separations exceeding given lengths.

c. Probability of exceeding set threshold levels.

d. Probability of clutter variations with range.

79. Clutter Patch Lengths and Discrimination. Two reports by the SHAPE Technical Centre {116} {117} on clutter in Europe, together with Rigden {118} in the UK and Briggs {119} in the USA, have been considered, the results are interpolated, and re-presented in different forms at Figs 7 to 10. Clutter patches vary in length from a few metres up to 1400m, although of course at varying signal levels. UK figures for a specific site {120} show that clutter $>1m^2$ does not exceed about 30m length while strong

levels such as $10m^2$ are limited to patches about 6m in length. It is not clear whether the available US results are wrt $1m^2$; however the main point of interest is the similarity of distributions at Fig 7. When replotted (plot not included) on log-normal graph paper these give sensibly straight lines over most of the patch lengths for $0.1<P<0.7$.

80. Clutter can be reduced by using pulse length discrimination. For the UK site about 75% of the clutter exceeds $0.1m^2$ (Fig 8) and is in patches longer than 30m - these could be removed simply by setting the appropriate thresholds. Fig 9 compares UK and European measurements.

81. If the probability of clutter exceeding given equivalent reflecting areas can be plotted from a knowledge of the terrain, this, together with the earlier data and data on clutter patch separations could lead to a model for radar tracking conditions by assessing the statistical opportunities when tracking can take place for given track lengths. These would of course be site specific assessments.

82. For tracking in clutter to be successful (as opposed to intermittent detection) the two cases are essentially:

a. Statistical likelihood of clutter patch separation such that the target may be tracked with no clutter present (ie target track held for a minimum time period).

and b. Those occasions where the target can be (additionally) tracked where the clutter level, though present, is negligibly low - or can be processed out in the receiver.

In both a. and b. above, conditions must exist with a sightline to the target (see Chap 2 - Screening) and a sightline to the clutter(in case b. above).

83. It is further proposed that from the statistics for a particular terrain area, an examination of track length unscreened, clutter patch length and the distribution of resolution cell slope facets, could produce a prediction for example "when a target enters an area Type A (eg flat terrain with 30% vegetation cover up to say 10m high) with known target velocity and altitude, with missile and radar type 'X' deployed, there will be a 20% probability of the system obtaining a firing opportunity in which a complete engagement could occur". Further it might be possible to vary the prediction to take account of the higher probability expected where the radar system is deployed in a premeditated manner on a previously surveyed (optimum) site. For example a higher probability would be expected from a presurveyed site in undulating terrain - since the probability of obtaining a target sightline is more likely as the target cannot maintain a set altitude clearance over terrain which undulates with a fast period. These points are considered further at Annex E and Chapter 10.

84. <u>Variation of Clutter with Range</u>. The SHAPE reports also express clutter probability in terms of range, the median values of which are replotted at Figure 10 (from fig 9 in {121} and Fig 4a in {122}), converted in each case to give relative echoing area by applying a R^4 correction by taking the average range in each interval. The UK and USA results are also shown for comparison. It is seen that the median clutter

value reduces almost linearly with range for all sites and although the individual values are site-specific, the rate of change of clutter level with range varies between approximately 0.5 $dB.Km^{-1}$ to 1.5 $dB.Km^{-1}$.

FALSE ALARM RATES

85. It is not the intention here to repeat receiver processing options, such as MTI, which are well covered in many standard texts. However a brief mention of false alarm rates is appropriate.

86. At the receiver input will be a combined signal of noise, clutter and wanted target; from which the receiver will adjust the ratios to separate the target from the other unwanted signals. The distribution of the noise envelope at the detector input is given by the Rayleigh distribution. In weak signal conditions (ie wanted signal near noise level) the action of a detector is square law and the distribution of the signal envelope modified by the square law action will be:

$$P_n (v)\, dv = \frac{1}{2a\sigma^2} \exp\left(-\frac{v}{2a\sigma^2}\right) dv \qquad (30)$$

where $2a\sigma^2$ is the mean value; a is a constant. v is the detector output voltage. If the noise envelope exceeds a threshold V_t a false alarm with probability P_{fa} is given:

$$P_{fa} = \frac{1}{2a\sigma^2} \int_{kn}^{\infty} e^{-\frac{v}{2a\sigma^2}} \qquad (31)$$

$$= e^{-kn} \text{ (normalised threshold for noise)} = \frac{V_t}{2a\sigma^2}$$

A threshold is chosen to give a tolerable false alarm rate eg 10^{-6} and the probability of detecting the presence of a signal (or the probability that signal + noise exceeds the threshold V_t) is then:

$$P_d = \frac{1}{2a\sigma^2 (1 + \bar{x})} \int_{k_s}^{\infty} \exp\left(- \frac{v}{2a\sigma^2 (1 + \bar{x})} \right) d_v \qquad (32)$$

$$= \exp^{-k_s}$$

Where k_s is a normalised threshold (signal + noise) $= \dfrac{V_t}{2a\sigma^2 (1 + \bar{x})}$

$\bar{x}$ is the mean signal to noise power ratio at the receiver input.

$$k_s = \frac{k_n}{(1 + \bar{x})}$$ (k_n defined on p113)

$$\text{hence } P_{fa} = e^{-k_n} \qquad (33)$$

$$P_d = e^{-k_s} \qquad (34)$$

$$\text{and } \log_e P_d = \frac{\log_e P_{fa}}{(1 + \bar{x})} \qquad (35)$$

87. For example if $P_{fa} = 10^{-6}$ and S/N = 10 then on the basis of a single echo:

$$P_d = \frac{10^{-6}}{1 + 10} = -1.26$$

and $P_d = \exp - 1.26 = 0.284$ (ie 28.4%)

88. Assuming a number of successive pulses N are integrated, each having crossed the threshold V_t then:

$$P_{fa} = \frac{N^N}{(N-1)!} \int_{k_n}^{\infty} x^{N-1} \left(\exp - N_x \right) dx \qquad (36)$$

Where $k_n = \frac{V_t}{2a\sigma^2}$; x is the value at any instant.

The solution to this integral is tabulated by standard methods as the incomplete Gamma function, of which a solution is:

$$P_{fa} = e^{-Nx} \left(1 + N_k + \frac{(N_{k_n})^2}{2!} \ldots\ldots\ldots\ldots \frac{(N_{k_n})^{N-1}}{(N-1)!}\right) \qquad (37)$$

and the probability of detection after integrating N samples of the signal noise is:

$$P_d = \frac{N^N}{(N-1)!} \int_{k_s}^{\infty} x^{N-1} \exp - Nx \, dx \qquad (38)$$

A solution is:

$$P_d = e^{-Nk_s} \left(1 + Nk_s + \frac{(Nk_s)^2}{2!} + \ldots\ldots\ldots \frac{Nk_s^{(N-1)}}{(N-1)!} \right) \qquad (39)$$

89. Assuming N = 2, $P_{fa} = 10^{-6}$ and x = 10 then P_d = 55%, compared with 28.4% when N = 1 (see para 87 above).

90. Figure 11 shows P_d when N = 8 for a radar operating on a number of frequencies (N_f), where the probability density function of N integrated pulses is:

$$P(x) - N^N \frac{x^{N-1}}{(N-1)!} \exp\left(-N_x\right) \tag{40}$$

for which the general case is

$$P(x) = \frac{a^b}{(b+1)!} x^{b-1} \exp\left(-ax\right) \tag{41}$$

a, b are constants where if b = 1 and $a = \frac{1}{\bar{x}}$ then

$$p(x) = \frac{1}{\bar{x}} \exp \frac{x}{\bar{x}} \tag{42}$$

a and b are deduced from:

$$a = \frac{N_f (1 - \bar{x})}{N_f - 1 + (1 + N_f \bar{x})^2} ; \; b = \frac{NN_f (1 + \bar{x})^2}{N_f - 1 + (1 + N_f \bar{x})^2}$$

91. For further details the reader is referred to Swerling {123}, {89} or Marcum {124}, to Chapter 6, para 14, and to Annex E, para 29.

92. Ideally an adaptive value of V_t is required to take account of the variations in clutter received from each resolution cell since the probability of detection is a function of false alarm probability and signal to noise

ratio as dictated by the statistical model. The overall probability of detection is found from:

$$\text{(overall) } P_d = \int_0^\infty P_d \, P(C) \, dC \tag{43}$$

93. If T_r and C_r are received Target and Clutter power respectively; and N is noise power (referred to receiver input) and if I is the improvement factor then, from (35):-

$$\log_e P_d = \frac{\log_e P_{fa} \quad (C_r + IN)}{1 + IT_r} \tag{44}$$

From (43) above, the overall probability of detection in clutter will be obtained:

$$\text{(overall) } P_d = \int_0^\infty P_{fa}^{\;(1/(1 + IT_r/C_r + IN)))} \, P(C)dC \tag{45}$$

and with C_r (assuming a log-normal pdf):

$$P(C_r) = \frac{1}{\sqrt{2\pi}\,\sigma\, C_r} \quad \exp.(-\log_e(C_r/C_m))^2/2\sigma^2) \tag{46}$$

Where C_m is the median of clutter power C_r.

Combining together (46) and (45):

$$\text{(overall) } P_d = \int_0^\infty P_{f_a} \quad (1/(1 + IT_r/C_r + IN))) \quad \frac{\exp\,(-\,(\log_e(C_r/C_m))^2/2\sigma^2)\; dC_r}{\sqrt{2\pi}\,\sigma\, C_r} \tag{47}$$

94. Some assumptions have been made here concerning the false alarm probability since the work by Marcum and Swerling are based on a constant false alarm rate whereas (as at para 92) this will not strictly be the case. However any prediction model will necessarily operate within constraints; since many modern radars will have MTI filters the basic eqns above will not always apply directly but will be subject to certain assumptions of clutter residue characteristics after passing through the MTI filter compared with receiver thermal noise levels. Similarly there may be receiver non-linearities which introduce changed statistics, however the above equations assume no receiver limiting. Pursuance of the relative performance of limiting circuitry is beyond the scope of this report. Threshold settings for Rayleigh, Ricean and Log-Normal clutter are at Figs 12-14.

CHAPTER SUMMARY

95. At the outset of this research it was decided to include many terrain types from a wide variety of sources to provide a broad basis for a general prediction model; rather than basing the conclusions on a few models albeit with more precise values which may be site-specific. A model is thus sought which is both simple and contains adequate statistical information to give reasonable integrity for a generalised prediction.

96. In the past it may be that excessive importance has been attached, to distributions and curve fitting to clutter prediction statistics. For acceptable false alarm rates the signal to clutter ratio must be very high, hence only the tails of distributions are of real interest. Predictions at these extremes may be based on excessive interpolation.

GRAZING ANGLES

97. It is clear that land statistics are less easily related to the surface than sea clutter statistics and that low grazing angles produce variable statistics which are much affected by 'shadowing'. As the grazing angle increases the shadowing effect diminishes and the s.d. decreases.

Rural Terrain

98. By careful examination of the plots of clutter values (figure 5) for grazing angle, and by rejecting the space-based results {94} {92} and {88} respectively shown at Figure 5 as curves (1) (2) and (12), a model is proposed for rural terrain as follows:

$$\sigma_m = A + B\ \psi \qquad (48)$$

By regression analysis A =-32.22, B = 1.017, with correlation coefficient - 0.99. This is plotted at Figure 5 at curve (17). It is seen that the model forms a reasonable median of the world-wide results surveyed. A gradient of 1.25 dB/degree is taken for $\psi > 3^{\circ}$ and 5dB/deg for $\psi < 3^{\circ}$

Forest Terrain

99. Similarly the coefficients proposed for forest are A = −33.1 B = +1.625. This is plotted at figure 6, curve (10). This proposal equates well with the model at eqn (8). An adjustment of 3 dB is necessary for vertical polarisation or with snow cover, and 5 dB for wet trees (see also para 101 below). Both rural and forest results are based upon analysis of worldwide data.

Radar Frequency

100. The general trend for low ψ and homogeneous terrain is that the median backscatter coefficient increases linearly with frequency for most terrain types, out to the horizon, and more variably thereafter (see also Page F1-41). A new model is proposed for K Band at App 1 to Annex F.

Snow Cover

101. Due to temporal, snow depth, water content and polarisation variations a reliable backscatter model is probably impossible to assess especially as these parameters may vary from one resultion cell to another in any but the most homogeneous conditions. Up to 10 dB should be added if conditions of free-water exist due to partial thawing and re-freezing.

Pulse Length

102. Median σ_o is taken to vary with τ as suggested by Dodsworth but (inconclusively) related to the Weibull shape parameter as investigated at Appendix 1 to Annex A.

Simulation of Clutter

103. Computer simulation of site specific data is possible within reasonable limits if a precise digital data matrix is available. In general however a digital landmass data base does not provide precise terrain screening information for vegetation. Therefore sightline information would be unreliable for an unknown site.

New Backscatter V Grazing Angle Model Based on Measurements at K Band:

104. The model developed by the author from raw radar measurements is also plotted at Figure 5 (Curve 18). Details of the analysis method are at Annex F, Appendix 1. They confirm the general model, although at a higher value of RF. When the data was taken as an entity it did not exhibit the reversal of σ_0 at low grazing angles reported by some other researchers. It is on interest that the values obtained clearly plot as a Weibull distribution and statistical tests show they are definitely not log-normal.

105. Selective Analysis: when the K Band data (at Annex F, Appendix 1) was examined critically, and outlying values from specular reflectors and probable sidelobe leakage removed; it became apparent that the clutter values did in fact rise at very low grazing angles. This confirms the reports mentioned above. Possible causes of this phenomena, including the possibility of terrain measurement errors, are at Annex F, Appendix 1, with many of the results. In the course of this analysis considerable care was taken in matching the measured backscatter to the terrain matrix and hence to the surface gradient concerned.

106. The results obtained compare favourably with Barton's latest unified clutter model proposed at this frequency, but not apparently supported by published measurements at present.

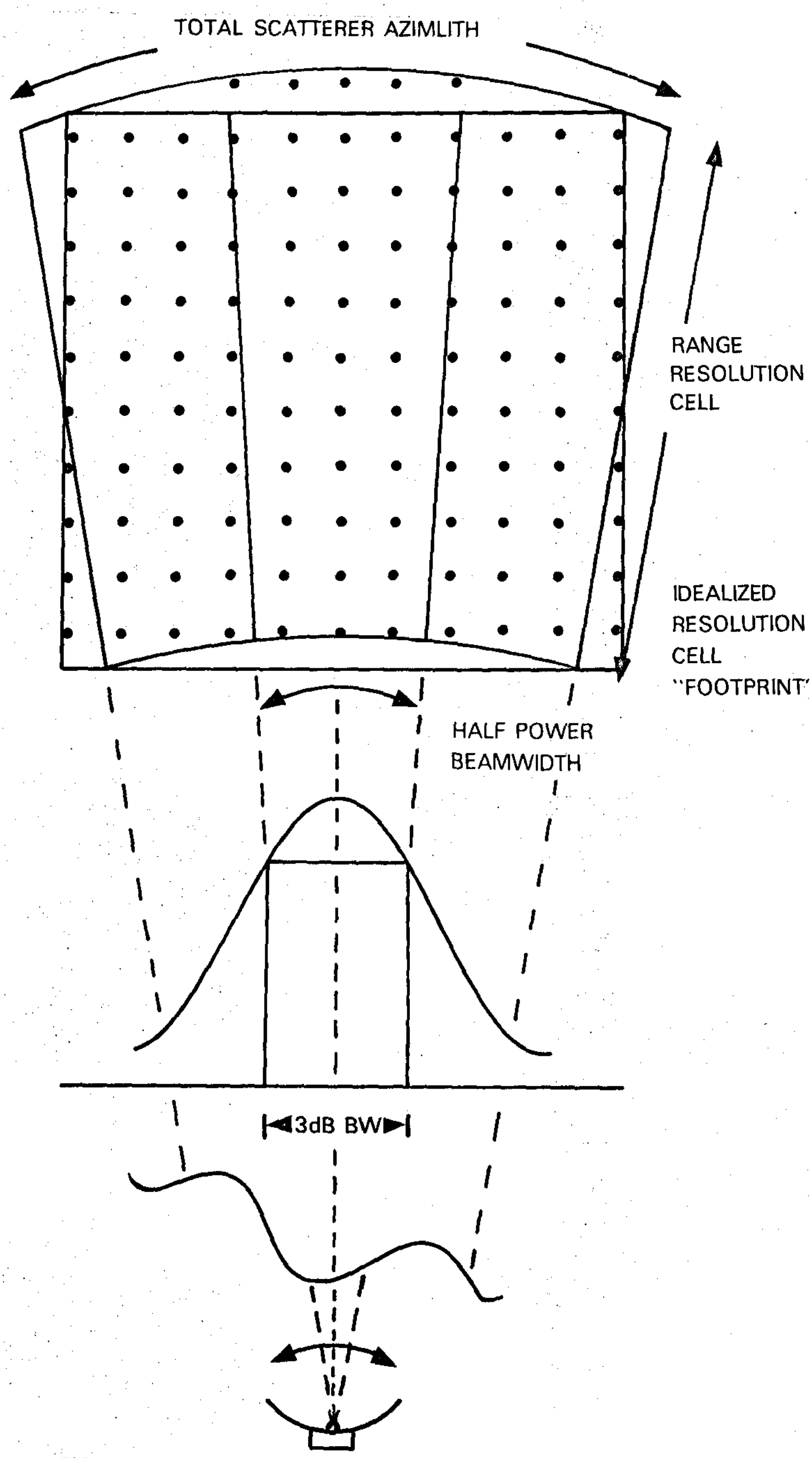

FIG 1 POINT SCATTERER CLUTTER REPRESENTATION

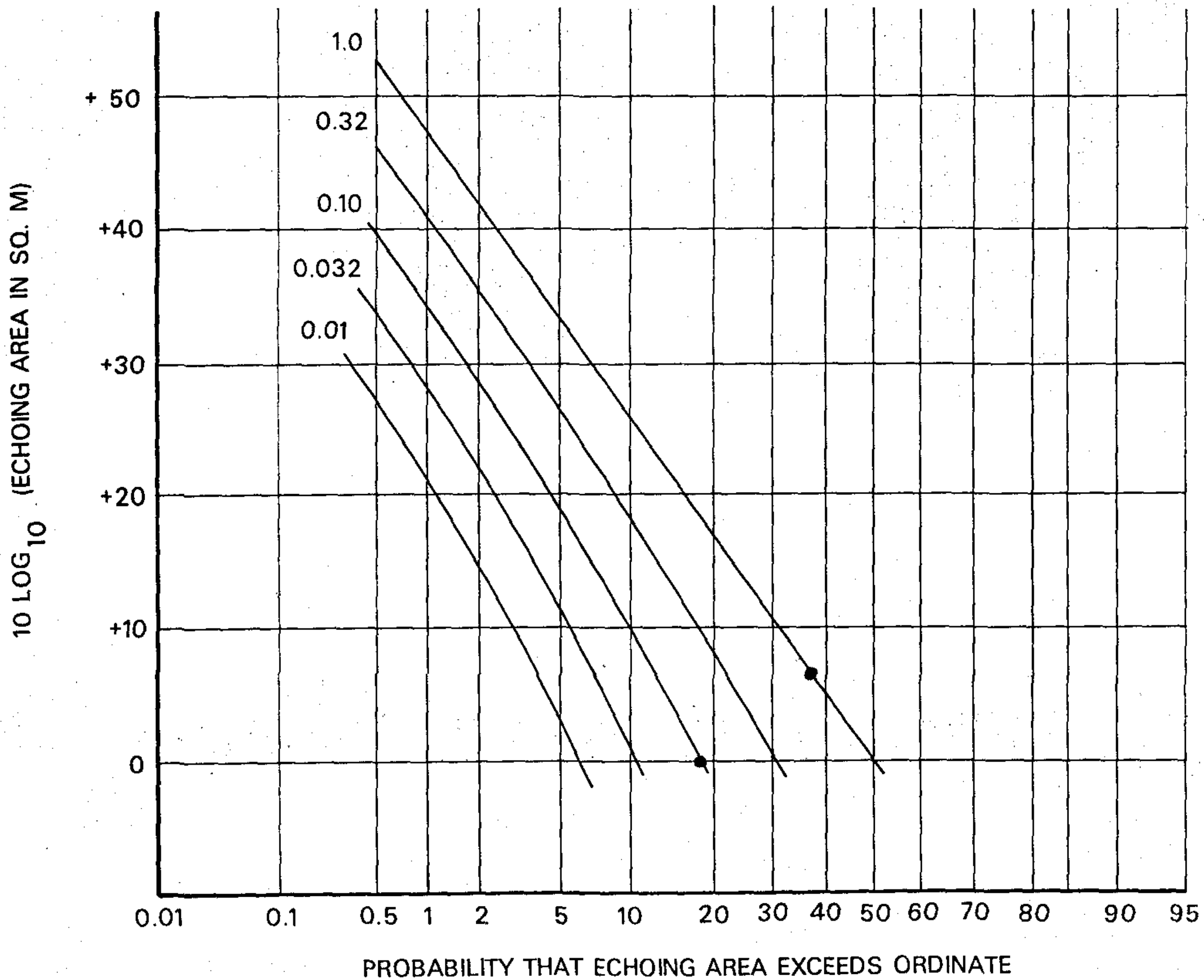

FIG 2 EFFECT OF PULSE LENGTH RATIOS ON CLUTTER PROBABILITY DISTRIBUTION

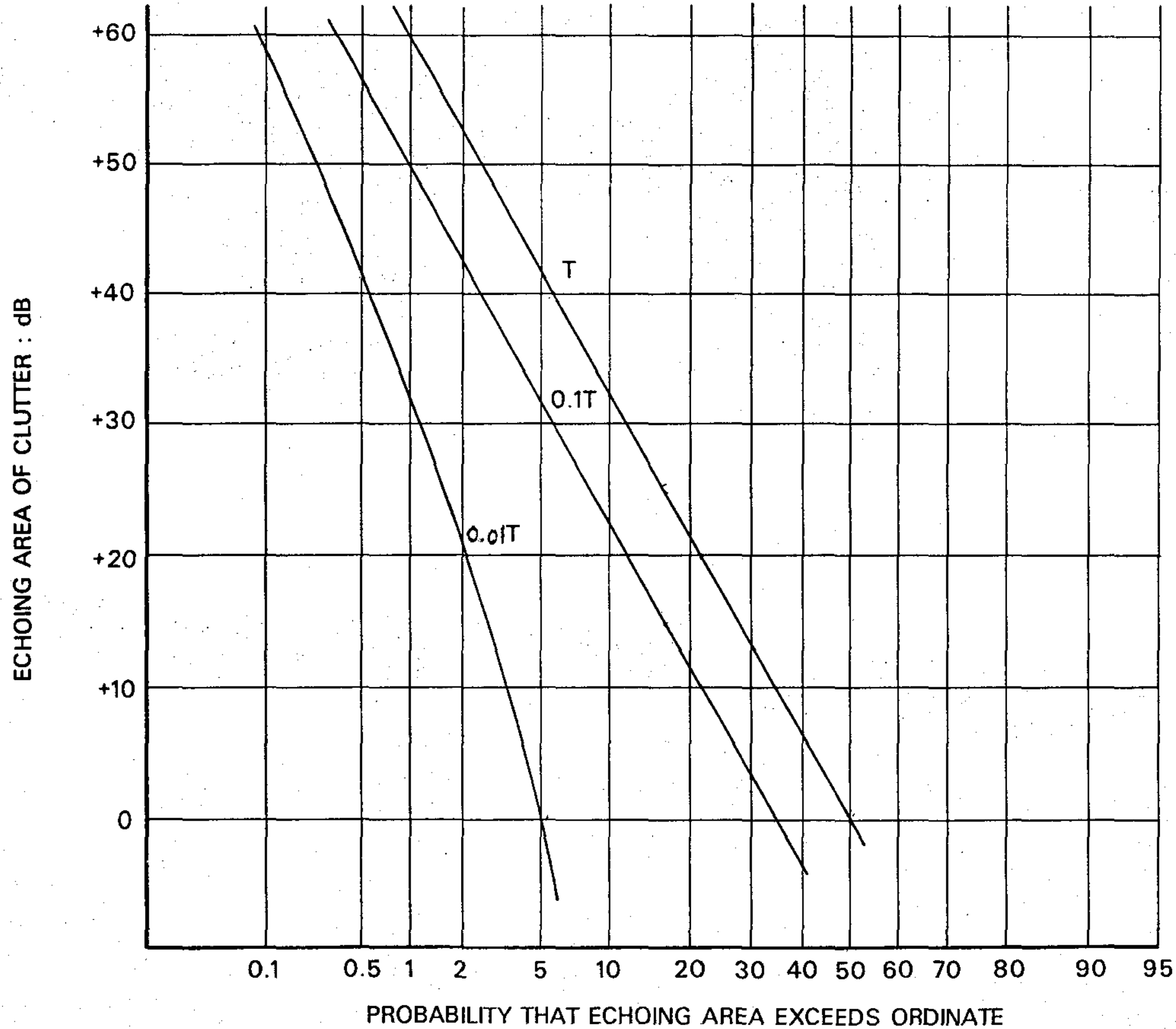

FIG 3 EFFECT OF PULSE LENGTH ON CLUTTER (after Dodsworth)

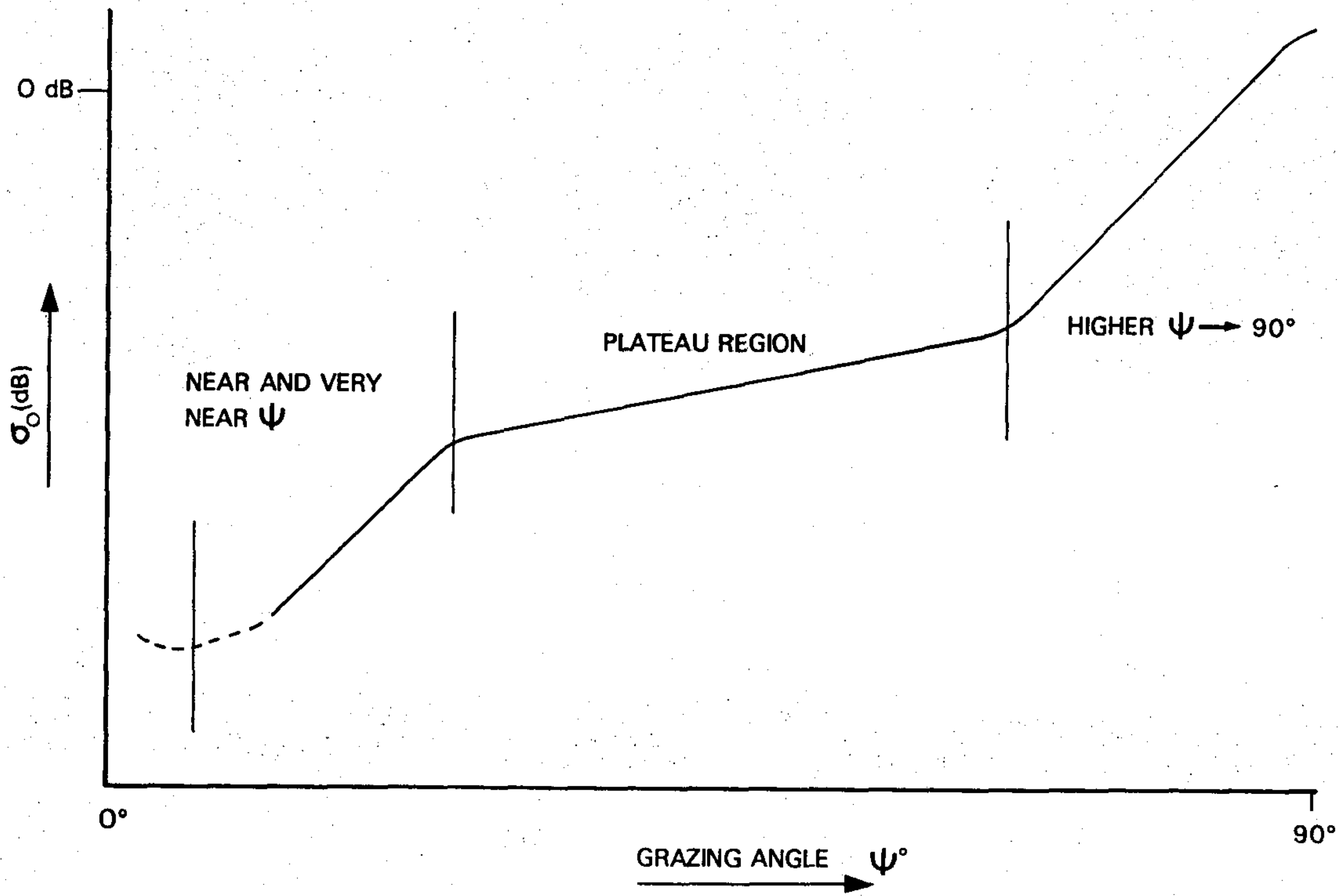

FIG 4 DEPENDENCE OF σ_o ON ψ

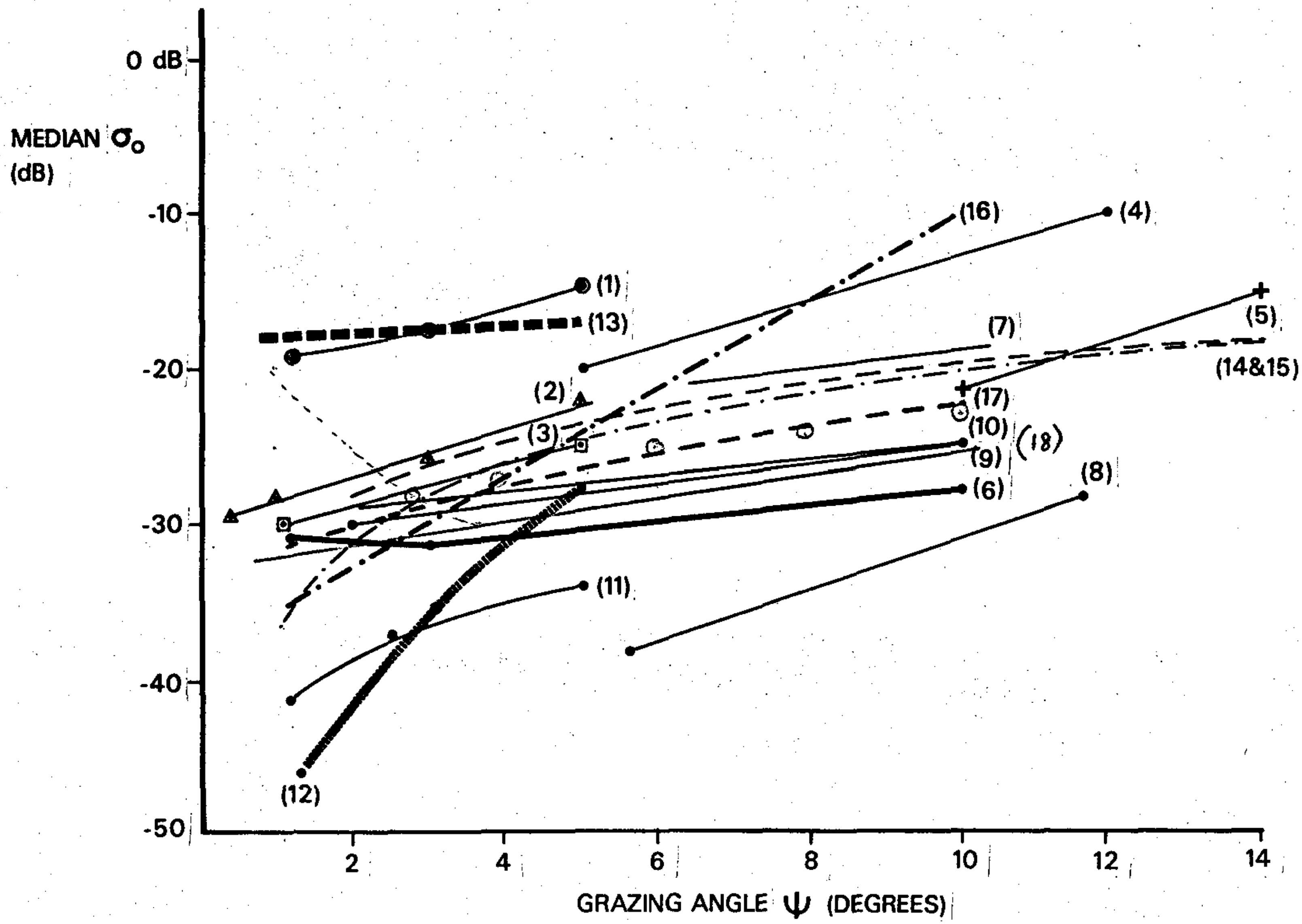

FIG 5 VARIATION IN σ_o WITH ψ FOR RURAL, FARMLAND & CULTIVATED TERRAIN AT (λ = 3cm)

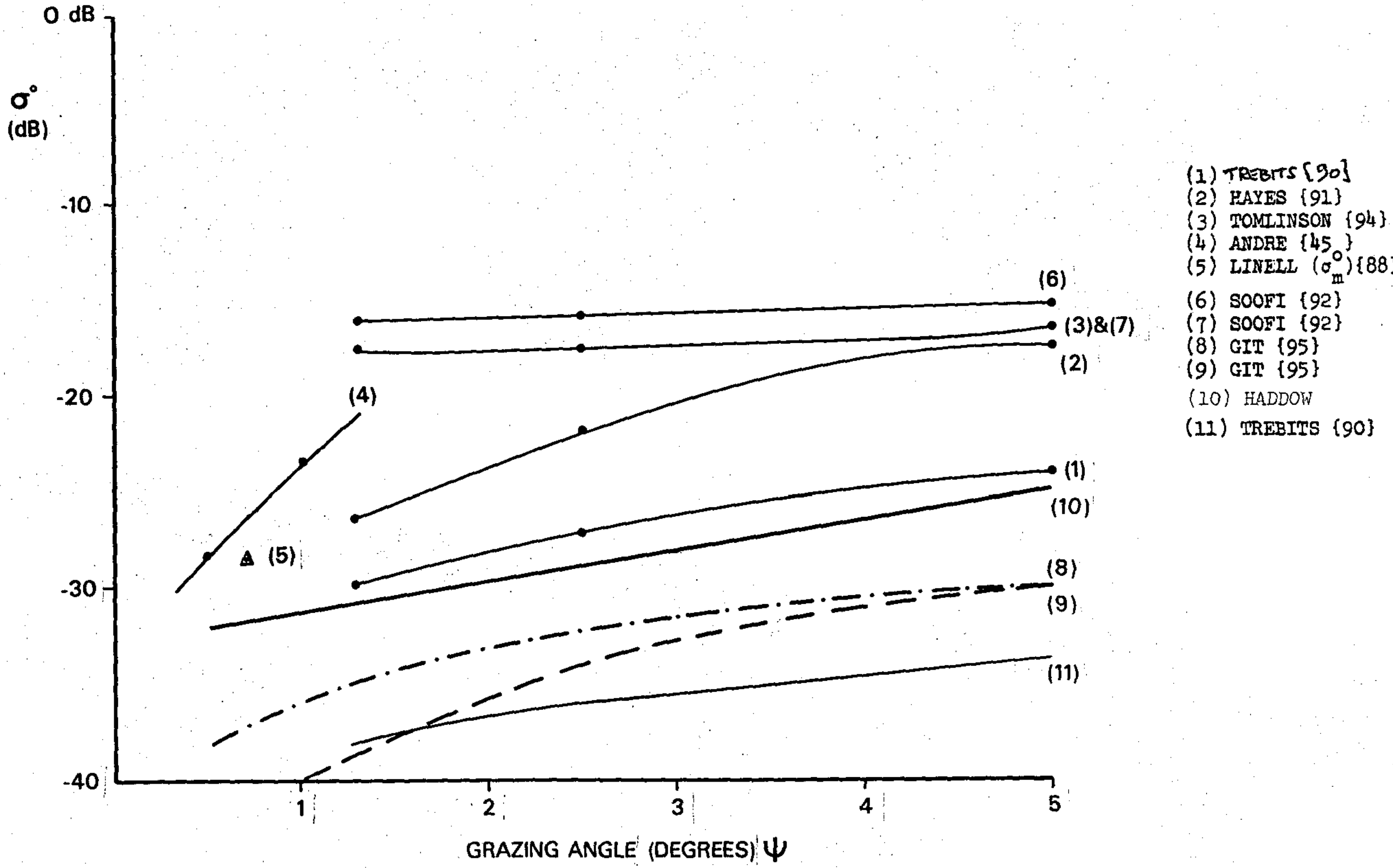

FIG 6 VARIATION IN σ_o WITH ψ FOR TREES, FOREST AT (λ = 3cm)

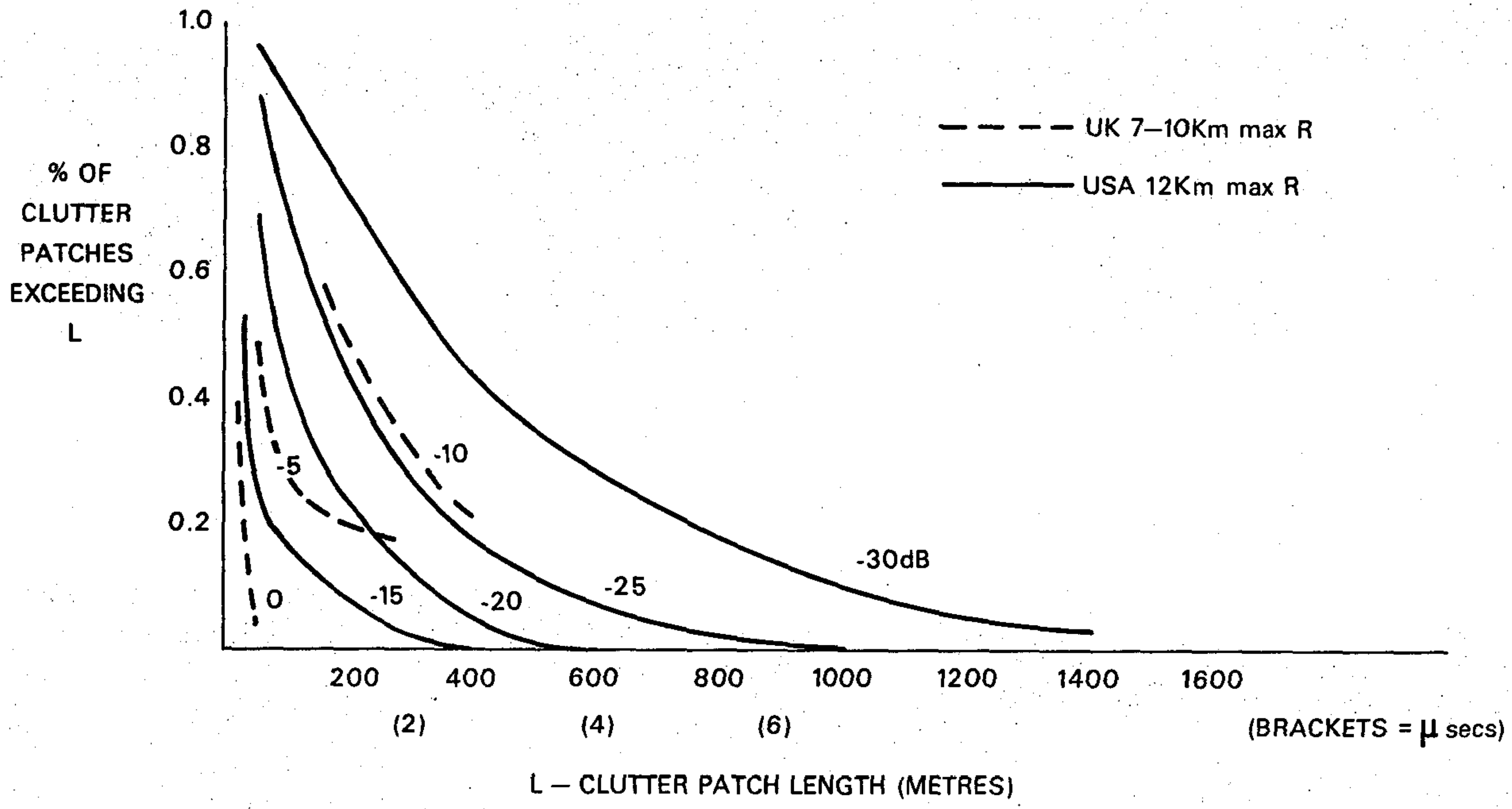

FIG 7 COMPARISON OF PROBABILITY THAT CLUTTER PATCH LENGTHS EXCEED RADIAL LENGTHS L - RURAL TERRAIN

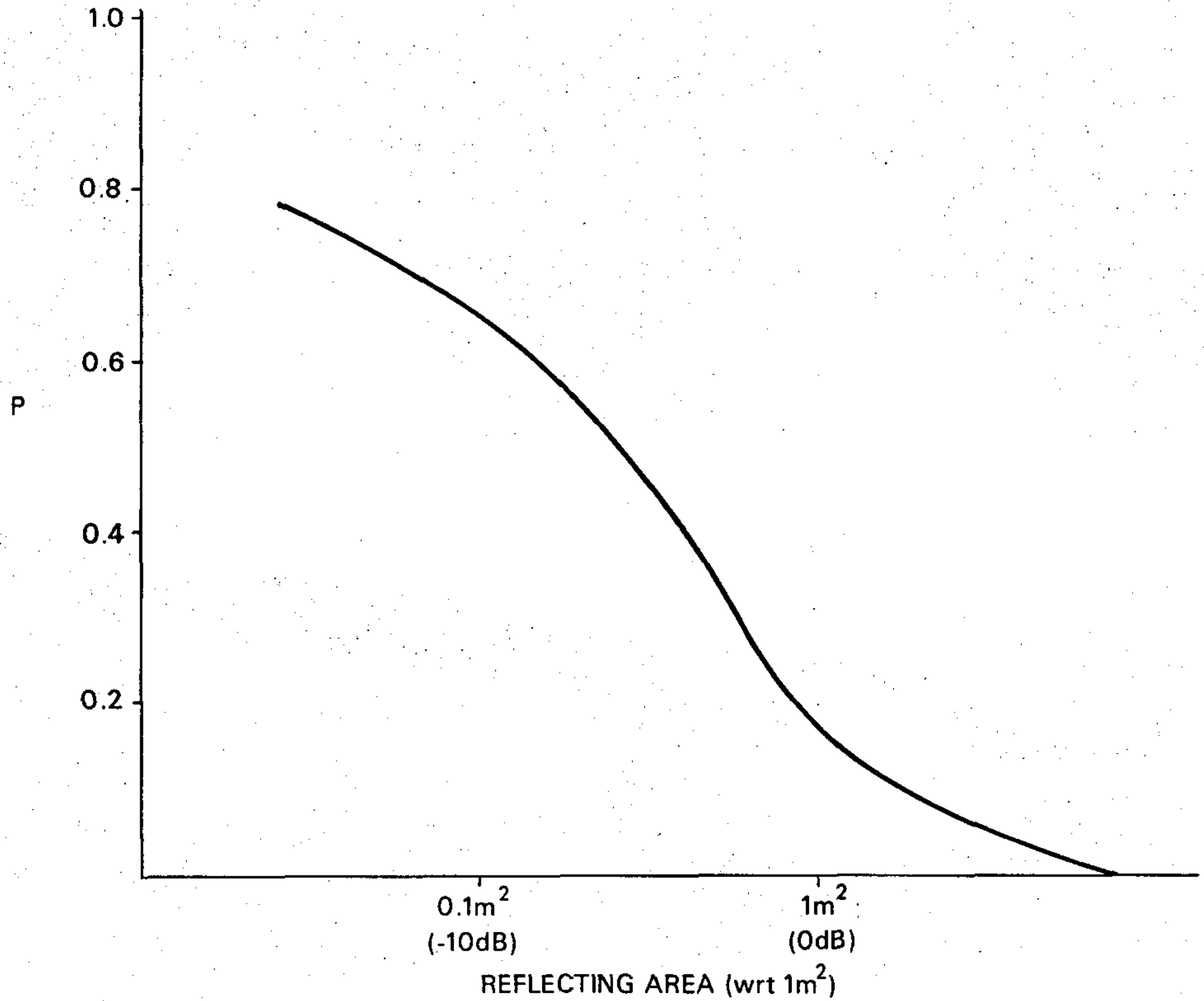

FIG 8 PROBABILITY DISTRIBUTION OF CLUTTER REFLECTING AREA RADAR CROSS SECTIONS FOR UK RURAL TERRAIN **(after Rigden)** (118)

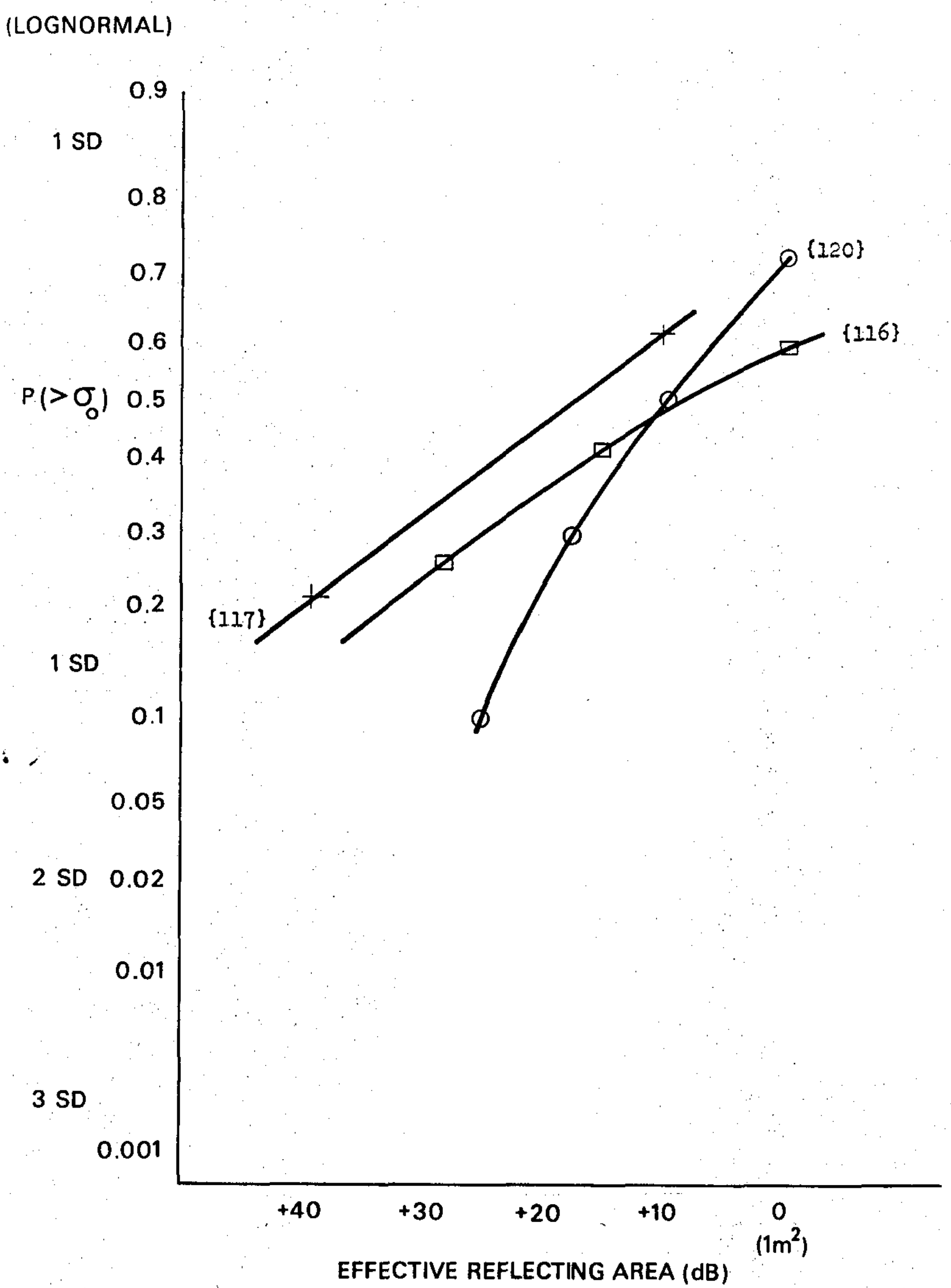

FIG 9 PROBABILITY OF EXCEEDING REFLECTING AREA FOR SPECIFIC UK AND EUROPEAN SITES

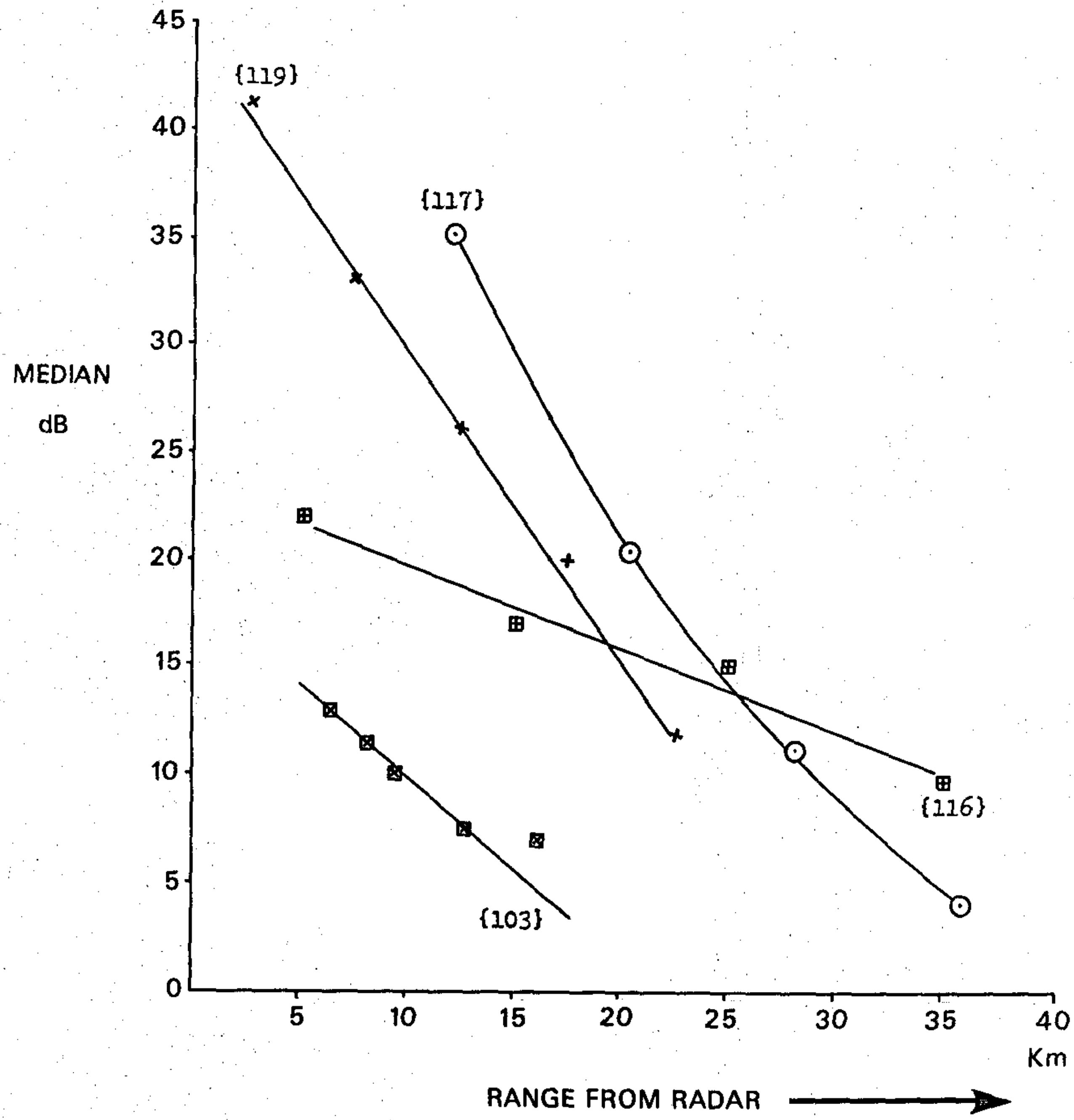

FIG 10 MEDIAN CLUTTER RETURN LEVEL (ABOVE MINIMUM DETECTABLE SIGNAL) FOR RANGE

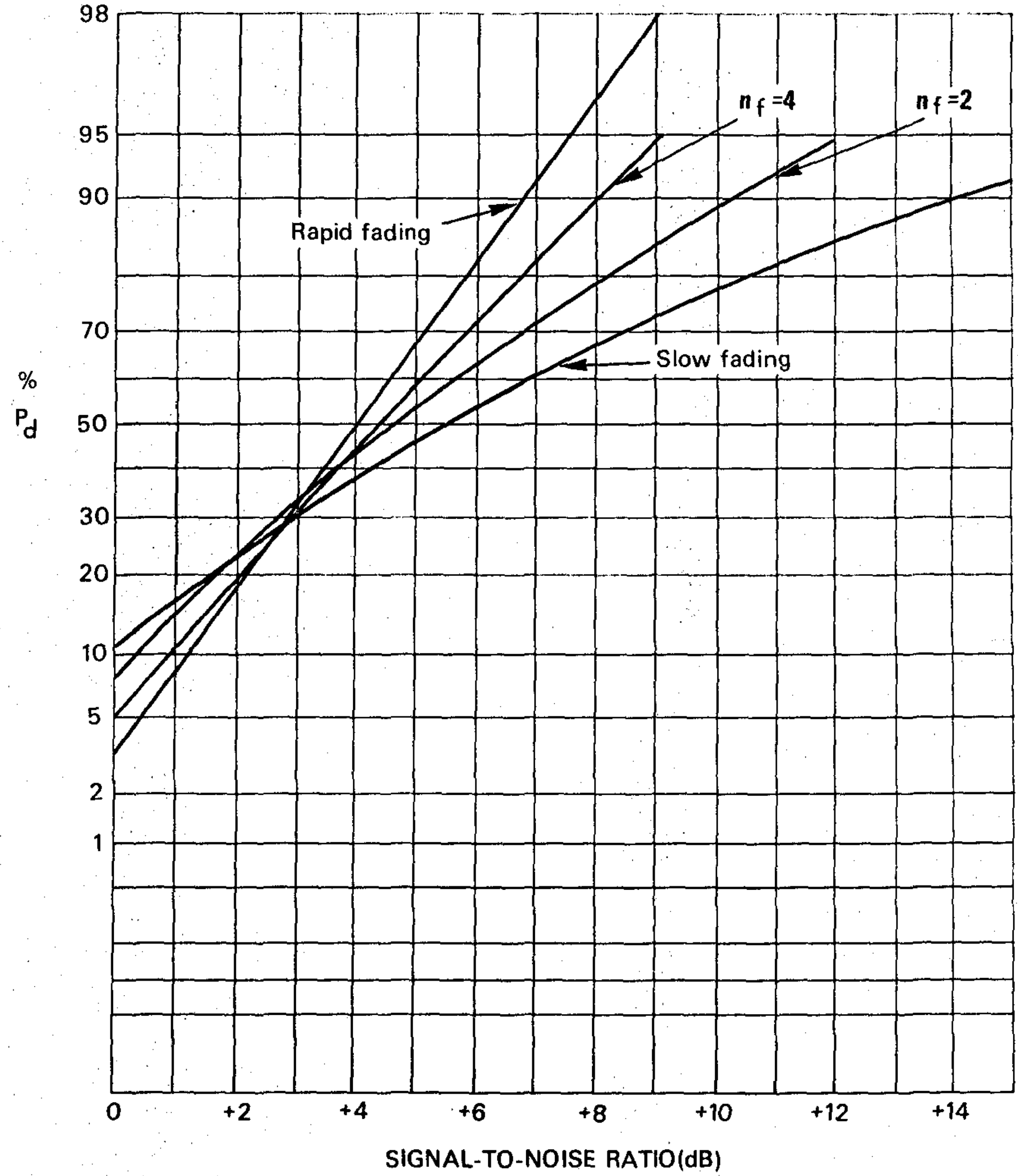

FIG 11 PROBABILITY OF DETECTION FOR GIVEN S/N (N=8, n=10^6)

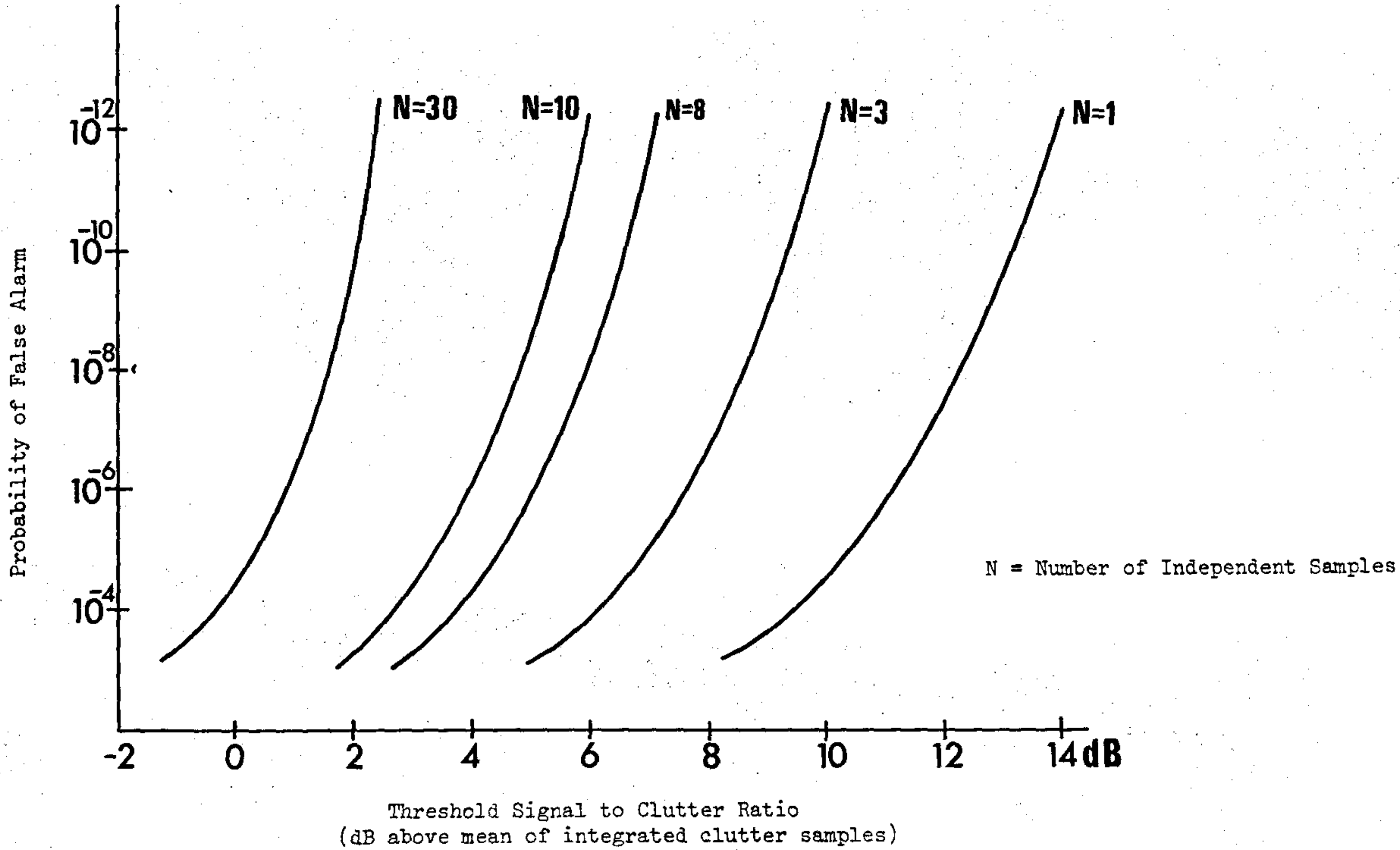

FIG 12 THRESHOLD SETTINGS ABOVE MEAN FOR RAYLEIGH CLUTTER

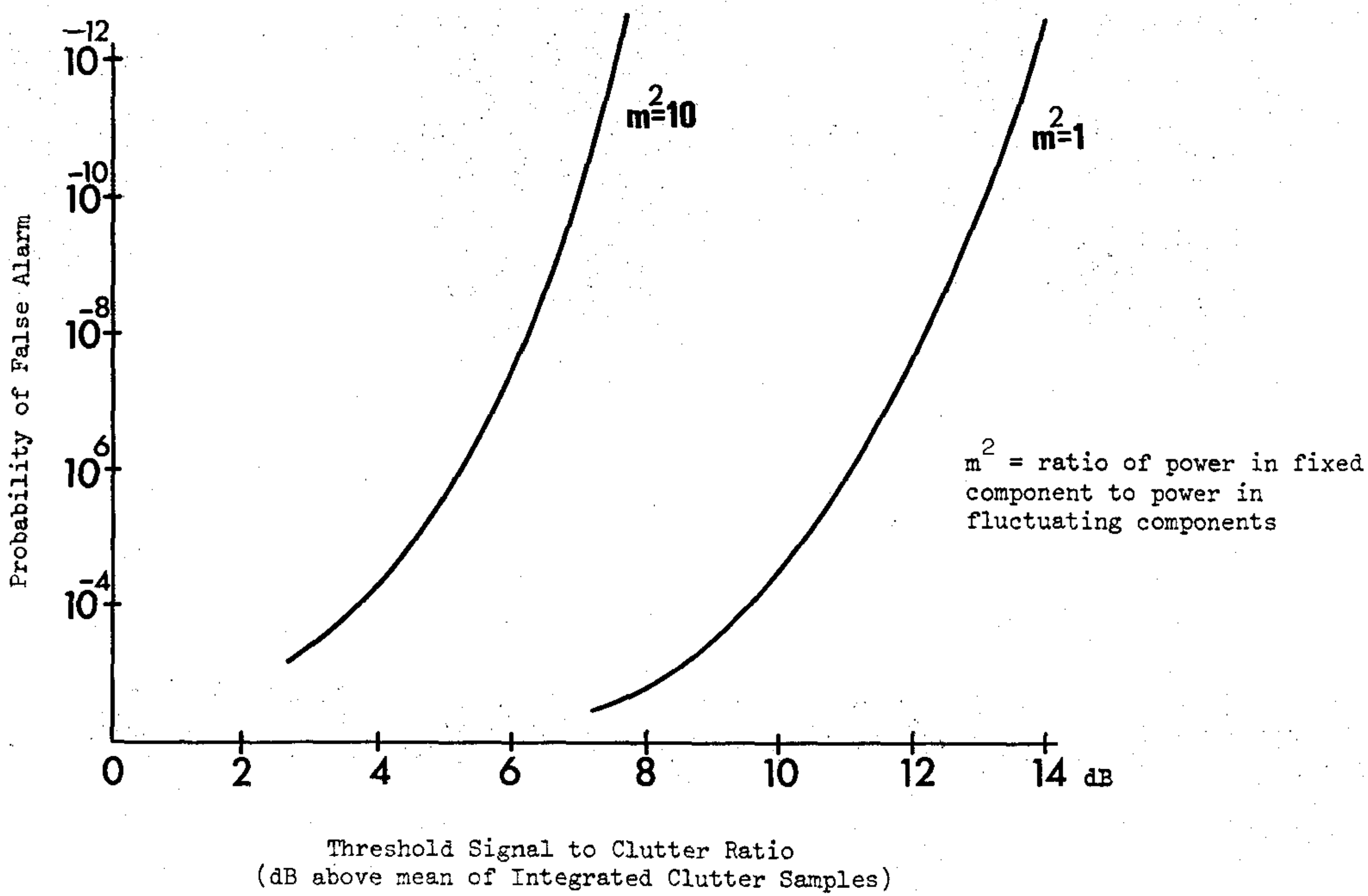

FIG 13 THRESHOLD SETTINGS FOR RICEAN CLUTTER

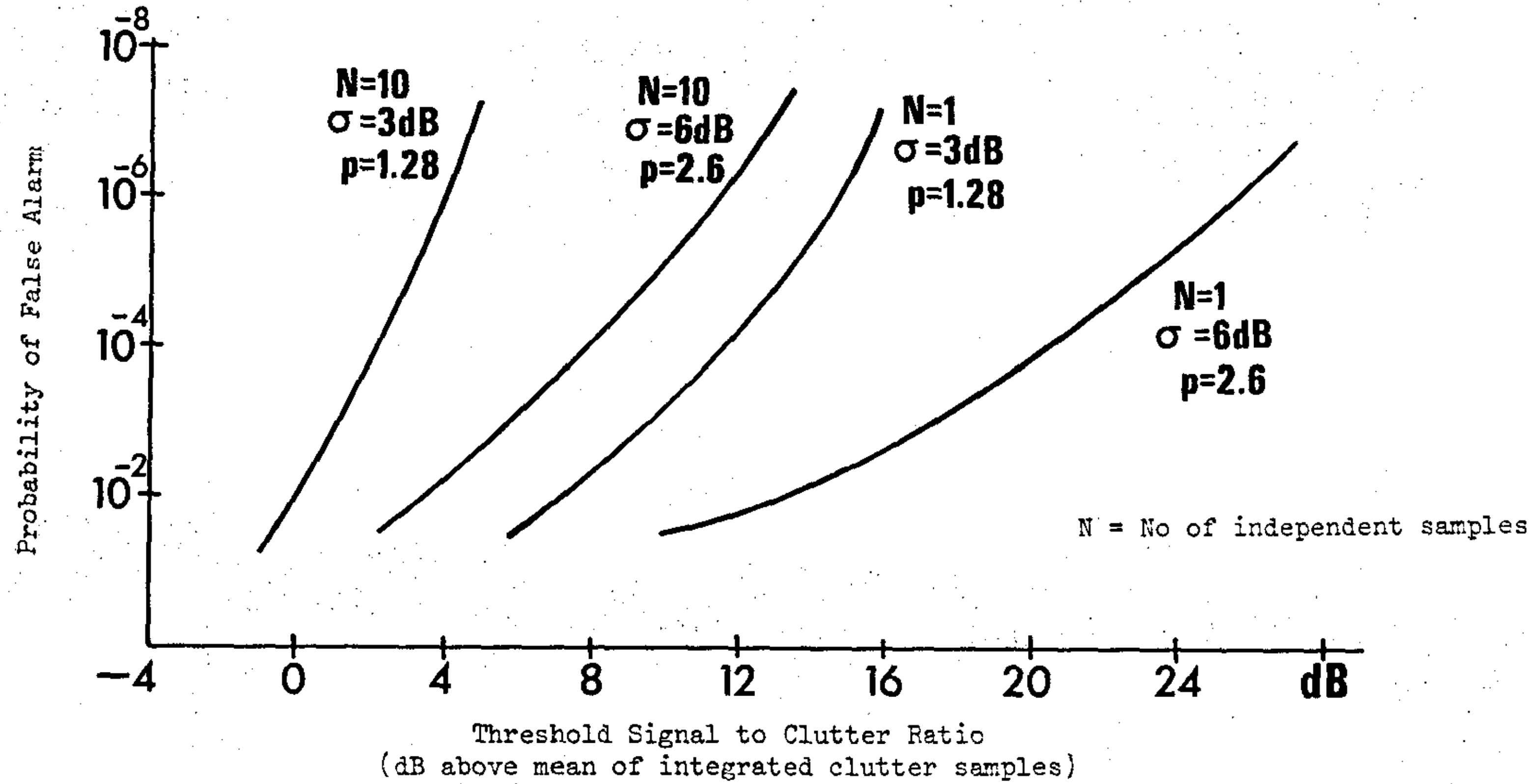

FIG 14 THRESHOLD SETTINGS FOR LOG-NORMAL CLUTTER

CHAPTER 5

NON STATIONARY CLUTTER

WIND, AIR TURBULENCE, CHAFF AND BIRDS

WIND EFFECT ON GROUND SCATTERERS

1. Since the re-radiation of electromagnetic energy from ground objects (and chaff) moved by the wind can have significant effects on backscatter, a survey was made to isolate practical wind or turbulence parameters for incorporation into the detection model. Twigs, branches, grass, crops etc all oscillate in the wind and when illuminated with centimetric (and especially millimetric) radar energy will contribute almost all possible electrical phases to the overall backscatter signal. Hayes {125} has shown a directly increasing relationship in signal fluctuation rate with increasing windspeed, as would be expected; but researchers have generally found a lack in correlation for measurements of tree fluctuations for varying polarisations; in particular when using a pencil beam at 3 cm wavelength. Radar observations on foliage have generally yielded Rayleigh-type statistics (See Annex A), with many researchers concluding that the ground echo from a resolution cell is likely to contain a sensibly steady component plus fluctuating echoes caused by oscillating surface motion; thus modifying the components into a Ricean distribution **(also see Annex A).**

2. Land and sea doppler spectra and surface radar cross section of foliage are all windspeed dependent. Kerr {126} confirmed ground echo amplitude to be peaked at a value near the amplitude of the constant component. As the wind increased, the ratio of the clutter emanating from the moving component increased, compared with the steady component of the overall signal. When the steady to moving ratio m^2 is small, ie <1,

there is little difference between equations (9) and (10) at Annex A. As m^2 increases, the distribution approaches a Gaussian shape centred about the ratio of the steady echo component. This effect has been well established at λ = 3cm to show variation with surface culture {127} with various polarisations, with and without snow cover, with small grazing angles and at different times of the year.

3. Sensitivity at Certain Windspeeds. Hayes and Walsh {128} found an abrupt increase in fluctuation rate comprising positive to negative reversals in slope and vice versa near windspeeds of 10 mph (44 ms^{-1}), and that leaves and twigs are likely to be in constant, rather than intermittent, motion at 8-12 mph. Other researchers (Barlow, Fishbein, Graveline, Kerr and Ritenbach) agree that the spectra are more complex than the basic Gaussian distribution. As an example, in wooded areas the sd of clutter using Gaussian values would be 25 Hz in 11 GHz. Wind-produced clutter is part of the overall clutter characteristic, where, for example, the Rayleigh characteristic is often seen in the homogeneous clutter of urban areas and very rough terrain having high intensity tails tending towards the lognormal.

4. Motion of Radar Beam. Additionally, wind spectra are found to be broadened by the motion of a radar beam {129}, but this is more appropriate to radars on moving platforms such as aircraft and it is not thought to be applicable to this particular study; since it is assumed that a low-level tracking radar will be stationary when tracking even though in a mobile radar system some associated acquisition radars may have limited ability to acquire on the move. **When tracking, the land-based radar tracker beam only moves slowly, compared with aircraft speeds.**

SURVEY

5. Table 1 summarizes a survey of 30 years work on windspeed effects

TABLE 1 SURVEY OF EFFECTS OF WIND ON SURFACE CLUTTER

Serial	Year	Researcher	Scatterer	λ (cm)	Wind Velocity (MPH)	Pol	Distribution	Remarks
1	1949	BARLOW *	Woods, Sea, Rain, Chaff	30	-	-	See para 5	
2	1951	KERR *	Woods, Sparse, Rocky	9.2 3.2 1.25	25-50 Gusts	-	Gaussian (Approx)	
3	1956	IVEY* et al	Deciduous and Coniferous	-	Moderate	H&V		Also at 35 GHz
4	1957	HAYES et al	" " "	3	0-7 2-15	//&X //&X	See para 5	1.86° Pencil Beam PW 0.25μsec
5	1959	HAYES et al	Deciduous	3	-	All	Rayleigh	
6	1963	LINNELL	Forest and Cultivated	3	-	Variable	Lognormal (approx) and Rayleigh	Grazing Angles 0.7°, 1.25° and 5°
7	1967	GUINARD * et al	Unknown	3	-	H&V	Ricean	Also P, L & C Bands down to 5°
8	1967	FISHBEIN * et al	Deciduous	3	10	H	See para 5	
9	1968	DALEY et al	Unknown	3	-	HH&VV	Rayleigh (see also Valenzuela)	Also P, L & C Bands

Serial	Year	Researcher	Scatterer	λ (cm)	Wind Velocity (MPH)	Pol	Distribution	Remarks
10	1974	ROSENBAUM * et al	Forest	23	Variable	-	Rayleigh	

<u>Note</u> 1. //&X represent parallel and cross-polarisations
2. "All" includes circular polarisation with //&X polarisations
*. Details of this reference in Part II bibliography

(made on λ = 3cm wherever possible), however few measurements are available at the lower grazing angles necessary for this study. The results of Hayes (serial 4) and Linnell (serial 6) most nearly use parameters of particular interest. Linnell {130} used a 25 metre resolution-cell radar mounted on a 30 metre tower with a vertical beamwidth of 30° and horizontal beamwidth 1.4°. Results included 15-17 dB standard deviation at 0.7° grazing angle and an approximately lognormal distribution. Fishbein et al (serial 8) produced a relationship which gave good agreement with measured power spectra but for deciduous foliage only and horizontal polarisation:

$$p(f) = \frac{1}{1 + \left(f/f_c\right)^3} \qquad \text{(1)}$$

Where $f_c = 1.33e^{0.1356V}$ $\qquad$ V = Windspeed (knots)

6. Wind Effect at Sea. Wind effects on the surface at sea also cause significant radar signal pertubations but since this report is only concerned with radar tracking overland, values for wind effects at sea are not required for the model.

CHAFF CHARACTERISTICS

7. Chaff is a feature of the modern military electronic countermeasures scenario and it is not the intention of this study to examine the possible disturbance effects of chaff on the radar tracking function when streamed or rapidly bloomed, but only as a clutter source. Statistical characteristics of chaff are similar to rain and therefore demand similar signal processing requirements to minimise degradation of radar performance; dependent on RF and the spectral width of the clutter so caused. The instantaneous position of chaff within the radar tracking beam is dependent upon windshear, windspeed and air turbulence. Windshear occurs when the radial windspeed varies

vertically through a radar beam. Dodsworth {131} in a note on windshear refers to {132} which shows windshear to be largely independent of altitude. Ref {133} gives typical windshear values of 1 or 2 m sec $^{-1}$km^{-1} of altitude. A typical MTI canceller can be made to eliminate the mean effect of wind velocity within limits.

8. Beam Broadening, Turbulence and Chaff Fall-Velocity distribution can all be considered as producing independent Spectra, but if all effects are summed, {134}, a Gaussian variance distribution can be taken as a good fit. Beam Broadening is a wind effect (small compared with windshear or turbulence) with a typical sd $\sigma_{beam} = 0.42V_0\theta_2 \mathrm{Sin}\beta$, where V_0 = Wind Velocity, θ_2 = 2 way half power beamwidth (rads) and β = azimuth angle relative to wind direction at centre of beam.

9. Chaff Dispersion. Once dispensed, chaff will disperse under the influence of the local turbulence. Windshear rates in the USA appear to be more severe than those in Europe, perhaps as high as 5 m sec $^{-1}$ km $^{-1}$ in altitude. This is contrasted with a typical maximum chaff fall-rate of 0.7 m sec^{-1} for 3cm wavelength chaff. Under turbulent conditions it has been shown {135} that chaff under the influence of eddy transport speeds can exceed mean wind speeds {136}, and this causes a considerable problem in assessment. Haddow {137}, concluded that the time-distance movement of eddy carried chaff cannot be quantified with any degree of accuracy under all conditions. Two aspects of chaff must however be considered - attenuation and backscatter.

10. Chaff Attenuation. The total RCS of dispersed chaff seen within the radar resolution cell will naturally depend upon a sightline, and, as described in earlier chapters, this may be intermittent, clear with no underlying clutter, or additional to underlying surface clutter. To completely obscure a target, ie to prevent energy reaching the target or

returning to the radar from the target, it can be shown that an exceptionally dense chaff cloud would be necessary. For 2-way attenuation of a uniform chaff cloud of thickness D and chaff dipole density of N per unit volume, then:

$$\text{attn} = e^{-\bar{\sigma}_s \, ND} \left(\text{as a factor}\right) \text{ ------------------ } (2)$$

Where $\bar{\sigma}_s$ is the average radar cross section per dipole. The product $\bar{\sigma}_s N$ is the volume reflectivity density $\Sigma\sigma$ in m^2 per unit volume. Expressing this in dB per metre

$$\text{2-way attn } (dB.m^{-1}) = -4.34 \, (\Sigma\sigma) \text{ ---------- } (3)$$

Where $\Sigma\sigma$ is in units $m^2 \, m^{-3}$. A heavy chaff cloud may comprise a chaff reflectivity density of approximately 3000 $m^2 \, nm^{-3}$ (corresponding to $475 \times 10^{-9} \, m^2 \, m^{-3}$). Therefore to attenuate a radar return by 3 dB would require a chaff cloud of thickness 800 nautical miles (1500 km); clearly an impracticable situation!.

11. Chaff Backscatter. Although signal attenuation due to chaff could occur momentarily under certain conditions when the chaff is self-dispensed and providing the dipole spacings are for a short period of the order a wavelength apart, significant volume attenuation is not a factor of consequence compared with that of backscatter. As implied at para 7 above, chaff may be dispensed by military aircraft so as to bloom rapidly within the radar resolution cell in the hope of breaking tracking capability or at the very least to disturb tracking accuracy by forcing the radar boresight to move to a different tracking centroid. Success or otherwise depends upon many factors in the radar system, such as tracking loop time constants,

resolution cell size, deceleration of the chaff, causing range gate pull-off and the effects caused upon velocity gates, and several other factors {138}.

12. After dispersion the chaff dipoles are randomly distributed by turbulence and researchers {139}, {140}, have discovered as many as six modes of fall when chaff of mixed characteristics is dispensed. Vakin and Shustor {141} suggest 2 main fall modes, one predominantly horizontal and the other vertical. In the absence of shadowing and clumping effects the idealised RCS of a number of dipoles N is:

$$\sigma_{total} = 0.18\lambda^2 N \qquad \text{-------------} \quad (4)$$

However the chaff may not be cut to precisely the radar transmission frequency (particularly with frequency agile radars), all dipoles may not contribute ideally and the chaff material will have some finite conductivity. More recent measurements {142} state that the RCS based on $0.14\lambda^2$ is more likely. RCS varies with dipole thickness as well as length, and maximum RCS can be approximated for practical purposes as:

$$\sigma_{total} = 0.14\lambda^2 EN \qquad \text{---------------} \quad (5)$$

E is the dispersal efficiency (ie a scattering efficiency factor) which may vary between 0.3 and 0.6. Actual RCS acheived per unit weight of dispensed chaff is of course also dependent upon the chaff type.

13. The use of MTI is likely to cancel most of the chaff spectral effects, where low frequency clutter over several KHz may be eliminated by a notch filter. If the entire chaff cloud was subjected to wind gusting in the same direction as an aircraft flying it could be evident in more than one

resolution cell, but it is of diminishing importance when using MTI; and as explained above could not shield radar energy from reaching a target at greater range.

BIRD ECHOES

14. Backscatter from birds can cause clutter at the very low altitudes relevant to this study. Bird clutter (also known as "angels") is briefly explored under the following headings:

a. Height and Velocity distribution.

b. Bird Radar Cross Section and distribution within a population.

c. Radar resolution cell, polarisation effects and spatial density.

Limited measurements were found at $\lambda = 3$cm, but the results of several papers at other RF's are in reasonable agreement.

15. Height and Velocity Distribution. Results from several researchers at different geographical locations show that 80% of all birds are encountered below altitudes of 250 metres and velocities spread between 10 and 25 m sec^{-1}.

16. Bird RCS and Distribution. Mean RCS per single (medium sized) bird is unlikely to exceed 10 cm^2 (pigeon at $\lambda = 3$cm), and in isolation will not be confused with an aircraft RCS. However flocks of birds very close together can reach clutter proportions. The distribution of echoing areas will naturally depend upon the proportion of birds of various sizes in a particular location, but in general will be lognormal.

17. Resolution Cell and Radar Polarisation. Effects of resolution cell size investigated by several workers, eg, {143}, {144}, were in some cases made using a pencil beam tracking radar, but with longer pulse lengths than applicable here. Although there is no accurate prediction of the effect of varying resolution cell size on bird echoes, a smaller cell size would split up larger groups of birds into perhaps a number of adjacent cells, reducing the observed RCS from the flock. Minimisation of bird returns by using circular polarisation has been shown {145} to be non productive since the clutter reduction obtained is approximately the same as for the wanted aircraft targets and hence target filtering is not acheived.

18. Spatial Density. Several researchers have attempted to quantify the density of bird clutter echoes likely to be present within a PPI search area (assuming these are not filtered out by the signal processing). Averaged over one year in UK, the probability of one bird echo per km^2 is slightly less than 0.5%. However, a typical PPI may typically scan 1000 km^2 on each 360^o sweep, and so the probability of some bird activity at most locations is high. With a target tracking radar following at target sight-line rate (or almost stationary for closing or receding targets), birds may enter, leave, or pass through the resolution cell of interest at any time.

CHAPTER SUMMARY

19. Factors selected for incorporation in the overall prediction algorithm from this chapter are:

a. Wind Effects. Values researched by Hayes are used in conjunction with the surface cover discussed at Chapter 4. Hayes uses $F = \frac{1}{1+\left(\frac{f}{9}\right)^3}$ for 9.4 GHz and $\frac{1}{1+\left(\frac{f}{35}\right)^2}$ at 95 GHz, giving, for a windspeed of 12 kts a half-power value of 9 Hz.

b. Chaff Attenuation and Backscatter. Equations (2) and (3) are used for modelling radar signal attenuation due to dispersed chaff between target and radar. Backscatter is incorporated using equation (5), for non-MTI radars only.

c. Bird Clutter - 'Angels'. Bird clutter can be expected in wooded locations and may cause significant signal returns at any time, but more particularly so in migratory periods and at sunrise and sunset. However, it is assumed that once a target is correctly range-gated and velocity-gated by a narrow-beam tracking radar with good discrimination (and since total tracking periods are likely to last for no more than 60 secs for really low level fast targets); then 'angel' effects are minimal for the tracking radar itself. It should be noted that overall system effectiveness may be reduced if 'angels' clutter degrades an area search radar's performance to the extent that "hand-on" to the associated tracking radar is delayed or prevented.

CHAPTER 6

RADAR SYSTEM AND TARGET DETECTION PARAMETERS

1. Preceding chapters have shown that the probability of successful detection and tracking very low - altitude targets is dependent on a great many variables. Additional to the very basic requirement of a direct sightline (or a set of fortuitous diffraction conditions), together with the imposition of clutter - and even jamming signals - the end result is finally dependent upon the radar system characteristics and the given target response. This chapter summarises the radar system parameters considered and their relationship in the radar equations used in the model. Some parameters, when varied slightly, become critical; since the very nature of the study involves targets which are likely to be often on the threshold of detection.

RADAR SYSTEM

2. Within the radar system, account must be taken of the radiation pattern, the transmitter waveform characteristics and the signal processing of the target and clutter returns in the radar receiver. Equations to describe clutter and target power received, receiver noise and jamming effects are fairly standard, however many basic texts generalise certain losses which have been considered here in more detail. Specialised references such as {146} and {147 } give adequate relationships for such topics as aerial motion and jamming. It has been necessary to include the whole range of parameters for a complete model, but it is not the intention to investigate every parameter in detail. Once the model was completed, further investigations, based on the model, were made into diffraction and terrain slope effects (Chapters 7 and 10).

3. Radar system parameters considered, together with typical values are shown below. A sample calculation for this system is shown at Annex G.

	Example System	
	TRACK-WHILE SCAN (TWS)	
a. Aerial Gain (Mainlobe) (dB).	2290	33.6dB
b. Aerial Gain (Sidelobes) (dB)		- 20dB
c. Peak Transmitter Power (Kw)	150	
d. Operating Frequency (GHz)	10 GHz (3cm)	- 15.2dBm
e. Receiver Noise Figure (dB)	8	9.03dB
f. System Losses (dB)	-	12dB
g. Pulse Duration (μ sec)	1	
h. Azimuth & Elevation Half Pwr Beamwidths (deg)	2 x 9	
j. Aerial Polarisation	H	
k. Integration Improvement in S/N ratio dB	-	
l. Radar Aerial Height above datum (m)	20	
m. Radar Type (eg MTI, PD)	PD	
n. Aerial Radiation Pattern	-	
p. PRF (Hz)	12000/10750	
q. Rotation (scan)	60 rpm	
r. Priority Target Size (RCS) (m^2)	0.05	-13 dBm^2
s. Signal Processing	-	

t. Range Accuracy (m)	± 30 (20% of resolution cell)	
u. Velocity Resolution ($m.s^{-1}$)	± 15	
v. Azimuth Resolution (deg)	± 0.5	
w. Frequency Agility	-	
x. Tracker mode (eg monopulse)	TWS	
y. Transmitter Characteristics	4 bursts of 10 pulses per scan	

RECEIVED TARGET, CLUTTER AND JAMMING POWERS

4. At the receiver, target, clutter, attenuation and jamming powers are largely dependent on statistical distribution dependent upon cross section and on PRF, pulse duration, transmitted power, and multipath. The overall signal/noise ratio is given by:

$$\frac{S}{N} = \frac{Sig\ (tgt).\ F\ (Attn\ 2).\ F\ (mult)}{N_{RX} + F_{(attn\ 2)}\ (Sig_{(clt)} + Sig_{(wtr)}) + F_{(attn\ 1)}.\ Sig_{(jam)}} \quad ...(1)$$

where $Sig_{(tgt)}$ = Signal from target

$F_{(attn\ 2)}$ = 2 way attenuation factor

$F\ (mult)$ = 2 way multipath effect

N_{RX} = Receiver Noise

$Sig_{(clt)}$ = Surface Clutter Signal

$Sig_{(wtr)}$ = Clutter Signal (Atmospheric and Weather)

$Sig_{(jam)}$ = Jamming Signal from Target

$F_{(attn\ 1)}$ = 1 way attenuation factor

5. Only the self-screening jamming signal (assumed to be noise) in the main beam is considered. Later it will also be seen that the numerator at (1) can be modified to allow for diffraction and the denominator adjusted to incorporate a factor for terrain clutter variation with slope.

6. Using the standard (unmodified) radar equation (pulsed radar) the received S/N ratio is:

$$\frac{S}{N} = \frac{P_T . G_T .^2 \lambda^2 \sigma_t . n\Sigma_i(n)}{(4\pi)^3 .K.To.b.NF.R^4 .L} \qquad \ldots\ldots\ldots\ldots (2)$$

where

R	=	Target range (m)
P_T	=	Peak Transmitter Power (watts)
L	=	System Losses (but see para 7)
b	=	Receiver noise bandwidth Hz (eg 30.8dB Hz for 1200Hz)
σ_t	=	RCS of target (m^2)
S	=	Minimum detectable signal (watts)
K	=	Boltzmans Constant (- 204 dBW)
To	=	Temperature (^oK) (290^o)
NF	=	Noise Figure
λ	=	Wavelength (m)
$n\Sigma_i(n)$	=	Integration Improvement Factor
G_T	=	Aerial Power Gain (Receiver or Transmitter)

7. <u>Losses</u>. System losses included as L, in this general form, can also be more exactly specified, according to conditions. The following losses are applicable, as appropriate to paragraphs 6 above and paragraphs 9 and 13 below:

L = All losses, both transmit, receive, propagation and beam pattern factor losses.

L_T = All transmitter losses eg waveguide, feeder, radome, TR-switching.

L_R = All receiver losses eg waveguides etc as above for L_T.

L_P = Beam shape and pattern lobing eg tracking radar cross-over losses.

L_a = Two way absorption or atmospheric propagation losses.

L_C = Collapsing losses.

L'_S = Signal processing losses applicable to jamming.

NOTE L'a and L'p are the one-way losses applicable to jamming.

8. G, the aerial power gain, must be modified according to the aerial radiation pattern. For example, if the (fairly common) cosine distribution is used G^2_T becomes $(G_o \text{ Cos}^2 (\pi\sigma/2\theta))^2$ where G_o is the on-axis power gain and θ the one way 3dB beamwidth.

9. Received Surface Clutter. Taking the basic equation the surface clutter power C_p at the receiver input is:

$$C_p = \frac{P_T \lambda^2}{(4\pi)^3} \frac{L_F \; G_T^2 \; \sigma_o \; A_c}{R_c^4} \qquad \text{......... (3)}$$

The illuminated surface clutter area A_c is:

$$A_c = R_c \theta_A \frac{C\tau}{2} \qquad \text{......... (4)}$$

but at very low grazing angles where $\tan \psi < \dfrac{2R_c \sin \theta/_2}{C\tau/_2}$ .... (5)

the clutter area is modified

$$A_c = R_c\, \theta_A \frac{C\tau}{2} \operatorname{Sec} \psi \qquad \text{......... (6)}$$

($\tan \psi < \dfrac{\theta_A R_c}{c\tau/2}$) See Annex B *also*,

giving $$C_p = \frac{P_T \lambda^2}{(4\pi)^3} \frac{L_F G_T^2 \sigma_o \theta_A C\tau \operatorname{Sec} \psi}{2R_c^3} \qquad \text{......... (7)}$$

or $$C_p = \frac{P_T G_T L_T L_a L_R A_e (\frac{C\tau}{2}) \theta_A \sigma_o}{(4\pi)^2 R_c^3 \operatorname{Cos} \psi} \qquad \text{......... (8)}$$

This modifies the basic S/C ratio (target/clutter ratio)

$$\frac{S}{C} = \frac{\sigma_t}{\sigma_o \frac{C\tau}{2} \theta_A R_C} \quad \text{into} \quad \frac{L_S L_P L_F \operatorname{Cos} \psi \sigma_t}{R(C\tau/_2)\, \theta_A \sigma_o} \qquad \text{......... (9)}$$

where σ_o = Average surface clutter per unit area (m^2)

$\bar{\sigma} = \sigma_o R_c \theta_A \frac{C\tau}{2}$

θ_A = Azimuth 3dB beamwidth, A_e = Effective Aerial Aperture

L_F = Loss factor in clutter receive chain (not necessarily the same as L in eqn (2)) (non-dimensional factor)

C_p = Received clutter power (watts)

R_c = Range of clutter cell

$\bar{\sigma}$ = Average clutter RCS

σ_t = Target RCS

10. Detection Range in Clutter. It is often convenient to assess the detection range in clutter simply by re-arranging (9). Calculations for an example radar system are included at Annex G.

11. Received Volume Clutter. Volume clutter is a combination of back-scatter, attenuation and chaff (see chaps 3 & 5).

For rain:

$$Sig_{(wtr)} = \frac{0.93\, P_T\, G_T\, C\tau\pi^4 Z}{128\, \lambda^2 R^2} \quad \text{......... (10)}$$

where $Z = 200\rho^{1.6}$ (See Chap 3).

It is assumed that only the single resolution volume containing the target is contributing volume clutter. Skolnik {148} produces a composite expression incorporating both attenuation and backscatter from the two terms at (12):

$$(\frac{S}{C}) = \frac{P}{N_r} = \frac{K_1\, \sigma_t}{R^4\, N_r} \quad \text{......... (11)}$$

where P = received echo power from target

$$K_1 = \frac{P G_T^2 \lambda^2}{(4\pi)^3}$$

N_r = receiver noise power

and

$$\frac{S}{N} = \frac{P_r}{N_r + N_c} = \frac{K_1\, \sigma_t\, \exp(-2\alpha R)}{R^4\, (N_r + N_c)} \quad \text{......... (12)}$$

where N_C = Clutter backscatter power

α = Attenuation coefficient

12. Chaff Clutter. Chaff backscatter is modelled at equation (5) Chapter 5.

13. Received Jamming Clutter. Although the foregoing clutter sources are almost always present, jamming will only apply to specific situations, and so the computer model can be initialised to include or ignore the jamming segment, as necessary. If the radar is modern, and assumed to have minimum sidelobes, with the mainlobe on the target all noise jamming energy enters along, or close to the mainbeam axis. Allowing for all losses the equation for signal to jamming noise ratio is:

$$\frac{S}{J} = \frac{P_T G_T L_T L'_p L'_c L'_s (\sigma_t)}{4\pi B_N R^2_J \qquad (P_J G_J)} \quad \text{.........} (13)$$

where R_J $(=R_t)$ = Range to jammer (ie target)

G_J = Jammer Aerial Gain

P_J = Power of jammer per unit bandwidth (watts for Hz)

B_N = Noise bandwidth of receiver (before detection)

Since only self screening jamming is considered R_J and R_t are equal.

TARGET CHARACTERISTICS

14. Targets are generally taken to comprise a predominant (steady) signal

re-inforced by many small reflectors (ie Ricean distribution of reflectors). Target fluctuations are taken to be independent scan to scan and based upon Swerling Type 3 detection probability.

$$p(\sigma) = \frac{4\sigma}{\sigma_{AV}^2} \exp\left(-\frac{2\sigma}{\sigma_{AV}}\right) \qquad \text{......... (14)}$$

for $\sigma \geq o$ (= 0 elsewhere)

where σ_{AV} is the average target RCS (m^2) and σ the instantaneous RCS. All relevant priority targets are 'aspect sensitive', as shown at fig 1, where a 0.05 (m^2) RCS target head-on can produce an enormous RCS on the beam (crossing target). Since the overall model detection probability is roughly the probability (excluding sightline blocking) that the target return signal will cross a detection threshold with a sufficient S/C ratio; it is seen that RCS can be a critical parameter. Because of the uncertainty of the instantaneous value of RCS, present when an aircraft is ostensibly in straight and level flight (and even more variable when the aircraft is deliberately manoeuvring), target RCS must be considered statistically. A Rayleigh distribution for larger targets has been found suitable by Ament et al {149} but aircraft and missiles of small RCS tend towards higher order chi-square functions. Typical radar cross sections for small aircraft range from 1.2 m^2 (head-on) to 20 to 60 m^2 (beam-on), giving a median of 1.3 to 5m^2 over 360^o and all roll plane aspects. For the purpose of the model 0.05 to 1m^2 has been used for head on targets and 4m^2 for beam targets. It is further assumed that the targets of interest are designed with profiled structures to minimise RCS and may comprise dielectric panels and possibly radar absorbent coating for a proportion of the observed echoing skin area (see also Chap 4 and Annex E).

15. RCS Spectra. Turbine and/or Propeller, and airframe spectra investigations are outside the scope of this report. Briefly, the airframe spectrum is due to the relative motion between target scattering points, and although an RCS range (eg 1.3 to $5m^2$) was easily selected for assessment purposes, the selection of a suitable airframe spectrum (due to random and systematic changes) is far more difficult. According to {150} the width of the airframe spectrum has the relationship:

$$\Delta f = K \left(\frac{Lo}{\lambda}\right) \left(\frac{\Delta\theta}{\Delta t}\right) \qquad \text{......... (15)}$$

With smaller targets likely to have a greater random motion than large aircraft. Further spectra information is available from the reference {151}. Measurement of the rate of change of target aspect ($\Delta\theta/\Delta t$) is complex although the factor L_o/λ, the characteristic length of the target, is more readily available. K is a proportionality constant.

16. Frequency Agility. Frequency agile radars have improved performance against fluctuating targets since the probability is reduced that the target will be at an aspect angle which gives a very low RCS or a null. Frequency agility can also reduce range and tracking errors caused by target glint and multipath (see Chap 9). Improvements in detectability of several dB have been measured when using frequency agility {152} at 10 cm wavelength. At the same time frequency agility can be used to decorrelate distributed clutter echoes (see Chap 4). The model incorporates an allowance, if required, to improve detection probability for frequency agile systems.

CHAPTER SUMMARY

17. Relationships stated in the chapter for Received Target power, Surface Clutter power, Jamming power, Signal/Noise ratio, Volume Clutter and Fluctuating target characteristics are incorporated in the model.

18. Radar Cross Section. Experimental distributions made by the US Applied Physics Laboratory indicate no simple solution for RCS modelling of all aircraft aspects. Much of the uncertainty in modelling RCS lies in the observation time used to obtain the distribution. Although the Rayleigh distribution is suitable for large aircraft, RCS modelling is necessarily a coarse procedure. Cumulative detection curves can be used if detection is required on an approaching target before it reaches a certain range. Missile targets have larger mean to median ratios; a log-normal distribution is more accurate in this case than Rayleigh. Equation (14) is used, for example, based on an average RCS with σ_t varied using a random number generated in the model to simulate target glinting. Distributions, Rayleigh or Log-Normal, are selected according to target type and appropriately for fixed RF or frequency agile radars, ie change of Swerling case.

19. Although the RCS of future aircraft will be reduced by careful design, stealth - low reflectivity coating, perhaps to lower than OdBSm; the range of terrain RCS (per m^2) may vary between - 30dB to possibly +30dB with -15dB as a typical average (see Chapter 4). A clutter signal may be present even when clutter from the target range gate is

masked but enters due to sidelobe clutter reception. Experience has shown that parameters such as target doppler, beamwidth (azimuth resolution) or range resolution may not be sufficient to separate targets from clutter, particularly at low level. The fluctuating target RCS can therefore be critical in the detection and tracking process since a tactical aircraft RCS may be of the order 10 to 20 dBSm.

20. Fluctuating Target. The problem of fluctuating target returns is closely related to FAR (see Chapter 4) and further considered at Annex E, where it is shown that a target fluctuating with low amplitude peaking is more easily detected at short range, while a more excessively fluctuating signal is more easily detected at longer range.

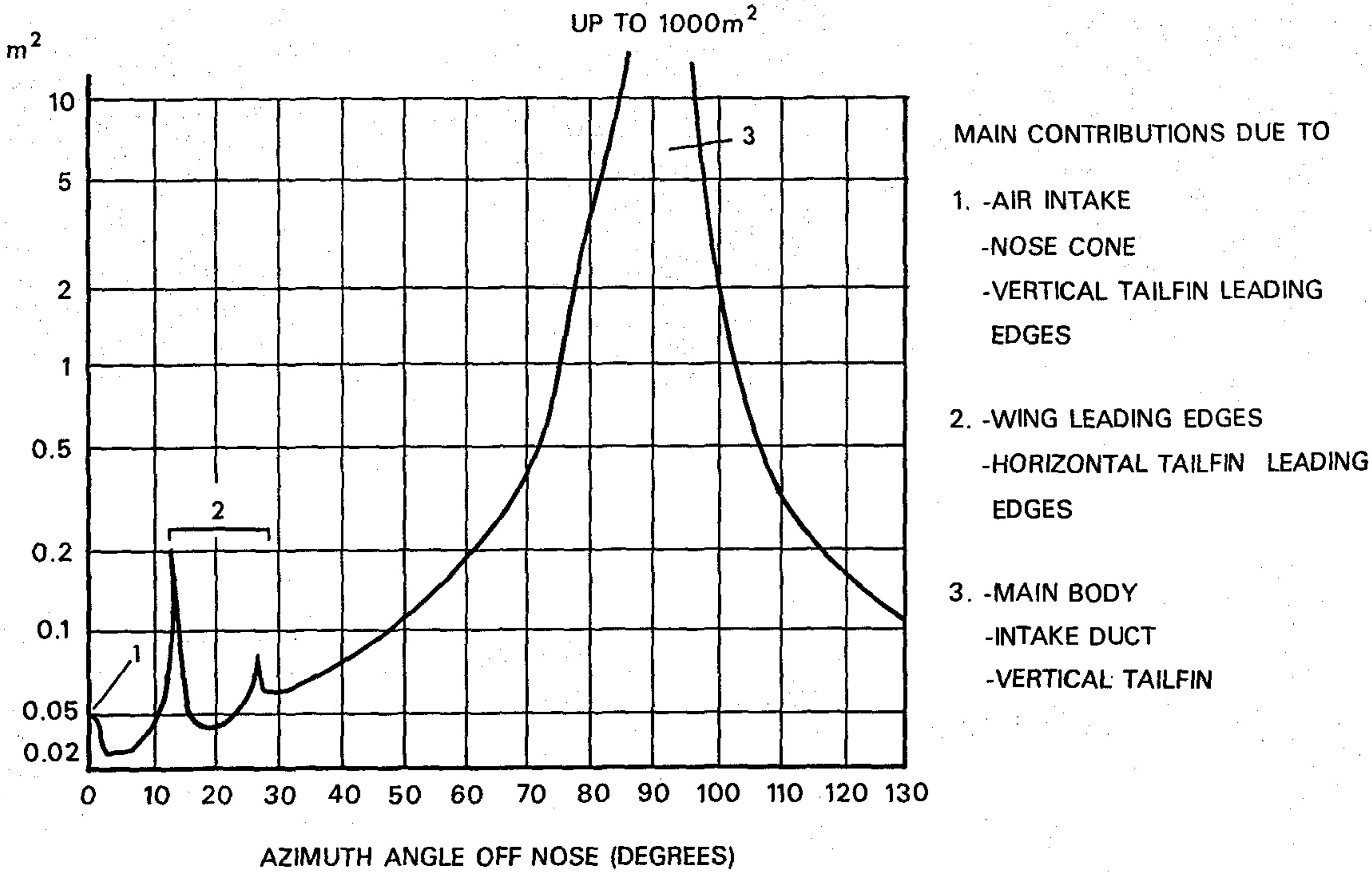

FIG 1 RADAR CROSS SECTION (RCS) - CRUISE MISSILE TYPE TARGET

CHAPTER 7

DIFFRACTION

1. Computer-aided and manual literature searches have revealed several comprehensive reports covering diffraction of data links at UHF and VHF, but with very limited research at microwave link frequencies. No detailed reports could be found on low level tracking radar diffraction, indeed practical prediction algorithms are thought not to exist. As recently as 1980 a report from the Lincoln Laboratory, MIT, {154}, stated "diffraction of radar transmissions over terrain obstacles has not received as much attention as refraction"; and, "diffraction has effects which should worry military mission planners"(military context of planning low level terrain-routing profiles to avoid detection). Also, "some obstacle problems remain unsolved - the debate continues over the proper way to estimate losses over terrain obstacles". To complete the radar performance prediction algorithm a detailed investigation is clearly necessary into diffraction effects.

DIFFRACTION PARAMETERS AND AIMS

2. There are several approaches to the theory of diffraction, including extended wave theory. The following research aims were selected:

a. Research the nature of diffraction in practical terms.

b. Determine the criteria under which diffraction is likely to enhance low level tracking.

c. Consider the substitution of terrain with cylinders or baffles for diffraction modelling purposes.

d. Consider diffraction effects with reference to modifications by reflection and multipath.

e. Determine diffraction path radar power values on outward and return paths.

f. Generate a diffraction subroutine for the main radar performance prediction algorithm.

g. Produce a subroutine capable of scanning a land area, given the terrain data base, and determining a general probability of diffraction from the nature of the surface profile for given target altitudes.

KNIFE-EDGE DIFFRACTION

3. Assuming that the local terrain does not support reflection, knife edge diffraction approximations are often used with the geometry shown at figures 1 and 2. With the radar transmitter near the earth's surface, and the target airborne (unlike the data-link case); the diffraction angle can be considered at figure 2 as fixed, while distance d_2 and hence R are reduced. This has the effect of moving the target upwards on the figure to the dotted position, changing d_2 to d_2^1 and R to R^1. From Fig 1, if the radius of the assumed diffraction edge (cylinder in practice) is large compared with λ, then:

$$\frac{{E_S}^2}{{E_I}^2} = \frac{1}{2\pi k R \alpha_1^2} = \frac{R}{2\pi k h^2} \qquad \text{-----------------------} \quad (1)$$

Where $k = \frac{2\pi}{\lambda}$, E_S = Scattered intensity from the target and E_I = Incident intensity. R, h and α_1 are shown in the figure. However, both figures are essentially the same as explained above.

4. The geometry at figure 2 is used to derive the further approximations at para 5 below, but at this stage it is necessary to discard the negative knife edge situation (ie diffraction ridge below radar horizon) since a direct sightline would exist simultaneously; hence detection capability would not be significantly impaired. Nevertheless, it is recognised that if the diffracted ray received via a negative knife edge exceeded the signal strength of the direct ray, an angle tracking error could occur.

5. Taking v as the dimensionless parameter of the Fresnel - Kirchoff diffraction formula (see Annex C) then:

$$v = +2\sqrt{\frac{\Delta r}{\lambda}} \qquad \text{------------(2)}$$

Where $\Delta r = r_1 + r_2 - R$ (or R^1 if the airborne target is used)

$$\text{or } v = +\sqrt{\frac{2R\alpha\beta}{\lambda}} \qquad \text{------------(3)}$$

$$\text{or } v = +\, h_t\sqrt{\frac{2R}{d_1 d_2 \lambda}} \qquad \text{------------(4)}$$

Where h_t is the obstacle height

α, β and θ are in radians

λ, R, d_1 and d_2 are in consistent units.

6. Comparison of the free space and diffracted fields to obtain the diffraction loss ratio A(v) gives :

$$A(v) = -20 \log_{10} |F(v)| \, dB \qquad \text{------------(5)}$$

$$\text{Where } F = \frac{1-j}{2} \int_{v}^{\infty} \exp\,(j\pi u^2/2)du \quad \text{-----(6)}$$

as v becomes large and positive $|F(v)| \longrightarrow 2^{\frac{0.5}{2\pi v}}$

$$\text{and } A(v) \text{ becomes approx} \quad -20 \log_{10} \left[\left(\frac{d_1 + d_2}{d_1\, d_2}\right)^2 \frac{\lambda^{\frac{1}{2}}}{2\pi\theta} \right] dB \quad \text{----(7)}$$

θ is the angle of diffraction.

7. For a single edge diffraction obstacle Deygout {155} uses a criteria to characterise the diffraction path to check that the first Fresnel Zone, of radius r, is not obstructed. Assuming $\lambda << h_t < \frac{d_1}{10}$ and $\lambda << h_t < \frac{d_2}{10}$, at a frequency f(MHz) separated by R kilometers, the free space loss is:

$$a_o = 32.5 + 20 \log_{10} f + 20 \log_{10} R \text{ (dB)} \quad \text{-----(8)}$$

Expressing the diffraction loss as a function of $\frac{h_t}{r}$

Where $r(m) = 548 \sqrt{\frac{d_1\, d_2}{f(d_1 + d_2)}}$ using f(mHz), d_1 d_2 (km)

$$\text{for } h_t > r,\ a_m = 20 \log_{10} \left(\frac{h_t}{r} + 16\right) \quad \text{-----(9)}$$

Where a_m = diffraction loss; total loss = $a_o + a_m$

8. When $\frac{h_t}{r}$ is used the results differ by $\sqrt{2}$ (see equation for v below). For comparison purposes in the use of v fig 3 shows the diffraction loss while figure 4 shows diffraction loss a_m against $\frac{h_t}{r}$ Again, using the diffraction loss ratio and including phase angle results and practical values for v:

$$A(v) = -20 \log_{10} \left|\frac{E_o}{E}\right| = -20 \log_{10} a(v) \qquad (10)$$

Where $E = E_o \, a(v) \exp\left[-j\phi(v)\right]$

$\Phi(v)$ = Phase lag of diffracted field with respect to free space field.

E, E_o respectively diffracted and free space fields

$a(v) = \left|\frac{E_o}{E}\right|$

$\phi(v) = 90v^2$ (deg) ie, the phase difference in degrees attributable to the path length difference Δr.

9. Ref {156} gives typical values for $v \geq 0$, $v < 0$ and $A(v)$ versus v:

$$A(v) = 12.953 + 20 \log_{10} v \quad \text{for } v \geq 2.4 \qquad (11)$$

$$A(v) = 6.02 + 9.11v - 1.27v^2 \quad \text{for } 0 \leq v \leq 2.4 \qquad (12)$$

$$A(v) = 6.02 + 9.0v + 1.65v^2 \quad \text{for } -0.8 \leq v \leq 0 \qquad (13)$$

and Larson {157} gives:

$$A(v) = 6.0 + 11.28v + 4.28v^2 \quad \text{for } -1.4 < v < 0 \qquad (14)$$

10. Fig 3 shows the variation of A(v) and phase shift with v, and Table 1 gives a selection of practical values for typical low level targets. In practice it is assumed that target altitudes vary between 30 m and 60 m and that the radar aerial will be no higher than 30 m AGL.

Obstacle (Ht(m)	d_1 (Km)	d_2 (Km)	v
50	15	15	4.7
40	15	15	3.5
30	15	15	2.6
20	15	15	1.7
50	25	5	8.2
40	25	5	6.5
30	25	5	4.9
20	25	5	3.2
500	10	20	50.0
500	25	5	141.0
250	15	15	14.1

Table 1 Example Values -v- for given Obstacle Heights and Ranges

INTERPRETATION

11. Where knife edge approximations are used, based on the relationship at Annex C, and the simplified criteria as used at paras 5 to 10; predictions have been found to be several dB above the measured values {158}, {159} and {160}. However, when account is taken of the practical situation, ie rounded hillcrests, as is so often the case instead of idealised knife edges, {161}, {162}, {163}, and a rough conducting surface is present; then {164} found general agreement with the conventional Fresnel-Kirchoff approach of ignoring the obstacle thickness. However {165} states that an additional or "excess loss" is largely dependent upon the crest curvature, the angle of diffraction and wavelength, but almost independent of distance for a given angle of diffraction. The Fresnel integral is sometimes produced as a set of curves or tables.

DIFFRACTION OVER ROUNDED HILLCRESTS

12. Up to 10,000 MHz it is considered at {166} that any rounded obstacle can be approximated by a knife edge, providing its radius of curvature R_c, satisfies:-

$$R_c < \frac{\lambda}{\theta^3} \quad 2.10^{-3} \text{ metres} \quad (\theta \text{ in rads}) \qquad \text{------(15)}$$

The geometry used for rounded hillcrests is shown at Figure 5, and {167} also suggested that the radius of curvature may be estimated by:

$$\text{Radius (m)} = \frac{2D_S \, d_{stx} \, d_{stgt}}{\theta(d_{stx}^2 + d_{stgt}^2)} \qquad \text{------(16)}$$

Where D_S = distance between transmitter and target horizons

($ie D_S = d - d_{Ltx} - d_{Ltgt}$)

d_{stx} = distance between transmitter horizon and horizon ray intersection points.

d_{stgt} = distance between target horizon and horizon ray intersection points.

A simplified solution {168} for rounded hillcrests assumes each obstacle to be represented as a cylinder of radius equal to the radius of curvature at the obstacle top. The following parameters are used and marked where appropriate on Fig 5.

H_1 Obstacle height

$$R_1 = \left[\lambda d_1 d_2/(d_1 + d_2)\right]^{\frac{1}{2}} = \text{First Fresnel zone radius}$$

(d_1, d_2 as at Fig 2.)

$\alpha = \lambda^{2/3}\, r_1^{\,1/3}/R_1$, where r_1 is the radius of curvature at the top of the obstacle, α is a curvature factor.

The main obstacle, assuming several lie on the path, is the one with the largest $\frac{H_1}{R_1}$ value. Figure 6 shows the relationship between $\frac{H_1}{R_1}$ and attenuation for various curvature factors.

EFFECTS OF SLOPE INCLINATION AND ROUGHNESS

13. Practical implications of diffraction are considered later in the chapter, but slope inclination and roughness should be mentioned since waves incident upon diffraction ridges may be expected to suffer depolarisation due to these factors. Experiments by Carlson {169} revealed no appreciable complications (in diffraction effects) by terrain scattering, but his conclusion may only have been applicable to conditions pertaining locally at the time. Similarly it is difficult to quantify the effects of foreground scattering and also of interference diffraction signals at longer ranges.

EFFECTS OF FREQUENCY ON DIFFRACTION

14. Delaney {170}, has shown that lower radar frequencies are better than higher frequencies in terrain where diffraction is dominant. Other results show that the coverage of lower frequency radars in reflection-dominated terrain can be quite adequate if sufficient power is transmitted.

RADAR POWER

15. In terms of radar power, the power at the target via the diffraction path will be:

$$P_{t_{gt}} = P_T G_T G_R \frac{\lambda^2}{64\pi^2 \, d, \, d_1 \, d_2 \theta^2} \qquad \text{------------------------(17)}$$

Troposcatter power is not considered here when using radars with narrow beams in the vertical, it could however be a contributory factor under other circumstances. Signals returned to the tracking radar are assumed to travel the same path in reverse and suffer therefore the same diffraction loss.

CHAPTER SUMMARY

16. By careful interpretation of the few available results it is found that adequate diffraction loss calculations can be made - subject to the existence of the necessary site-specific target, radar and terrain data. However, it is possible that the existence of diffracting paths over mobile or small fixed obstacles, close to the radar site, cannot be accurately assessed unless diffraction measurements are made in situ. Precise obstacle positions will be unknown and will not, of course, be recorded in the terrain data base overlay. Indeed many such objects would not be included - such as isolated buildings, unless the data base was very finely spaced.

17. It is shown to be possible to predict the likelihood that diffraction-path tracking may take place; by incrementally testing the data base azimuth profile using equations (15 and 16) together with the necessary radar receiver sensitivity values, radar transmission and target parameters. A segment of the computer program at Chapter 11 was developed to produce a plan output plot of the first assessed diffraction ridge - behind which a target would not always be invulnerable to radar tracking. (See also page F-10).

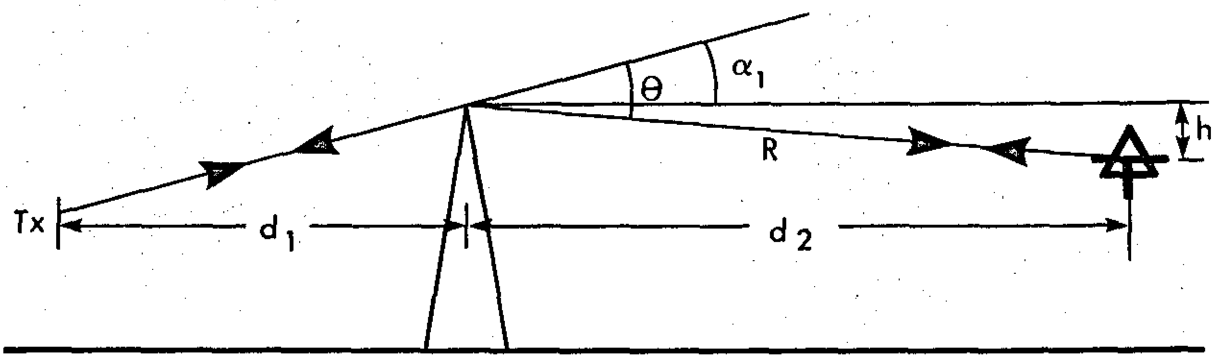

FIG 1 BASIC DIFFRACTION GEOMETRY

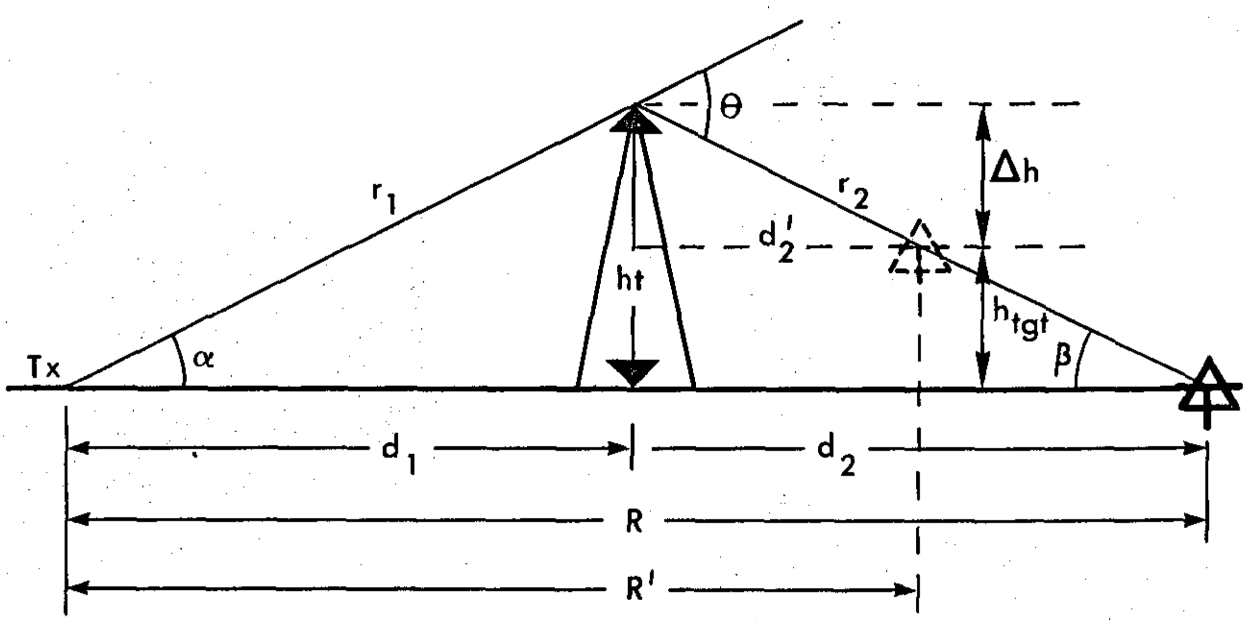

FIG 2 KNIFE EDGE GEOMETRY

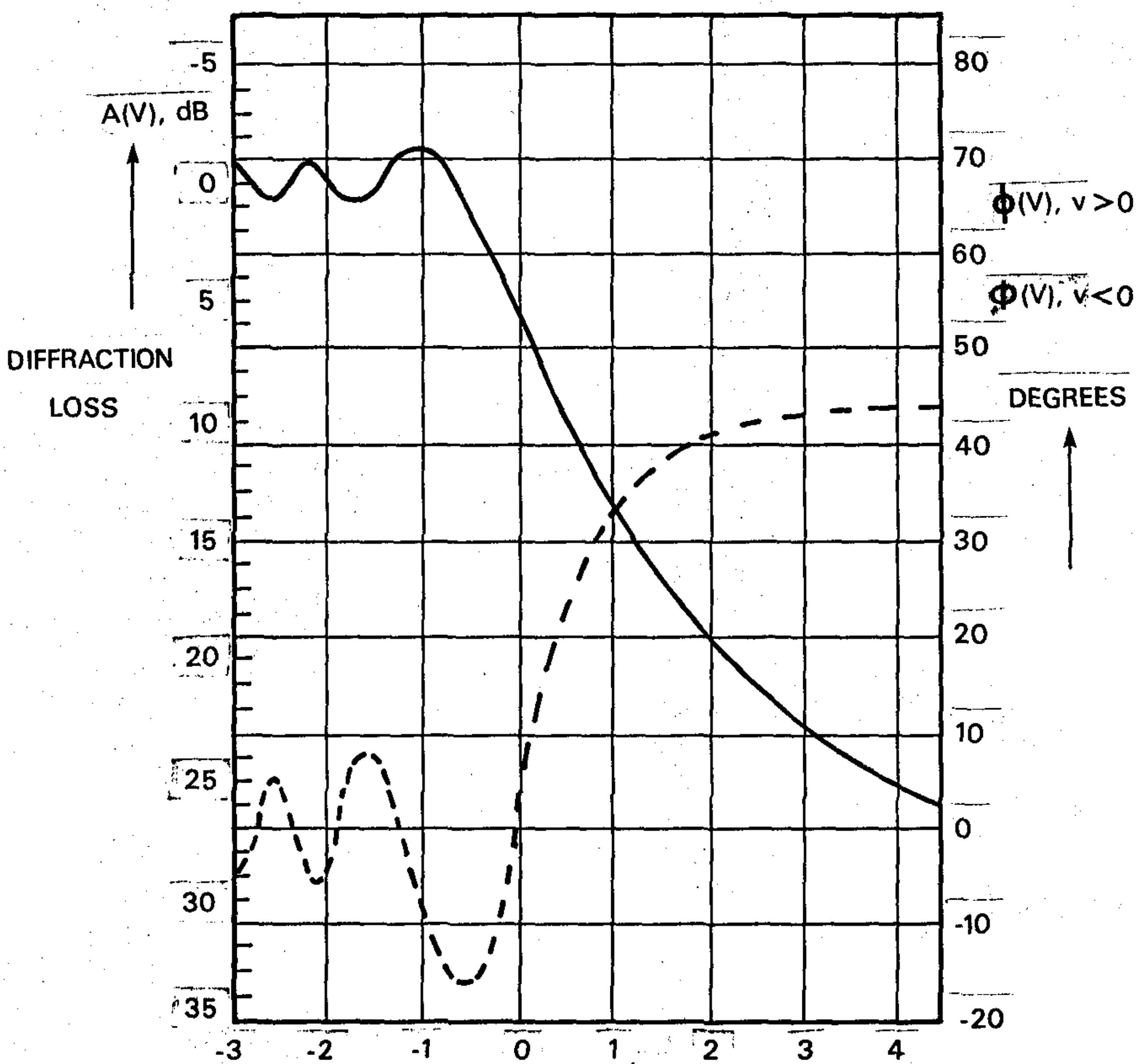

$$\left(\frac{k r_1}{\pi\,(r_1 + d_2^1)\,d_2^1}\right)^{\frac{1}{2}}\Delta h$$ NORMALISED DIST ⟶ V

NOTE: FOR LARGE V (SAY >2), $A(V) = -20 \log \sqrt{2\pi V}$

AND $\phi(V) = 45°$

FIG 3 PHASE LAG OF DIFFRACTED FIELD & DIFFRACTION LOSS WITH VARIATION OF V OVER KNIFE EDGE

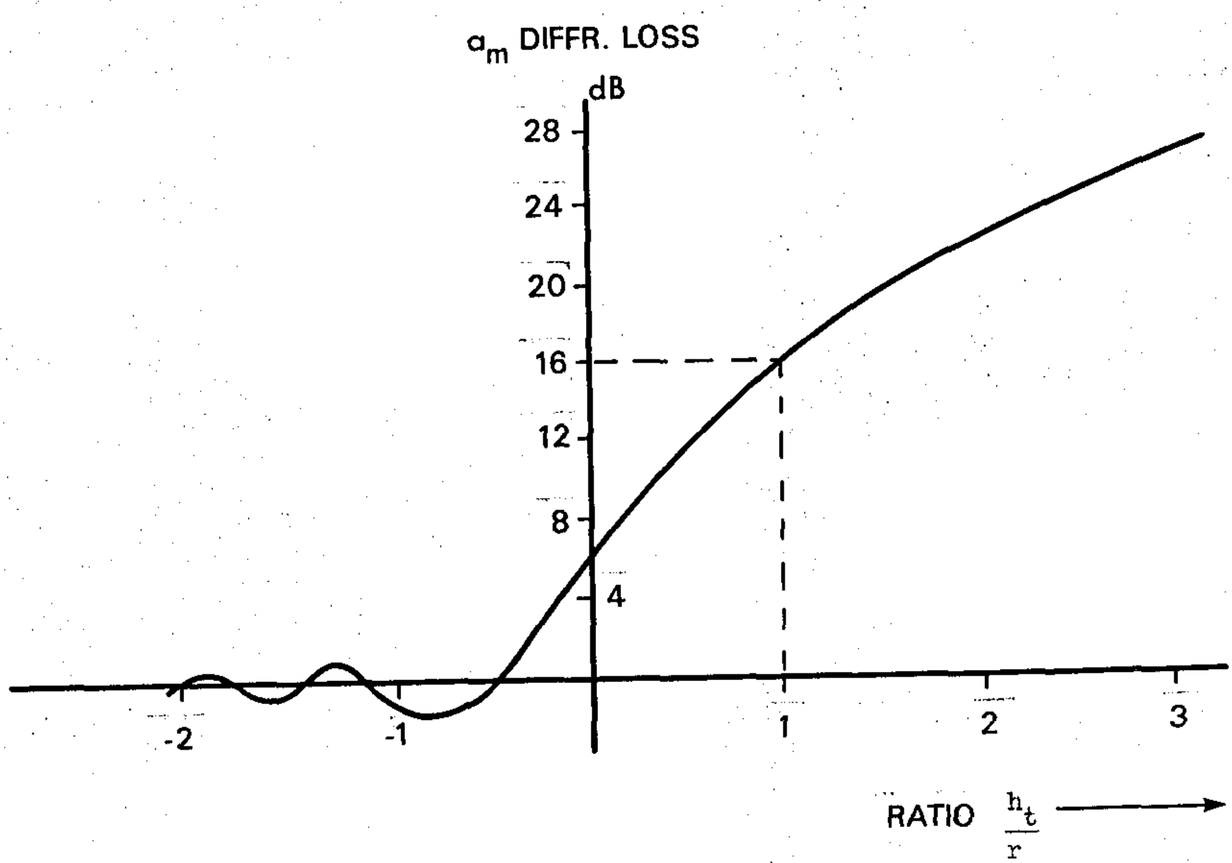

FIG 4 DIFFRACTION LOSS v OBSTACLE HT & FRESNEL ZONE RATIO

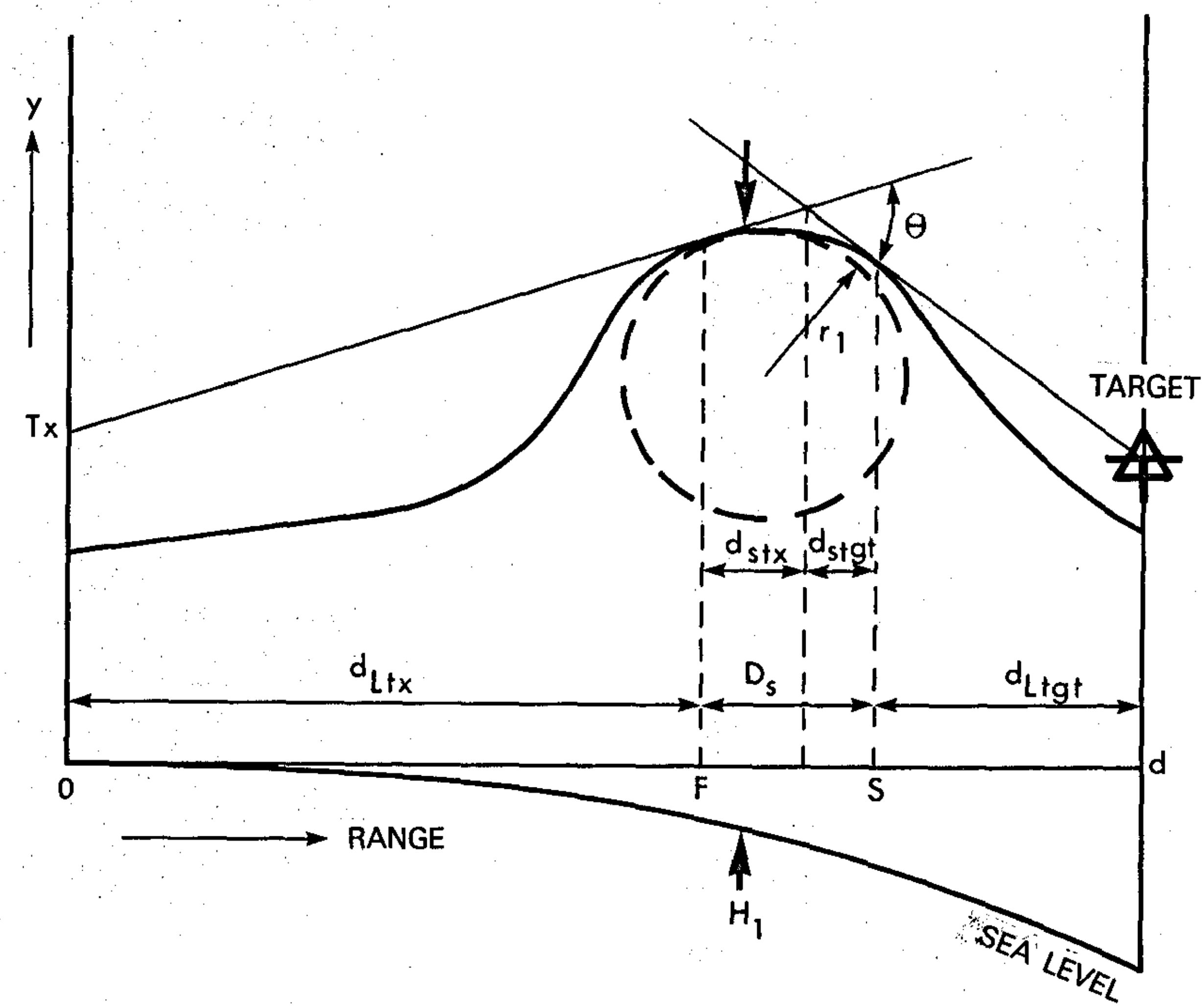

FIG 5 GEOMETRY OVER ROUNDED OBSTACLE

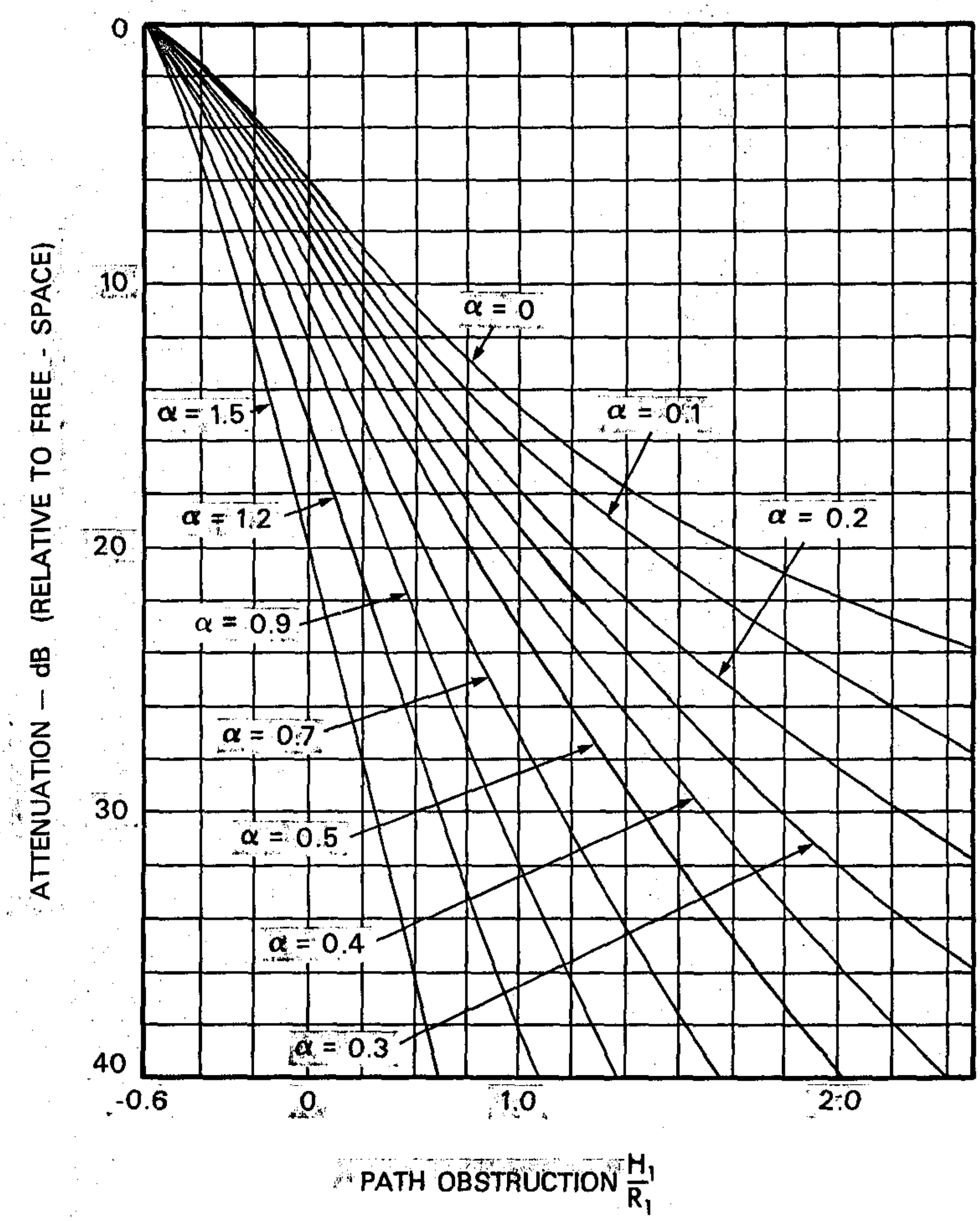

FIG 6 DIFFRACTION OVER ROUNDED OBSTACLES

(After de ASSIS {153})

FIG 7 ONE-WAY DIFFRACTION LOSSES FOR AIRCRAFT ALTITUDE REDUCTION Δh

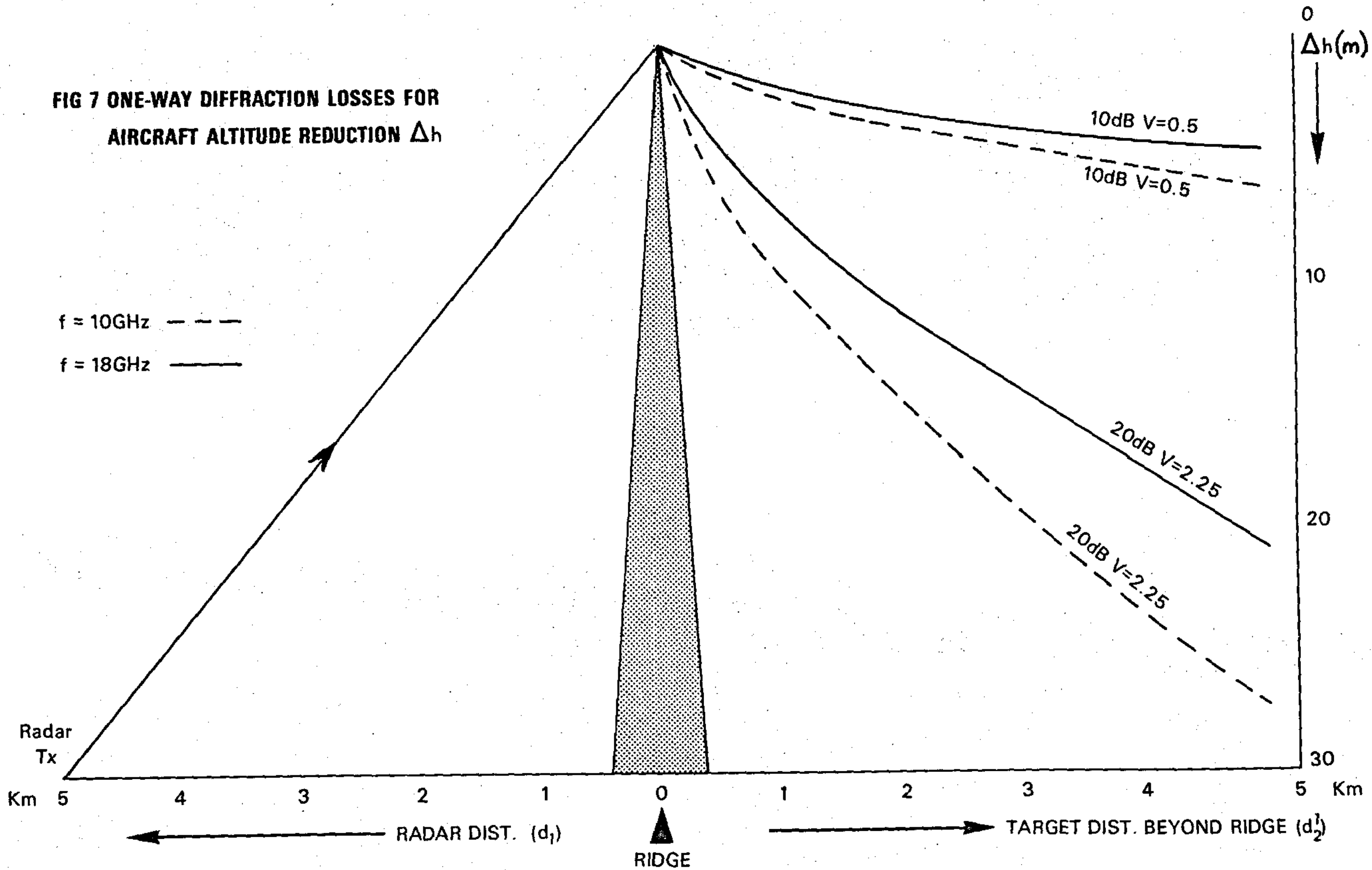

CHAPTER 8

PROPAGATION - REFRACTION AND REFLECTION

1. A number of standard texts and research papers are available on refraction and reflection, covering these phenomena in detail. However, some aspects are especially pertinent to the low level tracking case and so refraction and reflection are studied as a preliminary to the complete propagation model, which will finally include multipath and diffraction.

REFRACTION

2. Radar waves are bent primarily by water content in the atmosphere, which is normally denser at lower altitude. Two practical effects are considered here:

a. Radar range may be considerably increased by refraction under certain conditions; where the system may be able to detect targets around the curvature of the earth.

b. Tracking radars in particular, may obtain a false target elevation angle by measuring the tracker dish boresight angle - which is in fact not the true target sightline (Fig 1).

3. Radar wave refractivity due to the variation in the velocity of wave propagation is given by{172} as:

$$(n-1)\,10^{6} = N = \frac{77.6p}{T} + \frac{3.73 \times 10^{5} e}{T^{2}} \quad \text{------------} \quad (1)$$

Where N = refractivity

p = barometric pressure (mb)

e = partial pressure of water (mb)

n = atmospheric refractive index at zero altitude

T = Temperature (^{o}K)

The effective earth's radius is given by

$$a = a_o \left[1 - 0.04665 \exp (0.005577 N_s)\right]^{-1} \text{ km} \qquad \text{---------(2)}$$

Where N_s = refractivity at surface of earth.

If a_o, the actual earths radius is taken as 6370 km;

for $N_s = 301$, $\frac{a}{a_o} = \frac{4}{3} = k$, a good approximation to conditions in Europe.

4. Low Level Targets. Refraction effects can be significant at low grazing angles. For targets at 300 metres (or less), the 4/3 earth correction is an adequate approximation. Since radar ranges are limited for this study, extended refraction (ducting) is not relevant. A representative refractivity model from Bean and Thayers {173} is :

$$N = N_s \exp \left[- C_e \ (h_{tgt} - h_{tx})\right] \text{---------------------------} (3)$$

Where $C_e = \ln(N_s/N_1)$ N_1 = refractivity at 1 km altitude

h_{tgt} = altitude of target (m)

h_{tx} = altitude of radar aerial (m)

At the earth's surface a typical value for n is 1.0003, with a decrease rate of approximately 4×10^{-8} per metre increase in altitude. Computed values for low level targets and various radar mast heights are at Table 1.

Altitude (m)		Refractive Index (n)
Target	Radar	
30	0	1.0003
60	0	1.0006
30	4	1.0002
60	30	1.0003
30	30	1.0000
60	4	1.0006

Table 1 Variation of Refractive Index with Radar and Target Altitude

5. Refraction Errors. From {174} and interpolation from CRPL National Bureau of Standards data for appropriate target altitudes and given radar grazing angles, the vertical error values were obtained at Table 2.

GRAZING Angle (deg)	Angular Error (m rad) for Target Altitude (m)				
	0m	30m	60m	150m	300m
0	1.6	1.7	1.72	1.75	1.8
1	0.3	0.32	0.33	0.37	0.42
3	0.13	0.13	0.135	0.15	0.17
5	-	-	-	-	0.1

Table 2 Elevation Angular Error Due to Refraction

Taking, for example, the angular error and converting to altitude error at 17 km range a 300 m target at 1° grazing would be measured with a vertical error of 7.2 metres; or 0.5 metres for a similar target flying at 30 m. In each case the angular error is the angle between a straight line to the target and the apparent target elevation. Under refraction conditions the radar always measures a greater angle (ie greater altitude) of sightline than is actually the case.

6. Range Errors. Atmospheric refraction may also cause small errors in range, as shown at Table 3. To obtain the 2-way transmission path range errors the figures should be doubled.

Grazing Angle (Deg)	Range Error (m)
5	1.5
3	3
1	6
0	22

Table 3 Range Errors for Variation in Grazing Angle

7. The errors in both range and elevation angle, though small, are nevertheless present and may become significant where a tracking radar is being used in a commanded guided weapon system; since target position is degraded and eventual commanded miss distance may exceed the radius of effect of the weapon's warhead.

PROPAGATION OVER TERRAIN PROFILES

8. Spot terrain heights must be adjusted to allow for the effect of the average curvature of the earth's surface, as well as the refraction of the radar waves. Modified terrain height (y_i) at any distance (x_i) from the

radar location, taken along a great circle path is the height above a plane which is horizontal at the transmitter:

$$y_i = h_{si} - \frac{x_i^2}{2a} \quad \text{------------------------------------} (4)$$

Where h_{si} is the unmodified terrain spot height above sea level (m)

a = effective earths radius (km)

A proof of the validity of this approach is at {175}, and the geometry is shown at Figure 2 for a clear path.

9. Obstructed Sightline. When a path is obstructed the horizon ray grazing angles from the radar to the obstruction and from the target back to the obstruction are respectively given by:

$$\theta_{tx} = \frac{h_{L\,tx} - h_{tx}}{R_{L\,tx}} - \frac{R_{L\,tx}}{2a} \quad \text{------------------------------} (5)$$

and

$$\theta_{tgt} = \frac{h_{L\,tgt} - h_{tgt}}{R_{L\,tx}} - \frac{R_{L\,tgt}}{2a} \quad \text{-------------------------} (6)$$

Obstructed target sightline geometry is shown at Figs 3 and 4. Note that θ_{tx} and θ_{tgt} could be positve or negative - although a negative situation is unlikely to arise here since a levelled tracking radar does not usually depress below its nominal minimum tracking angle. Subsequent discussion of geometry will use the same notation as at (4) and (5) where:

$h_{L\,tx}$ and $h_{L\,tgt}$ = the horizon range of terrain obstacles from transmitter and target respectively. h_{tx} and h_{tgt} = radar transmitter and target heights respectively.

10. The geometry for obstructed sightlines is only of significance for tracking radars if diffraction occurs. In this case a single 'knife-edge' formed by terrain must be located beneath point X on fig 3 or 4. Multiple knife-edge diffraction is also considered at Chapter 7.

11. Unobstructed Sightlines. Figure 5 shows the situation where radars could be sited on a mast (at height h_{tx}) with a target flying at low level or nominally at surface level, (Point Q); or the target clutter on the surface (at point Q). It is assumed that targets will always be outside the Fresnel Zone since for $\lambda = 0.03$ m and for an aerial dimension D = 3 m, $\frac{2D^2}{\lambda} \approx 600$ m; for D = 4 m the Zone boundary would be about 1 km.

REFLECTION

12. Radar wave reflection theory is well covered in {176} and {177}. It is of prime importance under conditions of approximately plane (flat) reflecting surfaces such as the sea and under more isolated cases overland at low grazing angles. The reflection coefficients for vertical and horizontal polarisation respectively are:

$$\bar{R}_V = R_V e^{J\phi V} = \frac{\bar{n}^2 \sin\psi - \sqrt{\bar{n}^2 - \cos^2\psi}}{\bar{n}^2 \sin\psi + \sqrt{\bar{n}^2 - \cos^2\psi}} = \frac{\sin\psi - Z}{\sin\psi + Z} \qquad (7)$$

where $\bar{n}^2$ is defined at Annex B para 11.

$\bar{n}$ = complex dielectric const. of surface

ψ measured perpendicular to surface normal

$$Z = \frac{\sqrt{\bar{n}^2 - \cos^2\psi}}{\bar{n}^2}$$

and

$$\bar{R}_H = R_H e^{J\phi H} = \frac{\sin\psi - \sqrt{\bar{n}^2 - \cos^2\psi}}{\sin\psi + \sqrt{\bar{n}^2 - \cos^2\psi}} = \frac{\sin\psi - Z}{\sin\psi + Z} \qquad (8)$$

where $Z = \sqrt{\bar{n}^2 - \cos^2\psi}$

These equations may be approximated for low grazing angles for overland paths providing $\psi < 0.1$ rads (5.7°) and $f >> 30$ MHz, and are included in the computer programs described at Annex D. It is well established that horizontally polarised energy produces a greater reflection coefficient than vertically polarised energy. (See also Annex B page B-3).

13. A plane reflecting surface causes the continuous radar elevation coverage to break up into a lobed structure; where the approximate angle of the lowest lobe is approximately $\frac{\lambda}{4h_{tx}}$ radians.

Where h_{tx} = radar mast height (above local terrain level) for a 30 m mast at $\lambda = 0.03$ m the angle is 0.00025 rads and if the target elevation is less than a beamwidth direct ground reflected signals are received.

14. Multipath signal reception and reflected ray paths are synonomous, and curve fitting for terrain reflectivity profiles for smooth and rough earth situations using ray theory are considered at Chapter 9. In general, ray theory calculations are valid out to the radar horizon where radar aerial heights are sufficient for the surface wave to be neglected and with the restriction on grazing angle Ψ given by:

$$\operatorname{Tan}\psi > \left[\frac{0.3}{2\pi a\ f}\right]^{1/3}$$

(Where f is in MHz and a = effective earths radius in km).

For $\lambda = 0.03$ m and f = 10 GHz Tan ψ must exceed 0.0009 giving $\psi > 0.05^{\circ}$.

15. Smith {178} contrasts ray and mode propagation theory and observes that propagation theory is incomplete in some areas. A detailed discussion of the theory is outside the scope of this report, however figure 6 shows

measurements which compare the two approaches. The full line uses ray theory and the dotted line mode theory. Millington {179} uses the criterion $\psi > (\frac{\lambda}{2\pi a})^{1/3}$ to give the transition point (marked in Fig 6). Beyond this point as the horizon is approached the spreading of the rays due to earths curvature causes the ray theory to become unrealistic. For a radar mast height of 10 m at 3 cm wavelength it is of interest that the transition occurs at about 12 km, hence ray theory is used here with some confidence for targets out to 15 km range.

CHAPTER SUMMARY

16. Comments upon suitable factors to be incorporated in the radar performance prediction algorithm are:

a. Refraction. Out to 30 km range curvature (refraction) effects are small. However, it will be shown that small vertical errors may become significant under combined refraction and diffraction conditions. The 4/3 value for k is reasonable, but more precise values can be used for n from Table 1 and errors from Tables 2 and 3.

b. Refraction and Reflection Geometry. The approximations stated are used (see also Annex B), but these aspects are closely allied to the multipath and diffraction work covered in Chapters 7 and 9.

For radar trackers associated with low level SAM systems 'Ray theory' is used.

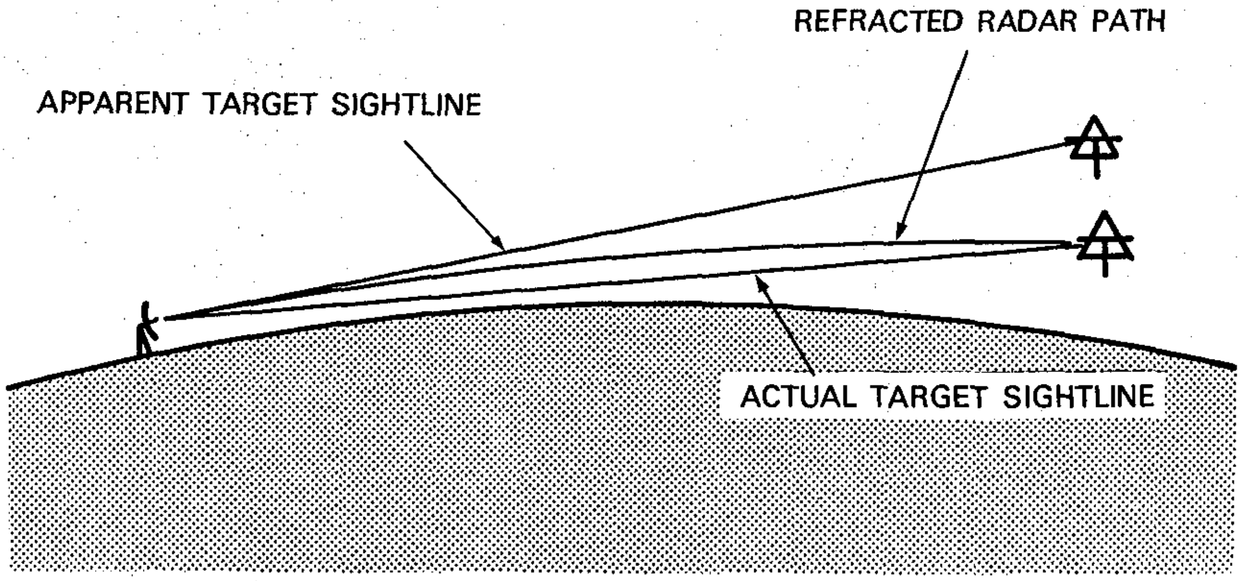

FIG 1 TRACKING RADAR REFRACTION ERROR

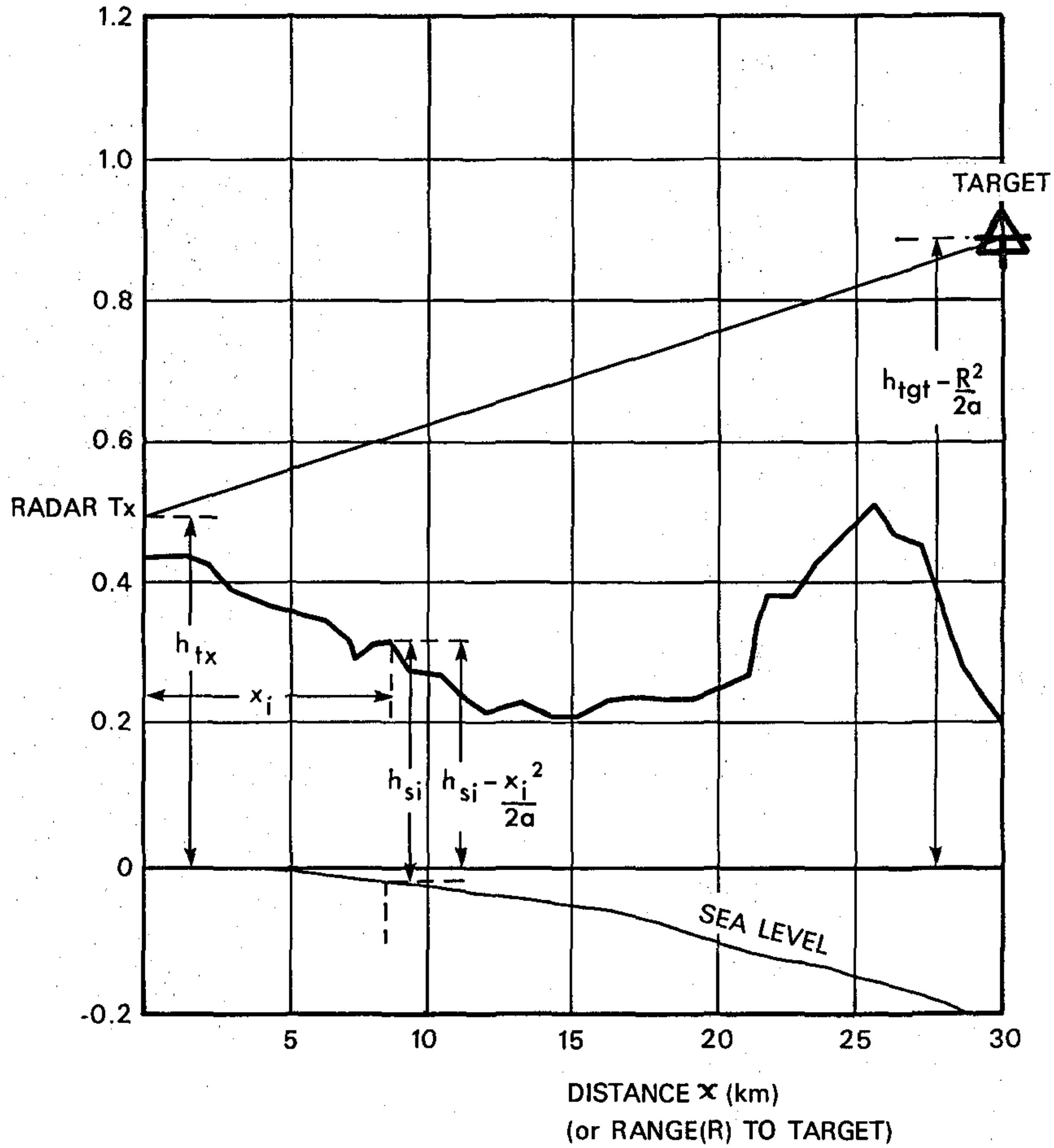

FIG 2 MODIFIED TERRAIN PROFILE

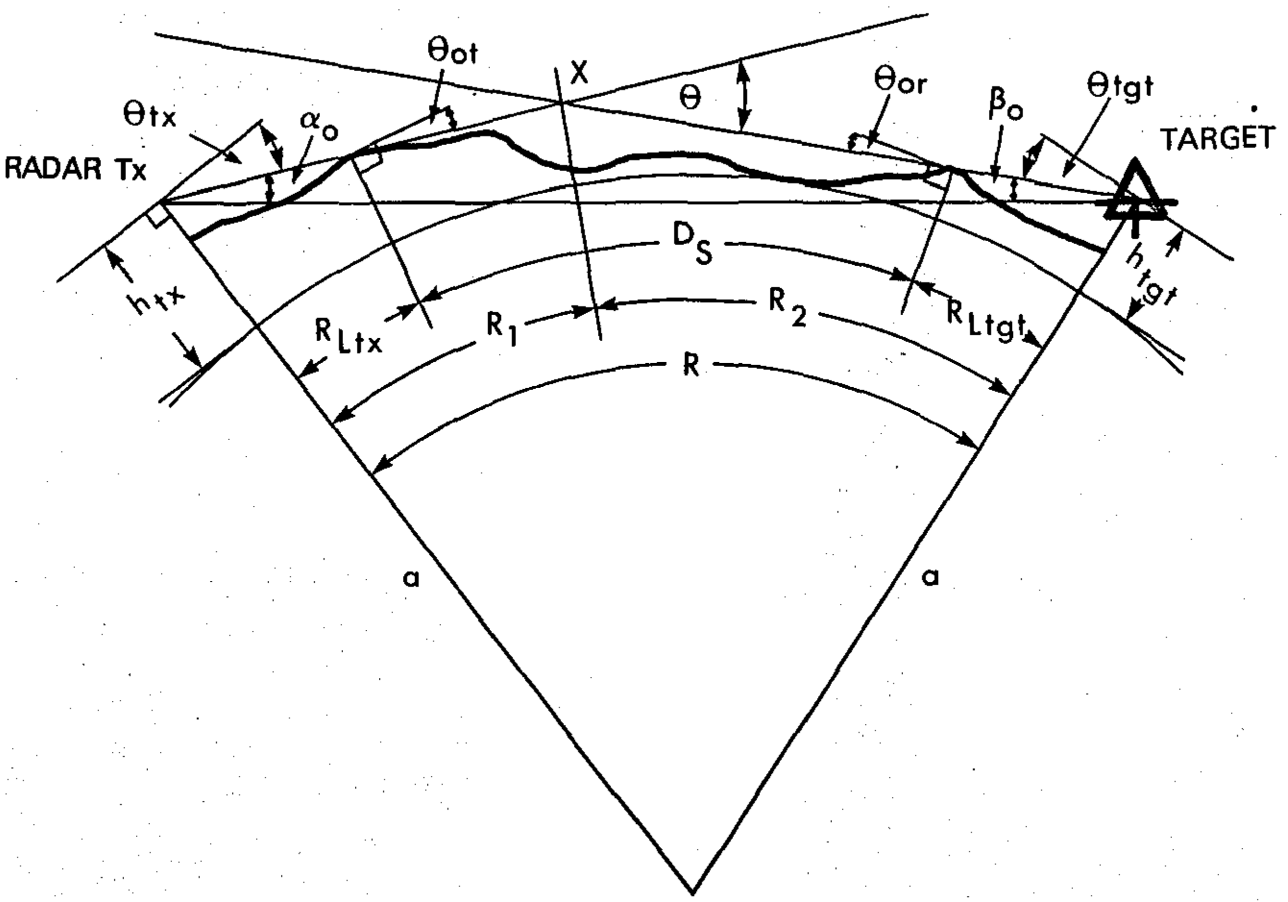

FIG 3 PATH GEOMETRY

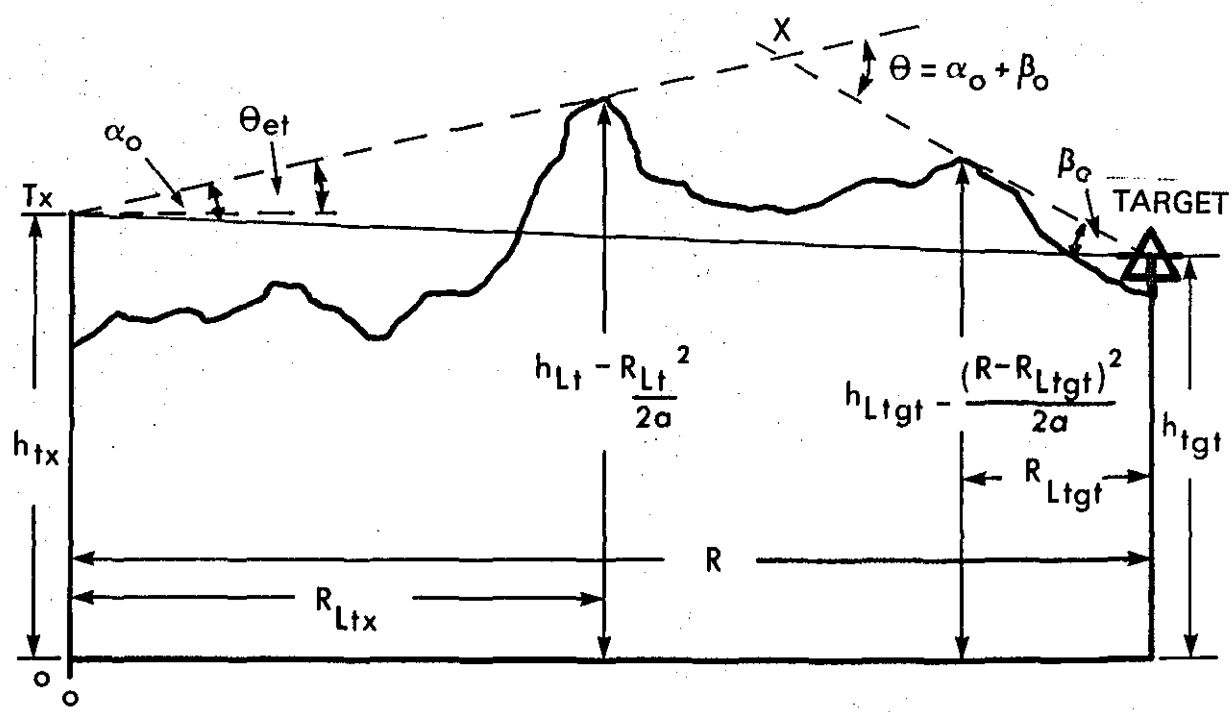

FIG 4 RANGE FROM RADAR TX

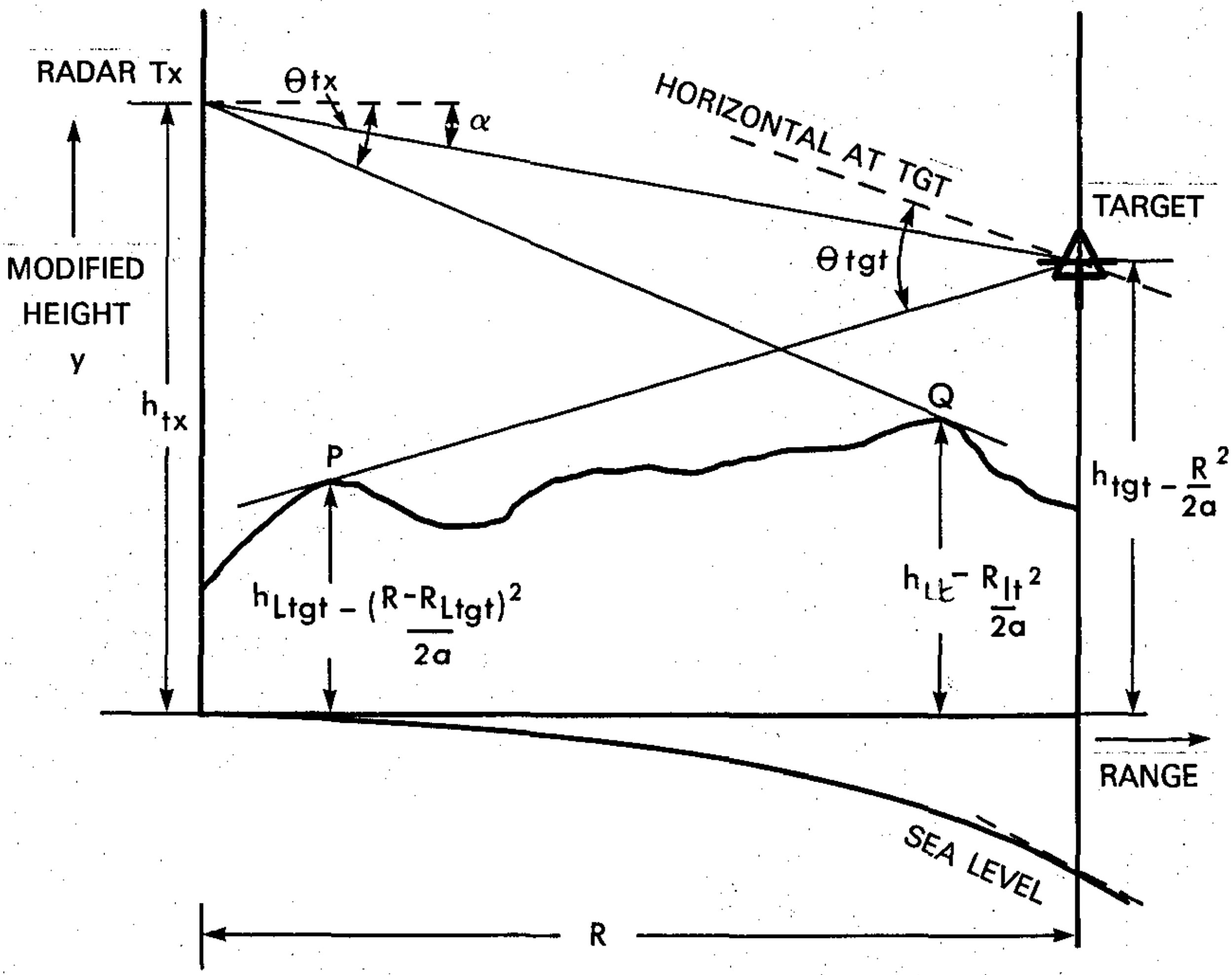

FIG 5 UNOBSTRUCTED SIGHTLINE

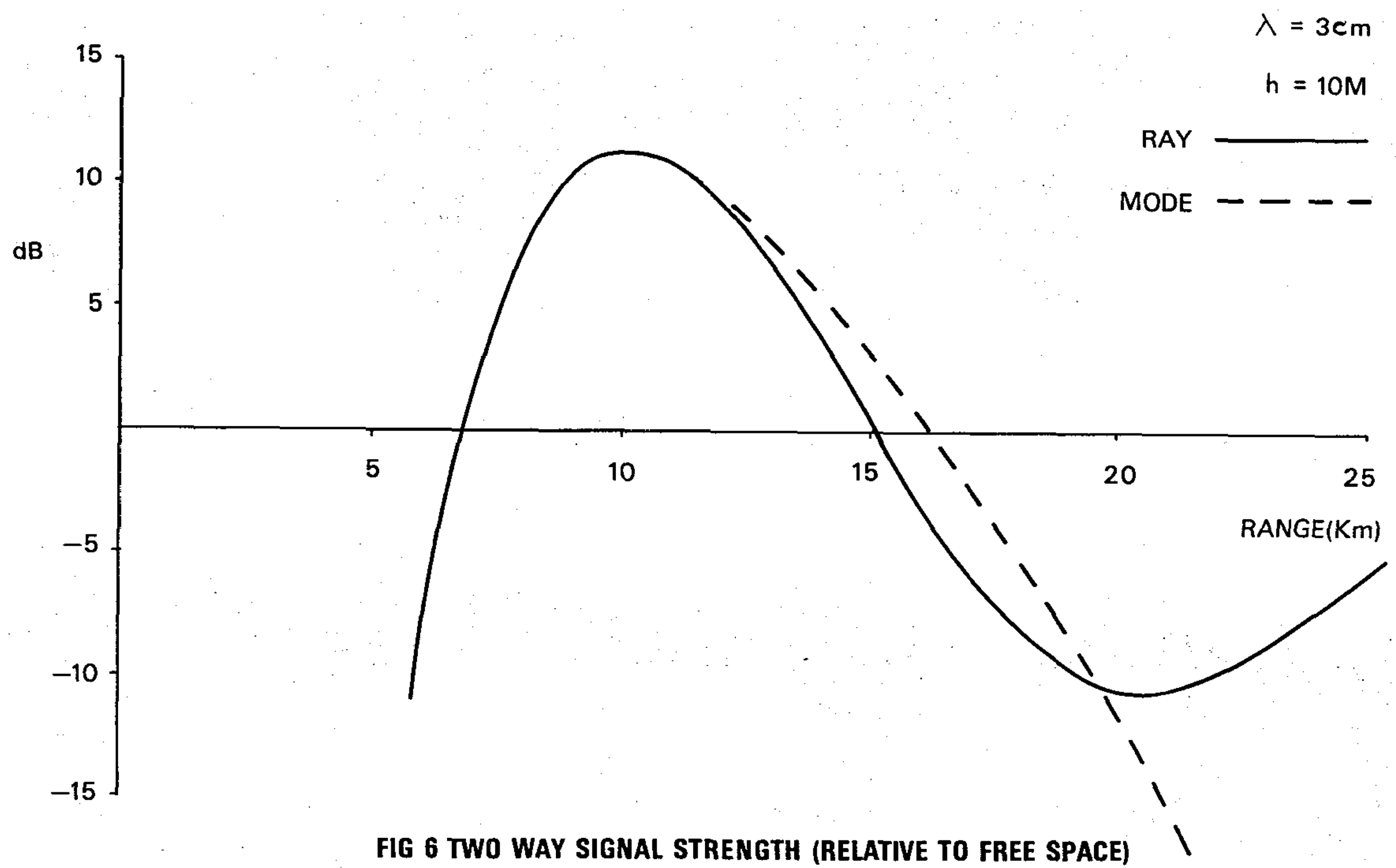

FIG 6 TWO WAY SIGNAL STRENGTH (RELATIVE TO FREE SPACE) FOR RAY AND MODE THEORY

CHAPTER 9

MULTIPATH

INTRODUCTION

1. Target tracking at very low grazing angles may be disturbed by the presence of unwanted surface-reflected waves; giving rise to two main effects which have been recognized since the early days of radar {180}:

a. Signals arriving from spurious angles cause the radar tracker boresight axis to be driven off the real target sightline.

b. The direct signal is contaminated by additional surface - reflected signals.

2. Surface reflections are usually classified as either 'specular' or 'diffuse', but here the objective is to consider practical means of incorporating multipath assessments into the computer model; rather than the detailed scattering processes. A brief survey of the effects of multipath on different tracker types is included. Minimisation of multipath at the design stage could be achieved by using narrower aerial beamwidths. This is not usually practicable with mobile systems since there is a limit to dish size, however there is a tendency for trackers to use higher RF's, giving some advantage in this respect. A number of techniques have been proposed {181}, but it is seen that the problem is mainly one of understanding terrain reflections rather than the hardware options available {182}. Indeed some techniques for reducing multipath may introduce other problems. One example of this {183} is to

insert a screen ('barrier' or 'fence') to prevent reception of signals from surface reflections. Although this can help at a pre-surveyed and prepared site, the screen itself introduces a diffracting edge with consequent interference with tracking results. The alternative is to accept multipath and use other techniques to minimise the effects.

RESEARCH AIMS

3. Specifically, the following aspects have been investigated:

a. Adjustment of S/N for variable (indirect) path lengths when transmit and receive signals are subject to multipath.

b. To achieve (a), identify the conditions under which multipath is likely to occur overland.

c. Quantify uncertainties in elevation angle measurement due to multipath.

d. Estimate likelihood of multipath combining with diffraction edges.

e. Assess the probability of degradation of target tracking due to multipath as the target traverses a specific area of terrain.

Items 3d and 3e above are also dependent upon some factors considered at Chapters 4 and 8.

4. Many papers are found to address multipath phenomena from the inevitable occurence at sea, but few results or conclusions are available for overland operation. Several overland research reports, eg, {184} {185} unfortunately quote results not applicable to this study - since they are concerned only with relatively close-range targets over smooth approaches relevant to airport runway approach radars. Delaney {186} has reported on the wider overland applications and it is clear that further data is required before really satisfactory assessment can be made. Delaney's model did not include target signal versus multipath clutter, but only the reflected signal for vertical angular errors.

5. The need for a multipath model which can be applied over general terrain with varying degrees of roughness has led to the development of a theory {187} which describes the effects of scattering from the terrain between the source and the receiver. Determination of the point at which diffuse reflections predominate over specular is dependent upon surface roughness - the rougher the surface, the lower the elevation angle at which diffuse scattering dominates. Separation of the resulting elevation errors has been the objective of {188} {189} and others. A good survey of options can be found at {190} {191} on bistatic solutions, and {192} {193} {194} {195} deal with other multipath compensation methods such as frequency agility, phased array processing and sidelobe reduction {196}. However, Barton {197} concludes that test data is extremely sparse in considering the arrival of diffuse multipath from angles other than the specular direction.

MULTIPATH GEOMETRY

7. Figure 1 shows the basic multipath geometry where illumination arriving

at the target via $R_1 R_2$ will be:

$$E_i = \frac{G\rho}{R_1 + R_2} E_t \qquad \text{---(1)}$$

Where G is the aerial voltage gain in the direction of the Specular point,

ρ is the surface reflection coefficient.

E_t, E_i transmitted and incident field intensities

The total illuminating field is the vector sum of the direct and indirect rays. Path lengths, direct and indirect are:

$$R_{(Direct)} = \{R^2 + (h_2 - h_1)^2\}^{\frac{1}{2}} \qquad \text{---(2)}$$

$$R_{(Indirect)} = \{R^2 + (h_2 + h_1)^2\}^{\frac{1}{2}} \qquad \text{---(3)}$$

h_1 and h_2 are small in practice compared to R, hence taking the first 2 terms of the binomial expansion of each:

$$R_D \simeq R + (\frac{h_2 - h_1}{2R})^2 \qquad \text{---(4)}$$

$$R_I \simeq R + (\frac{h_2 + h_1}{2R})^2 \qquad \text{---(5)}$$

8. <u>Path Difference.</u> $R_I - R_D = \Delta R$

$$\Delta R = \frac{2h_1 h_2}{R} \qquad \text{---(6)}$$

$$\text{Phase difference} = \Delta\emptyset = \frac{2\pi}{\lambda}\Delta R = \frac{2\pi}{\lambda}\frac{2h_1 h_2}{R} \qquad \text{---(7)}$$

To introduce a practical example here; given an aerial height of 7.5 metres at $\lambda = 0.03$ m and elevation angle of 0.5°, the multipath path-length difference will be of the order 5λ (15 cm).

9. Modified Signal. Interference from multiple lobes caused by the low grazing angle results in modified signal values. For small angles of ψ the pattern propagation factor (F) is:

$$F = 1 + \rho e^{-j(2\pi/\lambda)\ \Delta R + \emptyset} \qquad (8)$$

$$E_i = E_d \left[1 + e^{-j(2\pi/\lambda)\ \Delta R}\right] \qquad (9)$$

$$= E_d \left[1 + \rho e^{-j(2\pi/\lambda)\ \Delta R + \emptyset}\right] \qquad (10)$$

ρ is the reflection coefficient
Ed is directly backscattered energy

For small grazing angles (lobe raised by $\beta = \frac{\lambda}{4h_{tx}}$):

$$F(\beta) = \frac{4\pi\ h_{tgt}\ h_{tx}}{\lambda R_{tgt}} \qquad (11)$$

Where h_{tgt}, h_{tx} are target and transmitter heights. R_{tgt} = Target Range
Since the maximum range of a radar for detecting low flying targets is:

$$R_{max} = 8\sqrt{\frac{4\pi\ h_{tgt}^4\ h_{tx}^4\ P_T G_T{}^2 \sigma}{\lambda^2 S_{min}}} \qquad (12)$$

If $R_{max} > 10\pi\ h_{tgt}\ h_{tx}/\lambda$

$$\text{then } R_{max} = \frac{4\pi\, h_{tgt}\, h_{tx}}{\lambda} \sqrt[4]{\frac{P_T G_T^{\,2} \lambda^2 \sigma}{(4\pi)^3\ Smin}} \quad \text{------------(13)}$$

$$\text{Where } \sqrt{\frac{P_T G_T^{\,2} \lambda^2 \sigma}{(4\pi)^3\ Smin}} \text{ is the maximum free space range}$$

LOW LEVEL TRACKING

10. Fig 2 shows the multipath effect as a target reduces in altitude. At A the target is well clear of the surface without multipath, at B reflected energy enters the sidelobes causing oscillations of the aerial about a mean. Once the reflected energy enters the main beam at C considerable angular uncertainty can arise. Figure 3 indicates the typical situation where the tracking boresight moves from real to image target angular displacement. In a practical situation where the target is assumed to be moving rapidly through the fluctuations the tracking stability will much depend upon the inertia of the tracking control loop. At other times the system will jump to the image and lose track. Elevation tracking errors are considered below at para 12.

TRACKING MODES

11. As several tracking designs may be encountered in radar system assessment it is necessary here to take account of their individual vulnerability to multipath, briefly:

a. Monopulse. Standard monopulse uses Sum and Difference Channels to drive the aerial servo to zero error in the boresight. Under multipath conditions reflection signals also enter the Sum and Difference Channels. System vulnerable to multipath.

b. <u>'On-Boresight' Conical Scan</u>. Derivation of the error voltage takes a significant time in contrast to monopulse. There remains the problem of boresight target motion during a typical scan period (eg $\frac{1}{30}$ sec). Vulnerable system to multipath.

c. <u>Off Boresight</u>. The boresight is held at a fixed angle some 0.7 X beamwidth above the horizon. The error voltage is taken as giving the target elevation below this angle. Some angular discrimination is achieved since the image signal is attenuated by being appreciably further off-boresight than the target. Since the aerial is fixed, it cannot move onto the image, the system having switched from closed-loop to open-loop operation. The same technique can be used in both con-scan and monopulse systems. System resists elevation errors, but still susceptible to multipath clutter/noise.

d. <u>Double-Null</u>. Closed loop tracking is continued into the multipath region by generating an aerial pattern using monopulse, such that the difference function has 2 nulls equally dispersed about the horizon. Resistant to angular errors.

e. <u>Quadrature Components</u>. Three independent beams are used to make in-phase and quadrature measurements {198}. Resistant to angular errors.

f. <u>Complex Indicated Angle Monopulse</u>. Complex sum and difference signal can be processed to yield a complex indicated angle, and by combining this with more than one RF {199} the real angle can be uniquely determined. A marginal improvement is claimed overland, with a factor of 2 or better at sea. Some resistance to elevation angular errors.

g. <u>Frequency and Boresight Diversity</u>. One complex indicated angle technique uses frequency and boresight diversity as a means of resolving ambiguities. The radar must have frequency agility or beam steering respectively. The principle relies on storing representative calibration spirals using 2 or more boresight angles. Calibrations can be made for specific sites or a generalised model used. Howard {200} {201} {202} surveys these techniques and claims good results under multipath conditions on 90% measurements with elevation error Σ (rads) $0 \leq \Sigma \leq 0.5$.

ELEVATION TRACKING ERRORS

12. Para 10 introduced the oscillatory nature of the signals received through multipath. It is possible to find the optimum target height for a given range when using a specific tracker control loop bandwidth. The frequency beat between direct and reflected signals is obtainable:

$$\text{Since } F_t = \frac{2h_{tx}\ h_{tgt}\ V}{\lambda R^2} \qquad (14)$$

Assuming h_{tx} varies 5, 15 and 30 m, F_t = 1 Hz or 2 Hz, and V is the target velocity - nominally 300 m sec $^{-1}$ (ie Mach 1 at mean sea level) the following target table is produced for a spread of target altitudes:

	Target Altitude (m)			
	30	50	70	100
Tracker 2 Hz				
Radar Ht (m) 5	1.22 km	1.58 km	1.87 km	2.23 km
15	2.12	2.73	3.24	3.87
30	3.00	3.87	4.82	5.48
Tracker 1 Hz				
Radar Ht (m) 30	4.24	5.47	6.48	7.74

Table 1 Target Range at which Tracker Bandwidth is Critical

13. If the error cyclic variations fall within the radar tracker bandwidth the practical result shown above will be that targets at ranges greater than those shown will be difficult to track in the presence of multipath, unless one of the compensatory systems such as off-boresight tracking is used. Equation (14) above is obtained from the derivative of the phase difference expression:

$$\phi \simeq (4\pi/\lambda)\,(h_{tgt}\, h_{tx}/R) + \phi_R \qquad (15)$$

where ϕ_R = ground reflection and other phase differences in multiple paths.

i.e. $$F_t = |(1/2\pi)\,(d\phi/dt)| = |2\, h_{tgt}\, h_{tx}\, V/\lambda R^2| \qquad (16)$$

Example results are shown graphically at Figure 4.

RMS ELEVATION ERROR

14. Evans {203} conducted tests at λ = 0.03 m overland (ρ = 0.4), using a 1° beamwidth and shows ± 10' elevation tracking error at 0° target elevation. A suitable equation is derived, stated to be accurate down to

elevation angles of 0.5° (for a two beam static split system in elevation). At 1° elevation angle errors peaked at $\pm$ 3'. Targets were however at high level and long range. A graph of elevation tracking error is given by Barton {204} p 330 which illustrates these typical values, but his figures were obtained at "C' Band. The approximate RMS error can be found {205} from:

$$\sigma_{\phi} = \frac{\rho \, \theta_E}{(8G_s)^{\frac{1}{2}}} \qquad \text{---------------- (17)}$$

where ρ is the coefficient of surface reflectivity G_s is $\frac{\text{main lobe gain}}{\text{side lobe gain}}$ (as a power ratio) taken at an angle 2E below the beam axis (E is target elevation angle, θ_E is elevation beamwidth). Annex E contains more detailed analysis of track errors for low level systems.

CONDITIONS FOR MULTIPATH

15. Propagation Path Length. With a ground-based tracking radar, where the aerial and terrain remain fixed,the target scattering properties are strongly aspect dependent (see Chap 6). If the range gate width is T secs, then all scatterers contributing to the overall signal return must be located such that their return arrives in time interval t such that:

$$\left(\frac{2R}{c} - \frac{T}{2}\right) < t < \left(\frac{2R}{c} + \frac{T}{2}\right) \text{ and } \left(\frac{2R}{c} - \frac{cT}{2}\right) < D < \left(\frac{2R}{c} + \frac{cT}{2}\right) \text{ ----- (18)}$$

Hence $2R + \frac{cT}{2}$, is the maximum path length a signal can travel and still remain in the range gate (see fig 5). Distance = $PS_1 + S_1 S_2 + S_2P$ (max path D), hence:

$$= [R + \sqrt{h_2^2 (R_{max} - R_G)} + \sqrt{R_{max}^2 + h_1^2} \quad \text{------------} \quad (19)$$

This shows that some scatterers beyond the target will be in the range gate. At low elevations $R \rightarrow R_G$ and the maximum range of a scatterer of interest is then $R_{max} = (R + \frac{c\tau}{4})$

If $h_1 << R_{max}$ then:

$$R_{max} = \frac{[(R + \frac{cT}{2})^2 - R^2 - h_2^2]}{2\,(R + \frac{cT}{2} - R_G)} \quad \text{-------------} \quad (20)$$

16. The foregoing is expanded upon at {206}, where the minimum range at which an unwanted scatterer could interfere is calculated. Clearly if the range gate duration was zero, the problem would be eliminated, hence the need for a small gate width is established for low level tracking systems.

17. Burk addresses the problem of power levels arriving at the aerial via the multipath. Assuming the target is scatterer 1 (S_1) and the surface scatterer 2 (S_2). Then (using the notation at Fig 5):

$$P_{(at\ tgt)} = \frac{P_t\ G_R}{4\pi\ R^2} \quad \text{-----------------} \quad (21)$$

Overall Power scattered towards the surface scatterer S_2 (point S).

$$P_{(at\ S_2)} = P_{tgt}\ \sigma_{tgt} \quad \text{-----------------} \quad (22)$$

Power P_2 arriving at S_2 is:

$$P_2 = \frac{P_{tgt} \ \sigma_{tgt}}{4\pi \ q^2} \quad \text{------------------------} \quad (23)$$

q = dist S_1 to S_2

Overall power re-radiated as scatter:

$$= \frac{P_2 \ \sigma \ (S_2)}{4\pi \ r^2} \quad \text{------------------------} \quad (24)$$

Power at radar receiver

$$P_r = \left(\frac{P_t \ G_R \ \sigma_{tgt}}{4\pi \ R^2}\right) \left(\frac{\sigma_2}{4 \ \pi \ q^2}\right) \left(\frac{Ae}{4 \ \pi \ r^2}\right) \quad \text{---------} \quad (25)$$

Where Ae is the effective receiver aerial aperture towards the surface scatterer. If multiple scatterers exist the problem becomes complex. Methods to obtain the incident and scattered total field are beyond the scope of this study but can be found at {207}.

18. Path Calculations. The method used at {208} is used for path length determination, see fig 6 . With the multipath angle very small $R_T \rightarrow R_1 + R_2$ and $h_1 + 2 \ RE \rightarrow 0$, shows that:

$$R_1^{\ 3} + \left[-\frac{3}{2} RT\right] \ R_1^{\ 2} + \left[\tfrac{1}{2} \ RT^2 - RE \ (h_1 + h_2)\right] R_1 + \left[RE.h_1. \ RT\right] = 0 \quad \text{---} \quad (27)$$

from which R_1, one of the three roots of (27) can be found, R_2 is then found from.

$$R_2 = h_2 + \text{Sin} \ \Psi \quad \text{-------------------} \quad (28)$$

The accuracy of R_2 decreases at long range using equation (28), but it is satisfactory for the relatively short ranges in this study. An iterative process is used:

$$\text{Cos}\ (\theta_1 + \theta_2) = \frac{(RE + h_1)^2 + (RE + h_2)^2 - R_T^{\ 2}}{2\ (RE + h_1)\ (RE + h_2)} \quad \text{-------- (29)}$$

Although the sum of $\theta_1 + \theta_2$ is known, their individual values are not. In the first iteration let $\theta_1 = \frac{1}{2}\ (\theta_1 + \theta_2)$ and calculate R_1:

$$\text{Cos}\ \theta_1 = \frac{RE^2 + (RE + h_1)^2 - R_1^{\ 2}}{2\ RE\ (RE + h_1)} \quad \text{-------------- (30)}$$

$$\text{Hence}\ R_1 = \sqrt{RE^2 + (RE + h_1)^2 - RE\ (RE + h_1)\ \text{Cos}\ \theta_1} \quad \text{-------- (31)}$$

Using R_1, θ_1 and Ψ_1 are found (Cosine Law).

$$\text{Cos}\ (\tfrac{\pi}{2} - \Psi_1) = \frac{RE^2 + R_1^{\ 2} - (RE + h_1)^2}{2\ (RE)\ (R_1)} \quad \text{----------- (32)}$$

$$\text{Sin}\ \psi_1 = \frac{(RE + h_1)^2 - (RE^2) - (R_1^{\ 2})}{2\ RE\ (R_1)} \quad \text{-------------- (33)}$$

Hence R_2 can be found:

$$R_2 = \sqrt{RE^2 + (RE + h_2)^2 - 2\ RE\ (RE + h_2)\ \text{Cos}\ \theta_2} \quad \text{-------- (34)}$$

19. Testing ψ_1 against ψ_2, if $\psi_1 < \psi_2$ the interval is re-defined for θ_1 (as $\theta_1+\theta_2$). If $\psi_1 < \psi_2$, re-define the interval 0 degrees to θ_1 degrees. ψ_1 and ψ_2 are then recalculated with θ_1 assumed to be half the new interval. An extremely accurate result is obtained in 31 iterations; in excess of the accuracy required here to determine the location of the surface specular point. The method reduces the error between the initially assumed θ_1 and the actual θ_1 by $\frac{1}{2^N}$; where N is the number of iterations.

MONOPULSE RADAR TRACKING ERRORS

20. One agency has produced a desk-top computer program {209} which splits the multipath signal components into diffuse and specular; and assumes small angles over a "flat earth". For completeness the relevant equations to achieve the error calculation are shown at Annex E.

CHAPTER SUMMARY

21. To meet the aims at para 3 the following items are incorporated in the model for low level tracking:

a. Multipath Conditions. After determination of the position of the probable specular point using equations (27) to (34), the algorithm (see programs at Annex D) examines the slope and surface material to assess whether multipath is likely.

b. Elevation Tracking Errors. Equation (12) is used as a check to ascertain the target is within radar range; while equation (14) is used to find the optimum target range beyond which elevation tracking accuracy will probably become degraded.

c. Adjustment of Signal Levels. If multipath is assessed as likely, equation (1) is used to adjust E_i, incorporating the assessed ρ from the terrain data base (see Annex B).

d. Multipath Coincident with Diffraction. Using the terrain data base the algorithm can produce a radial PPI-type plot for small azimuthal increments to indicate where diffraction edges could exist. Multiple diffraction edge assessment is complex and not thought to be particularly reliable at the higher RF's; especially since it is unlikely that more than one really significant diffraction edge will occur within the range brackets of interest here.

Further, double diffraction is only probable under limited conditions when plateaus between adjacent diffraction edges are sensibly smooth and horizontal. However, by using the same method as at (a) above, the fitting of a second specular point could be achieved by treating the first diffraction edge as the position of the radar transmitting source. The first diffracting edge would of course be considered in the first instance and would probably be the only edge relevant to short-range tracking systems.

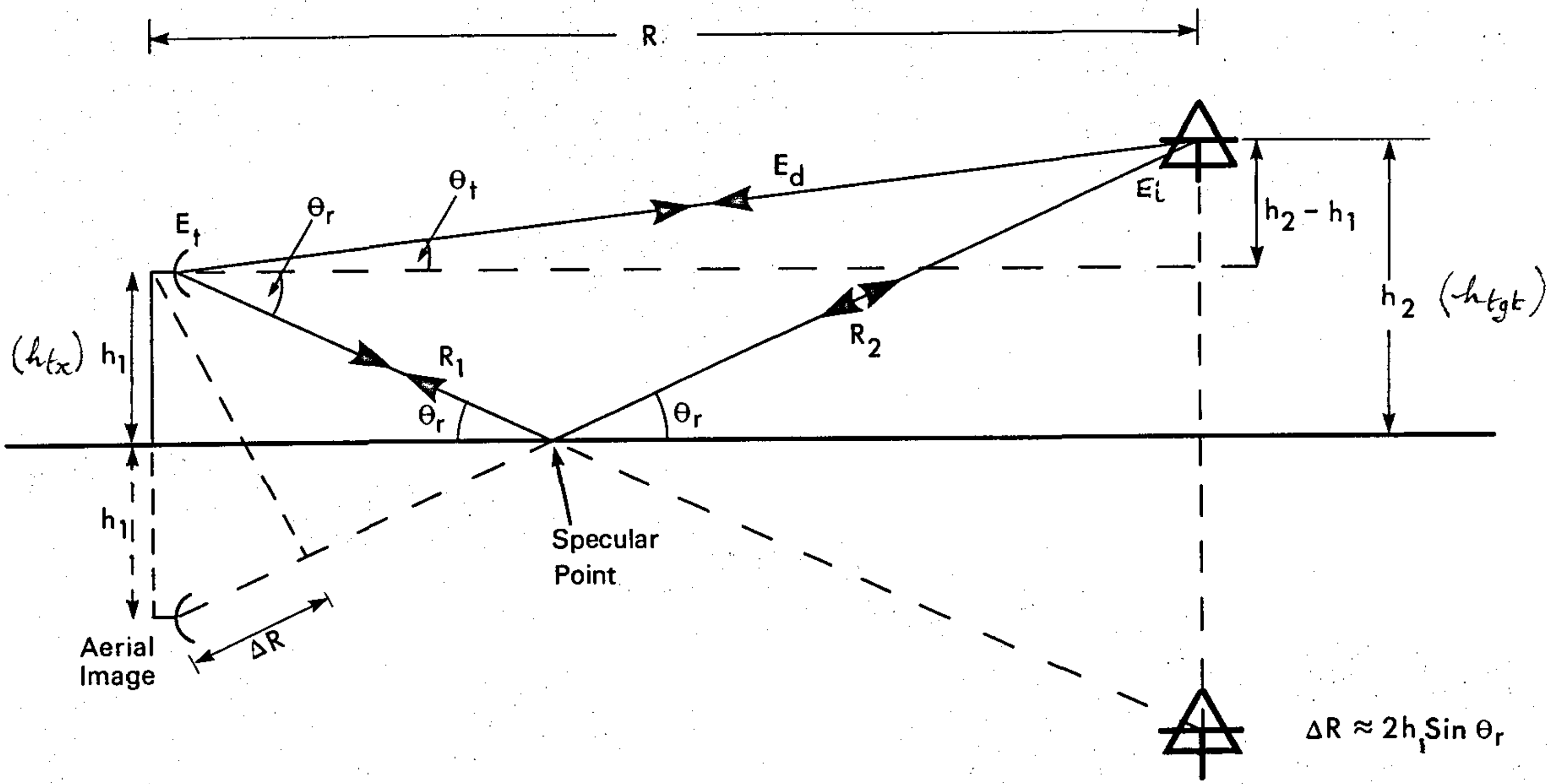

FIG 1 MULTIPATH GEOMETRY

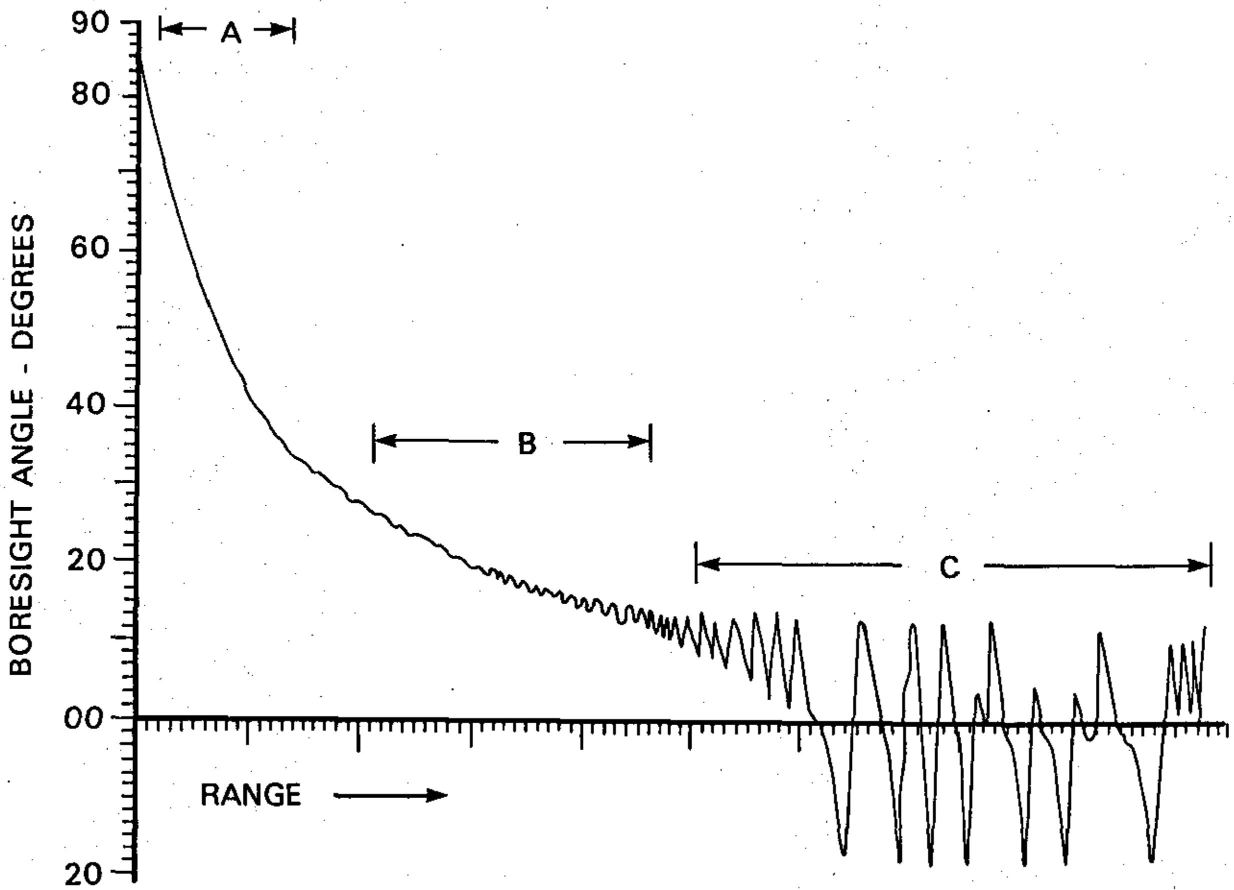

FIG 2 RECEDING TARGET - REDUCING IN ALTITUDE

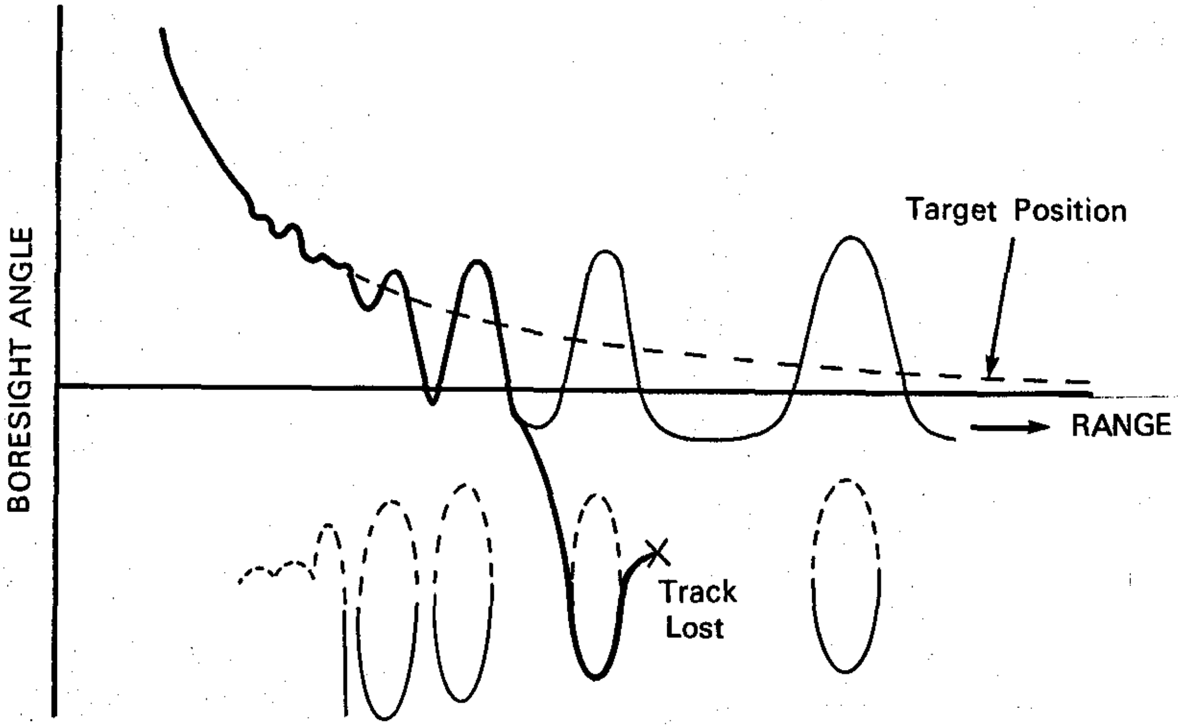

FIG 3 TARGET TRACKING UNLOCK

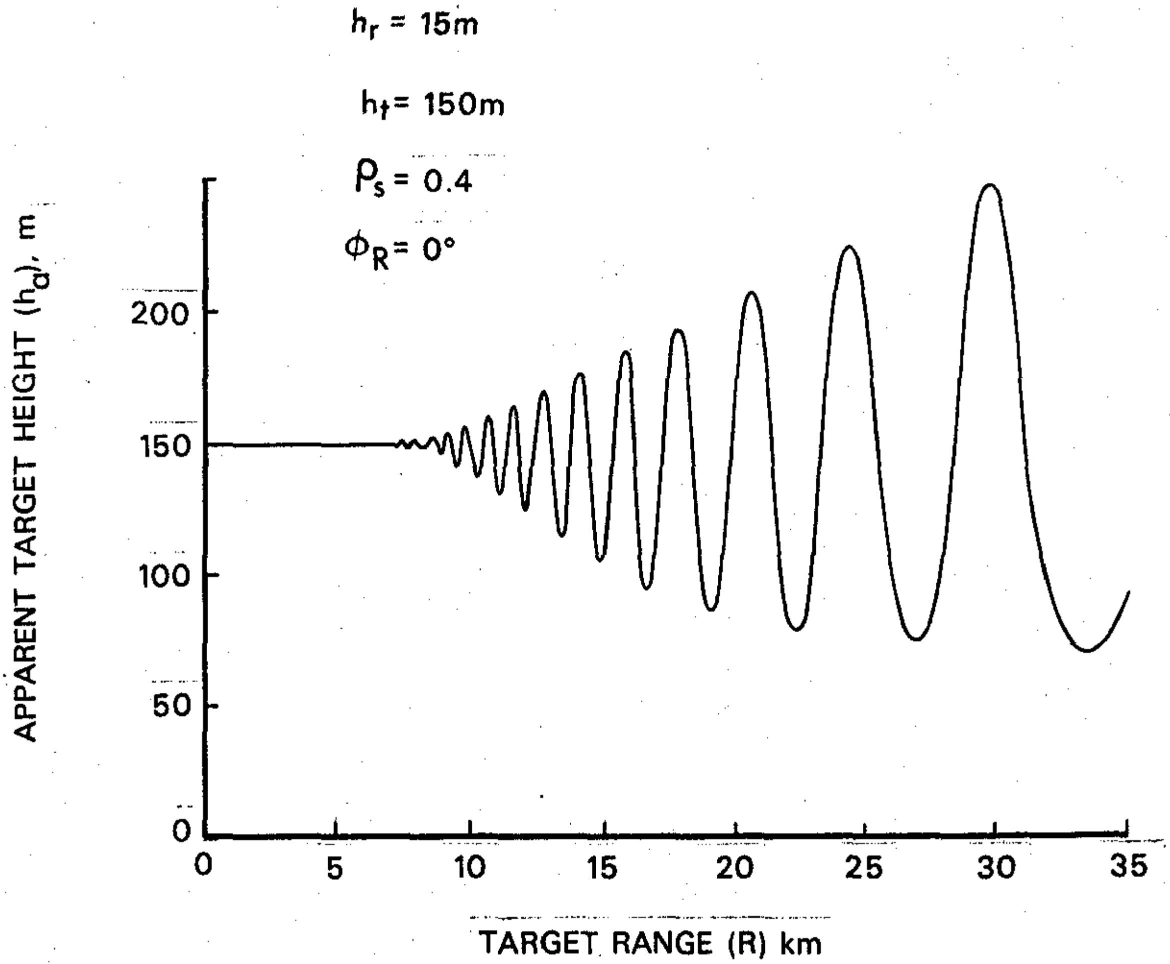

FIG 4 APPARENT TARGET HEIGHTS

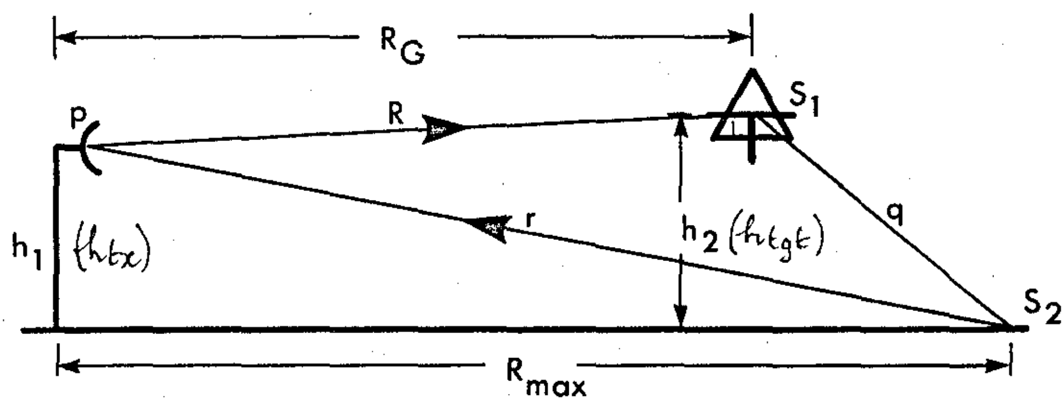

FIG 5 MAXIMUM PATH PROPAGATION

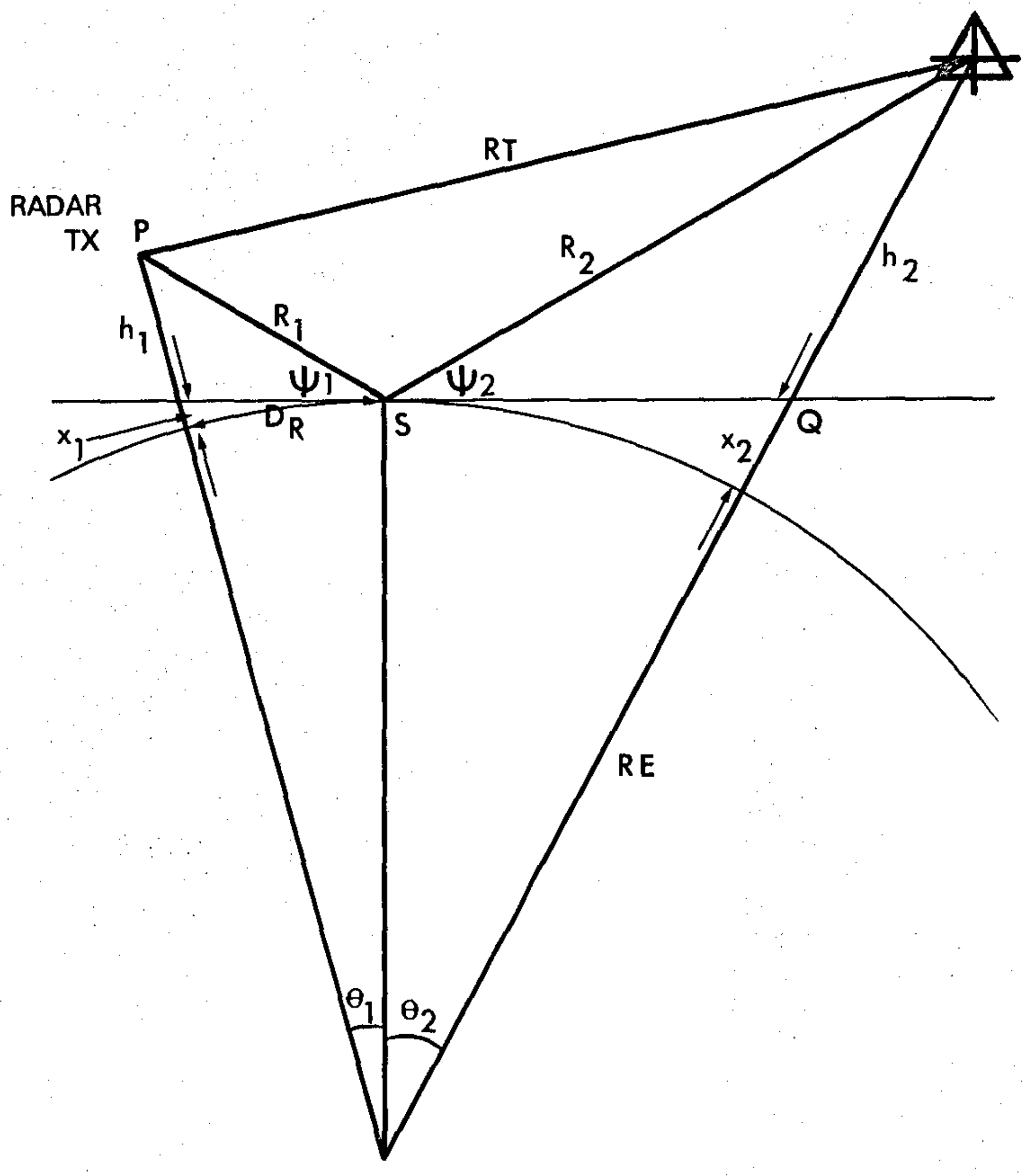

FIG 6 GEOMETRY FOR MULTIPATH CALCULATIONS (after Kirk)

CHAPTER 10

TERRAIN SLOPE - CLUTTER EFFECTS WITH AND WITHOUT TREE COVER

1. Sloping terrain implies a change in radar grazing angle since the surface resolution cell "tilt" as viewed by the radar, will vary. Land surface tilted away from the radar will be shadowed. Changes in slope gradient (1) and 'aspect angle' (2) may vary from cell to cell in areas of the roughest terrain, although spatially there is fairly high probability that adjacent cells may have the same slope and aspect in gently undulating conditions. If the period of undulation is less than the resolution cell length, the actual grazing angle could vary within the cell. Since clutter is strongly dependent upon Ψ, σ_o can be expected to show significant variation with slope. Of the many radar research papers studied none considers slope in any detail; {210} and {211} mention that the 'slope effect' exists. The general geometry is shown at Figure 1. It is seen that the resolution cell 'footprint' on the surface, or 'facet', can be tilted at almost any angle depending on the local terrain aspect when viewed along the radar boresight. If gradient is zero, aspect is indeterminate. For mapping and geomorphological purposes Evans {212} proposes methods of slope representation and statistical terrain comparison; this is explained in some detail at Annex F and converted to the radar slope and aspect situation found during measurement analysis by the author.

(1) Gradient is defined as the rate of change of terrain altitude with horizontal displacement (range 0-90°) ie, gradient is tangent to profile.

(2) Aspect angle is the compass azimuth angle (either with respect to the radar beam, or measured from North datum), along which the maximum gradient falls (range 0-360°)

GEOMETRY

2. For investigative purposes terrain with regular undulations could be approximated to a sinusoidal profile. Amplitude and period would then dictate the probability density function for any grazing angle and surface RCS could be computed for given values of θ_E and θ_{AZ} and τ, as a function of amplitude and period. Gentle rolling hills for example may give an amplitude to period ratio of 0.05 (figure 2a), whereas very hilly terrain might produce a ratio of 0.1. Such a surface profile would have to be considered together with the existence of a sightline to the aircraft target. At the lowest grazing angles shadowing is of course at a maximum. In every case a sightline is assumed to the clutter patch with no intervening obstacles, apart from shadowing.

3. From Figure 3, the revised value of Ψ_1 (taken to be Ψ^1), towards a clutter patch is given by:

$$\Psi^1 = \text{Sin}^{-1} \left[\frac{-(h_t^2 - h_{tx}^2)}{2R\ (\frac{4}{3})\ r_o} - \frac{h_t - h_{tx}}{R} - \frac{R}{\frac{8}{3}r_o} \right] \quad \text{---------} \quad (1)$$

Where h_t = height (average) of clutter patch (m)

h_{tx} = height of radar aerial (m)

R = range to clutter area (m)

r_o = Earths radius (nominal 6500 km, 4587 n.ml.)

4. Figure 2b shows the pdf's for the probability that the actual grazing angle Ψ^1 falls between Ψ and $\Psi + d\Psi$ for a nominal value $\Psi = 5^o$ for amplitude/period ratios of 0.05 and 0.1 (respectively undulating & hilly terrain) and allowing for masking effects. The radar is raised (or the terrain passes beneath an airborne radar platform) such that the set value of Ψ is 5°. By siting a mobile radar at any point the probability of achieving the expected Ψ is very low. (see also ANNEX F APPENDIX 1 para 11

5. It has been observed {213} that as large areas of shadowing and hence facing slopes are illuminated, a pronounced 'knee' appears in the curves, for example where about 20% of the area was shadowed and 50% of the area sloped. Therefore the expected probability distribution is most likely to be contaminated in some way.

6. Providing radar reflectivity measurements are available it was realised that using terrain spot heights and a culture database, it should be possible to isolate and study those cells containing like foliage and with a particular slope - perhaps using Ψ and $\Psi + d\Psi$ as a working range of aspect angles - to make correlation studies. Various errors such as aerial gain and propagation loss error should be taken into account, since these are site - specific, together with other relevant radar parameters present at the time.

7. It will be expected that the more heterogeneous the data becomes, then more areas are shadowed. However, if very large resolution cells are observed (large value of τ), the probability distribution will take on a smooth transition from a small rate of change at the 50% percentile to a large rate of change at low percentiles. Detailed results of the author's correlation studies are at Appendix 1 to Annex F for radar measurements taken by British Aerospace over varying terrain.

PRACTICAL EFFECTS OF 'SLOPE'

8. Area. Equation 1 (above), does not however contain all the geometrical information necessary to define the slope and the associated radar footprint. If a very narrow (tracking) beam radar is considered several other effects are observed. Some examples are shown at Annex F, where the illuminated

plane dimensions can be less than the resolution cell dimensions with very steeply sloping terrain. Within the bounds of the aerial vertical beamwidth the surface footprint may exceed the resolution cell length τ if the plane is located at a maximum defined by the diagonally opposite edges of the resolution volume. As the terrain slope increases beyond α (CRIT) the surface footprint is reduced, and if it is assumed that the slope is centred on the point O, at the plane centre; then the illuminated plane is reduced in length and hence area at both ends by an amount dependent upon the slope. This extreme condition would occur in practice only in very rough terrain.

9. If small resolution cells are used (and ignoring the occasions when a specular reflector happens to be centred in the cell), it is assumed that the clutter from the cell centre gives a reflection typical of the whole cell. Surfaces tilted to the left or right similarly cause variations in radar footprint size.

10. Curvature. It is clear that many researchers have found it is inconvenient - or perhaps too tedious - to consider these effects in detail. Apart from the more obvious variations in radar footprint area caused by gradient, and calculated from the terrain altitude matrix, (shown at Annex F) the second derivative is that of curvature. In this study curvature is of interest; both convexity and concavity. Surface concavity is likely to produce radar shadowing, while profile convexity may be used to predict the curvature values necessary to test for the likelihood of diffraction in accordance with the criteria selected at Chapter 7 and also detailed in Annex F.

VARIATION OF VEGETATION (TREE COVER) WITH TERRAIN ALTITUDE

11. In an attempt to obtain correct terrain screening data (see Chap 2), it has been the normal practice in the worldwide clutter models studied, to add a set value for tree height to the terrain (contour) spot heights. Investigations by the author have shown that this approach is not strictly correct. For a given type of tree cover, measurements {214} {215} suggest that trees at the bottom of sloped terrain grow to a greater height than trees at the top of the slope. Nature's reasons for this phenomena are of no concern here, however the practice of adding a constant height for tree cover must result in slight inaccuracies in the calculated grazing angle of radar energy striking the tree canopy.

12. Tree growth rates vary with tree types as well as with altitude, further, all tree *mensuration is made* on a volume yield basis ($m^3.ha^{-1}$). A brief examination of a forest of pine/spruce types - prevalent in larger quantities than deciduous in some parts of Europe - has shown a probable variation of the order 25% over a slope altitude change of 200 m. Interpolation of measurements provided by {216}, (assuming tree height (h) is approximately proportional to volume yield), leads to the conclusion that a nominal 20 m tree cover over the terrain can be expected to reduce to 19 m if the terrain rises 30 m; ie, an approximate rate of reduction of tree cover of -1m per 30 m elevation increase. The relationship between yield and elevation is linear.

13. Translating this into practical significance means that grazing angle can only be approximate since the rate of change of tree height with terrain altitude also varies geographically. For example, the effect is more marked in the North. For precise clutter investigations under laboratory instrumentation conditions against a sloping forest area the effect should be noted as an extra input variable.

GRAZING ANGLES

14. Nathanson {217} uses a simplification for depression angle α_d (see figure 3a), where $r_e = \frac{4}{3} r_o$:

$$\alpha_d = \mathrm{Sin}^{-1} \left[\frac{2r_e h_{tx} + h^2_{tx} + R^2}{2R (r_e + h_{tx})} \right] \qquad (2)$$

then if $\frac{h_{tx}}{r_e} << 1$ and $\frac{h_{tx}}{2r_e R} << \left(\frac{h_{tx}}{r_e} + \frac{R}{2r_e} \right)$ an

approximation gives:

$$\alpha_d = \mathrm{Sin}^{-1} \left[\frac{h_{tx}}{R} + \frac{R}{2r_e} \right] \qquad (3)$$

and similarly for grazing angle (assuming flat terrain) as at figure 3b

$$\Psi = \mathrm{Sin}^{-1} \left[\frac{h_{tx}}{R} \left(1 + \frac{h_{tx}}{2r_e}\right) - \frac{R}{2r_e} \right] \qquad (4)$$

reducing to:

$$\Psi = \mathrm{Sin}^{-1} \left[\frac{h_{tx}}{R} - \frac{R}{2r_e} \right] \qquad (5)$$

A plot of ψ v Range for typical radar mast heights is at Figure 4.

15. Using the above equations and applying the error and hence slope variation in estimating true gradients over tree-tops, we get the situation where the appropriate gradient must be added to the result at Eqn (4) to get the true grazing angle; since Nathansons model is for the illumination to strike the surface at nominal sea level. It is usually the case that the terrain facet is not only sloped but raised above sea level (or above radar transmitter level for land-based radars). The geometry is shown at figure 5 and is assumed to have forest cover of varying depth as explained at paras 11-13 above.

16. Actual grazing angle, at which radar boresight energy strikes the sloped tree tops will be $(\psi^1 + \alpha_t)$:-

a. <u>Sloped Terrain near Transmitter Level</u>

$$\Psi^1 = \mathrm{Sin}^{-1}\left[\frac{h_{tx}}{R}\left(1 + \frac{h_{tx}}{2r_e}\right) - \frac{R}{2r_e}\right] + \alpha_t \qquad \text{------------ (6)}$$

b. <u>Sloped Terrain below Transmitter Level</u>. ψ^1 is greater ; the calculation is repeated but assuming the radar height to be at a greater height than the terrain thus:

$$\Psi^1 = \mathrm{Sin}^{-1}\left[\frac{h_{tx} - h_t}{R}\left(1 + \frac{h_{tx} - h_t}{2r_e}\right) - \frac{R}{2r_e}\right] + \alpha_t \text{----- (7)}$$

When $h_{tx} = h_t$, $\psi^1 \rightarrow \alpha_t$

17. If terrain height exceeds radar transmitter height (as will often be the case with ground based radars), the same equation can be used for Ψ^1 by interchanging h_{tx} and h_t in Eqn (7) and subtracting from gradient:

$$\Psi^{1}\ (h_t > h_{tx}) = \alpha_t - \mathrm{Sin}^{-1}\left[\frac{h_t - h_{tx}}{R}\left(1 + \frac{h_t - h_{tx}}{2r_e}\right) - \frac{R}{2r_e}\right] \quad \text{-- (8)}$$

18. With increasing height of tree cover and the radar height fixed, the grazing angle intersecting the terrain becomes shallower and as trees and terrain reduce in height grazing angle Ψ^1 approaches the value at Eqn (4).

19. In practice the difference in gradient, $\Delta\Psi^1$, is:-

$$\Delta\psi^{1} = \alpha_{t_1} - \alpha_{t_2} - 2\sin^{-1}\left[\frac{h_t - h_{tx}}{R}\left(1 + \frac{h_t - h_{tx}}{2r_e}\right) - \frac{R}{2r_e}\right] \quad \text{------- (9)}$$

For example, if the terrain rises 30 m (in a 1 in 4 gradient) then X (horizontal distance) = 120 m, Assuming tree cover of 20 m (19 m at top of slope), then $\Delta\Psi^1 = 0.45^\circ$. Similarly for a terrain gradient of 1 in 10 the value of $\Delta\Psi^1 \approx 0.2^\circ$. It is seen therefore that the radar energy striking angle does vary significantly, and that the correct allowance should be made for tree cover height variations. This may explain why some results, such as those plotted at Chapter 4 Figure 6, exhibit such a wide spread of rate of change of median σ_o at low values of Ψ.

POLARISATION WITH SLOPE

20. Hevenor {218} made measurements which strongly indicate that slope in the field of incidence "influences the calculation of radar backscatter in an entirely different manner than the slope in a plane orthogonal to the plane of incidence for a given polarisation". His experiments concerned a slightly roughened surface, although an analysis of his results shows that they are probably applicable to the homogeneous surfaces presented by continuous forest cover or rural terrain, since the correlation period will be shorter than the roughness period.

21. It is clear that significant errors of up to 5 dB will occur, as measured {218} if for example, single slope only is used. This may explain why, in the absence of computing in the past, many sets of raw results could not be fully reduced but were plotted and compared - such that often like has not been compared with like - leading to inaccurate conclusions.

SUMMARY

22. A method of categorising aspect and slope of terrain which is 'tilted' to the incident radar energy is recommended at Annex F. Backscatter effects caused by terrain 'tilt', ie aspect and gradient, have been investigated using raw radar data on a specific site with controlled radar parameters. These results are detailed at Appendix 1 to Annex F.

23. The computer program is also capable of separating resolution cell footprints of like 'slope' and 'aspect' and will plot these on a PPI-type layout on hard copy. This information is then converted onto acetate overlays for comparison purposes on survey maps.

24. Probability statistics for slope for any grazing angle can be produced for a terrain area where the database of spot-height matrix and culture exists.

25. It is possible that backscatter from terrain sloped at exceptionally low angles may have little practical effect upon radars using modern anticlutter processing.

26. The majority of clutter is likely to fall in the first 5-10 n miles of range, and within the amplitude range 0·1–100m² (wrt 1m²) with only a small proportion in the range 100-1000m², although these values would increase in rough terrain. About 95% of clutter is typically > 30dB above minimum detectable signal out to 5 n mls and 60% out to 15 n mls, however precise measurements should always allow for the changing grazing angle as the terrain slope varies. It is possible that Linell's (and others) results (see Chapter 4) would have been different if some slope effect had been incorporated.

27. Models. Equations shown in paras 14 to 19 are used, as appropriate, for investigations and the performance prediction algorithm. 3dB boundaries are used for statistical analysis although it is naturally understood that the radar footprint spreads over a larger area in practice. It is further assumed that the radar aerial distribution is such that energy levels fall rapidly outside the 3dB limits while energy distribution within the 3dB volume is sensibly evenly spread.

28. Surface Reflectivity Reversal Phenomenon. The pdf's at figure 2b are of particular interest since they clearly show the wide variation in actual grazing angle obtained in practice when illuminating undulating terrain. Several sets of worldwide research results have shown a hitherto unexplained reversal in the clutter values obtained at very low grazing angles (see Chapter 4, figure 4). It is the author's opinion that this could be partly explained by the pdf's shown. For example when nominally grazing at $\psi = 5^{\circ}$, the probability of obtaining the expected grazing angle is extremely low. As the terrain gently undulates $\psi = 5^{\circ}$ occurs on only 8% of occasions, while more hilly terrain reduces the probability to 4%. The pdf's at Figure 2b clearly

show that $\psi = 11°$ or $27°$ would be obtained as the actual grazing angles on the majority of occasions, hence the radar reflectivity measured would be greater at these angles that the value to be expected at the shallower angles. There is, of course, zero (main beam) backscatter from the shadowed areas caused by surface undulations, unless diffraction occurs, and the pdf will depend upon the period of undulations - how many reflecting facets are contained within the resolution cell, their angles and amplitude.

29. Slope Correlation Studies: Some additional investigations have been made into the above proposals and detailed at Appendix 1 to Annex F. Actual grazing angles are shown to be larger than measured grazing angles in all cases when the suggestions at paragraph 28 above are applied to the author's terrain data base. Backscatter Distributions plotted, give a straight line on Wiebull paper, and detailed methods and discussion are at Appendix 1 to Annex F. Care was taken to identify slope and aspect for every terrain facet and to correct slope for radar boresight. Correlation tests were carried out between those parameters which were likely to be in relationship, for grazing angles taken in steps of 2° and 3° and by median and mean filtering.

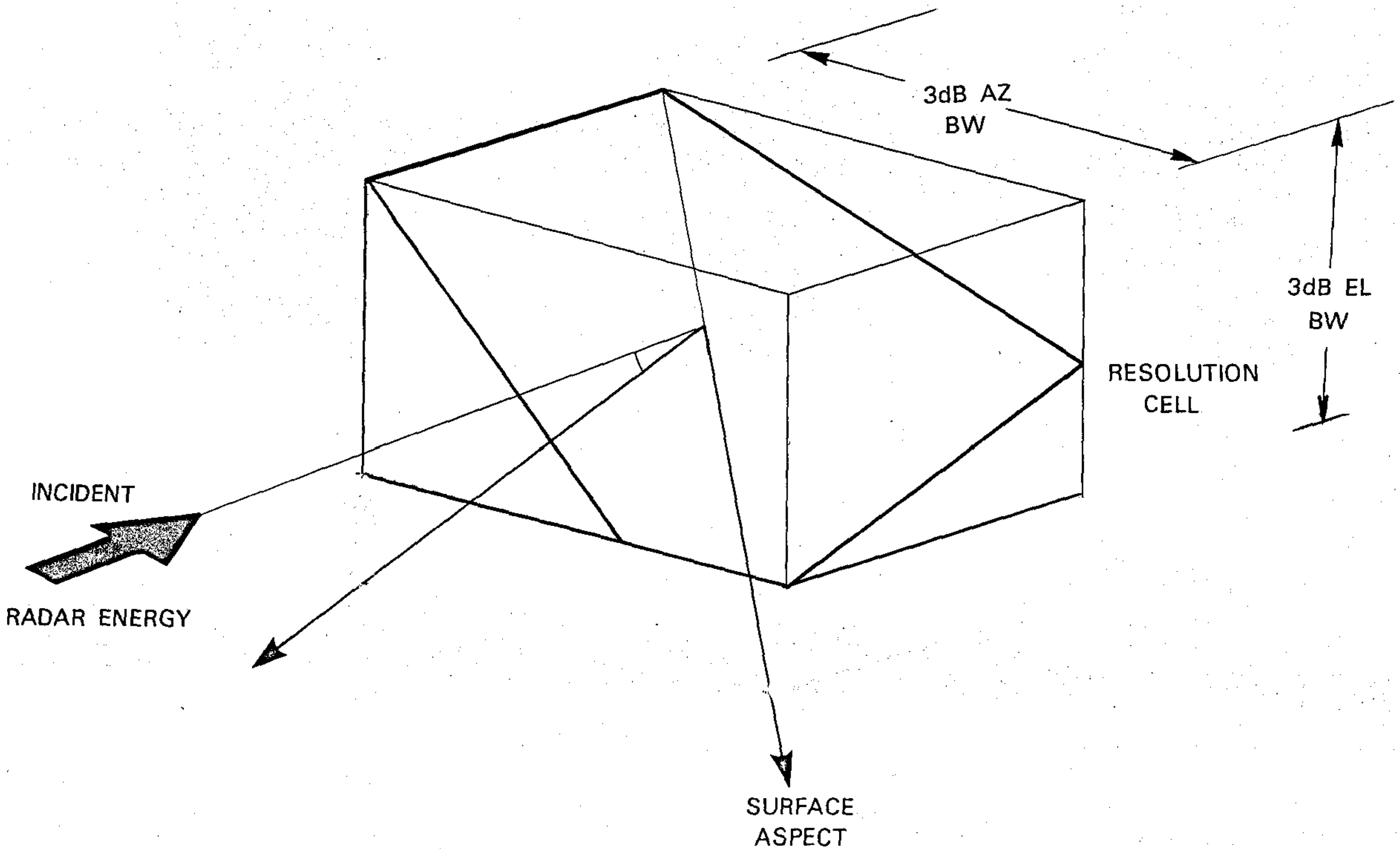

FIG 1 GENERAL GEOMETRY – GRADIENTS & ASPECT OF TERRAIN

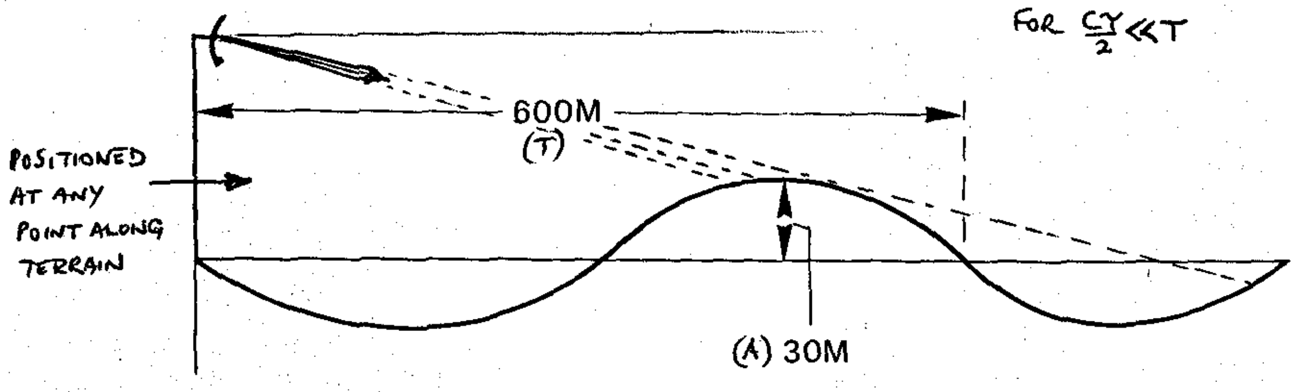

FIG 2a TERRAIN EXAMPLE (RATIO 0.05) ROLLING
A/T

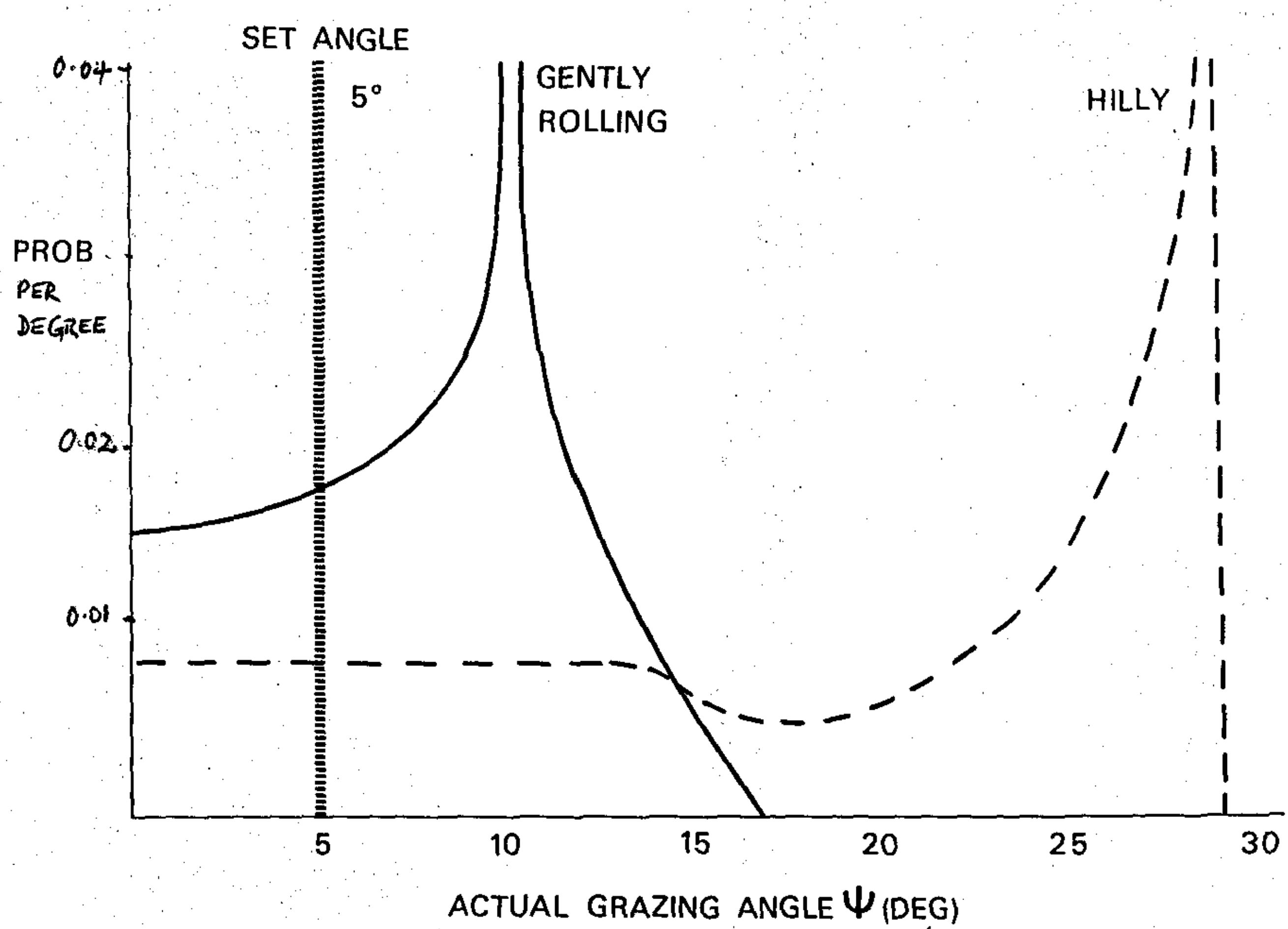

FIG 2b ACTUAL PDF'S FOR Ψ (RATIOS 0.05 & 0.1) FOR Ψ = 5°

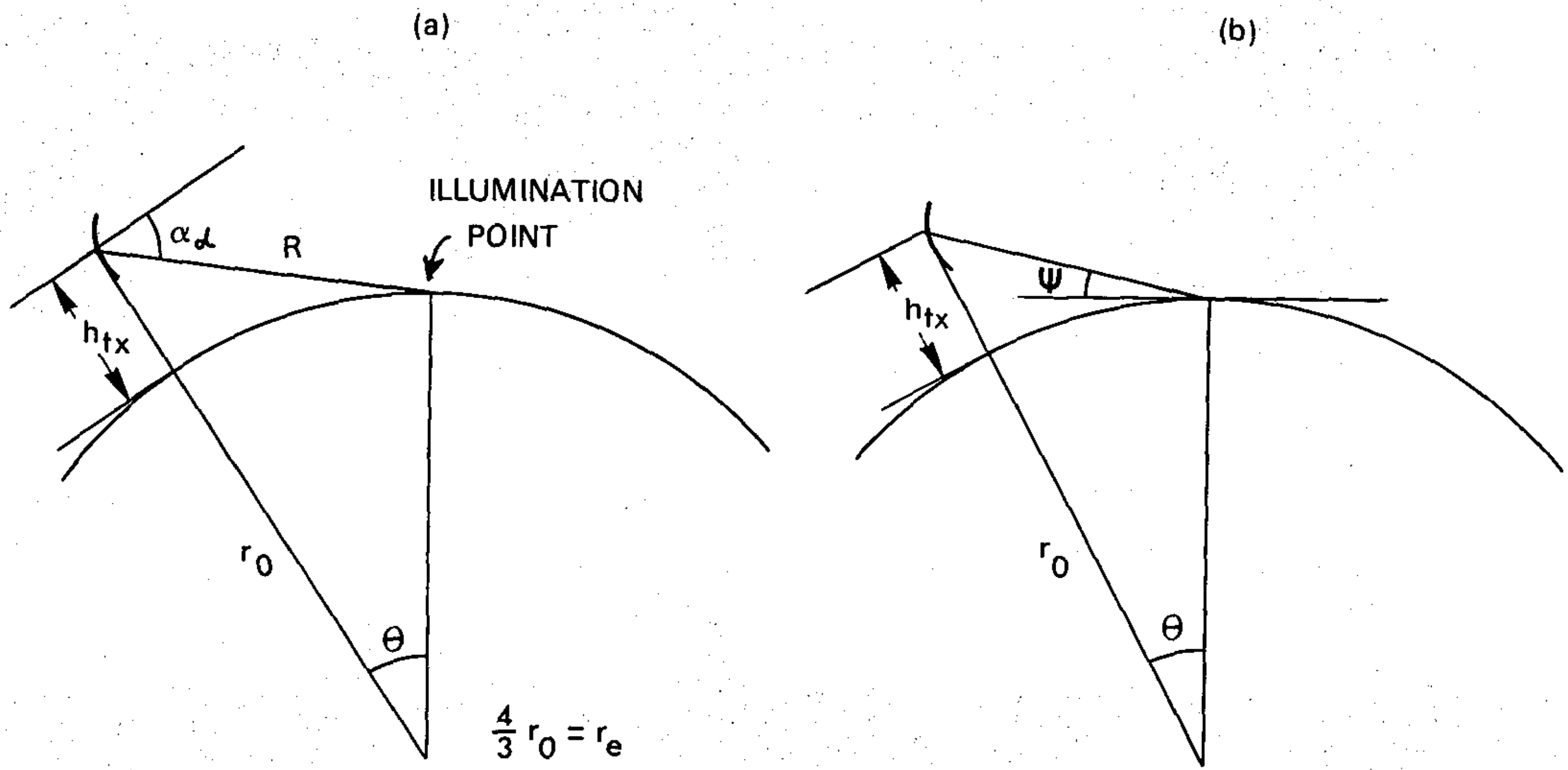

FIG 3 GRAZING ANGLE v RADAR RANGE

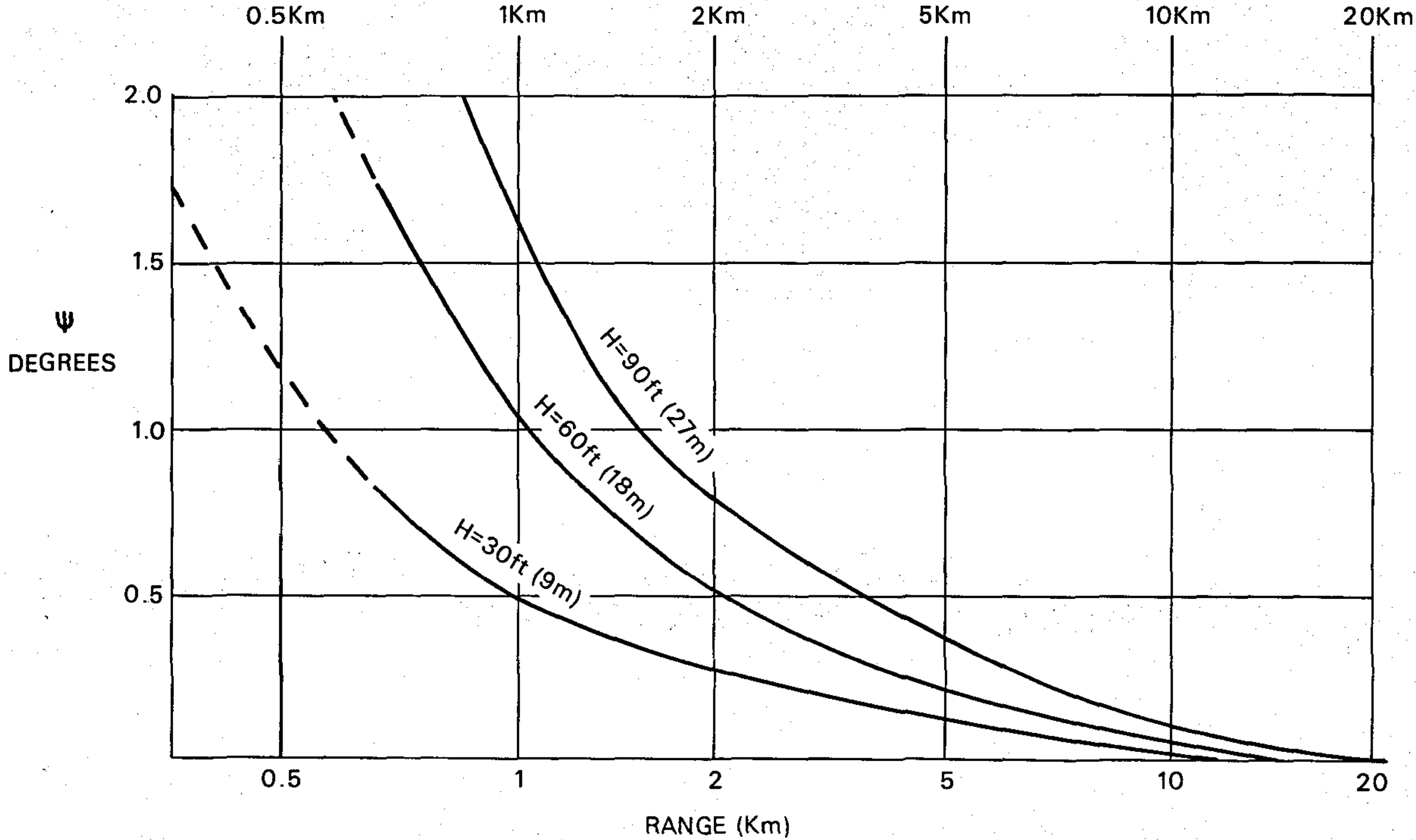

FIG 4 GRAZING ANGLE v RADAR RANGE

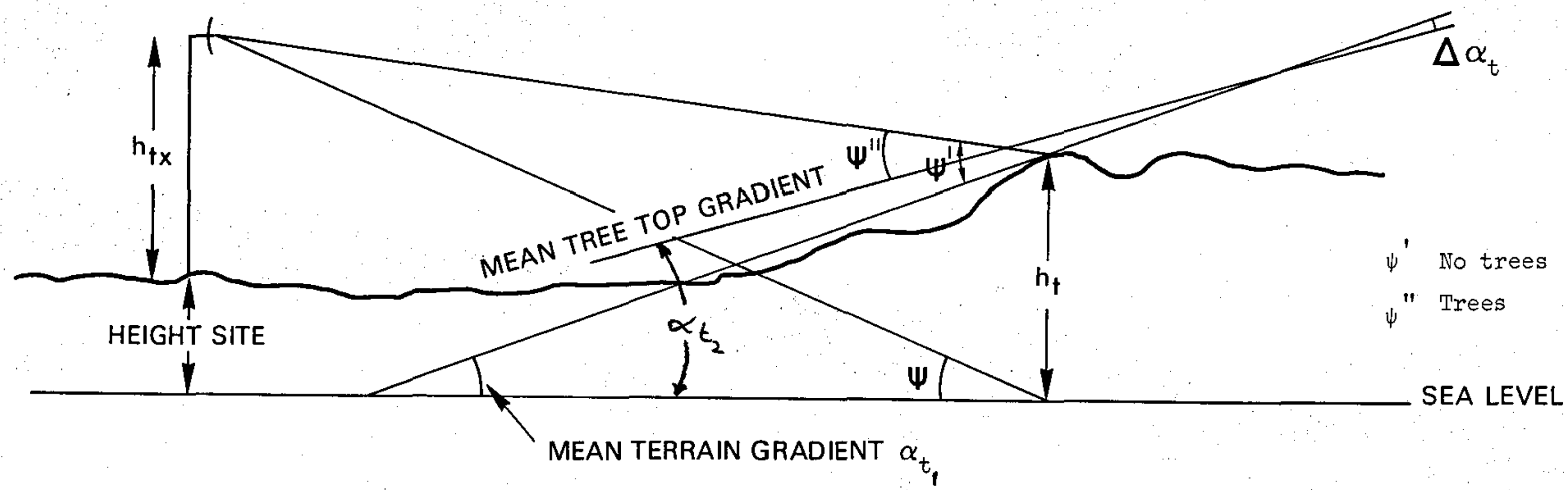

FIG 5 VARIATION IN GRADIENT DUE TO TREE COVER

10-220

CHAPTER 11

SYSTEM PERFORMANCE ASSESSMENT MODEL

1. The general sequence of inputs necessary for the assessment model are shown at Fig 1. A more detailed procedure is at Fig 2, showing the inter-relationship of optical and radar tracking with the terrain data and with certain operational factors which directly affect overall system assessment.

2. In applying the sequence, different circumstances may pertain, for example, assessments may be required for:

a. A general (and quickly produced) assessment, where reasonably accurate radar emission characteristics are known but with limited detail on the terrain obscuration affecting a deployed mobile system. The signal processing capability of the radar under these terrain conditions may also have to be assessed empirically.

OR b. Fully documented terrain data available from presurveyed sites to which a radar may be deployed and where details of the radar are known. Examples, which use typical figures are at Annexes G and H.

TERRAIN MODEL

3. Typical results for observable target track lengths in various types of terrain are shown at Annex E Fig 5a. It should be noted that the lower curve on this figure shows flat terrain with evenly distributed but not dense surface obscuration. A curve for flat terrain with sparse surface cover will usually approximate to the position of the higher curve on

Fig 5a and thus possess a higher probability of obtaining a given track length.

MISSILE SYSTEM MODEL

4. For a particular system reaction time, target altitude and target and missile velocity, the probability of obtaining minimum track length required at a given crossing range is calculated using the technique at Annex E paras 16-21. This is considered sufficiently accurate for prediction purposes without getting into the detail of missile trajectory shaping. Further factors which may affect a prediction might be included, for example, radars associated with point defence systems are more likely to engage radially approaching targets than those area coverage systems which will also engage crossing targets. Radial observable track lengths are often likely to be longer than the majority of crossing observable track lengths. The value of P_{T_L} obtained from this process is not of course the tracking or missile success rate - merely the opportunity value for a particular area which meet the minimum track length requirements. In an optically controlled system the assessment sequence next moves into P_{OE} and P_{MX} as seen at Fig 2 (but see also paras 6 and 7 below).

RADAR SYSTEM MODEL

5. In a radar tracking system the next step is to assess the probability of gaining and maintaining radar track within the observed track length periods. At times the sightline will include clutter plus target, while at other times clutter will be shadowed. Terrain may be flat or sloped hence backscatter model values proposed at Chapters 10, Chapter 4 and Appendix 1 to Annex F should be used; together with the known or assessed radar

parameters. Propagation conditions should be incorporated, as necessary. It may be advantageous to work through the sequence under 'best case' and 'worse case' conditions to determine the 'spread' of performance to be expected. Ideally, System, Environmental and Statistical values should be taken into account each time with a range of possible values. Attempts have been made to simplify the 'paper' operation of the sequence at Annexes G and H, however a modular computer program was also written in Fortran for analysis purposes for terrain and radar signals.

SYSTEM AVAILABILITY AND OPERATOR PERFORMANCE

6. Adjustment of the predictions at the bottom of Figure 2 are often a matter of "military judgement" in an operational environment. A point of contention between manufacturers and the author in the past! In some cases fairly reliable figures may be available, eg MTBF, while in others, such as availability of spares for radars and associated equipments and reloads for missile systems may be more difficult to assess. The effect of learning curves and operator climatic degradation are also part of the equation and cannot be ignored.

SYSTEM PERFORMANCE IN COUNTERMEASURES

7. This is considered separately from the system performance in a benign environment because two aspects exist - that of inherent or incorporated automatic design features which minimise the effectiveness of countermeasures and that of operator involvement of reducing countermeasures effectiveness by his skill. The effect of target manoeuvre and chaff degradation in any given situation is applied as a reduction factor, for example, due to target

glinting or range gate disturbance leading to an increase guidance system miss-distance. (See Annex E Figs 1 to 4) and is at present often a matter of considered judgement rather than hard fact from trials because of the number of variables involved.

APPROXIMATE PREDICTIONS

8. Approximate predictions can be obtained by applying empirical values, based on experience to the simple model P_{DET} x P_{TL} x P_{MX} with the extra factor P_{OE} inserted as appropriate. Further adjustment may be necessary for multiple fire channel or refire situations where a second attempt is necessary if the initial tracking and the first missile fails - providing of course sufficient observable track length is available to accommodate target response analysis, refire reaction time and missile flyout time for a refire.

HIGH AND LOW RISK TRACKING AREAS

9. Aircraft in transit, while encountering point defences at their destination - which they must radially approach, will inevitably be forced to transit through area defences en-route in both directions. Area defences may also be enhanced by other point defences,both mobile and fixed.

10. Area defences are likely to be on pre-determined sites in the main with higher P_{TL}; the value of P_{TL} varying invalue with terrain cover and surface undulation. Sharp ridges in an area will enhance the possibility of tracking under diffraction conditions, and may slightly increase the system performance in these areas.

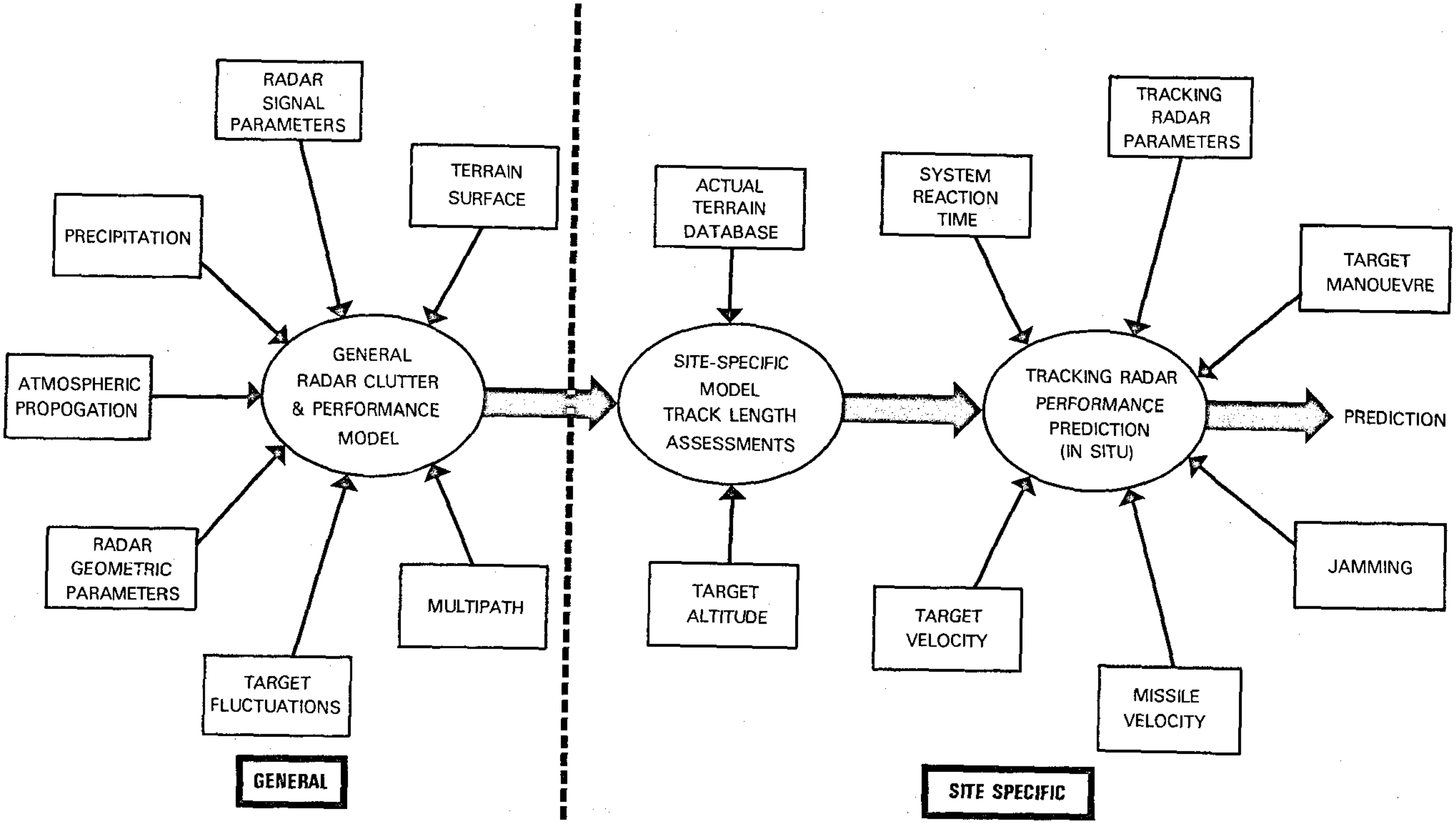

FIG 1 GENERAL SEQUENCE - PREDICTION MODEL

FIG 2 OVERALL PREDICTION SEQUENCE

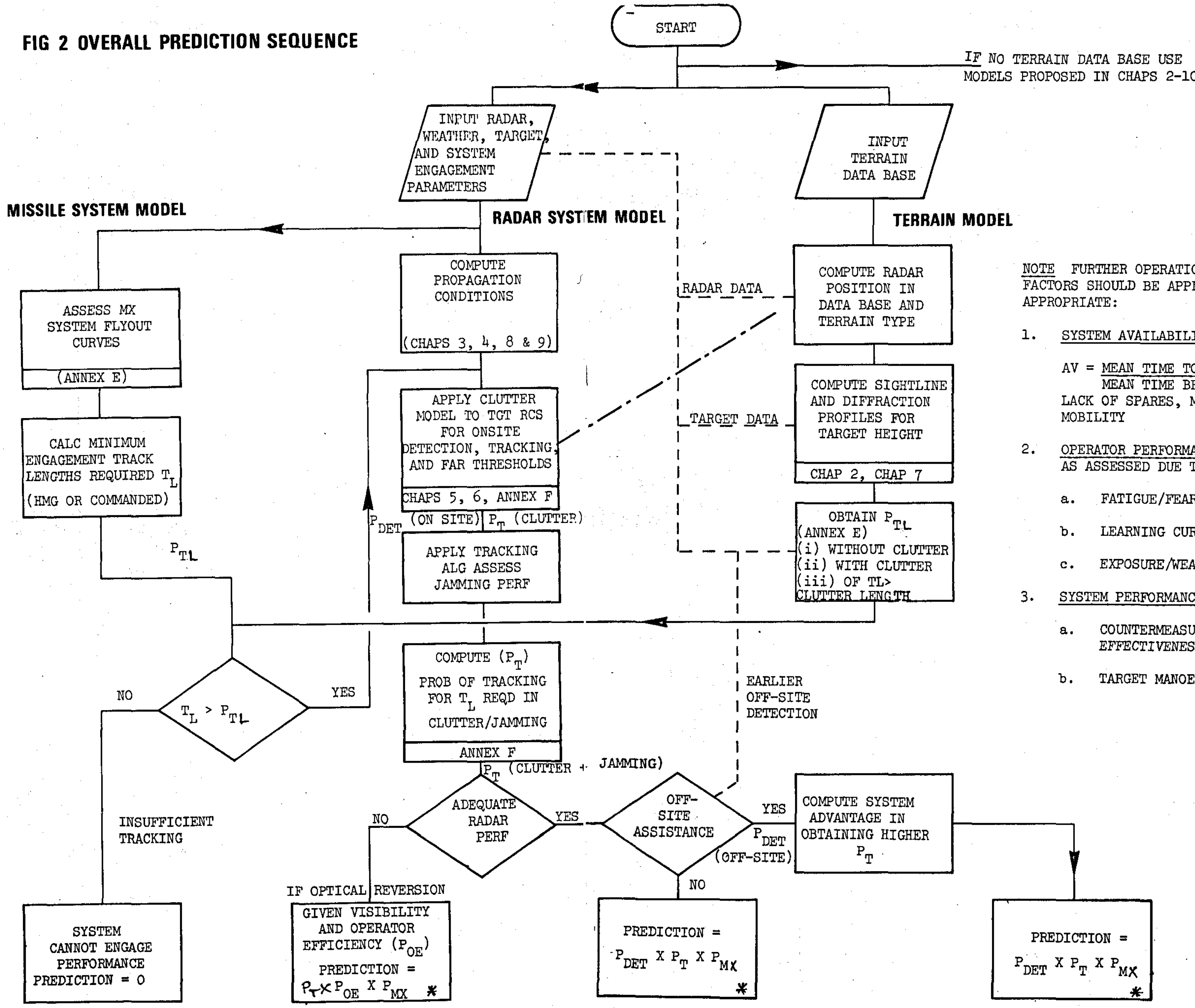

NOTE FURTHER OPERATIONAL DEGRADATION FACTORS SHOULD BE APPLIED AS APPROPRIATE:

1. SYSTEM AVAILABILITY (P_R)

   $AV = \frac{\text{MEAN TIME TO REPAIR}}{\text{MEAN TIME BETWEEN FAILURES}}$

   LACK OF SPARES, MX RELOADS, MOBILITY

2. OPERATOR PERFORMANCE AS ASSESSED DUE TO:

   a. FATIGUE/FEAR AND MORALE

   b. LEARNING CURVES

   c. EXPOSURE/WEATHER

3. SYSTEM PERFORMANCE

   a. COUNTERMEASURES EFFECTIVENESS

   b. TARGET MANOEUVRE

* MULTIPLY BY P_R WHERE APPLICABLE

CHAPTER 12

SUMMARY OF RESEARCH AND RECOMMENDATIONS

GENERAL OBSERVATIONS

1. Sightline. It has been shown that the predominant factor in detecting and tracking a low level target successfully is the ability to obtain a sightline, ie, a minimum unscreened, or 'unmasked' track length. For most terrain this will only occur with certainty if the radar aerial is raised on a mast, clear of immediate obstacles and vegetation. In flat terrain this may be sufficient for all-round coverage, however in undulating and hilly terrain targets at longer range may remain obscured due to shadowing. A terrain data base allows an initial assessment of sightline probability in a given area to be made on a statistical basis. Precise sightline information can only be obtained by optical survey of the actual radar site and this will vary from season to season and with changes in local obstacles such as the proximity of mobile vehicles (or smoke in optical systems). In the past it has not been the normal practice to raise tracking radars on masts because of the difficulties of stabilising the radar beam under conditions of wind-gusting. Although raised tracking radars may now be (theoretically) possible, while maintaining accuracy by the use of mast-mounted accelerometers and associated error correction by computer; radars with low aerial heights will be widespread for many years, hence the sightline prediction will be of continued importance, since all other radar tracking functions are dependent upon it.

2. Clutter. Given a sightline, clutter is of next importance since the radar beam will invariably strike the surface when directed at low level targets even if on a raised mast. It is then necessary to model the clutter levels expected at the low grazing angles as suggested at Chapter 4, and

extended with actual results at Annex F. At this point the significance of the prediction model depends on whether an offensive or defensive viewpoint is taken. The clutter model will enhance the apparent performance of a defensive radar if the clutter level is assessed as lower than is actually the case; or if the radar's clutter processing capability is over-assessed. Conversely if the clutter level is assessed as 'high' radar performance will be predicted as relatively 'poor', where even the best clutter processing may not enable a target to be separated from the clutter for tracking purposes. Example predictions at both extremes have been shown in the report (ANNEX H).

3. Validation of Models. Clutter models are difficult to validate because of the paucity of reliable measurements. It is the author's opinion that although a particular clutter model may be selected for practical purposes - if for no other reason than to give a starting point for predictions - it would be wrong to assume that this can be much better than a reasonable estimate. No existing clutter model could be said to be really adequate or scientifically precise unless it is site-specific and radar-specific, resulting from on-site measurement in all weather and seasonal conditions. Much of the uncertainty is due to the very large number of variables which are so dependent on local conditions.

4. It is seen therefore that the scope for a study of this type could be almost open-ended, since, as more results of clutter research become available the conclusions can be influenced slightly - first one way and then the other. However clutter itself is just one part of the overall input required for a useful prediction model for a low level tracking radar.

5. Results from some systems and measurements studies have been made using search (acquisition) radars, where clutter is often measured over longer ranges, at different RF's and longer pulse durations (hence larger resolution cells); such results often indirectly affect the overall performance of a radar tracking system - since search radars are often used to 'hand-on' targets to associated tracking radars which operate in the same area. Both surface scanning and airborne radars, though providing clutter measurements are noted to suffer "smeared" clutter effects because of the speed of the radar beam's swift traverse from one resolution cell to the next. These effects have not been considered significant for stationary systems.

6. It is possible that too much is made of the clutter problem in isolation in the context of tracking radars, since in practical terms clutter is only of interest on those azimuths where a target sightline exists simultaneously with a sightline to the underlying clutter. Furthermore it is of interest only in those sectors where sufficient track length can be observed for a useful period of time (distance). Once within the "useful" part of the radar site's field of view the radar parameters and the many other variables such as chaff, multipath, diffraction and weather also become important.

SENSITIVITY TO PARAMETER CHANGES

7. The sensitivity of the overall prediction to variations in the individual parameters is of particular interest. Target altitude is a critical parameter in determination of observable track length probability (P_{TL}). For example a reduction in height (seen in one practical case from 300 ft to 200 ft) gave a 10% reduction in P_{TL} - a much more significant effect in the overall result than say a change in target speed of 40 $m.s^{-1}$ which, in the same case, changed P_{TL} by 4%. Similarly degradation due to target scintillation, multipath and the many other factors considered in the report cause only minor

changes in the overall prediction, varying to a greater or lesser extent due to circumstances.

MODEL VALUES

8. Suitable model values, included in each chapter summary must be supplemented by an assessment of the signal processing capability of the particular radar. This may be difficult to assess, since clutter processing may be assisted by pulse to pulse frequency agility, polarisation agility, MTI, multiple channel operation with different processing in each channel, (such as ground clutter filtering and moving clutter filtering) noise or precipitation or chaff filtering. For the relatively short ranges for tracking, clutter is always assumed to be present at low grazing angles unless shadowing is present. A reduced effect will be felt if off-boresight modes are used (see Chap 9 para 11c).

9. Assuming the clutter values to be averaged and taking figures from the extensive survey and measured values, a reliable median value for σ_o (in flat terrain) is about - 25 dBm^2m^{-2} with a standard deviation of 9 to 10 dBm^2m^{-2}. These values will vary slightly with changes in pulse duration, RF, polarisation etc, but are considered suitable for I and J band tracking radars. (10,000 MHz to 18,000 MHz). As RF increases σ_m is likely to reduce to $-30 dBm^2m^{-2}$. (see also discussion at App 1 to Annex F)

10. From the purely radar aspects the overall P_D used (Chap 4 eqn 47) must be converted to the probability of tracking. Given the observable track length probability for a given geographical area and assuming a percentage of shadowing during an observed track length, multipath and other radar degradations are applied as reduction factors which will affect different tracking systems in

different ways. For example, a judgement must be made on the effect of short-term loss of sightline for optical or radar tracking as appropriate. Some systems will be able (by rate-aided tracking) to withstand narrow sectors of obscuration quite successfully. For some optical systems a slight adjustment will be necessary for the improved tracking of targets through deciduous trees when defoliation occurs in winter.

CONCLUSIONS

11. The selected method of overall system performance prediction is suggested to be the most reliable approach available within the constraints set out at Chapter 1, the limited worldwide results directly applicable to this study, and the large number of variables involved. It is thought that overall performance predictions will never be exact in the scientific sense, since apart from the measurable parameters there are also those human factors in an unknown operational environment. In addition the possibility of such occurances as electro-magnetic incompatibility, the variable and surprise effects of jamming and the largely unknown effectiveness of ECCM response all influence the results in practice.

12. Many related studies have been made but totally accurate predictions cannot be made for all the unknowns- since even those results obtained from tracker radars and associated missile systems used in action in N Vietnam, the Middle East or in the Falklands cannot be read-across to other geographical locations with any degree of reliability.

RECOMMENDATIONS

13. Since raised tracker aerials will not totally overcome the problem of obscuration in hilly terrain, and since P_{TL} is such a predominant factor in the

prediction process it is recommended that:

a. Further studies should be made into the distribution (density) of surface culture and buildings in those areas for which P_{TL} is known, in order to search for possible correlation between P_{TL}, undulation and surface coverage. The intention would be to assign a P_{TL} to an area (of limited extent) by examination of accurate maps and stereo photographs. 'Good' or 'Bad' areas for deployment could possible be determined - or conversely safe or less safe areas to fly.

b. More clutter measurements are needed using carefully controlled conditions with as many radar parameters varied as possible. These should be made in areas typical of the intended deployment with particular attention to terrain slope measurement.

c. Some practical diffraction trials are required where an aircraft transits behind ridged terrain with and without tree cover and with accurate ridge profile measurements. Accurate instrumentation over a number of target runs would be necessary to compensate for target RCS fluctuations due to minor manoeuvres. Alternatively it might be possible to make diffraction measurements using a balloon-mounted reflector tethered behind the ridge.

REFERENCES

CHAPTER 1

1. Warden M P — "An Experimental Study of some Clutter Characteristics". RSRE AGARD Conf Proc No 66 1970

2. Riley J H — "An Investigation into the Spatial Characteristics of Land Clutter at 'C' Band". ASWE Tech Rep TR 71-6-1971

3. Allan D — "Predicting the Performance of Surface Radars in Land Clutter". Thesis (MSc), Loughborough University of Technology (through RAFC Cranwell) Aug 1980

4. Billingsley J B and Briggs D L — "Survey of Terrain Reflectivity Measurements". MIT CMT8 Vol 2, MIT Lincoln Laboratories Massachusetts, May 1980

5. Skolnik M — "Radar Handbook" McGraw Hill, New York 1970 and "Introduction to Radar Systems". McGraw Hill 1962

6. Long M W — "Radar Reflectivity of Land and Sea". Lexington Books 1975

7. Nathanson F E — "Radar Design Principles". McGraw Hill New York 1969

8. - — "The Canadian System of Soil Classification". Canadian Dept of Agriculture Publication 1646 Ottawa 1978

CHAPTER 2

9. Francois R E — "Geometric Radar Coverage Predictions using Digital Terrain Elevation Data". MIT Lincoln Laboratories IEEE International Radar Conference 1980

10. Adgie R L — "The Effect of Terrain Screening on Clutter Visibility". RSRE Malvern DIV Note 1/79 June 1980

11. Theresby G B — "Some of the problems in Digital Terrain Model Construction". AGARD Conf Proc 269 September 1979

NOTE: Ibid references are 'within chapter' only.

CHAPTER 3

12.	Skolnik M	"Introduction to Radar Systems". McGraw Hill 1962 (a)
13.	Nathamson F E	"Radar Design Principles - Signal Processing and the Environment". McGraw Hill 1969 (a)
14.	Ibid	"Rayleigh Distributed Vector". 1963 (b)
15.	Battan L J	"Radar Observations of the Atmosphere". Univ of Chicago Press 1973 (a)
16.	Dodsworth E J	"Rain Clutter". Unpublished personal notes RSRE Malvern July 1974
17.	Barton D K	"Radar Systems Analysis" Prentice- Hall Inc 1964
18.	Ibid	1973 (b)
19.	Ibid	1973 (c)
20.	Ibid	1973 (d)
21.	Harrold T W	"Estimation of Rainfall Using Radar - A Critical Review". Meteorological Office Scientific Paper No 21 MET 0.767 1965 (a)
22.	Warden M P and Dodsworth E J	"A Review of Clutter 1974". RRE Tech Note 783 September 1974
23.	Reiss et al	"Land and Precipitation Clutter Measurements at 'C' Band" ASWE Lab Note XRE-68-10 June 1968
24.	Ibid	1969 (b)
25.	Ibid	1965 (b)
26.	Bilham E G	"The Climate of the British Isles". McMillan & Co 1938
27.	Long M W and Zehner S P	"Effects of the Sea on Radar Echo". IEEE Trans Aerospace and Electronic Systems Vol AES 6 November 1970

CHAPTER 4

28. Rivers W K — "Shipboard Surveillance Radar Prog Assessments 1985-2000". Vol II Radar Clutter J Hopkins Univ. AD A061136 Mar 1978 (a)

29. Ibid — March 1978 (b) Ref List p 3-70.

30. Ibid — March 1978 (c) Ref List p4-25.

31. Ibid — 1978 (d) Ref List p4-25

32. Chatfield C — "Statistics for Technology" Penguin 1970

33. Mitchell R L — "Radar Cross-Section Statistics of Randomly Orientated Disks and Rods" Trans IEEE AP 17 May 1969

34. Allan D — Ref 3 Chapter 1

35. Valenzuela G R — "Point Scatterer Formulation of Terrain Clutter Statistics" NRL Rep 7459 AD750668 Sep 72 (a)

36. Ibid — 1972 (b)

37. Ibid — 1972 (c) at his ref (13)

38. Ibid — 1972 (d)

39. Ibid — 1972 (e)

40. Ibid — 1972 (f)

41. Ibid — 1972 (g)

42. Ibid — 1972 (h)

43. Peake W H — "Theory of Radar Return from Terrain" IRE Nat. Conf. Record 7(1) 1959 27-41

44. Zubkovitch S G — "Statistical Characteristics of Radio Signals Refl from the Earths Surface". Russian FTD Translation MT 24-780-74 AS 783046 Jun 1974

45. Andre, Bechtel & Foster — "Radar Clutter Research" Cornell Aero Labs AD 673938 July 1968

46. Plaza T J — "Clutter Cell Maps Guide Radar Simulation" General Dynamics Pomona. Microwaves Apr 1966

47. Ibid — 1978 (e)

48. Hayes R D — "Clutter Returns from Ground Radars" Rem Sens Wkshop on Radar Backscatter Jan 1979 (a)

49. Drake & Schuchman — "Feasibility of Using Multiplexed SLAR Imagery for Water Resources Management and Mapping Vegetation Communities". Proc Int Symp Rem Sens Vol 1 Apr 74

50. Meuche C E — "Moving Target Detector - An Improved Signal Processor". MIT Report

51. Long M W — "Radar Reflectivity of Land and Sea". Lexington Books 1975

52. Hayes, Currie & Long — "An X Band Polarisation Measurements Program" Univ Michigan Fen 1957

53. Ament W S, MacDonald & Shewbridge — "Radar Terrain Reflections for Several Polarisations and Frequencies". Trans Symp Radar Return 1959

54. Hayes R D — "Radar Clutter Models at 95 GHz". US Armament R&D Command Rep AD AO 89986 ARSCD-MR-80001

55. Long M W — "Radar Reflectivity of Land and Sea". Lexington 1975

56. Linell T — "An Experimental Investigation of the Amplitude Distribution of Radar Terrain Return" 6th Conf. Swed Ntal. Comm. Sci. Radio. Stockholm Mar 1963 (a)

57. Katz I — "Radar Backscattering from Land at 'X' Band". APL Rep CLO 4-002 June 1963

58. Erikson L O — "Terrain Return Measurements ----". Proc 6th Conf. Swed Natl. Comm. Sci. Radio Stockholm 1963

59. Lindquist & Staleby — "Ground Clutter Model for Radar Applications". Proc Int Conf IEEE Oct 1973 (a)

60. Ibid — 1973 (b)

61. Ibid — 1963 (b)

62. Kusters E R — "Biological and Geophysical Factors of EM Wave Propagation and their use in Digital Data Banks AGARD Conf Proc Sep 1979

63. Hoekstra & Spanogle — "Backscatter from Snow and Ice Surfaces at Near Incident Angles". IEEE Trans. Ant and Prop. Nov 1972

64. Krason and Randig — "Terrain Backscattering Characteristics at Low Grazing angles". Proc IEEE No 12 Dec 1966

65. Moore R K, Soofi K A Purduski S M — "A Radar Clutter Model: Average Scattering Co-efficients of Land and Ice". IEEE Trans-Aerospace Elect Syst Vol AES 16 No 6 Nov 1980 (a)

66. Linlor W I et al — "Snow, Wetness Measurements for Melt Forecasting". NASA Spec Pub SP 391 Aug 1975

67. Ibid — 1979 (b)

68. Reiss et al — "Land and Percipitation Clutter at C Band". ASWE Lab Note XRE 68-10 June 1968

69. Tomlinson P G — "A model for Space Radar Clutter" RADC Final Tech Rep. TP 336 Jun and RADC-TR-79-166, AD 072-990 Jun 1979 (a)

70. Dodsworth E J — "Unpublished Note". No 2 RSRE

71. Dodsworth E J — "Unpublished Note". 1974 (a) RSRE. Note 9 and "Overall Probability of Ground Clutter for Ground Based Surveillance Radar".

72. Boothe — "The Weibull Distribution" RE-TR-69-15 AD 691-109 Jun 1969

73. Sekine et al — "Log Weibull Distributed Sea Clutter". Proc IEE Vol 127 No 3 Jun 1980

74. Shelerher D C — "MTI Radar" Artech 1978

75. Dodsworth E J — "Sea Clutter". Unpublished Personal Note. RSRE Jan 1974

76. Riley J H — "An Investigation into the Spatial Characteristics of Land Clutter". ASWE Tech Rep TR-71-6 Feb 1971 (a)

77. Dodsworth E J — "Overall Probability Distribution of Ground Clutter for Ground Based Surveillance Radar". RSRE Memo 3066

78. Warden M P & Wyndham — "A Study of Ground Clutter Using a 10cm Surveillance Radar". RRE Tech Note 745 AD 704874 Sep 1969

79. De Loor G P & Jurriens A A — "The Radar Backscatter of Vegetation" Physics Lab RVO-TNO. The Hague AGARD CP90-71 Jun 1971

80. Ibid — 1978 (c)

81. Warden M P — "An Experimental Study of Some Clutter Characteristics" RSRE AGARD Conf Proc No 66 1970

82. Goodyear Corporation — "Radar Return Study: Measurements of Terrain Backscatter X Band". GERA 463 Sep 1959

83. Ericson L O — "Terrain Return Measurements ----". Proc 6th Conf Swed Natl Comm Sci Rad Stockholm 1963

84. Nathanson F E — "Radar Design Principle" McGraw-Hill 1969

85. Nathanson F E & Reilly J P — "Clutter Statistics that Affect Radar Performance Analysis" ESACON Proc IEEE Vol AES 6 Nov 1967

86. Long M W — "Radar Reflectivity of Land and Sea". (Page 212) Lexington Books 1975

87. Ibid — 1980 (b)

88. Ibid — 1963 (c)

89. Pollon G E — "Course Notes Topics in Radar Clutter Modelling Tech Serv Corp Santa Monica March 1973

90. Trebits R N et al — "Mm Reflectivity of Land and Sea" (GIT) Microwave Journal pp 49-53 August 1978

91. Hayes R D — "Radar Clutter Models at 95 GHz". US Armament R&D Command Report. AS AO 89986 ARSD-MR-80001.

92. Ibid — 1980 (c)

93. Ibid — 1980 (d)

94. Ibid — 1979 (b)

95. HQAF Staff — "Low Altitude Clutter and Multipath Models for TAC ZINGER". Georgia Inst of Tech April 1979

96. Arafiles V P — "Comparison of Radar Clutter Models". HQ FTD/SDER 1981 (a)

97. Ibid — 1981 (b)

98. Cosgriffe, Peake & Taylor — "Terrain Scattering Properties for Sensor Design" Univ Ohio Eng Exp. Bulletin May 1960

99. Barton D K — "Radar Systems Analysis pp 165-286 Prentice Hall 1964

100. Ibid — 1979 (c)

101. Ament W S et al — "Radar Terrain Reflections for Several Polarisations and Frequencies". Symp. Rad. Ret. AD 320-390 May 1959

102. Rider G C — "A Polarisation Approach to the Clutter Problem" IEE Conf. Proc. Radar 1979

103. Reiss et al — "Land and Precipitation Clutter at C Band". ASWE Lab Note XRE 68-10 June 1968 (Restd)

104. Gent H et al — "Polarisation of Radar Echoes, including Aircraft, Percipitation and Terrain". Proc IEE Vol 10 1963.

105. Brindley et al — "A Joint Army/Air Force Investigation of Reflection Coefficients". IIT Res. Inst. Chicago AS 031-403 AFFDL TR76-67 July 1976

106. Daley et al — "NRL Terrain Clutter Study Phase II". NRL Rep 6749 October 1969

107. Reitz E A — "Radar Terrain Return Study". Final Report GERA 463 AS 229-104 September 1959

108. Katz and Spetner — "Polarisation and Depression Angle Dependence of Radar Terrain Return". J. Res. Nat. Bureau Stds. Vol 64D No 5 Sep/Oct 1960

109. Ibid — 1973 (c)

110. Simkins, Vannicola & Ryan — "Seek Igloo Radar Clutter Study". RADC TR 77-338 October 1977

111. Ibid — 1974 (b)

112. Ibid — 1978 (d)

113. Ibid — 1971 (b)

114. Ibid — 1979 (c)

115. Kayal et al "Extension to the ORT Clutter Model" ITT Rep Contract F 33615-69-C138 1971

116. Jernigan J J "Results and Analysis of Ground Clutter Measurements" SHAPE Tech Centre Memo 133

117. Jernigan J J "Ground Clutter Distribution Measurements". SHAPE Tech Centre Memo 186

118. Rigden C J "High Resolution Land Clutter Characteristics". ASWE Tech Rep TR 73-6 January 1973

119. Briggs D L & Billingsley J B "Briefing to US Army and UK Representatives on Systems Analysis". 16 June 1981

120. Ibid 1971 (c)

121. Ibid Ref 116 above

122. Ibid Ref 117 above

123. Swerling P "Detection of Fluctuating Pulsed Signals in the Presence of Noise". IRE Trans Vol IT 3 Sep 1957

124. Marcum J I "A Statistical Theory of Target Detection by Pulsed Radar" IRE Trans App Vol IT 6 APR 1960

CHAPTER 5

125. Hayes R D, Currie C H, & Long M W "An 'X' Band Polarisation Measurements Program". Univ. Michigan 3rd Conf Proc February 1957

126. Kerr D E (Ed) "Porpagation of Short Radio Waves". MIT McGraw-Hill NY. 1951

127. Linell T "An Expermental Investigation of the Amplitude Distribution of Radar Terrain Return" 6th Conf Swed. Ntnl. Comm. Sci. Radio. Stockholm March 1963 (a)

128. Hayes R D et al "Study of Polarisation Characs of Radar Targets". Georgia Inst. Tech Final Rep 1958

129. Ridenour L N "Radar System Engineering". McGraw-Hill

130. Ibid 1963 (b)

131. Dodsworth E J "Windshear" Unpublished personal note RSRE. Malvern January 1974

132. MRC "Statistics of Wind" MRC Note 408 April 1948

133. Nathanson F E "Radar Design Principles" McGraw-Hill New York 1969

134. Rivers W K "Shipboard Surveillance Radar Prog. Assessments 1985-2000". Vol II Radar Clutter. J Hopkins Univ. AD-AO-61136 March 1978

135. Elderkin & Powell "Measure to Time-Space Relationships in Atmospheric Turbulence". Batelle Pacific N W Labs. Washington (PRE 1974)

136. - "An Assessment of Turbulent Data for Aeronautical Applications" USAF Flight Dynamics Lab RAeS. CASI AIAA Conf 1971

137. Haddow R W "The Feasibility of using Chaff to Break Radar Lock at Low Level". CRAN. REP. September 1974 (a) (Classified)

138. Ibid 1974 (b)

139. Sunderan C S "Expendables in Electronic Warfare" IDR No 9 December 1976

140. Puskar R J "Radar Reflector Studies". Proc IEEE 1975 EASCON p 177. May 1974.

141. Vakin S A & Shustor L M "Principles of Jamming and Electronic Reconnaissance". Sovetskoy Radio Moscow FTD Transl. FTD MT-24-115-69. AD 692 642

142. Brown B M "Dipole Cross-Sections Calculated by Variational Techniques". AF TM 59. Univ. Texas Def. Lab. April 1961

143. Konrad T G et al "Radar Characteristics of Birds in Flight". Science 195 January 1968

144. Pollon G E "Distribution of Radar Angles" IEEE Trans. AES 8 November 1972

145. Dodsworth E J "Bird Clutter". Unpublished personal note. RSRE Malvern July 1974

CHAPTER 6

146. Barton D K "Radar System Analysis" Prentice-Hall 1964

147. Nathanson F E "Radar Design Principles - Signal Processing and the Environment". McGraw-Hill 1969 (a)

148. Skolnik M I — "Introduction to Radar Systems" McGraw-Hill 1962

149. Ament et al — "Radar Terrain Reflections for Several Polarisations and Frequencies" TRANS SYMP. Radar Return. Univ New Mexico 1959

150. Ibid — 1969 (b)

151. Ibid — 1969 (c)

152. Warden M P and Wyndham B A — "A Study of Ground Clutter using a 10 cm Surveillance Radar" RRE Tech Note 745 AS 704874 September 1969

CHAPTER 7

153. de Assis M S — "A Simplified Solution to the Problem of Multiple Diffraction over Rounded Obstacles" IEEE Trans Ant and Prop March 1971

154. Delaney J R and Meeks M L — "Prediction of Radar Coverage Against Very Low Altitude Aircraft" AGARD CP 269 September 1979 (a)

155. Deygout J — "Multiple Knife-Edge Diffraction of Microwaves" IEEE Trans Vol AP 14 No 4 July 1966

156. Rice P L et al — "Transmission Loss Predictions for Tropospheric Communications Circuits" NBS Tech Note 101 1967 (a)

157. Larson J V — "A Study of Propagation over Rough Terrain" Thesis Dept of Elect Eng. Univ Maryland USA 1963

158. Crysdale et al — "An Experimental Investigation of the Diffraction of EM Waves by a Dominating Ridge". IRE Trans. Ant & Prop Vol AP5 April 1957

159. Barsis A P & Kirby R S — "VHF and UHF Signal Characteristics Observed on a Long Knife Edge Diffraction Path". NB5 Rep. 6751, March 1961

160. Cassell P L et al — "Experimental Investigation of Mountain Obstacle Path Transmission at Microwave Frequencies". Motorola Riverside Res. Lab Rep. RL 3824-4. August 1957

161. Rice S O — "Diffraction of Plane Waves by a Parabolic Cylinder" Bell. Sys. Tech J. Vol 33 No 2 1954

162. Nengabauer H E J & Backynski M P — "Diffraction by Smooth Cylindrical Mountains" Proc IRE Vol 46 September 1958.

163. Wait J R & Conda A M — "Diffraction of EM Waves by Smooth Obstacles for Grazing Angles" J. Res. NBS Vol 63D No 2 1959

164. Carlson A B & Waterman J R — "Microwave Propogation over Mountain - Diffraction Paths". IEEE Trans. Ants and Prop Vol AP 14 No 4 1966 (a)

165. Hacking K — "Approximate Methods for Calculating Multiple Diffraction Loss". Electronic Letters Vol 2 No 5 May 1966

166. - — "Atlas of Radio Wave Propagation Curves for Frequencies between 30 and 10,000 MHz". Radio Res. Lab. Ministry of Postal Services Japan. 1957

167. Ibid — 1967 (b)

168. Dougherty H T & Maloney L J — "Application of Diffractions by Convex Surfaces to Irregular Terrain Situations". Radio. Sci. Vol 68D No 2. February 1964

169. Ibid — 1966 (b)

170. Ibid — 1979 (b)

171. Self A G — "The Prediction of Site Coverage at Radio and Radar Frequencies". RSRE Memo 3339 January 1981

CHAPTER 8

172. Skolnik M I — "Introduction to Radar Systems". McGraw-Hill 1962

173. Bean B R & Thayers G D — "Models of Atmospheric Radio Refractive Index". Proc. IRE. Vol 47 May 1959

174. Felix C — "Investigation of Propagation Prediction and Modelling Techniques". BAC Filton ESS/SS 339 March 1972

175 Reed H R & Russel C M — "Ultra High Frequency Propagation". Wiley & Sons NY 1953

176. Rice P L et al — "Transmission Loss Predictions for Tropospheric Communications Circuits". NBS Tech Note 101 1967

177. Sherwood E M & Ginzton E L — "Reflection Co-efficients of Irregular Terrain at 10 cm". Proc IRE Vol 43 1955

178. Smith J M — "Propagation Problems in Radar Systems Analysis" Marconi Radar Syst. IEEE Int. Radar. Conf 1980

179. Millington G et al — "Double Knife Edge Diffraction in Field Strength Predictions" Proc IEE Vol 109c 1961 (see also Marconi Review No 80 1946)

CHAPTER 9

180. Senior T B A — "The Elevation Errors Involved in the Radar Location of a Low Flying Target". RRE Memo 1220 March 1956

181. Barton D K — "Low Angle Tracking" Microwave Journal December 1976

182. Mrstik A V & Smith P G — "Multipath Limitations on Low Angle Radar Tracking" IEEE Trans. Aerosp & Elect Syst. Vol AES 14 No 1 January 1978

183. Becker & Sureau — "Control of Radar Site Environment by the Use of Fences". IEEE Trans. Ant & Prop Vol AF 14 November 1966

184. Evans G C — "Influence of Ground Reflections on Radar Target Tracking Accuracy" Proc IEE Vol 113 No 8 August 1966 (a)

185. Smith J M — "Propogation Problems in Radar Systems Analysis" Marconi Radar Syst. IEEE Int Rad. Conf 1980

186. Delaney J R & Meeks M L — "Prediction of Radar Coverage Against very low Altitude Aircraft". AGARD Conf. Proc. No 269 September 1979

187. Armstrong & Cornwell — "Multipath Measurements" ER 74-4316 AD 001-064 August 1974 (a)

188. Ibid — 1974 (b)

189. Fanti, Franchi & Taylor — "Effect of Multipath on the Height Finding Capability of Fixed Radar". RADS TR 77-47 AS AO 38-833 January 1977

190. Merrill — "Analysis of Bistatic Radar" IRE Trans. Aerospace and Nav March 1961

191. Davis D E N — "Bistatic Radar" Electronic Letters Vol 4 May 1968

192. Shearman S M — "The Use of Complex Indicated Angles in Monopulse Radar to Locate Unresolved Targets". Proc NEC Vol 22 1966

193. Peebles P E et al — "Multiple Target Monopulse Radar Processing Techniques". IEEE Trans. Aerospace & Elect. AES Vol 4 November 1968

194. Graf & Nagle — "Frequency Diversity and Signal Processing to Reduce Glint Pointing Errors". Tech Rep No 1 Army Missile Command June 1972

195. Peebles P E — "Multipath Angle Error Reduction Using Multiple Target Methods". IEEE Trans Aerospace & Elect Vol AES 7 November 1971

196. Burks D G et al — "Frequency Agility and Radar Pointing Errors Due to Multipath". Auburn Univ. Army Missile Command AD 787-390 October 1974 (x)

197. Barton D K & Ward — "Handbook of Radar Measurement". Prentice-Hall Inc Englewood Cliffs NJ 1969 (a)

198. Dax D R — "Keep Track of that Low Flying Target" Microwaves April 1976

199. Symmonds M D & Smith J M — "Multifrequency Complex-Angle Tracking of Low Level Targets". Int. Conf. Radar Past and Present October 1973

200. Howard D D et al — "Experimental Result of the Complex Indicated Angle Technique for Multipath Correction". IEEE Trans. Aerospace & Elect. Syst Vol AES 10 No 6 November 1974

201. Shearman S M — "Complex Indicated Angles Applied to Unresolved Radar Targets and Multipath". IEEE Trans. Aerospace & Elect Syst. Vol AES 7 No 1 January 1971

202. Ibid — 1969 (b)

203. Ibid — 1966 (b)

204. Ibid — 1969 (c) p 330

205. Long M W — "Radar Reflectivity of Land and Sea". p 39, Lexington Books 1975

206. Ibid — 1974 (y)

207. Ibid — 1974 (z)

208. Kirk K — "A Radar Detection Model" Center for Naval Analysis, Arlington. AS-A049-261 March 1977

209. Texas Instr — "Radar Multipath Error" PP X 59 Professional Program Exchange

CHAPTER 10

210. Simkins, Vannicola & Ryan — "Seek Igloo Radar Clutter Study". RADC TR77-338 October 1977 (a)

211. Tomlinson P G — "A Model for Space Radar Clutter". RADC Final Tech Rep. TR 336 June 1979

212. Evans I S — "An Integrated System of Terrain Analysis and Slope Mapping". Final Report DAERO 591-73-G0040 Univ. Durham 1979

213. Ibid — 1977 (b)

214. Edwards P N & Christie J M — "Yield Models for Forrest Management" Booklet 48 ISBN 0855 38 092-6

215. Mayhead G J — "The Effect of Altitude above sea level on the Yield Class of Sitka Spruce". Scottish Forrestry Vol 27 1973

216. Christie J M — Personal Conversation, Forestry Research Station, Bentley Hants.

217. Nathanson F E — "Radar Design Principles". McGraw-Hill 1969

218. Hevenor R A — "Backscattering of Waves from a Tilted, Slightly Rough Surface". AETL Fort Belvoir AD A047-668 June 1977

ANNEX B

219. Ruck G T et al — "Radar Cross Section Handbook" Plenum Press 1970

220. Beckmann P & Spizzichino A — "The Scattering of Electromagnetic Waves From Rough Surfaces". McMillian NY 1963

221. Smith B G — "Geometric Shadowing of a Random Rough Surface" IEEE Trans Ant & Prop Vol AP 15 - No 5 1967

ANNEX C

222. Schelleng J C et al — "Ultra-Short-Wave Propagation" Proc IRE Vol 21 March 1933

223. Anderson L J & Trolese L G — "Simplified Method for Computing Knife-Edge Diffraction in the Shadow Region" IRE Trans Ant & Prop Vol AP 6 July 1958

ANNEX E

224. Maksinov M V — "Radar Anti-Jamming Techniques" (Transl from Russian) Zaschita Ot Radiopomekh Artech Books 1979

225. Barton D K — "Low Angle Radar Tracking" Proc IEEE June 1974 (a)

226. Barton D K — "Radar Systems Analysis" (P 330) Prentice-Hall Inc 1964

227. Ibid — 1974 (b)

228. Powell D — "Radar Cross-Section Studies" BAe Paper APN 356 July 1981 (a)

229. Swerling P — "Probability of Detection for Fluctuating Targets" Rand Memo RN 1217 Mar 1974

230. Heidbreder & Mitchell — "Detection Probability for Log-Normally Distributed Signals" IEEE Trans Aerospace January 1967

231. Ibid (Powell) — 1981 (b)

ANNEX F

232. Evans I S — "An Integrated System of Terrain Analysis and Slope Mapping" Final Rep D A ERO 591-73 G0040 Univ Durham 1979

233. Evans I S — "General Geomorphometry, Derivatives of Altitude and Descriptive Statistics". "Spatial Analysis in Geomorphology" Chorley R J (ed) Methuen London 1972

234. Barton DK. — "Flat & Rolling Terrain Clutter Model" Raytheon memo DKB:82:10/7011:82:169 dated 17 May 1983.

DISTRIBUTIONS FOR FLUCTUATING RADAR SIGNALS

THE WEIBULL DISTRIBUTION

1. The Weibull distribution (1951) is widely applicable and has a probability density function given by:

$$f(x) = m\lambda x^{m-1} \exp\left[-\lambda x^m\right] \qquad (1)$$

Variable m and λ are known as the shape and scale parameters respectively, and must be estimated from the data available. The function is re-written:

$$p(x) = \frac{c}{b}\left(\frac{x}{b}\right)^{c-1} \exp.\left[-\frac{x}{b}\right]^c \qquad (2)$$

Where b and c are now the scale and shape parameters. The use of λ is avoided here, since λ is used for radar wavelength elsewhere.

When c = 2 this distribution reduces to the Rayleigh Distribution (see below).

From (2), the probability of a signal level x being exceeded is

$$\int_x^\infty p(x)\,dx = \int_x^\infty \left\{\frac{c}{b}\left(\frac{x}{b}\right)^{c-1}.\exp\left[-\left(\frac{x}{b}\right)^c\right]\right\} dt$$

$$= \exp.\left[-\left(\frac{x}{b}\right)^c\right]$$

If x_m is the median value then:

$$\exp.\left[-\left(\frac{x_m}{b}\right)^c\right] = 0.5$$

$$\text{hence}\quad \left(\frac{x_m}{b}\right)^c = -\ln 0.5 = -(-0.69315)$$

$$\text{and}\quad b = \frac{x_m}{(0.69315)^{\frac{1}{c}}} \qquad (3)$$

2. The second moment of distribution is:

$$\int_0^\infty \frac{c}{b}\left(\frac{x}{b}\right)^{c-1}.\exp\left[-\left(\frac{x}{b}\right)^c\right] x^2\,dt$$

$$= b^2\Gamma\left(1+\frac{2}{c}\right)$$

$$= \frac{2b^2}{c}\Gamma\left(\frac{2}{c}\right) \qquad (4)$$

Where $\Gamma(n)$ is the Gamma function.

3. If the Weibull parameters for a normalized distribution[1] are b_o and c_o and new values are required after scaling for a different resolution cell size (by a factor N), then:

$$\frac{1}{N} \frac{2b^2}{c} \Gamma\left(\frac{2}{c}\right) = \frac{2b_o^{\,2}}{c_o} \Gamma\left(\frac{2}{c_o}\right) \qquad (5)$$

As the median value for the normalised distribution is:

$$x_{m_o} = (0.1)^{\frac{1}{2}} = 0.31623$$

$$\text{from } (3), \quad b_o = \frac{0.31623}{(0.69315)^{\frac{1}{c_o}}} \qquad (6)$$

The median value of the new distribution is:

$$x_m = 0.31623N$$

$$\text{and} \quad b = \frac{0.31623N}{(0.69315)^{\frac{1}{c}}} \qquad (7)$$

substituting (7) in (5) gives

$$\frac{1}{\left((0.69315)^{\frac{1}{c}}\right)^2} \cdot \frac{2}{c} \cdot \Gamma\left(\frac{2}{c}\right) = \frac{10}{N} \cdot \frac{2b_o^{\,2}}{c_o} \Gamma\left(\frac{2}{c_o}\right) \qquad (8)$$

(8) can be solved graphically to obtain a value for $\frac{2}{c}$ hence c, and b can then be found from (7).

RAYLEIGH DISTRIBUTION

4. If the average returned signal level is essentially constant in time and there are a large number of statistically (independently positioned) scatterers, the probability of echo amplitude being between a level P and an infinitesimally larger level P + dP is given by the pdf:

$$W(P)dP = \frac{1}{\overline{P}} \exp\left(\frac{-P}{\overline{P}}\right) dP \qquad (9)$$

$\overline{P}$ is the average power.

RICEAN (RICIAN) DISTRIBUTION

5. Also called the non-central Rayleigh density function. This distribution describes a received signal containing an essentially constant echo in addition to a Rayleigh-distributed fluctuation.

1 By making the median a suitable apparent echoing area (eg $0.1m^2$) set by the desired detection threshold.

$$W(P)dP = (1+m^2)e^{-m^2} e^{-P(1+m^2)/\bar{P}} \, J_o\left(2m\sqrt{1+m^2}\sqrt{P/\bar{P}}\right)(dP/\bar{P}) \qquad (10)$$

J_o is the Bessel function $\left(J_o(jx) = I_o(x) \right)$

$$J_o = 1 - \frac{x^2}{2^2} + \frac{x^4}{2^2\,4^2} - \frac{x^6}{2^2 4^2 6^2} + \text{-------}$$

NORMAL (GAUSSIAN) AND LOGNORMAL DISTRIBUTIONS

6. Large amplitude signal components may cause an appreciable departure from the Rayleigh or Ricean distributions. The Lognormal distribution can be used, and the normal distribution curve is:

$$f(x) = \int_{\infty}^{x} \frac{1}{s\sqrt{2\pi}} \exp.\left[-(x-\mu)^2 / 2s^2 \right] \qquad (11)$$

where s = standard deviation (to avoid σ, used elsewhere for target echoing area).

μ = median value of x

x = normally distributed variable

The pdf for the lognormal distribution can be obtained from (11) by using the transformation $x = \ln Y$:

$$\text{giving } f(Y) = \int_{\infty}^{x} \frac{1}{Ys\sqrt{2\pi}} \exp.\left[-\frac{1}{2s^2}\left(\log_e \frac{Y}{Y_m}\right)^2 \right] \qquad (12)$$

Where Y = Lognormally distributed variable

Y_m = Median value of Y

s = standard deviation of $\log_e\left(\frac{Y}{Y_m}\right)$

APPENDIX 1 TO

ANNEX A TO

"THE PROBABILITY OF

DETECTING AND TRACKING

RADAR TARGETS IN CLUTTER

AT LOW GRAZING ANGLES"

DATED 30 SEPTEMBER 1982

WEIBULL SHAPE PARAMETER AND σ_M CORRELATIONS

1. Investigations were made into:

a. Correlation between Beamwidth - Pulse Duration product and median backscatter σ_m.

b. Correlation between Beamwidth - Pulse Duration product and Weibull Shape Parameter 'C', for each of the following:

(1) By applying Dodsworth's algorithm to the calculated values ($\theta_A \gamma$) for the worldwide survey.

(2) By applying the author's model for 'C' derived by statistical analysis of the worldwide results by measuring slopes of all results replotted on Weibull paper.

2. It was also possible to compare measured results for 'C' (obtained from slope) with values predicted by the algorithms.

3. No account was taken of different RF's. It was however noticed that some values were suspect or at extreme values (eg Serial 7 at Table 1 Chapter 4 page 4-92). This was confirmed by computer plots where the correlations could be seen if extremes were deleted. Several other sets of data became available in addition to those at Chapter 4, and the total test was run with a reasonable selection of data from USA, UK and Continental Europe.

4. <u>Correlation Matrix</u>. Correlation results for C with $\theta\tau$

measured Slope C	2	0.32 (0.31)			
Rad Sec $\theta_A\tau$	3	0.74 (0.75)	0.24 (0.19)		
	4	0.70 (0.72)	0.30 (0.23)	0.68 (0.57)	Authors Model
		1 Dodsworth	2 Measured Slope C	3 Rad Sec ($\theta_A\tau$)	

5. Correlation between measured slope (2) and proposed models by Dodsworth (1) and the author (4) are not high. Correlation between $\theta_A\tau$ product and the models proposed by Dodsworth and the author are good. Correlation between the author's and Dodsworth's values are also high. It is noted that the correlations did not change significantly in most cases when Dodsworth's and Warden's UK figures (on which Dodsworth originally based his premise) were deleted and the correlation tests repeated. The figures shown in brackets on the correlation matrix are those using USA and European results other than RSRE results.

6. A poor correlation of 0.11 was found between $\theta_A\tau$ and σ_m with $dB = 39.7 + 0.24\ (\theta\tau) \times 10^{-9}$.

RECEIVED CLUTTER POWER FROM RESOLUTION CELL AND REFLECTION COEFFICIENTS

1. The Radar Cross Section (RCS) is defined as the area intercepting that amount of power, which, when scattered isotropically, produces an echo equivalent to that received from the object. An idealised received signal clutter power can be found using the radar range equation:

$$S_R = \frac{P_T \, G \, Ae \, \sigma}{(4\pi)^2 R^4} \qquad (1)$$

or, since $G = \frac{4\pi Ae}{\lambda^2}$

$$S_R = \frac{P_T G^2 \lambda^2 \sigma}{(4\pi)^3 R^4 L} \qquad (2)$$

Where P_T = Peak Transmitted Power

G = Peak Aerial Gain

Ae = Effective Aerial Capture Area

R = Range to Target (assuming $R_i = R_r$, ie monostatic radar)

σ = RCS

L = Combined System Losses

λ = Wavelength

2. Figure B1 shows the resolution cell geometry; from which it can be seen that the resolution cell range dimension AB approaches $\frac{c\tau}{2}$ as $\psi \to 0$. θ_A is the azimuth 3dB beamwidth. τ is the radar pulse length.

SCATTERING RCS PER UNIT AREA

3. To express the clutter in terms of the scattering cross section per unit area (σ_o) then:

$$\sigma = \sigma_o R\,\theta_A \frac{c\tau}{2} \sec\psi \qquad (3)$$

Eqn (3) is the result of introducing a characteristic γ such that $\sigma_o = \gamma \sin\psi$, thus removing the geometrical dependence of σ_o, and the other assumptions are made at para 4 below.

4. The area of illuminated terrain depends upon the grazing angle. If, for example a flat plate (ideal) reflector is used, and assuming sidelobes are minimal at practical ranges, the effective capture area and gain are dependent on grazing angle. The incident area will then be:

$$\text{Area} = R\,\theta_A \frac{c\tau}{2} \tan\psi \qquad (4)$$

Where θ_A and θ_E are respectively the 3dB azimuthal and vertical beamwidths. A pencil beam (having small $\theta_A = \theta_E$) produces an elliptical ground "footprint" such that the ellipse axis lengths are $R\theta_A$ and $R\theta_E$ Cosec θ (providing Tan (θ_A) " θ_A). Area of footprint is hence $(2R \tan\frac{\theta_A}{2})\,(\frac{c\tau}{2}\sec\psi)$ ——— (5)

If $\tan\psi < 2R \sin\frac{\theta_E}{2} / \frac{c\tau}{2}$ then (5) is used for area.

5. It is also assumed that the clutter scatterers are small in relation to λ,

the transmitted wavelength, in which case σ varies as λ^4 (dependent on the Rayleigh Law). For general angles of depression the RCS (of a flat target perpendicular to the incident beam) is a function of the angle of incidence which varies rapidly if the wavelength is small compared with the target size. This is more complex at sea because dependence of reflectivity varies with both the sea state and the angle of arrival. The radar cross section variation with shape has been researched by RUCK {219}.

SURFACE REFLECTION COEFFICIENTS

6. Multipath and backscatter values are dependent upon the magnitude and spatial origin of surface reflected waves. The effect of surface roughness in changing the relative proportions of amplitude and phase from specular towards diffused has been expressed as the specular scattering factor:

$$\rho_s^2 = \exp-\left[\left(\frac{4\pi(\sigma_h)}{\lambda} \sin\psi\right)^2\right] \qquad \text{------------------------------(5)}$$

σ_h is the rms height standard deviation relative to an idealised surface. Values such that $\frac{\sigma_h}{\lambda}\sin\psi > 0.066$ significantly reduce the specular reflection (ie $\rho_s < 0.7$). For most terrain the largest part of the non-specular energy appears as forward scatter, or is absorbed by the vegetation.

7. It has been shown {220}, using small scale diffuse reflection theory that a scatter lobe of width $4\sigma_\alpha$ will be formed about an axis corresponding to the position of the specular reflector. (σ_α is the rms slope of the illuminated facet). Viewed from the radar receiver this diffuse scattering "will appear to originate from a glistening surface surrounding the specular centre of the facet".

8. The diffuse scattering coefficient (ρ_d) depends upon the integration of the reflected power density η_d, together with the radar receiver aerial gain over the angular extent of the glistening surface:

$$\rho_d^2 = \int \eta_d G_r d\Omega \quad \text{--(6)}$$

Thus when $4\sigma_\alpha > \theta_E$ (elevation Beamwidth), θ_E rather than the surface becomes the predominant factor in establishing the reflected fraction of diffuse power.

9. Magnitude of Reflection Coefficients. Terrain coefficient values near 1 give strong specular reflections. Reflection coefficients can be established over an interval from the relationship:

$$\rho = - \rho_A \rho_B \rho_S e^{j 2\pi \Delta R/\lambda} \quad \text{------------------------------------(7)}$$

Reflection coefficient ρ is therefore dependent upon:

ΔR = Difference in path length (direct and indirect)

ρ_A = Absorption coefficient

$$\rho_B = \exp \left[- \frac{(4\pi\sigma_h \sin\psi/\lambda)^2}{2} \right]$$

$$\rho_S = \frac{1 + \text{erf}(\alpha)}{1 + \text{erf}(\alpha) + e^{-\alpha^2}/\sqrt{\pi}\,\alpha}$$

Where $\alpha = \dfrac{\sin\psi}{\sqrt{2}\sigma_s}$

ρ_S is a correction to ρ_B to account for shadowing in the Fresnel Zone (Smith Factor) {221}. ρ_B is known as the Bechmann-Spizzichino factor. σ_s is the slope (facet) standard deviation (rads). σ_h = height sample standard deviation.

10. For the above conditions for strong specular reflection $\psi \leq 0.037\lambda/\sigma_h$ and $\psi \geq 1.4\sigma_s$. Taking σ <10 mrad, σ_h >10m then strong specular reflection would be rare at λ = 0.03m.

11. Reference is made to Chapter 8 eqns (7) and (8), where

$$\bar{n}^2 = \varepsilon_r - j60\sigma\lambda = \varepsilon_r - \frac{j1.8\sigma 10^4}{f_{MHz}}$$

σ = surface conductivity mho.m.m^{-2}

ε_r = relative permittivity

Typical values for insertion at Chapter 8 and Annex E are given at Table 1:

SURFACE	CONDUCTIVITY σ	DIELECTRIC ε_r	TYPICAL ρ for $\Psi < 1^\circ$
Dry, Flat	1×10^{-4}	5	0.3
Farmland Rural Low Hills	1×10^{-2}	15	0.1–0.2
Medium Hills	5×10^{-3}	13	
City	2×10^{-3}	5	
Sea	8×10^{-5}	81	0.6–1.0

Table 1. Table of Typical Values for Reflecting Terrain

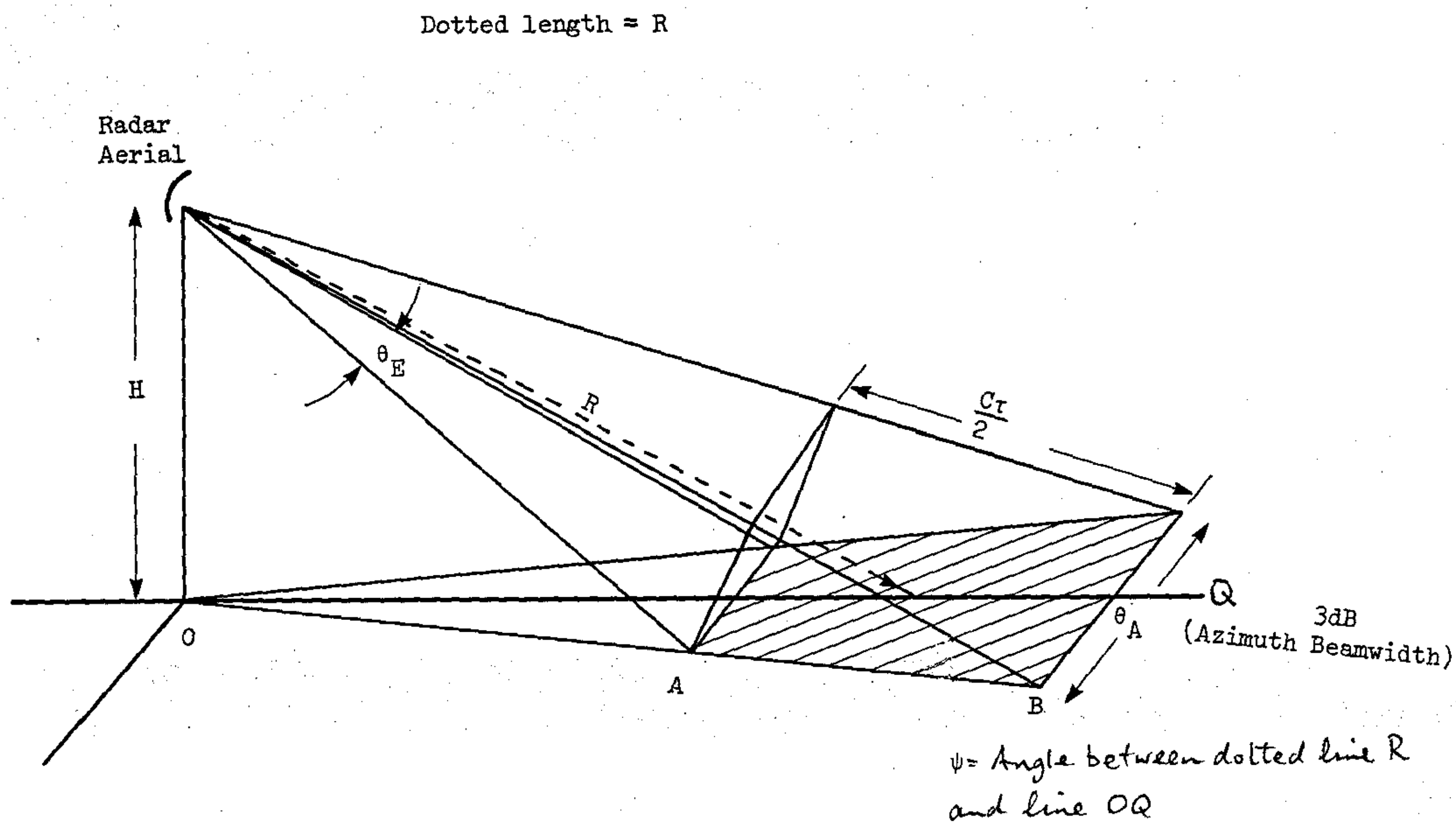

FIG B1 RESOLUTION CELL FOR LOW GRAZING ANGLE

FRESNEL-KIRCHOFF SINGLE KNIFE EDGE DIFFRACTION SOLUTION

1. Assuming small grazing angles, and using the previous notation at Chapter 7 figure 2:

$$E = \frac{1}{2d}\left[1 - (1 + j)(C - jS)\right] \quad \exp\left[-j\, k\,(d + d_1\alpha - d_2\beta)^2/2d\right] \quad \text{--(1)}$$

Where E = Electric Field at receiver (target) from unit source

S, C = Fresnel integrals of argument

θ = diffraction angle (see diagram), ie $\alpha + \beta$

v = $\theta\sqrt{d_o/\lambda}$

k = $2\pi/\lambda$ (known as wavenumber)

d_o = $2d_1d_2/d$ $\quad d = d_1 + d_2$

Simplified {222} then (1) becomes:

$$E = \frac{1}{2\pi\theta}\sqrt{\frac{\lambda}{dd_1d_2}} \quad \exp\left[-j\,(k(r_1 + r_2) + {}^{\pi}/4)\right] \quad \text{------------(2)}$$

2. This approximation is developed from {223}:

$$E = \int_{x_o}^{\infty} e^{-jx^2}\,dx \approx \frac{1}{2x_o}\, e^{-j\,(x_o{}^2 + {}^{\pi}/2)} \text{ for } x_o >> 1 \quad \text{----------(3)}$$

$$\text{Thus} \quad C(v) - jS(v) = \int_{0}^{v} e^{-j\pi u^2/2} du \text{ -----------------------------(4)}$$

$$\approx \frac{1}{\sqrt{2}} e^{-j\pi/4} - \frac{1}{\pi v} e^{-j\pi(v^2+1)/2} \text{ -------------(5)}$$

$$\text{for} \sqrt{\pi/2}\, v >> 1$$

3. For engineering purposes the approximation condition is:

$$\theta^2 \geqslant 8\lambda/\pi d_o \text{ ---------------------------------------(6)}$$

Which is interpreted physically as requiring the receiver (target position in this report) to be deep in the shadow zone, or equivalently, that the first Fresnel zone on the obstacle path is well masked by the obstacle. This condition is satisfied by most microwave diffraction paths.

4. Although the above is included here for completeness, extended rigourous treatment of the wave theory of the solutions are often complex and cannot be directly applied to this practical case.

ANNEX D TO

"THE PROBABILITY OF

DETECTING AND TRACKING

RADAR TARGETS IN CLUTTER

AT LOW GRAZING ANGLES"

DATED 30 SEP 82

COMPUTER PROGRAMS AND FLOWCHARTS

1. It is not intended to include lengthy program listings or detailed flowcharts in the report, but to describe the programs and datafiles briefly.

DATA

2. The following data was available for clutter and other investigations either at the start of, or was generated as the project progressed:

a. Plotted results from the worldwide clutter survey, from which values could be interpolated for correlation studies for ψ, Weibull, etc.

b. Raw radar measurements taken at a set range over a known sector in the Malvern area (E J Dodsworth RSRE on his retirement).

c. A Malvern terrain data base (produced at Malvern) but with a larger matrix spacing than satisfactory for the particular work envisaged.

d. Two area data matrix (manually produced by the author) to a finer spacing for the project. (Malvern and Scottish).

e. Raw radar measurements in considerable quantity (unfortunately no tape available), from British Aerospace Stevenage. From these extensive listings, data was re-entered onto disc for the slope correlation studies.

f. Files generated for radar parameters.

PROGRAMS

3. A brief resume follows for each of the main programs (written in FORTRAN to run on the DEC 20 at Cranwell) which were used to calculate, process or plot results during the research. A number of smaller programs were also written to manipulate data bases in support.

a. SLINE.FOR Scans through 360° in any increment and to any range, from any given site location within a terrain matrix (spot height) data base; for any target and radar site height and produces sightline (obscuration) data for plots of the type at Chapter 2 (2-36). Incorporates height of surface obstacles eg trees, which it combines with the terrain/matrix data from the files at para 2c and 2e above.

b. RADS.FOR Makes terrain data for a particular resolution cell match the corresponding backscatter signal. Calculates terrain slope, aspect, actual grazing angle and σ_m. Creates a new file containing all data necessary for slope correlation studies. Also produces terrain profile data and through convexity calculations diffraction plot data files.

c. SNOISE.FOR Makes all radar propagation, range equation, pencil beam weather and surface clutter calculations. Including fluctuating target, main and sidelobe jamming and chaff jamming subroutines. Also includes multipath calculations and tracker range checks.

d. IRADAW.ALG/PAS Originally in ALGOL but now also in PASCAL and modified, this program flys the actual missile aerodynamic and control functions to produce a time readout of the missile trajectory. Apart from some interest in the tracker control functions it was decided for this report that a mean missile flyout range was adequate for the type of prediction envisaged.

e. PPI This plotter program produces a circular (PPI) radar type display for surface obscuration or diffraction plots of the type shown at Chapter 2 (2-38).

4. STATPK. STATPK, the college statistical library, was used to produce correlation matrices, regression and all other statistical results.

DOCUMENTATION

5. Working flowcharts were made for each program, and hard-copy program and data listings were maintained for each revision. All outputs from STATPK were taken on hard copy for detailed analysis; these include regression plots, scatter plots, sorts, correlation matrices, histographs, bargraphs, frequency tables, Kolmorogov-Smirňov tests, and basic statistical measurements.

LOW LEVEL TRACKING ERRORS AND TRACK LENGTH PROBABILITY

1. Probability Density Function for Tracking Error. An expression can be derived for the probability density function of the tracking error, in terms of target altitude h_{tgt}, linear error ε, and the power ratio of the direct signal reflected from the target compared to the multipath (surface reflection signal - see fig 1) ${q_s}^2$:-

$$w(x) = \frac{2q_s^2}{\sqrt{1+q_s^2}\left[(1+x^2) + q_s^2\,(1-x^2)\right]^{3/2}} \qquad (1)$$

$x = \varepsilon/h_{tgt}$, the relative centroid tracking error.

From Figure 2, the mean relative error M_ε is given by:

$$\frac{M_\varepsilon}{h_{tgt}} = \int_{-\infty}^{\infty} x w(x)\, dx = \frac{q_s^2 - 1}{q_s^2 + 1} \qquad (2)$$

$$\text{and } M_\varepsilon = h_{tgt}\,\frac{q_s^2 - 1}{q_s^2 + 1} \qquad (3)$$

2. Assuming the target maximum dimension (ie wingspan or fuselage length) is s, then the probability that the sightline will fall on the target during tracking is shown at Figure 3 {224}, from:

$$p = \int_{\varepsilon_2}^{\varepsilon_1} w(x)\, dx = \phi(\varepsilon_1) - \phi(\varepsilon_2) \qquad (4)$$

$$\text{Where } \phi(\varepsilon) = \frac{(1 + q_s^2)\,\varepsilon + (1 - q_s^2)}{2\sqrt{1+q_s^2\left[(1+\varepsilon)^2+q_s^2(1-\varepsilon)^2\right]}} \qquad (5)$$

$$\varepsilon_1 = \frac{2h_{tgt} + s}{2h_{tgt}}$$

$$\varepsilon_2 = \frac{2h_{tgt} - s}{2h_{tgt}}$$

3. Figure 3 shows the relationship, where for a target flying at an altitude of 50m, target size 10m, linear error ε of 10m and $q_s^2 = 10$, then the probability of the sightline falling on the target is approximately 10%. At maximum tracking range it would be expected that to track correctly the system should remain within 10m vertical error for 70% of the time. (Fig 4a)

4. Angular Tracking Error. Assuming the radar aerial receives 2 signals, ie direct and multipath, respectively $S_1 = V_1 \cos \omega_1 t$, $S_2 = V_2 \cos \omega_2 t$. (6)

If ω_o is the carrier frequency and v_1 and v_2 are the apparent approach (radial) velocities of the target and its image, then

$$\omega_1 = \omega_o \left[1 + \left(\frac{v_1}{c}\right)\right] \; ; \; \omega_2 = \omega_o \left[1 + \left(\frac{v_2}{c}\right)\right]$$

Combining (6) above $(S_1 + S_2)$

$$= V_1 \cos \omega_1 t + V_2 \cos \omega_2 t \qquad (7)$$

$$= 2 V_1 V_2 \cos\left(\frac{\omega_1 - \omega_2}{2}\right) t \cos\left(\frac{\omega_1 + \omega_2}{2}\right) t \qquad (8)$$

5. Assuming a quadratic detector in the radar receiver then its output voltage is:

$$V_{tgt} = K \left[1 + \tfrac{1}{2} \cos 2\omega_1 t + \tfrac{1}{2} \cos 2\omega_2 t + \cos (\omega_1+\omega_2) + \cos (\omega_1-\omega_2)t\right] \qquad (9)$$

K is a constant. A beat frequency $\omega_1-\omega_2$ causes disturbance in the tracking accuracy if the radial velocities v_1 and v_2 are close to the aerial scanning frequency Ω_{sc} ie $\frac{2\omega_0}{c}(v_1-v_2) \approx \Omega_{sc}$.

6. Multipath propagation causes the output from the radar tracker aerial to be:

$$= S_1 L_1(\alpha) \left[1 + m_1 (\alpha) \cos \Omega_{sc} t\right] \cos \omega_1 t + S_2 L_2(\alpha, \Delta\alpha)\left[1 + m_2 (\alpha, \Delta\alpha) \cos \Omega_{sc} t\right] \cos \omega_2 t \qquad (10)$$

$$L_1(\alpha) = \tfrac{1}{2} \left[f(\alpha_o - \alpha) + f (\alpha_o + \alpha)\right] \qquad (11)$$

$$L_2 (\alpha_1 \Delta\alpha) = \tfrac{1}{2} \left[f (\alpha_o - \alpha + \Delta\alpha) + f (\alpha_o + \alpha - \Delta\alpha)\right] \qquad (12)$$

$$m_1(\alpha) = \frac{f (\alpha_o - \alpha) - f (\alpha_o + \alpha)}{f (\alpha_o - \alpha) + f (\alpha_o + \alpha)} \qquad (13)$$

S_1 is required signal. S_2 is interfering signal.

$$m_2(\alpha, \Delta\alpha) = \frac{f(\alpha_o - \alpha + \Delta\alpha) - f(\alpha_o + \alpha - \Delta\alpha)}{f(\alpha_o - \alpha + \Delta\alpha) + f(\alpha_o + \alpha - \Delta\alpha)} \qquad (14)$$

α_o = Displacement of aerial beam peak relative to equal signal line.

α = tracking error for target.

$\Delta\alpha$ = Angular separation between true target and image.

Signal detection and amplification at $F = \Omega_{sc}$, assuming $\omega_1 - \omega_2 = \Omega_{sc}$, the phase detector output voltage S_3 (zero at balanced condition) is:

$$S_3 = S_1^2 L_1^2(\alpha)\, m_1(\alpha) + S_1^2 L_1^2(\alpha, \Delta\alpha) m_2(\alpha, \Delta\alpha) + S_1 L_1(\alpha)\, S_2 L_2(\alpha, \Delta\alpha) + \frac{3}{4} S_1 S_2 L_1(\alpha)\, L_2(\alpha, \Delta\alpha)\, m_1(\alpha) \left[m_2(\alpha, \Delta\alpha)\right] \qquad (15)$$

Using equations (10) to (15) above, the angular radar tracker error is given by:

$$f^2(\alpha_o - \alpha) - f^2(\alpha_o + \alpha) + q_n \left[f^2(\alpha_o - \alpha + \Delta\alpha) - f^2(\alpha_o + \alpha - \Delta\alpha)\right] + \frac{q_n}{4} \{ f(\alpha_o - \alpha + \Delta\alpha) \left[7f(\alpha_o - \alpha) + f(\alpha_o + \alpha)\right] + f(\alpha_o + \alpha - \Delta\alpha) \left[f(\alpha_o - \alpha) + 7f(\alpha_o + \alpha)\right] \} = 0 \qquad (16)$$

$$q_n = \frac{1}{q_s}$$

7. Placing practical values into eqn (16), provides the relationship between tracking error and angular separation angle between target or image. If plotted with normalized error and separation over a range of $\Delta\alpha$ and q_n values, it is seen that for conditions where the interfering

signal is comparable to the wanted signal ($q_n \approx 1$) the effective target position is above the real target position; whilst for a swamping value of interference signal for very shallow grazing (ie $\Delta\alpha \rightarrow 0$) the effective target position is lower than the actual target position. Interference, causing inaccuracies may be minimised in practice by changing the scanning frequency or narrowing the tracker receiver pass band. Alternatively the technique known as 'complex indicated angle' can be used to minimise the multipath effect {225} For accurate tracking it is stated {226} p 330 that for a 1^{o} beam width and 0.1 mrad measuring accuracy:

$$\frac{\rho}{\sqrt{8G_s}} \ll 0.005 \qquad (17)$$

A value of $\rho = 0.3$ (typical for land) is used.

G_s = Specular Power Gain Ratio

8. Effect of Terrain Slope. It is of course possible that multipath reflections, (including tracker error), could come from a sloping patch of terrain, and for clutter and other effects, the relative height of the radar transmitter, slope of the terrain and target altitude must be used for calculations.

MULTIPATH TRACKING ERROR USING MONOPULSE TRACKER

9. For short ranges and assuming a flat earth the multipath tracking error of a monopulse radar is given by {227}:

$$\Sigma \text{ (mrads)} = \frac{\theta_E \rho_v}{k_m} \sqrt{\tfrac{1}{2}\left(\sum_{i=1}^{n} I_i + I_s\right)} \qquad (18)$$

Where I_i, I_s are the diffuse and specular components, (eqns 19, 20 below)

θ_E the aerial beamwidth in elevation

ρ_v vegetation absorption (commonly 0.1 to 0.3 for $\Psi = 0.5$ to 2 deg).

k_m monopulse slope ($\approx$ 2)

n number of depression angle elements summed

Eqn (18) then uses Eqns (19) to (26) below.

Separately I_i and I_s are given by

$$I_i = \Delta_i^2 \, \rho_{oi}^2 \, \eta_{di} \, \Delta_\theta \qquad (19)$$

$$I_s = \Delta_s^2 \, \rho_{oi}^2 \, \rho_s^2 \qquad (20)$$

The Fresnel reflection coefficients are not repeated here. η_{di} is the diffuse reflection density, Δ_i and Δ_s the difference pattern gains, Δ_θ the width of element in depression angle, ρ_s the specular scattering factor.

10. The difference channel illumination is assumed to be of the distribution x cos x . For which

$$\Delta = \frac{6\left(\frac{\pi^2}{4} - U^2\right) \text{Sin } U - 2U \text{ Cos } U}{\left(\frac{\pi^2}{4} - U^2\right)^2} \qquad (21)$$

$U = \frac{3.77\theta}{\theta_E}$ $\theta = \theta_b + \psi_1$ where θ_b is elevation of beam axis.(rads).

ψ_1, ψ_2 grazing angle from radar to surface and target to surface.(rads).

For the reflection coefficients it is taken that $\psi = \frac{\psi_1 + \psi_2}{2}$ and the surface complex dielectric constant is calculated in the usual way to get ρ_o.

Assume $\sin\psi \approx \psi \approx \tan\psi$. $\rho_o > 0.8$ for $\psi < 2°$ for both V & H polarisations.

11. Diffuse power density per radian of depression angle is:

$$\eta_d = \frac{R}{R-x} \frac{\psi_1 + \psi_2}{4\sqrt{\pi}\, S_o\, \psi_1} \exp\left[-\left(\frac{\psi_1 - \psi_2}{2S_o}\right)^2\right] F_d^2 Z \qquad (22)$$

Where

S_o is the RMS surface slope deviation

$\psi_1 = h_{tx}/x$, and $\psi_2 = h_{tgt}/R-x$ (rads)

x = range from radar to surface

R = radar range of target

F_d = Roughness Factor (eqn 23 below)

Z = Low grazing angle correction factor (see eqns 25, 26)

12. Roughness Factor and specular scattering factor are given by:

$F_d = \sqrt{1-\rho_s}$ where ρ_s = specular scattering factor

$$\text{hence } F_d^2 = \sqrt{1-\rho_{s1}} \cdot \sqrt{1-\rho_{s2}} \qquad (23)$$

$= F_{d_1} \cdot F_{d_2}$ For ψ_1, ψ_2

ρ_{s_1}, ρ_{s_2} from eqn (24) for $\psi_1\ \psi_2$ respectively.

$$\rho_s^2 = \exp\left[-\left(\frac{4\pi\,\sigma_h'}{\lambda}\,\psi\right)^2\right] \qquad (24)$$

$$= \exp(-\psi^2/\psi_c^2)$$

σ_h' = RMS surface height deviation corrected for shadowing

ψ_c = critical angle for $\rho_s^2 = \frac{1}{e}$

13. For low grazing angles 2 correction terms are used

$a = \psi_1/2S_o \quad , \quad c = \psi_2/2S_o$

$a^1 = \min(a,c) \quad c^1 = \max(a,c)$

(which is used depends on the smaller of the 2 angles).

Effective surface roughness is corrected for shadowing

$\sigma_h' = \sigma_h \; 5\sqrt{4a'}$ where $4a' \leqslant 1$

or $\sigma_h' = \sigma_h$ where $4a' \geqslant 1$

14. Low grazing angle correction for diffuse power density, where $b = \psi_c/2S_0$:

$$Z_1 = \frac{8\sqrt{1-\rho_{sa}^2}}{\frac{1}{a'} + 4 + 3a' - \frac{b^2}{3a'} - b} \quad \text{for } b \leqslant 1 + a' \qquad (25)$$

$$Z_2 = \frac{24}{\frac{2}{a'^2} + \frac{9}{a'} + 12 + 5a'} \quad \text{for } b \geqslant 1 + a' \qquad (26)$$

Where

$$b = \frac{\psi_c}{2S_o} = \frac{\lambda}{8\pi\,\sigma_h' S_o}$$

$$\rho_{sa} = \exp(-a'^2/b^2)$$

15. The specular error component is only present in the absence of nosediving ie for $\theta_b > 0.7\ \theta_E$ or for lower angles if $\rho_{os}\rho_s < 0.5$ (ρ_{os} is Fresnel specular reflection coefficient). A calculator program for the above is available as a Texas Instruments master library module.

TRACK LENGTH PROBABILITY

16. An initial survey or terrain data base may be used to produce (see Fig 5a) unscreened track lengths. This may be difficult in practice, but it is hoped that by examination of typical sites a pattern of probabilities might emerge so as to act as a starting point in predicting defensive performance or conversely offensive survivability when operating aircraft against these low level radar systems. Short periods of target obscuration might be considered negligible since modern systems, rate aided, may be able to track a target 'through' a narrowly obscured sector of, say, 1^o; the exception is of course when the target is headed radially towards the radar along an obscured flight path.

17. Example. For explanation purposes an example is used:

a. Target Parameters. Velocity 300m sec^{-1} (V_{tgt}), Mean target range (crossing target) 3 km (R_{tgt}), Altitude 60m (h_{tgt}).

b. Missile Parameters. Velocity 600 m sec^{-1} (V_m), Radar Site Reaction Time 15 sec (t_r). V_m is assumed constant over unmasked time interval.

c. Obscuration. Probability of obtaining track length of x metres is p.

18. For a given aircraft velocity a non-obscured target must be tracked on radar for T secs. Useful tracks are dependent on range from the radar and V tgt, since the geometry of a track at longer ranges (though perhaps visible for the same time as a track at shorter range) may not allow an engagement to succeed because of the longer missile flight-time to reach the required range. This is especially so in a commanded missile system where missile and target must be observable at all times up to impact if they are to be tracked on radar and the appropriate guidance commands derived and transmitted to the missile. Using the example figures an approximation for crossing targets at mean range is:

$$t_f = \frac{R_{tgt}}{V_m} = \frac{3000}{600} = \underline{5 \text{ secs}} \quad \text{and } T = t_f + t_r = \underline{20 \text{ secs}}$$

where $t_f + t_r$ is the minimum observation time required. An approximate track length T_c necessary for an engagement for a target crossing at sensibly constant range is:

$$T_c = V_{tgt}\,(t_f + t_r) = 300 \times 20 = \underline{6 \text{ Km}}$$

The probability of obtaining this track length is about 0.25 at Figure 5b. For a radially approaching target a close approximation is:

$T_c = t_r V_{tgt} + t\,(V_{tgt} + V_m)$ where $t > \frac{d}{V_m}$ given that d is the minimum possible impact range. If d = 600 m, for this example $t > 1$, hence $t\,(V_{tgt} + V_m) > 900$ and $T_c \approx \underline{5.4 \text{ Km}}$.

Accurate computations for system and target parameter change can be made from weapon trajectory programs written by the author, however the above method is adequate for manual prediction purposes.

19. If the aircraft altitude is changed to h_{tgt} = 200 m, the same timing calculations apply if the range is unchanged. However, a decrease in

obscuration due to the increased target altitude will cause the probability of obtaining the critical track length T_c to (typically) rise to 0.7 for flat terrain. Table 1 shows the effect in similar terrain but with changes in target and missile parameters.

TABLE 1 PROBABILITY OF OBTAINING MINIMUM TRACK LENGTH REQUIRED

Target : V_m = 600 m sec^{-1} System Reaction 10 sec

Terrain: typical flat terrain with scattered clumps of trees.

	TARGET PARAMETERS			
	V_{tgt} 260 m sec^{-1} (500 kts)		V_{tgt} 220 m sec^{-1} (420 kts)	
Mean Range to target Km	h_{tgt} 200 (ft)	h_{tgt} 300 (ft)	h_{tgt} 200 (ft)	h_{tgt} 300 (ft)
1	0.62	0.75	0.66	0.77
3	0.37	0.52	0.41	0.55
5	0.22	0.37	0.26	0.40

20. As expected the probability figures are more sensitive to a change of target height, than of target velocity. It is of interest to note that doubling the missile speed (and using the same t_r) would marginally (0.01) increases the probability of engaging targets at close range, t_r is more sensitive for close range targets. However, the higher missile speed increases probability values by 0.08, ie almost 10% at 5 Km range, with the example terrain used here.

21. In the above examples the radar aerial is almost at ground level and it is assumed the missile flies in a straight line (rather than the more

usual curved trajectory). This approximation will make little difference for a general assessment, since it is assumed also that the target is being tracked at a mean range. In practice with the variation of ground tracks sometimes the target will be nearer at the beginning or end of an engagement if no evasive manoeuvres are used, the missile velocity will also vary, depending on range. Clutter is ignored for the moment. If the tracking aerial is raised above the immediate obscuration the situation will be changed significantly and in general at short ranges the target's only hope of evading a tracking situation is either by the inability of the radar to follow the high sightline rate, to separate the target from surface clutter, or by deliberately degrading the sytem by introducing noise or deception jamming and hard target manoeuvre.

TRACKING ALGORITHM

22. It may seem from the foregoing in this Annex that radar detection theory has been temporarily forgotten. The picture is now completed by considering an example tracking algorithm as part of the overall detection process. Assuming a tracking situation (unobscured target - which may or may not last for minimum track length T_c at para 18), then a statistical algorithm to separate genuine detection opportunities from false alarms can be used to detect an acceptable sequence of detections and a track is then declared. Markov chains can be used to study such sequences with the criterion that a tracking state should be held for a minimum number of time intervals and at a correct signals to noise ratio. The relationship between p (detection probability) and declared tracking status is derivable. Results are not only dependent upon the number of observations chosen when setting up the algorithm, {228} but the degree of correlation between individual target returns (hits) during the observation time interval.

23. <u>Derivation of Algorithm</u>. If the detection opportunities are taken in time sequence, as triplets, where p = P (next digit is a 1), q = P (next digit is a 0), then there are 8 3-bit patterns. Initial and final states (i, j) are plotted below; where P_{ij} occurs in one change:

i \ j	0	1	2	3	4	5	6	7
0	q				p			
1	q				p			
2		q				p		
3		q				p		
4			q				p	
5			q				p	
6				q				p
7				q				p

(q = 1 - p)

If two 1 states are required for tracking (2 our of 3, ie n = 3, k = 2), then non tracking will be represented by the binary pattern for 0, 1, 2 or 4 and tracking by 3, 5, 6 or 7. The above plot can be re-written, with T and $\overline{T}$ representing tracking and non-tracking respectively. Although the example used here assumes 2 "hits" out of any successive observations (ie 2 signal returns out of 3 produce 1 states by crossing the detection threshold), other radars may use algorithms which use a larger number of observations (n) and require more hits (k). The values of the transition matrix at equation 35 will change accordingly. Performance prediction of a radar with unknown tracker processing characteristics will require exploration of a range of values for n and k. The technique used here is known as a 'sliding window' algorithm.

	i \ j	$\overline{T}$ 0	1	2	4	T 3	5	6	7
$\overline{T}$	0	q			p				
	1	q			p				
	2		q				p		
	4			q				p	
T	3		q				p		
	5			q				p	
	6					q			p
	7					q			p

$P_o = P\ (000) = q^3$

$P_1 = P\ (001) = P_2 = P_4 = pq^2$

$P_2 = P\ (011) = P_5 = P_6 = p^2q$

$P_3 = P\ (111) = p^3$

24. If each quadrant (ie $T\overline{T}$, TT, $\overline{T}T$ and $\overline{T}\overline{T}$) is taken separately:
(JOINT PROBABILITIES)

a. <u>$T\overline{T}$ = P (T and $\overline{T}$) - Tracking to Non Tracking</u>. Starting in a tracking state, ie 3, 5, 6 or 7. Moving from state 3 to state 1. P (of being in state 1 at (time t) x P (transition from state 3 to state 1 at t + 1).

$$P_3,\ P_{3,1} = p^2q \times q = p^2q^2\ (P_3 \times q)$$

The only other non-zero term is $P_5 \times P_{5,2}$

$$= p^2q \times q = p^2q^2$$

Combining ($P_3P_{3,1}$ with $P_5P_{5,2}$) gives the transition P ($T\overline{T}$).

$$\therefore \; P(\overline{T}\overline{T}) = \Sigma P_i P_{ij} = 2p^2q^2 \qquad \text{———} \qquad (27)$$

i, 3, 5, 6, 7

j, 0, 1, 2, 4

b. <u>$\overline{T}T = P(\overline{T}$ and T) – Non Tracking to Tracking</u>. We have P_2, $P_{2,5}$ and P_4 $P_{4,6}$

$$\therefore \; P(\overline{T}T) = \Sigma P_i P_j = (pq^2 \times p) + (pq^2 \times p) = 2p^2q^2 \qquad \text{———} \qquad (28)$$

i, 0, 1, 2, 4

j, 3, 5, 6, 7

c. <u>TT = P (T and T) – Tracking Maintained</u>. Six items are considered

$$P_3 P_{3,5} + P_5 P_{5,6} + P_6 (P_{6,3} + P_{6,7}) + P_7 (P_{7,3} + P_{7,7})$$

$$= (p^2q \times p) + (p^2q \times p) + (p^2q \times 1) + (p^3 \times 1)$$

$$= 2p^3q + p^2q + p^3 = p^2 (2pq + q + p) = p^2 (2pq + 1)$$

$$\therefore P(TT) = \Sigma P_i P_{ij} = p^2 (2pq + 1) \qquad \text{———} \qquad (29)$$

= i, 3, 5, 6, 7

j, 3, 5, 6, 7

d. $\overline{T}\overline{T} = P(\overline{T} \text{ and } \overline{T})$ - Non-Tracking Maintained

$$P_0 (P_{0,0} + P_{0,4}) + P_1 (P_{1,0} + P_{1,4}) + (P_2 \times P_{2,1}) + (P_4 \times P_{4,2})$$

$$= (q^3 + pq^2) + (pq^2 \times q) + (pq^2 \times q)$$

$$= q^3 + pq^2 + 2pq^3$$

$$\therefore \; P\,\overline{T}\overline{T} = \Sigma P_i P_{ij} = q^2 (2pq + 1) \qquad (30)$$

i, 0, 1, 2, 4

j, 0, 1, 2, 4

25. The transition matrix is that of conditional probability.

a. To get the entry for $\overline{T}T$, start in state $\overline{T}$ and finish in T

if $P(\overline{T}) = P(T\overline{T}) + P(\overline{T}\overline{T})$

and $P\left(T/\overline{T}\right) = \frac{P(\overline{T}T)}{P(\overline{T})}$ (ie probability of T given $\overline{T}$)

$$= \frac{2p^2q^2}{2p^2q^2 + q^2 (2pq + 1)} \qquad (31)$$

b. Similarly for $P\left(\overline{T}/T\right)$ then $P\left(\overline{T}/T\right) = \frac{P(\overline{T}T)}{P(T)}$

where $P(\overline{T}/T) = P(TT) + P(\overline{T}T)$

$$= \frac{2p^2q^2}{2p^2q^2 + p^2 (2pq + 1)} \qquad (32)$$

c. For $P(T/T)$ then,

$$\frac{P(TT)}{P(T)} = \frac{P(TT)}{P(TT) + P(T\bar{T})}$$

$$= \frac{p^2(2pq+1)}{2p^2q^2 + p^2(2pq+1)} \qquad (33)$$

d. Finally for $P(\bar{T}/\bar{T})$ then,

$$\frac{P(\bar{T}\bar{T})}{P(\bar{T})} = \frac{q^2(2pq+1)}{2p^2q^2 + q^2(2pq+1)} \qquad (34)$$

Giving the matrix, after cancellation:

Final State

Initial State		T	$\bar{T}$
	T	$\frac{2pq+1}{2q^2+2pq+1}$	$\frac{2q^2}{2q^2+2pq+1}$
	$\bar{T}$	$\frac{2p^2}{2p^2+2pq+1}$	$\frac{2pq+1}{2p^2+2pq+1}$

(35)

From matrix above $P_{T,T} = 1 - P_{T\bar{T}}$

$$= \frac{2pq+1}{2q^2+2pq+1} \qquad (36)$$

26. The probability of obtaining a number of successive detections N is:
(declarations)

$$P_{T(N)} = (P_{TT})^N P_{T\bar{T}}$$

$$P_{T(N)} = \left[\frac{2pq + 1}{2q^2 + 2pq + 1}\right]^N \quad \frac{2q^2}{2q^2 + 2pq + 1} \qquad \text{(37)}$$

The mean track length (taken from the geometric distribution at (38)) and measured in terms of the number of successive detections is plotted at Fig 6.

$$\bar{L} = \frac{2q^2 + 2pq + 1}{2q^2} = 1 + \frac{p}{q} + \frac{1}{2q^2} \qquad \text{(38)}$$

27. From the above, the probabilities of interest are; in summary (and subject to a continued sightline once a track is declared):-

$$P_T \text{ (at any time)} = p^3 + 3p^2q \qquad \text{(39)}$$

$$P_{\bar{T}} \text{ (no tracking)} = q^3 + 3pq^2 \qquad \text{(40)}$$

$$P_{\bar{T}T} \text{ (New track commencing)} = \frac{2p^2}{2p^2+2pq+1} \qquad \text{(41)}$$

(given a sightline and at least 2 out of 3 successive threshold crossings in the sampling timeframe)

PRACTICAL INTERPRETATION

28. Each detection is of course dependent on the signal/clutter ratio, both of which are fluctuating. In the first case this is due to target RCS variations (glint) and secondly as a function of the clutter level being simultaneously received. Swerling and Rayleigh distributions {229}, and Heidbreder and Mitchell {230} show that lognormal distributions may be applicable to certain types of target.

29. The probability of an integrated group of N signals (with noise samples) exceeding a threshold V_t has been examined by Powell {231}. For the distribution (Swerling 3) this can be approximated with four degrees of freedom as:

$$P_{N_4} = \left(1 + \frac{2}{N\bar{\sigma}}\right)^{N-2} \left[1 + \frac{V_t}{1 + \frac{N\sigma_{AV}}{2}} - \frac{2\ (N-2)}{N\sigma_{AV}}\right] \exp\left[- \frac{V_t}{1 + \frac{N\sigma_{AV}}{2}}\right] \text{--(42)}$$

and may be compared with the other Swerling distributions with two degrees of freedom (from $p(\sigma) = \frac{1}{\sigma} \exp. \left(- \frac{\sigma}{\sigma}\right)$):

$$P_{N_2} = \left(1 + \frac{2}{N\sigma}\right)^{N-1} \exp. \left(- \frac{V_t}{1 + N\sigma_{AV}}\right) \text{---------------------(43)}$$

30. At short ranges $N\sigma_{AV} \to \infty$, therefore in equations (42) and (43) above $P_{N_2} > P_{N_4}$. At longer ranges $N\bar{\sigma}$ will decrease. If strong signal peaks are received from time to time from targets at range they may nevertheless exceed V_t, even though the required target mean signals are below detection threshold. A critical or "crossover" range must exist, where $P_{N_2} \approx P_{N_4}$, at which this takes place. By further approximations taken over shorter ranges the "crossover range" may be deduced which shows that a low 'noise' target is more easily detected at short ranges, while a noisy, peaking or spiky target is more easily detected at long ranges. Using the range at which signal/noise ratio is 1 (0 dB), $P_{N_2} < P_{N_4}$ when $p < 1.256$ ie:

$$R = 1.059 \left(\frac{V_t - N + 1}{N}\right)^{\frac{1}{4}} R_{(0dB)} \text{ ---------------------------- (44)}$$

31. With FAR = 10^{-6} and N = 1000 the crossover range is $0.835R_{(dB)}$. Beyond this range the target signal fluctuations enhance the probability of detection and hence tracking. If $R_{(0dB)}$ is approximately twice the detection range for $P_{det} = 0.9$, then R (crossover) is $\approx 1.7R_{(P_d = 0.9)}$. It is seen therefore that a large signal variance does not always coincide with a high probability of detection.

32. Although this approach may be acceptable for certain aircraft targets, it is thought that they must exhibit fairly angular structural shapes, ie mutually orthogonal reflecting surfaces, in order to produce the large dynamic range of "spiked" returns. The technique is probably not applicable to small targets with smooothed profiles.

33. In all cases there is a crossover range beyond which fluctuations enhance P_d, but inside which fluctuations detract from P_d. When integration number N is plotted against crossover range, the following applies:

a. <u>Low Integration Numbers</u> e.g. Acquisition radars, crossover range is low.

b. <u>High Integration Numbers</u> e.g. Tracking radars P_d at corssover is at greater range ($0.75 < \frac{R}{R_o} < 0.90$). Within this range a closing small target will be more difficult to track if it is "spiky".

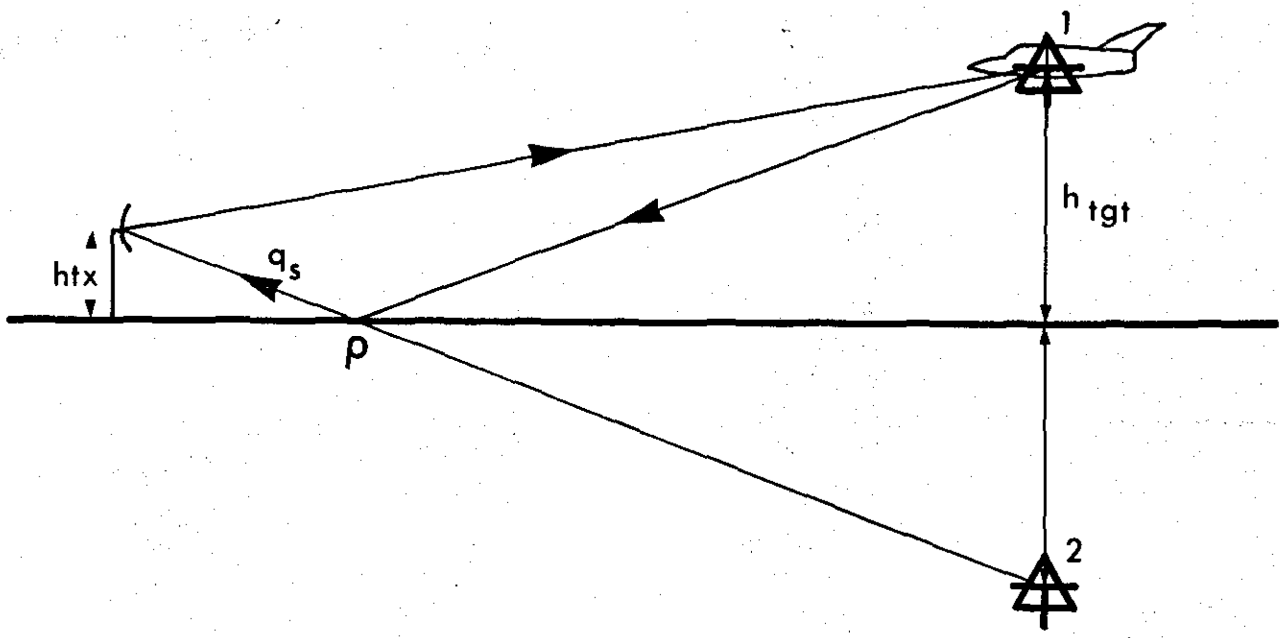

FIG 1 REFLECTION CENTROID OF LOW FLYING AIRCRAFT

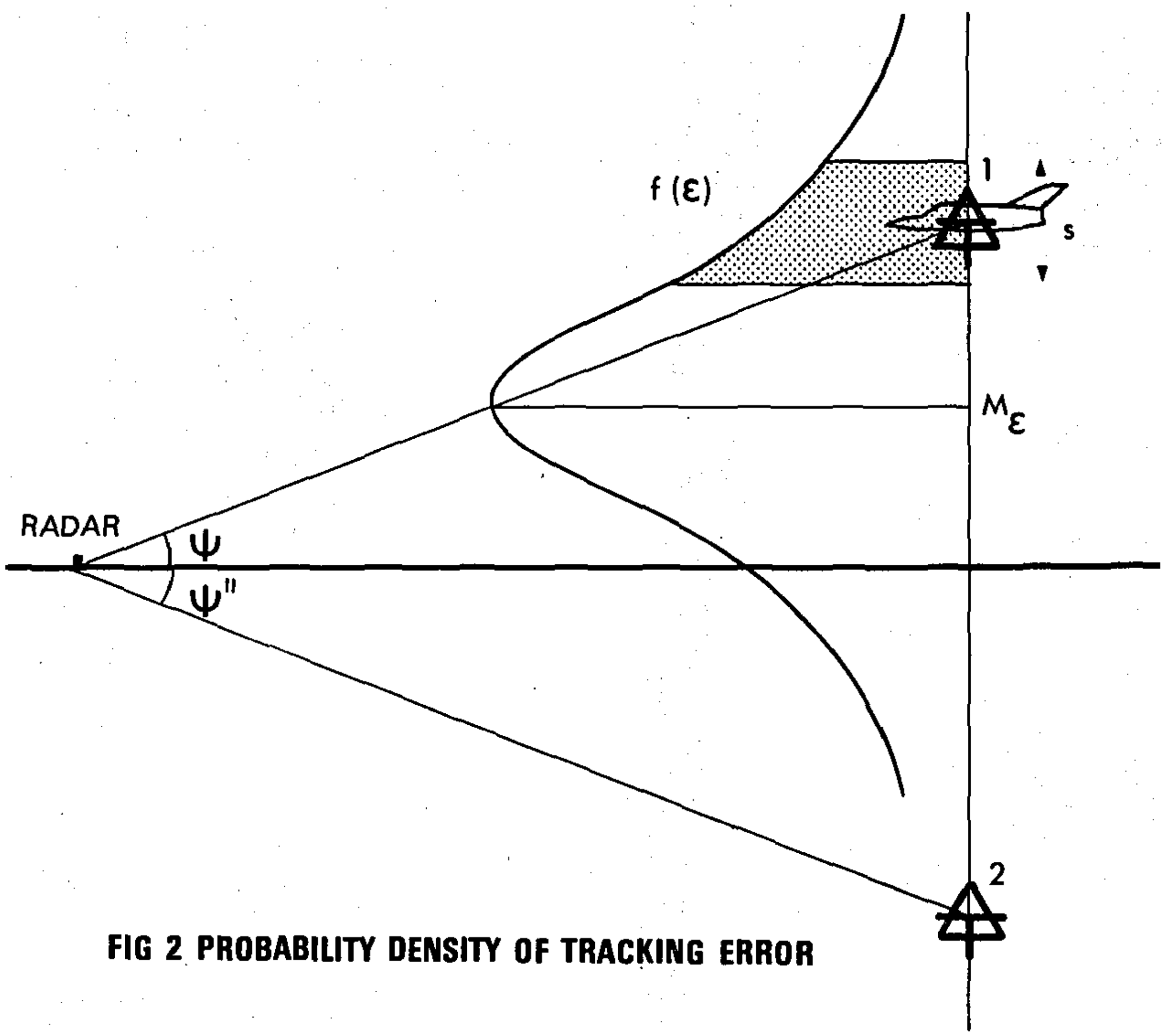

FIG 2 PROBABILITY DENSITY OF TRACKING ERROR

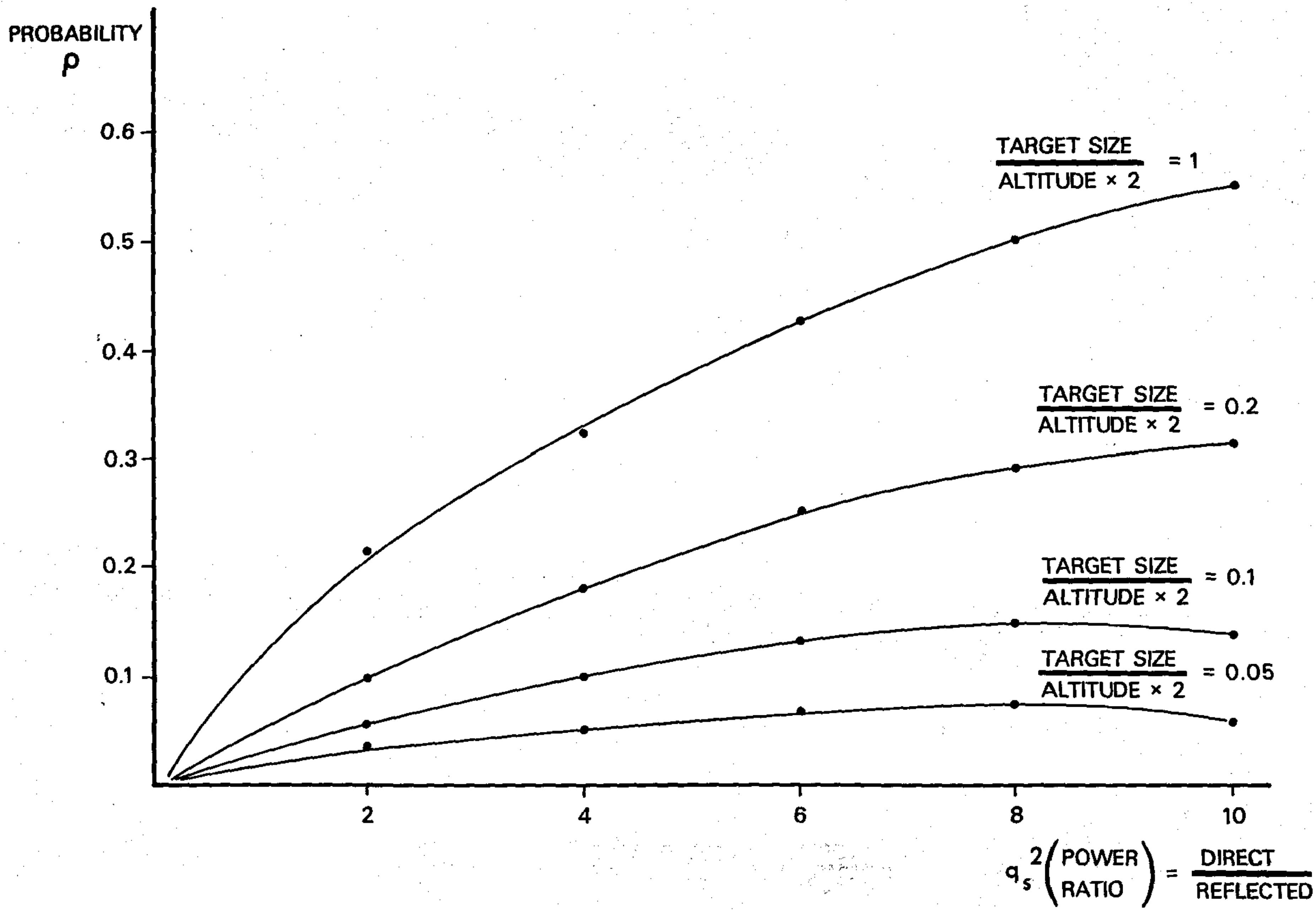

FIG 3 PROBABILITY OF SIGHTLINE FALLING ON TARGET

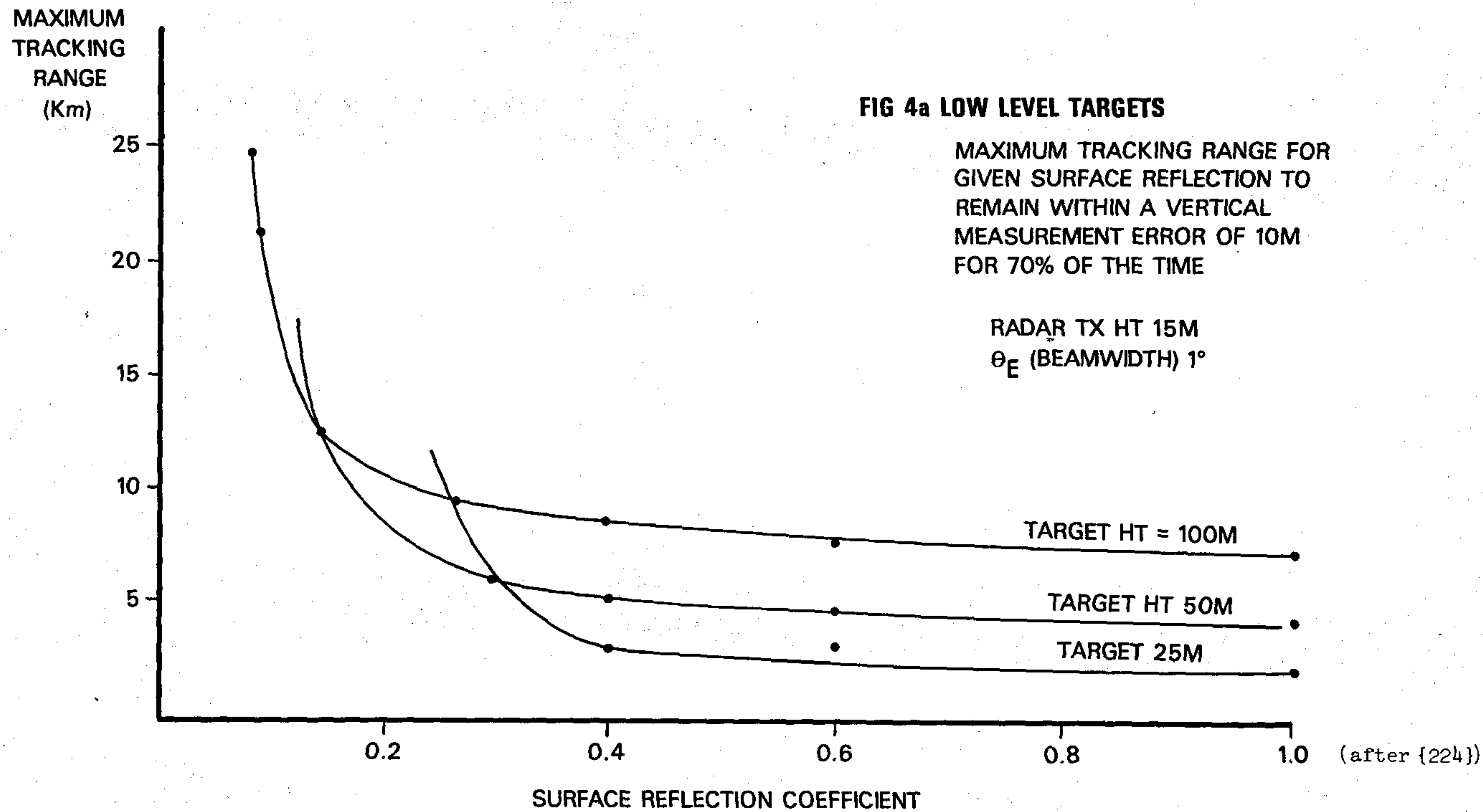

FIG 4a LOW LEVEL TARGETS

MAXIMUM TRACKING RANGE FOR GIVEN SURFACE REFLECTION TO REMAIN WITHIN A VERTICAL MEASUREMENT ERROR OF 10M FOR 70% OF THE TIME

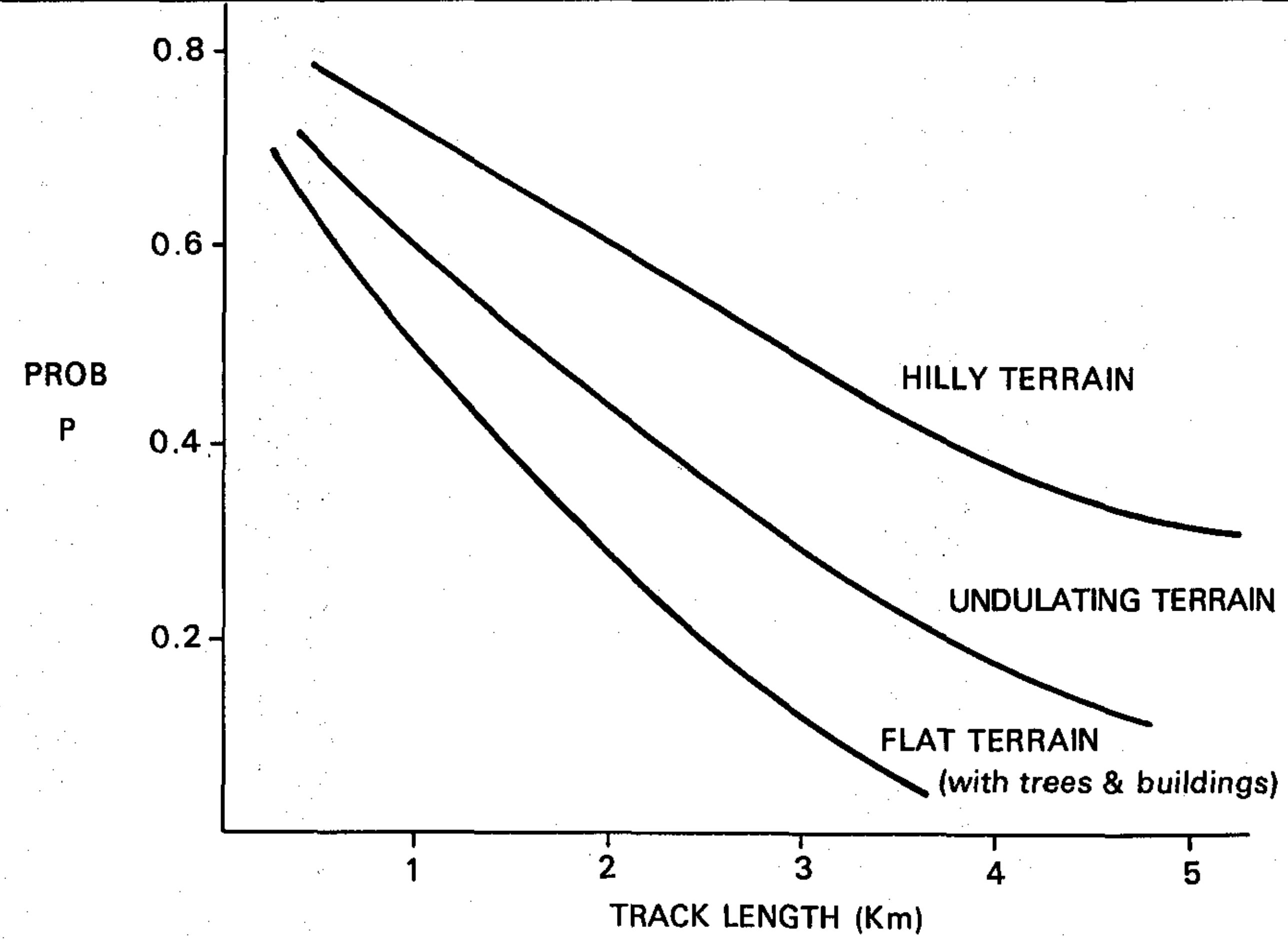

FIG 5a PROBABILITY OF OBSERVING A GIVEN TRACK LENGTH

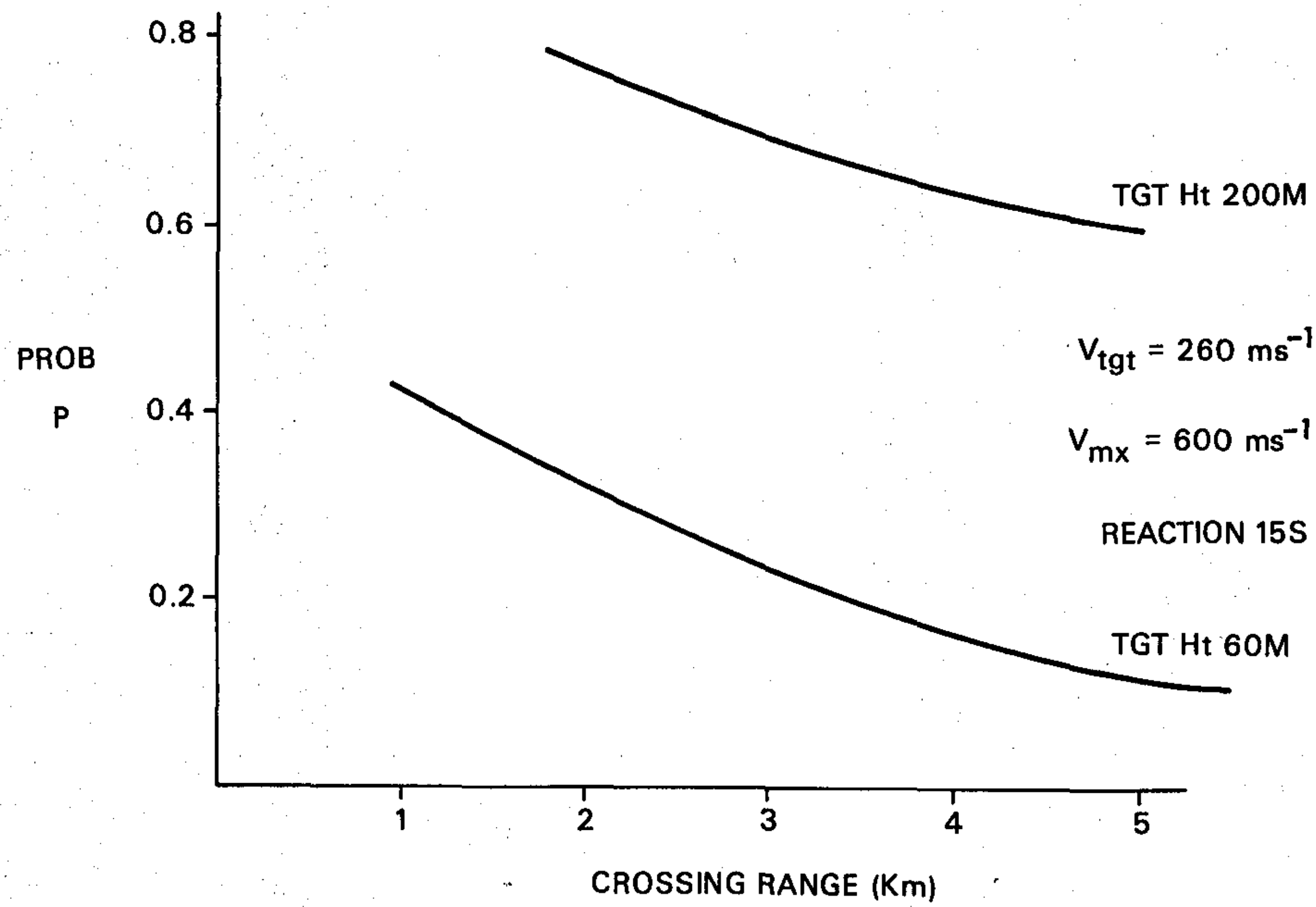

FIG 5b PROBABILITY OF OBTAINING A GIVEN TRACK LENGTH AT A GIVEN CROSSING RANGE

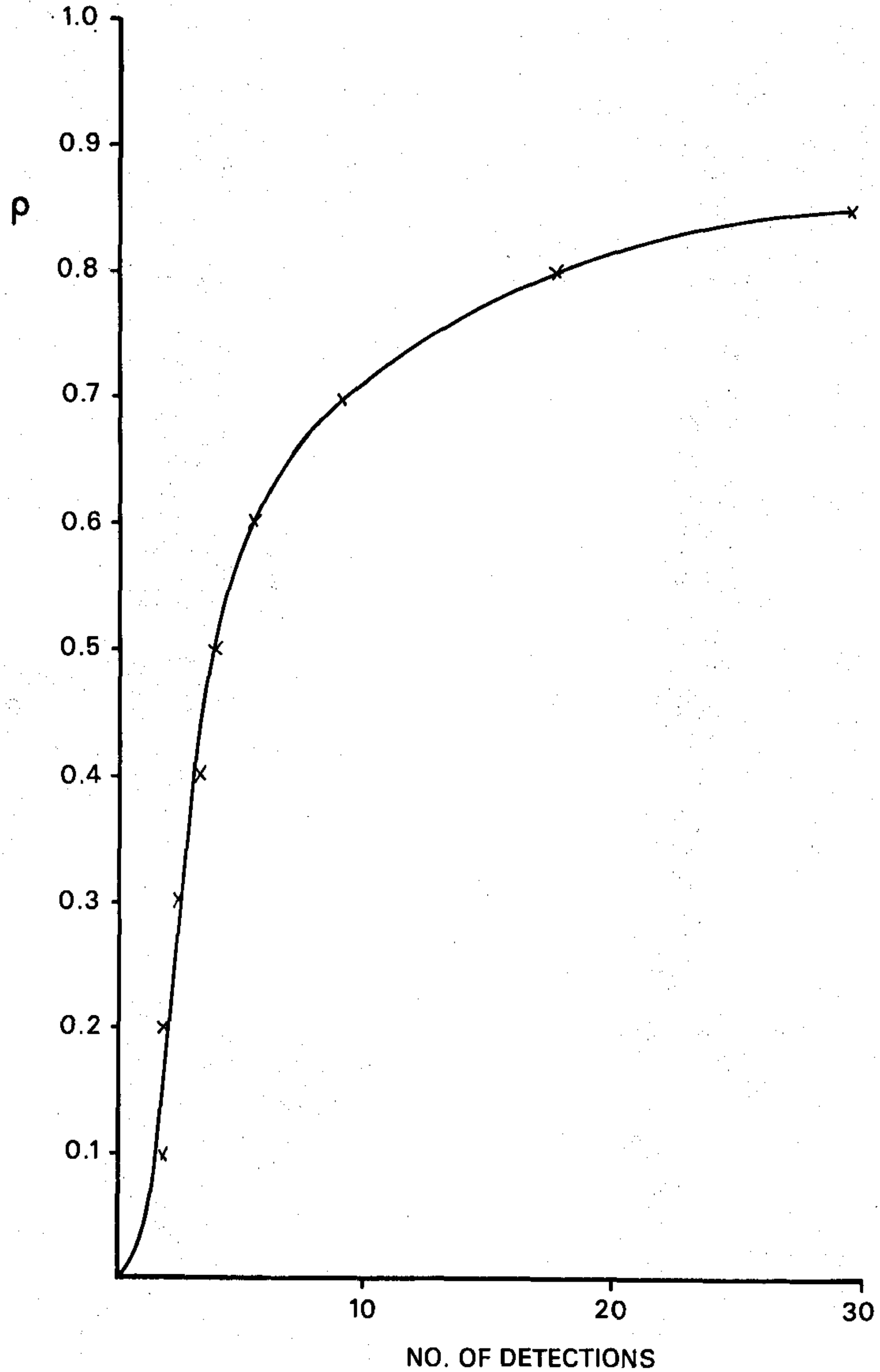

FIG 6 PROBABILITY OF OBTAINING A GIVEN TRACK LENGTH EXPRESSED AS A NUMBER OF DETECTIONS

ILLUMINATED SURFACE AREAS AND TERRAIN CURVATURE

1. Reference is made to Figure 1, where the average gradients of a surface-illuminated tilted 'facet' between adjacent matrix terrain spot heights (ABCD) are:

a. In Range

$$\alpha_R = \frac{\alpha_{R_1} + \alpha_{R_2}}{2} \qquad (1)$$

b. In Azimuth

$$\alpha_A = \frac{\alpha_{AZ_1} + \alpha_{AZ_2}}{2} \qquad (2)$$

2. The simple facet shown can be taken as the illuminated area beneath the resolution cell for shallow surface gradients. Although it is realised that the radar energy will also strike the surrounding area, for the following statistical studies the 3dB area is taken. Sidelobes are ignored since only sharp-beamed tracking radars are considered here. Facet range (along beam boresight) gradients will cause radar reflectivity to vary appreciably due to the changes in the illuminated surface area, as seen with the aspect variation at Figure 2. The critical condition for a reduced area in the range direction (as τ, θ_E and θ_A vary) is given by (3) and (4). R is taken as the radar range to the facet centre, R^1 and R^{11} as range to the nearest and furthest cell edges respectively:

$$\alpha_{R(CRIT)} = \text{Arctan} \quad \frac{\theta_E R}{\tau} \tag{3}$$

$$\alpha_{AZ(CRIT)} = \text{Arctan} \quad \frac{\theta_E R}{\theta_A R} = \text{Arctan} \frac{\theta_E}{\theta_A} \tag{4}$$

θ_E, θ_A in rads, τ as a length

3. If the illuminated facet is assumed to be a flat plane (ie no significant undulations within the area bounds) its area can be calculated for any tilt angle within the volume of the resultion cell. Only those terrain facets which are tilted towards the source of radar energy are assumed to create backscatter. These are declared "illuminated" by the computer program. For this to occur α_R must be a positive value or zero.

4. Non-Critical Slope Values. For a simple set of conditions (Fig 1) $\alpha_R < \alpha_{R(CRIT)}$ and $\alpha_{AZ} < \alpha_{AZ(CRIT)}$; the average dimensions of the sides of the illuminated area are $\tau/\cos \alpha_R$ and $R\theta_A/\cos \alpha_{AZ}$. More precisely, account should be taken of the accurate lengths of all four boundaries of the illuminated area by allowing for the slight beam divergence in azimuth; such that $R^1\theta_A/\cos \alpha_{AZ1} < R^{11}\theta_{AZ2}$

The basic shape is a regular quadilateral with maximum possible side-lengths for $\alpha_{AZ(CRIT)} > \alpha_{AZ} \geqslant 0$, $\alpha_{R(CRIT)} > \alpha_R \geqslant 0$ will be:

Rear $R\theta_A/\cos \alpha_{AZ2}$

Front $R\theta_A/\cos \alpha_{AZ2}$ (5)

Sides $\tau/\cos \alpha_{R1}$ or $\tau/\cos \alpha_{R2}$

$$R\theta_A \leqslant AB < R\theta_A \cos_{AZ(CRIT\ 1)}$$
$$R\theta_A \leqslant DC < R\theta_A \cos_{AZ(CRIT2)} \qquad (6)$$
$$\tau \leqslant AD < \tau/\alpha_{R(CRIT1)}$$
$$\tau \leqslant BC < \tau/\alpha_{R(CRIT2)}$$

Giving average azimuth X Range product area:

$$\text{Area} = \frac{\tau\ (\cos\alpha_{R1} + \cos\alpha_{R2})\ R\theta_A\ (\cos\alpha_{AZ1} + \cos\alpha_{AZ2})}{4\cos\alpha_{R1}\cos\alpha_{R2}\cos\alpha_{AZ1}\cos\alpha_{AZ2}} \qquad (7)$$

5. Critical Slope Values. Figure 2 shows the effect of $\alpha_{AZ} > \alpha_{AZ(CRIT)}$, $\alpha_R < \alpha_{R(CRIT)}$ and $\alpha_{AZ1} < \alpha_{AZ2}$

Calculation of illuminated areas for any condition thus becomes more difficult than the first case, since facet tilt either results in an irregular hexagon (figure 4) or a reduced area in which the plane does not cut either the range boundaries or the azimuth boundaries as at Figure 3. For calculative purposes the area at figure 4 is taken as a plane quadilateral TD^1QB^{11} and the area within the resolution cell is defined by TUVQRS (ie TD^1QB^{11} less the corner areas). Calculations are detailed at para 17 below.

6. Terrain data base interpolation can provide the spot heights TD^1QB^{11} if required. However, as will be shown below, these are not strictly necessary if facet gradient and aspect can be calculated from nearby data matrix points without the need for interpolation. In any event spot heights U, V, R, S cannot be obtained by simple interpolation.

7. Gradient and Curvature. Several techniques for the optimum calculation of surface parameters have been developed by geomorphological researchers as part of their studies for soil erosion, drainage and similar requirements. Such a study is considered at {232}, giving a demonstrably satisfactory method for estimating both surface gradient and curvature derivatives directly from the altitude matrix.

8. To apply this to radar here, using gradient to investigate clutter returns (as a function of facet slope and aspect) and curvature on a larger scale (for diffraction investigations); involves the inclusion of the eight nearest spot heights surrounding the centre of the required cell - which is the centre of the radar resolution cell "footprint".

9. The central spot height with the four nearest points define simple gradient, with the furthest four points additionally for curvature. It is assumed that the basic matrix dimensions are adequate to produce the required accuracy. It should be noted that gradient or curvature 'maps' produced by this method cannot be compared with others unless the matrix spacing is similarly defined.

10. Grid Definition. A nine-point altitude sub-matrix is defined at Figure 5a. By using the full quadratic a complete surface description can be obtained at equation (8). Gradient is more accurately calculated using 9 data points for the coefficients at eqns (9) to (14).

$$A = ax^2 + by^2 + cxy + dx + ey + f \tag{8}$$

Using the notation defined for the matrix of spacing (m) the coefficients are calculated as follows:

$$a = \frac{A_1 + A_3 + A_4 + A_6 + A_7 + A_9}{6m^2} - \frac{A_2 + A_5 + A_8}{3m^2} \tag{9}$$

$$b = \frac{A_1 + A_2 + A_3 + A_7 + A_8 + A_9}{6m^2} - \frac{A_4 + A_5 + A_6}{3m^2} \tag{10}$$

$$c = \frac{A_3 + A_7 - A_1 - A_9}{4m^2} \tag{11}$$

$$d = \frac{A_3 + A_6 + A_9 - A_1 - A_4 - A_7}{6m} \tag{12}$$

$$e = \frac{A_1 + A_2 + A_3 - A_7 - A_8 - A_9}{6m} \tag{13}$$

$$f = \frac{3(A_4 + A_2 + A_8 + A_6) - (A_1 + A_3 + A_7 + A_9) + 5A_5}{9} \tag{14}$$

Hence gradient, aspect and profile convexity are obtained respectively from:

$$\begin{aligned} \text{grad} &= \arctan\ (d^2 + e^2)^{\frac{1}{2}} \text{ deg} \\ &\text{or } \arctan\ (d \cos \theta + e \sin \theta) \end{aligned} \tag{15}$$

$$\text{aspect} = \theta = \text{Arctan}\ \frac{e}{d}\ \text{deg} \qquad (16)$$

$$\text{Conv} = \frac{-200\ (ad^2 + be^2 + ced)}{e^2 + d^2\ (1 + d^2 + e^2)^{3/2}}\ \text{deg} \quad (100\ \text{m})^{-1} \qquad (17)$$

(for 100m matrix)

11. Frequency Distributions. Gradient frequency distributions were also considered by the author as a possible aid to the overall prediction process for a given area. Gradient steepness distribution shows an increase with altitude with moderately strong correlation, but in a non-linear way {232}. In general no single transformation is found to be universally valid {233}.

12. Therefore although it is possible to statistically summarize a surveyed area in terms of gradient frequency distribution, the results would be site-specific. However it seems quite possible that a frequency distribution for an area might be representative (within reasonable limits of judgement) of another area, unsurveyed, but with similar general characteristics.

13. Convexity distributions tend to be balanced by concavity (negative convexity) since the mean or median convexities tend to cancel {232}. Profile convexity has a weak positive correlation with altitude.

14. Gradient and Aspect Examples. Gradient calculations present no problems using the above method, but aspect values have orientations which depend upon simple rules developed below.

15. Aspect. It is seen that the actual aspect value can be defined with respect to North or with respect to the radar beam boresight. With respect to the beam boresight the relative direction of aspect depends upon the arithmetic sign combination of both numerator and denominator of eqn (16), as

seen at Table 2; where the terrain surface is in the quadrant 0 to 90° (wrt North). Similar tables can be deduced for other quadrants. The slope reflectivity studies in this report were made using the 0-90° quadrant. Actual angle "Aspect" $\pm$ (90- angle of Radar (wrt N)) = 0 in this quadrant.

Table 2 Determination of Terrain Aspects

Serial	e	d	Orientation
1	+	0	↓
2	0	-	→ Negative Slope
3	0	+	←
4	-	0	↑ Negative Slope
5	+	1	↘
6	-	+	↖
7	+	+	↙ Towards Radar
8	-	-	↗ Negative Slope
9	0	0	Flat Terrain

16. Serials 2, 4 and 8 produce radar shadowing(ie zero backscatter is assumed), aspect values close to serial 7 would be expected to give a maximum backscatter, serials 1 and 3 intermediate levels and serials 5 and 6 minimum levels. Absolute values of aspect (degrees) are measured as shown at figure 5b.

17. Calculation of Area - First Critical Case. The illuminated facet at figure 3 can be calculated as follows, since once aspect (θ) is known this also corresponds to the angle θ marked on the diagram. The conditions are $\alpha_{AZ} > \alpha_{AZ(CRIT)}$ and $\alpha_R < \alpha_{R(CRIT)}$ then:

$$\text{Since } TS = \frac{\tau}{\cos\theta},\ PT = \frac{R\theta_E}{\cos\,(90 - \alpha_{AZ})}$$

Quadrilateral PQST

$$\text{Area} = \frac{R\theta_E \tau}{\cos\ \theta \cos\ (90 - \alpha_{AZ})} \tag{18}$$

R = mean range, as before.

18. <u>Calculation of Area - Second Critical Case</u>. Consideration was given to the use of Direction Cosines since the required area of a surface can be calculated with respect to its normal position.

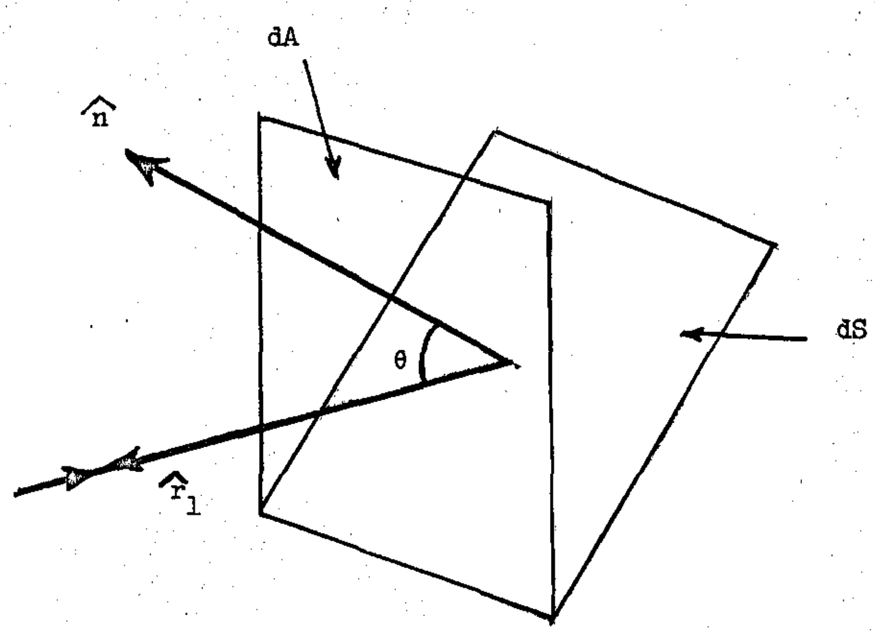

$dA = dS \cos\ \theta$ Terrain $\hat{n} = (l, m, n)$

Radar Beam $\hat{r}_1 = (\lambda, \mu, \gamma)$

$\cos\ \theta = \hat{r}_1 \hat{n} = (\lambda l + \mu m + \gamma n)$ etc ....

But to produce the required area a three-co-ordinate direction cosine system would be needed and the required terrain co-ordinates are not readily accessible for the typical, but awkward shapes, as at figure 4. Hence in the long term it was simpler to use trigonometric methods.

19. If $\alpha_{AZ} > \alpha_{AZ(CRIT)}$ of if $\nless \alpha_{R(CRIT)}$ the side TD^1 (fig 4) will cut AD and with $\alpha_R < \alpha_{R(CRIT)}$ then QD^1 must cut DC. Hence the quadrilateral TD^1QB^{11} is a terrain plane passing through the resolution cell. Points UVSR are positioned dependent upon α_R, α_{AZ}. It is points TUVQRS which define the illuminated area and which are not directly available from the spot height data base. The plan diagram accentuates the beam divergence, but for practical purposes, with small values of τ, sides UA, CR are assumed to be parallel. Aspect is calculated from the terrain matrix - it's direction is shown in the diagram (in direction OB^{11} since this is the lowest terrain point). Gradient is available from eqn (15) and is angle $D^1 B^{11} D^{11}$. α_{AZ} and α_R are computed as Arctan (eqn 12) and Arctan (eqn 13) respectively.

20. From the figure, if the centre of the illuminated terrain is also the centre of the resolution cell, then

$VQ = TS$, $SR = UV$, $\alpha_{AZ1_1} = \alpha_{AZ_2}$, Area UD^1V = Area $SB^{11}R$.
$B^{11}Q = TD$ and $TB^{11} = D^1Q$.

$$\text{Then } B^{11}Q = \frac{\tau}{\cos \alpha_R} \text{ and } TB^{11} = \frac{\theta_A R}{\cos \alpha_{AZ}} \qquad (19)$$

$$\text{Quadrilateral Area } TD^1QB^{11} = \frac{\tau\theta_A R}{\cos \alpha_R \cos \alpha_{AZ}} \qquad (20)$$

Since $\alpha_R \ngtr \alpha_{R(CRIT)}$ then $UD^1 \cos \alpha_{R_1} = \frac{\tau}{2}$

$$\text{hence } UT = UD^1 = B^{11}R = RQ = \frac{\tau}{2\cos\alpha_R} \qquad (21)$$

$$TA^1 = R\theta_E - UT \, Sin \, \alpha_R = TS \, Sin \, \alpha_{AZ} \qquad (22)$$

$$\text{giving } TS = \frac{Sin \, \alpha_{AZ} \, Cos \, \alpha_R}{R\theta_E Cos\alpha_R - \tau Sin\alpha_R} \qquad (23)$$

$$TB^{11} = SB^{11} + TS = \frac{\theta_A R}{Cos\alpha_{AZ}} \quad \text{from (19)}$$

$$\text{Hence Side } SB^{11} = \frac{\theta_A R}{Cos\alpha_{AZ}} - \frac{Sin \, \alpha_{AZ} \, Cos \, \alpha_R}{R\theta_E \, Cos \, \alpha_R - \tau Sin\alpha_R} \qquad (24)$$

Area of both triangles is given by the product of eqn (24) and eqn (21). Subtraction from eqn (20) gives the radar illuminated area:

$$A = \frac{\tau\theta_A R}{Cos\alpha_R Cos\alpha_{AZ}} - \left[\frac{\tau}{2Cos\alpha_R}\left(\frac{\theta_A R}{Cos\alpha_{AZ}} - \frac{Sin\alpha_{AZ} \, Cos\alpha_R}{R\theta_E Cos\alpha_R - \tau Sin\alpha_R}\right)\right] \qquad (25)$$

It is therefore possible to obtain the required area without direct knowledge of the terrain spot heights which define the illuminated area spot heights.

TERRAIN CURVATURE APPLIED TO DIFFRACTION CONDITIONS

21. Reference is made to Chap 7 eqns (15) and (16), which define the criteria for approximating the terrain as a diffracting knife edge. The intention here is to use the convexity calculation at eqn (17) above to estimate the curvature - and then to test it against the criteria. By taking typical dispositions for target, obstacle and radar site together with the matrix values at figure 5a, example calculations are:

From Fig 5a, coefficients are:

$$a = -0.00055$$

$$b = 0.001833$$

$$c = 0$$

$$d = \frac{5}{600}$$

$$e = \frac{-30}{600}$$

$$f = 35.5$$

hence from eqn (17) convexity = 0.356 deg $(100m)^{-1}$

22. The criteria for approximating an obstacle as a knife edge can be expressed from known obstacle radius or diffraction angle θ. However, θ is normally available only if a complete set of conditions are known (ie range from radar to obstacle, and beyond to the target). Converting the above value to the rate of change of slope (Ø) by taking the tangent at 2 successive matrix points; where R is radius of curvature of obstacle (m):

$$R = \frac{180m}{\varnothing\pi} = \frac{180 \times 100}{0.356\pi} = \underline{16094m} \qquad (26)$$

Clearly the rate of change of slope is insufficient to produce diffraction. R is excessively large, as shown by the typical values at Table 1. Typical terrain profiles obtained from the terrain database used for slope reflectivity reported at Appendix 1 to this Annex had limited azimuth cover. In practice a full 360° sweep would be required to produce an area assessement. If it is found that the correct conditions exist to aid tracking on a small % of occasions then the probability of tracking is increased for the area in question eg $P_{TL} = P_{TL}$ x Diff Factor where Diff Factor >1. An example diffraction plot is at Figure 6.

Table 1 Typical Radar, Obstacle and Target Conditions

Ser	Tgt Ht (m) h_{tgt}	Radar Ht (m) h_{tx}	Obstacle Ht (m) h_t	Obstacle Rng Km d_1	Target Range (m) $d_1 + d_2$	Radius (m) R
1	70	0	100	10	15	7.46
2	70	15	100	10	15	19.7
3	70	20	100	10	15	22.17
4	70	30	100	10	15	27.0
5	70	30	100	5	10	7.6
6	20	0	50	10	15	60.0
7	30	0	50	10	15	82.0
8	30	0	30	10	15	2221
9	40	0	30	10	15	480

Using the notation at Chap 7.

$$\alpha = \text{Arctan} \; \frac{h_t - h_{t_x}}{d_1} \qquad (27)$$

$$\beta = \text{Arctan} \; \frac{h_t - h_{t_{gt}}}{d_2} \qquad (28)$$

Diffraction Angle $\theta = \alpha + \beta$

23. Retracing the steps to obtain θ for R = 16094 gives $\theta = 0.0888^\circ$. Using the scenario at Table 1 serial 8, the target would have to climb by approximately 7 metres (ie new target height 37m) if this larger terrain radius existed at the same obstacle range. The conditions at Serial 8 are such that the target would be just visible by direct sightline at an altitude of 45m.

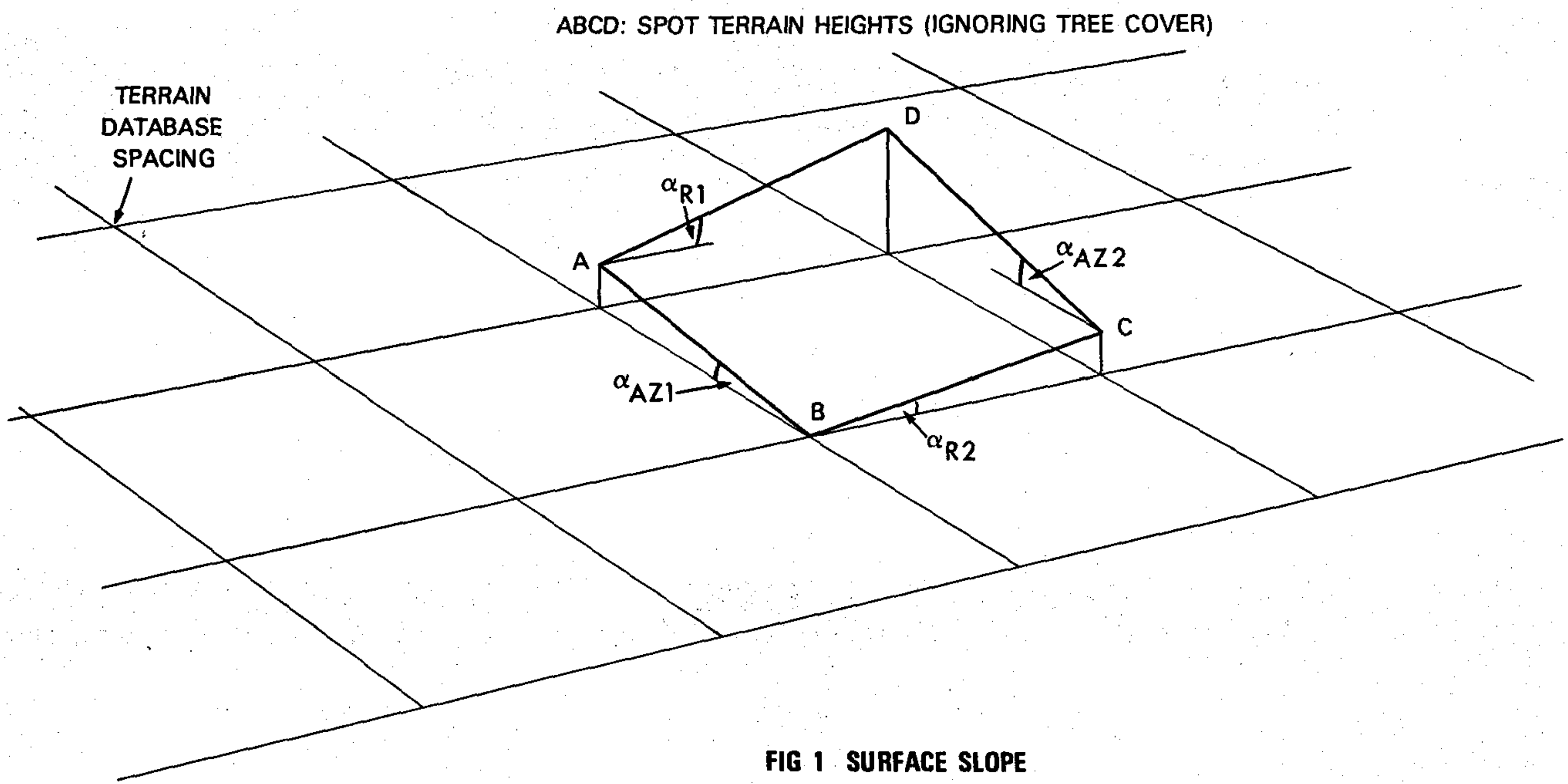

FIG 1 SURFACE SLOPE

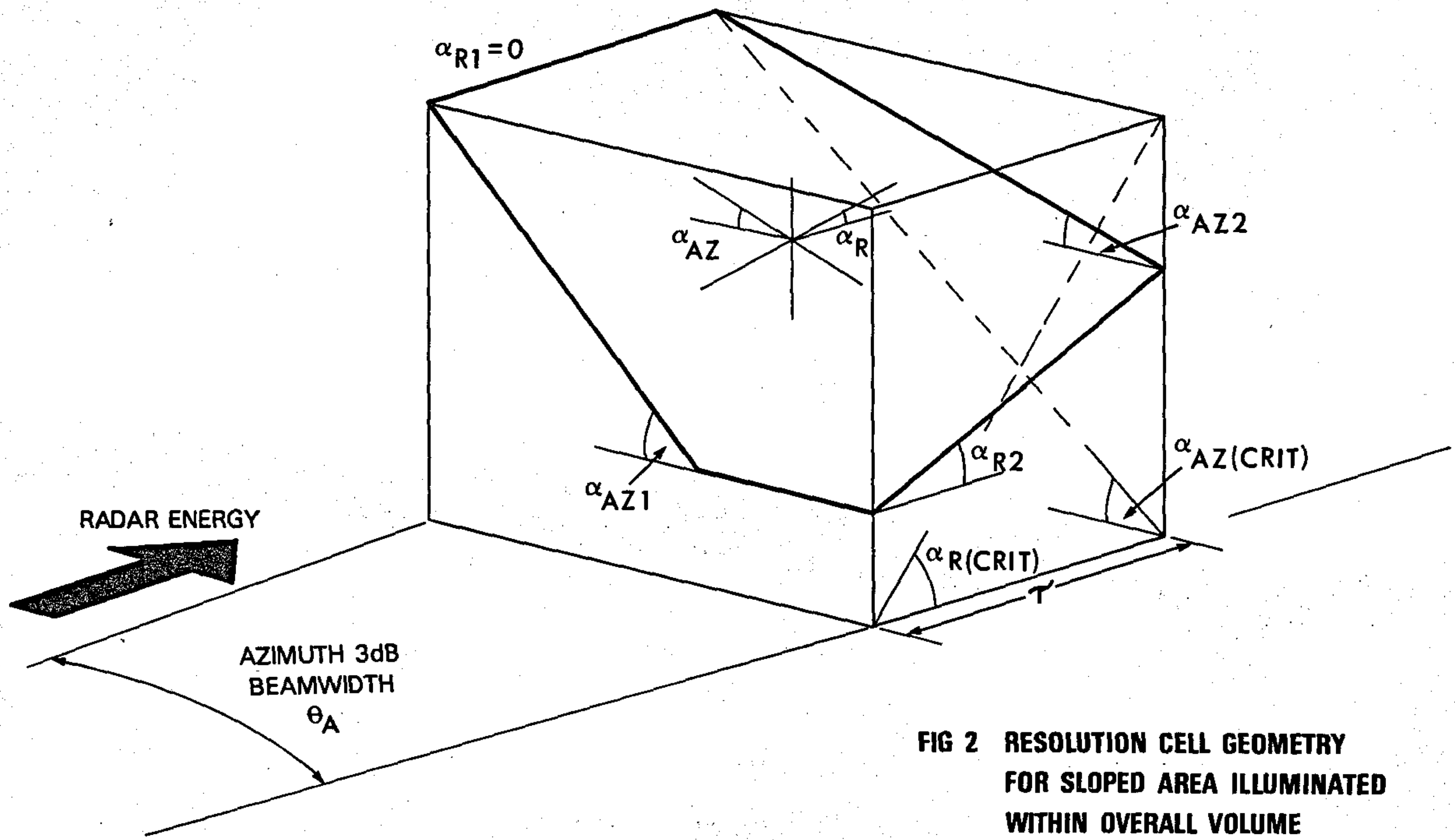

FIG 2 RESOLUTION CELL GEOMETRY FOR SLOPED AREA ILLUMINATED WITHIN OVERALL VOLUME

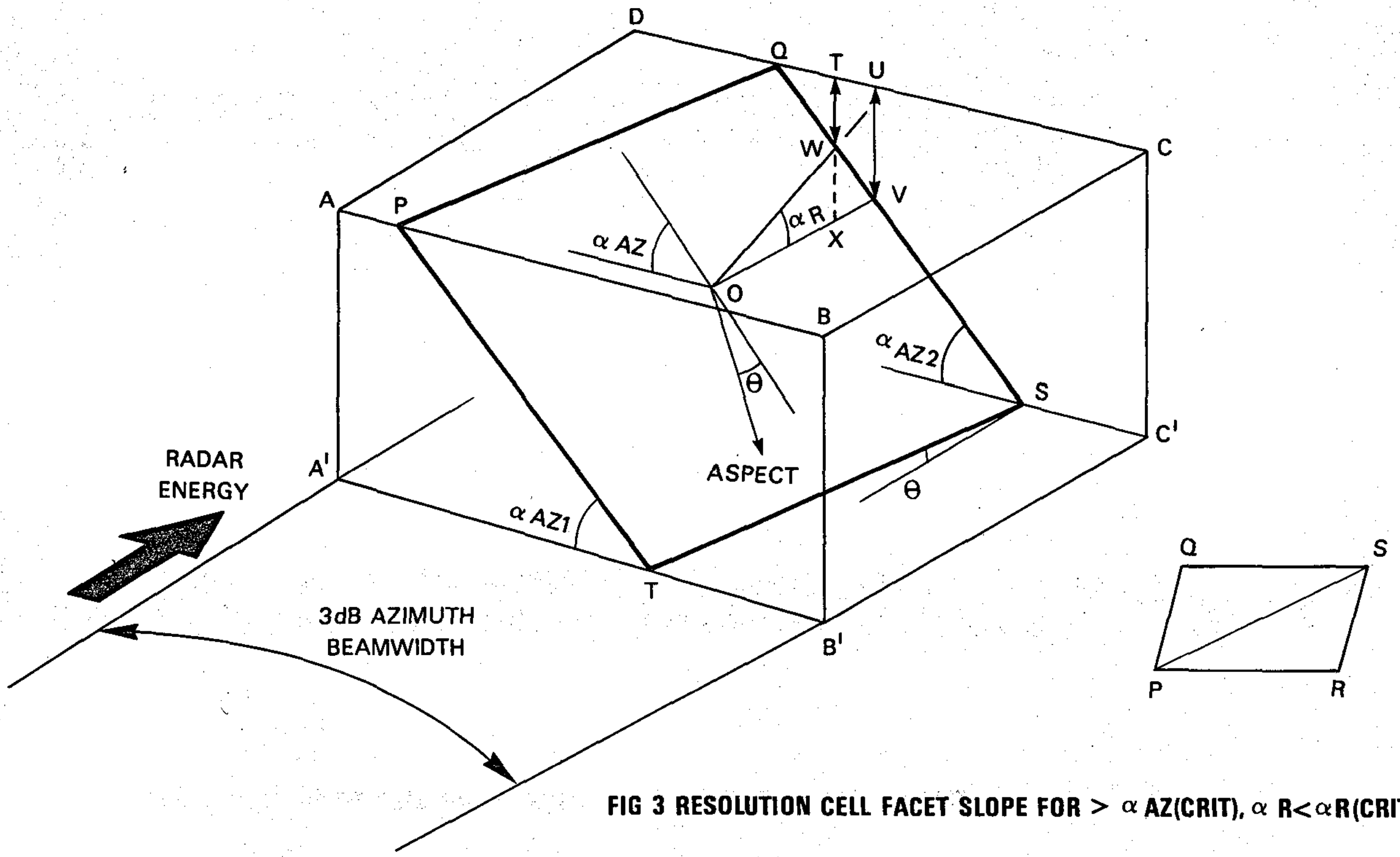

FIG 3 RESOLUTION CELL FACET SLOPE FOR > α AZ(CRIT), α R<αR(CRIT)

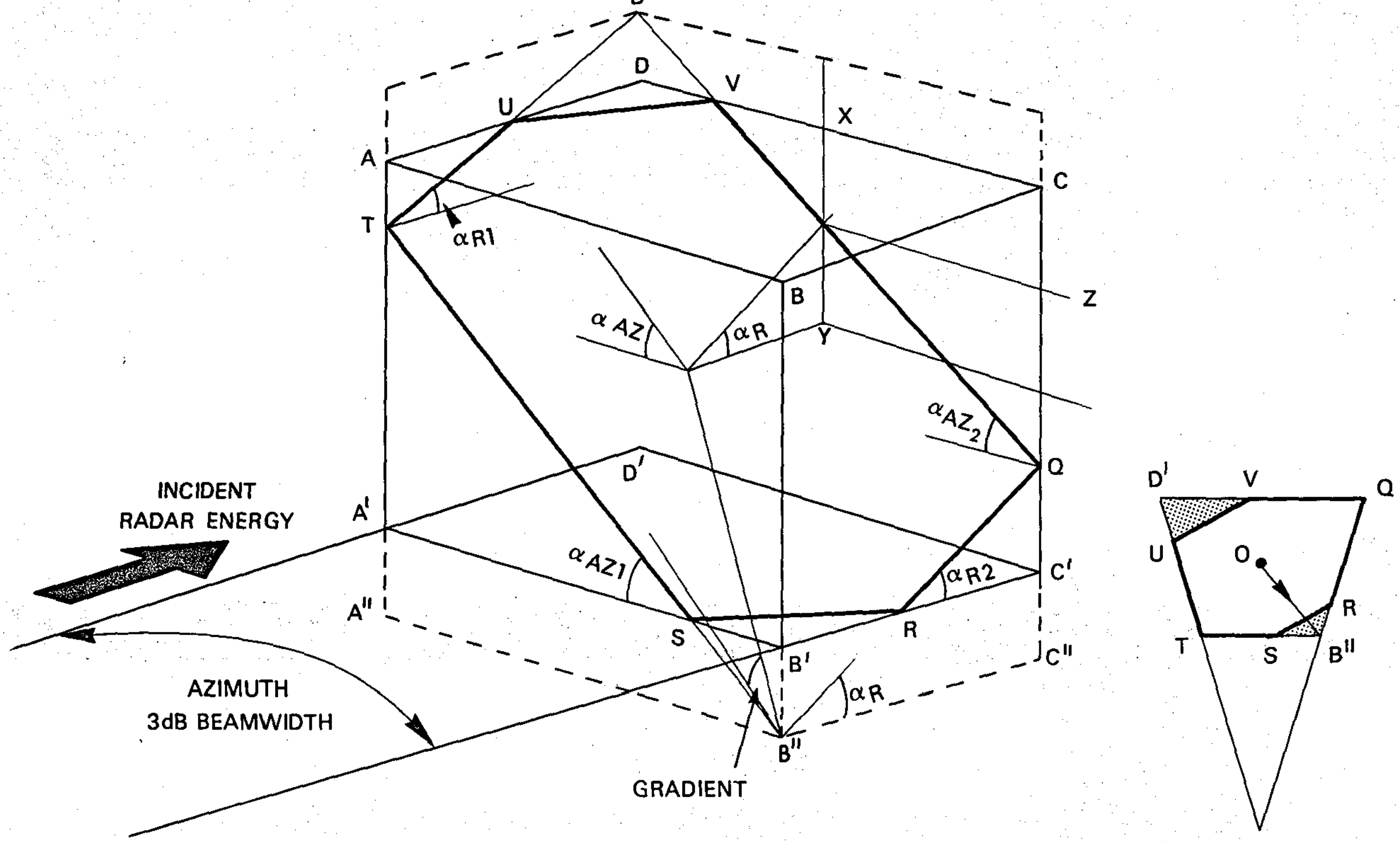

FIG 4 RESOLUTION CELL GEOMETRY FOR > AZ(CRIT) α < α CRIT

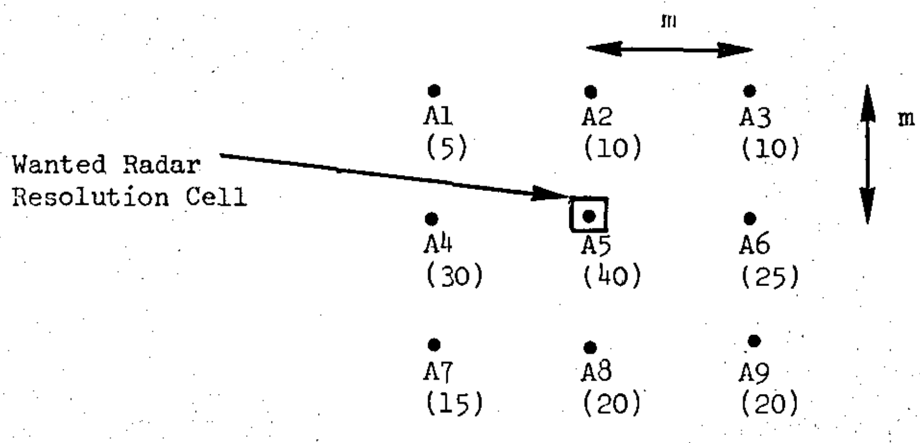

Notes 1. Bracketed figures are example altitudes.

2. m = 100 m (for example).

FIG 5a DEFINITION OF ALTITUDE SUB MATRIX

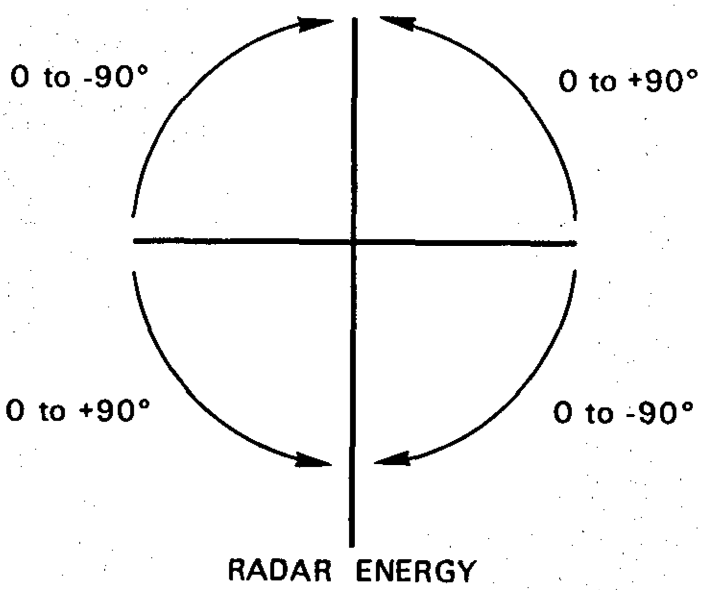

FIG 5b MEASUREMENT OF ASPECT

FIG 6 IDENTIFIED DIFFRACTION RIDGE

STATISTICAL ANALYSIS OF RAW RADAR MEASUREMENTS TO OBTAIN A DISTRIBUTED CLUTTER MODEL OVER SLOPED TERRAIN

1. Full statistical analysis of the raw radar measurements commenced after initially correcting the range (see para 5 below), with the formation of a multivariable array containing some 20k of measured and calculated values. All data reduction programs were written by the author in FORTRAN to run on the RAF College DEC 20 computer facility. Initial analysis was backed by a terrain data base interpolated (tediously) by hand from non-standard survey maps specially provided by the Mapping and Charting Establishment at Tolworth with a contour notation at 5 metre intervals. By photographic enlargement it was possible to interpolate matrix spot heights to within ± 1 metre or better, subject to the original accuracy of the contours. Using 50 metre grid spacing the data base produced extends for 9 square kilometres.

2. For calculative purposes, given the range and azimuth bearing of each radar discrete clutter signal, it was thus possible to extract the corresponding terrain data using the matrix method for terrain slope and

RANGE (m)	S/N	CLT σ	BRG (Deg)	TERR SLOPE	ASPECT (Deg)	$\sigma\ m^{-2}$	AREA (m^2)	TRUE GRAZE (Deg)	$\sigma\ m^{-2} m^{2}$ dBs
6125	21.7	0.5185	58.5	6.322236	12.28579	0.0008034	645.3984	6.162382	-30.9507900
6130	20.7	0.4132	58.5	6.322236	12.28579	0.0006397	645.9253	6.162395	-31.9402200
6135	19.7	0.3294	58.5	6.322236	12.28579	0.0005096	646.4522	6.162408	-32.9281300
6140	22.8	0.6690	58.5	6.322236	12.28579	0.0010340	646.9790	6.162420	-29.8546400
6145	29.0	2.8330	58.5	6.322236	12.28579	0.0043752	647.5059	6.162433	-23.5899700
6150	35.3	12.0000	58.5	6.322236	12.28579	0.0185176	648.0327	6.162446	-17.3241600
6155	31.3	4.8210	58.5	6.322236	12.28579	0.0074334	648.5596	6.162459	-21.2881300
6160	20.3	0.3788	58.5	6.322236	12.28579	0.0005836	649.0864	6.162471	-32.3389300
6165	9.2	0.0297	58.5	6.322236	12.28579	0.0000458	649.6133	6.162484	-43.3902200
6100	22.3	0.5859	57.8	6.322236	11.58579	0.0009115	642.7642	6.176984	-30.4022800
6105	20.0	0.3438	57.8	6.322236	11.58579	0.0005344	643.2911	6.176998	-32.7210200
6110	17.7	0.2018	57.8	6.322236	11.58579	0.0003134	643.8179	6.177012	-35.0384200
6115	15.3	0.1184	57.8	6.322236	11.58579	0.0001838	644.3448	6.177026	-37.3576700
6120	13.0	0.0695	57.8	6.322236	11.58579	0.0001078	644.8717	6.177040	-39.6748800
6125	10.7	0.0407	57.8	6.322236	11.58579	0.0000632	645.3985	6.177054	-41.9927400
6130	8.4	0.0239	57.8	6.322236	11.58579	0.0000371	645.9254	6.177068	-44.3105800
6135	6.0	0.0140	57.8	6.322236	11.58579	0.0000217	646.4522	6.177081	-46.6286000
6140	7.2	0.0182	57.8	6.322236	11.58579	0.0000283	646.9791	6.177095	-45.4867700
6145	11.0	0.0445	57.8	6.322236	11.58579	0.0000687	647.5059	6.177109	-41.6288400
6150	14.9	0.1083	57.8	6.322236	11.58579	0.0001671	648.0328	6.177123	-37.7696900
6155	18.7	0.2635	57.8	6.322236	11.58579	0.0004063	648.5597	6.177137	-33.9116900
6175	13.8	0.0870	59.5	6.299493	1.60725	0.0001338	650.6391	6.283281	-38.7357100
6180	7.3	0.0193	59.5	6.299493	1.60725	0.0000297	651.1659	6.283292	-45.2723500
6185	8.0	0.0229	59.5	6.299493	1.60725	0.0000352	651.6928	6.283304	-44.5345000
6190	12.6	0.0668	59.5	6.299493	1.60725	0.0001024	652.2196	6.283316	-39.8955200
6195	17.3	0.1946	59.5	6.299493	1.60725	0.0002981	652.7464	6.283327	-35.2560200
6200	21.9	0.5668	59.5	6.299493	1.60725	0.0008676	653.2733	6.283339	-30.6166500
6205	26.5	1.6510	59.5	6.299493	1.60725	0.0025252	653.8001	6.283351	-25.9769800
6210	31.2	4.8090	59.5	6.299493	1.60725	0.0073495	654.3270	6.283362	-21.3374000
6215	30.2	3.8770	59.5	6.299493	1.60725	0.0059204	654.8538	6.283374	-22.2764900
6220	27.0	1.8500	59.5	6.299493	1.60725	0.0028228	655.3806	6.283385	-25.4932200
6105	32.5	6.0740	59.5	6.299493	1.60725	0.0094425	643.2635	6.283525	-20.2491400

TABLE 1 SAMPLE DATA ARRAY

aspect detailed at Annex F. Illuminated radar footprint size could then be calculated, taking into account resolution cell size, slope and aspect and (by mean terrain height) the actual arrival angle of the radar wavefront. Generated data examples are at Table 1.

3. Clutter returns were processed radially (ie incrementally by increasing range at 5 metre steps) and incrementally in azimuth at either 0.3 or 0.4^{o} steps. The geographical area was chosen to include both flat and sloped terrain. For convenience this was divided into 4 sectors which contain predominately 'sloped' terrain and one sector which is mostly 'flat' - although it will be shown below that terrain is rarely flat in the scientific sense. Data was analysed by sectors and as an integral data bank. Figure 1a is a photograph, with OS map showing the location of the measurements, at Figure 1b.

4. Generally the extent of range measurements did not greatly exceed 7 km as indeed many would fall in shadow at this range behind the hill ridges; as seen on the map. The terrain, (as viewed in the photograph along the boresight) contains scattered trees, but not in sufficient density to classify as 'forest'; for the purpose of backscatter studies the terrain is clearly 'rural'. There are a few features which may exhibit specular reflector characteristics in the form of small buildings - and possibly in places the railway line or associated fencing. It is difficult to specify how much of this is masked by the earth railway cuttings. However, much of the area of interest was at a higher angle of elevation than these reflectors - or excluded by the sharp beamwidth of the trials radar. It should be mentioned that some of the analysis was made by filtering out spurious values, taking these to be 'outliers' in the statistical sense.

5. It is re-iterated at this point that by assuming 3dB aerial beamwidth limits the backscattered energy is taken to be that only from the idealised surface "footprint" area. Clearly any sidelobe effects or backscatter, (for example from a large reflector just outside the 3dB beamwidth) will contribute in some instances. However, it is proposed that although this instance can occur they are likely to do so with relatively low incidence. As can be seen, the area immediately ahead of the radar is clear of such obstacles. Further, the terrain chosen is more or less homogeneous at any given time, at the least for several 'footprints' dimension in both the range and azimuth directions. This was proved by making a correlation study between adjacent footprints in both along-boresight and across-boresight directions.

EXPERIMENTAL ERRORS AND LIMITATIONS

6. Although the raw radar signal measurements were not taken by the author, the prevailing conditions are known. Wind was light, weather fine and time of year - June. Other information suggested the possibility of range errors for which a correction would be necessary. Clearly any constant range error would cause the incorrect terrain data to be coupled to each backscatter reading - hence an incorrect grazing angle model could result.

7. At the outset the areas selected for distributed clutter analysis were especially chosen to avoid any major man-made specular reflectors such as pylons or metal buildings which might contaminate the statistical distributions. It is of course realised that such reflectors may occur when a tracking radar is deployed in practice. The absence of a really distinct reflector to act as a range calibrator in the sector of interest, resulted in an additional computation task - that of producing several additional data files, each with an iterative signal strength

shift relative to range along all azimuths, while simultaneously checking correlation values. These shifts were made in 5 metre increments both towards and away from the radar with correlation checks between several variables on each occasion. Although there was reason to believe that an error of up to 100 metres might exist, the plot at figure 2 most convincingly shows a range under-reading by only 5 metres. All data was therefore range-corrected by +5m before statistical analysis commenced. Table 1 shows example data after processing to obtain σ for given terrain conditions.

ERRORS IN CALCULATED TRUE GRAZING ANGLE

8. True grazing angle comprises 2 main components. The first is obtained by calculation of the terrain slope and aspect angles, with the remaining part determined by the angle of arrival of the wavefront from the radar. Slope and aspect are critically dependent upon the accuracy of the terrain data base as is the mean terrain height used in the determination of angle of arrival, always calculated at the centre of the radar footprint.

9. Raw signal amplitudes were corrected at source by a calibrated standard at the time of measurement. There may be slight propagation errors to apply, discussed at paras 26 & 27 below.

10. On the majority of occasions terrain which appears to be flat will undulate slightly, giving rise to false grazing angles if the mean slope is used. Additionally, slope (and hence grazing angle) will depend on the accuracy of each of the spot heights representing a 'facet' on which the radar energy is impinging. Precise grazing angle will also depend upon range, earth's curvature, propagation, radar transmitter height; each of which is subject to small angular error. Additionally the surface culture varies, eg trees (see Chapter 10 page 209). There are 2 ways of considering the

magnitude of surface error. Either way it is clear that the effect of errors, as a proportion will be greatest at small grazing angles.

11. <u>GENERAL SLOPE ERROR</u> The magnitude of errors in true grazing angle ψ can be easily demonstrated by using the example at Figure 3. A sinusoidally varying surface with A = 7.5 m and T = 150 m is used to represent gently undulating terrain. Ignoring vegetation the surface gradient at point P will be:

$$\phi = \tan^{-1} \frac{d}{d\theta} A \sin \theta \qquad \ldots\ldots (1)$$

where P is defined $y(P) = 7.5 \sin \theta$, $x(P) = \frac{37.5\theta}{90}$

hence at any point

$$\phi = \tan^{-1} 0.314 \cos \theta \qquad \ldots\ldots (2)$$

12. Accurate grazing angles are therefore not only dependent upon the underlying mean terrain gradient, since the true value of ψ can be significantly different than that obtained by pure facet geometry using spot heights, radar range and radar transmitter height.

13. Direct energy cannot reach point R, which is shadowed. Point S is the highest point to which a direct energy path exists at a grazing tangent (i.e. $\psi = 0°$). If the underlying terrain is flat and the elevation angle E is known, θ, (which defines point S) will be given by:

$$\theta = \cos^{-1} \left[\frac{\tan E}{0.314} \right] \qquad \ldots\ldots (3)$$

If the terrain is sloped, as on Figure 3, point S will move to a higher point on the curve.

14. For example, for E = 2.5° energy will reach S at θ = 82°, with distance OT = 82/90 x 37.5 m. The surface distance OS will be slightly longer and is the distance over which the wavefront is spread, depending upon the resolution cell dimension. At point S the true grazing angle is zero. At point 0 the surface gradient is 17.4°, hence the value of ψ is 14.9. Thus, no single value of ψ is correct for the surace illuminated. A mean could be taken (7.45°) which does not compare favourably with the value using facet geometry ($\mathrm{Tan}^{-1} \frac{4A}{T} = 11.3$).

15. PROBABILITY DENSITY FUNCTION. Only at θ = 73.5° will a true graze of 2.5° be obtained. If it is assumed that N parallel direct energy paths exist from the emitter to the surface then the probability of obtaining 2.5° is $\frac{1}{N}$ in this particular case -providing the resolution cell length ≤ 37.5 m. If cell length is increased (due to larger τ), shadowing beyond the point V will eventually occur, as shown at Figure 4; where it is seen that the resolution footprint could embrace a number of sloped and shadowed areas, dependent on its length. By considering changes in the variables A, T, τ, E it is seen that the pdf will change. In the example shown energy arising at the surface between point 0 and 73.5° will graze at a steeper angle than 2.5°; almost 90% of the energy is grazing at angles greater than 2.5°. This leads to the conclusion, that in general terrain observations it is likely that "the actual grazing angle from which backscatter is measured is higher in value than plane terrain geometry suggests, and would reasonably be expected to produce higher backscatter values". Practical results will of course depend also on the finer terrain texture and wavelength used.

16. For any grazing angle or terrain amplitude and period, mean surface gradient and mean true grazing angle, taken over N intervals with respect to mean terrain gradient, are respectively given by:

$$\phi_m = \frac{1}{N} \sum_{o}^{s} \tan^{-1} \left\{\frac{d}{d\theta} A \sin \theta\right\} \qquad \ldots\ldots (5)$$

and

$$\psi_m = \frac{1}{N} \sum_{o}^{s} \left(\tan^{-1} \left\{\frac{d}{d\theta} A \sin \theta\right\} - E\right) \qquad \ldots\ldots (6)$$

17. COMPARISON OF METHODS. A comparison of mean ψ and mean surface gradients calculated from data base terrain spot heights (which assumes a plane facet between adjacent values) with the example method above show significant differences and confirms the hypothesis that backscatter values have almost certainly in the past been attributed to incorrect grazing angles. Ranges are those to give grazing angles of zero with the A/T ratio shown.

RADAR	SINUSOIDAL POSTULATION		PLANE FACET	
ELEVATION E	RANGE ψ $S \to 0$	MEAN ψ	MEAN SURFACE GRADIENT	MEAN ψ
0.5°	0° → 16.9°	8.54°	11.3°	10.8°
1.5°	0° → 15.9°	7.95°	11.3°	10.8°
2.5°	0° → 14.9°	7.45°	11.3°	10.8°

Error values will clearly vary with terrain conditions and the above figures are used only to show that a more rigorous treatment is necessary in studying and representing terrain than is at first apparent; hence the importance placed on terrain studies at Chapters 2, 10 and Annex F. In practice, with typical ranges of 6 km, E will be very small unless the mean terrain height is about 250 metres above the radar.

18. It is seen that the method shown above for illustrative purposes for obtaining true grazing angle would be difficult to use for experimental measurements -since a sinusoidal approximation may not be representative. Further there are usually insignificant terrain data to set up accurate concavity and convexity profiles along any specific azimuth -especially with aspect changes and discontinuities with shadowing. However, the concept shows how easily errors can occur in mean grazing angle measurements within the radar footprint even under experimental conditions.

19. Effect of Matrix Errors. It was argued earlier that the matrix method of terrain representation was preferable for practical as well as experimental expediency, despite the greater overheads in digital storage requirements.

20. Returning to the 2 components of true grazing angle which change due to spot height errors, sensitivity of each is outlined below, taking a spot height error of Δh_t. True slope angle (as seen from the radar) is slope times (cos θ), where θ is the aspect. Sensitivity of aspect change with Δh_t is important since it is not constant, and depends significantly upon errors being across, rather than along, boresight. A small error across boresight will significantly change θ, with error magnitudes proportionally greatest at low slope angles (both along and across), and least when near slope angles are highest.

21. The reader is referred to Annex F (eqns 9 to 16) together with diagram 5 at page F17, for matrix slope and aspect methods; and to Chap 10 page 211 for the equations for beam boresight angles.

22. Beam Boresight Angular Errors. Referring to Chap 10 Eqn 8 and applying a Δh_t of $\pm$ 1 metre, each of the 3 terms, when examined, have differing significance. When $h_t - h_{t_x}$ is very small or zero, Δh_t can impose a shadow situation, a small gradient where non existed before, or can change a shadowed situation into a flat terrain. Shadowed areas are detected and discarded by the computer program, whereas some shadowed areas should be included if errors exist; while other areas included should have been deleted. There is no reason to believe that instances of positive or negative errors predominate, and over the large amount of data they may well cancel for statistical purposes. The magnitude of beam boresight

errors, if they exist, was calculated to be approximately $\pm$ 0.01° ie $\simeq \sin^{-1} \frac{\Delta ht}{R}$ where $\Delta h_t = \pm 1$ and R = 6 Km. This holds at approximately an error of .01° for each metre of error in spot height at the centre of the footprint.

23. <u>Slope Errors</u>. Slope is calculated by using 8 of the 9 spot heights representing a group or 'facet' in which the illuminated footprint falls. The facet is dimensioned 100 m x 100 m with heights at 50 metre intervals. Slope (given by Arctan $\sqrt{d^2 + e^2}$),is thus susceptible to errors in e or d or both. It is assumed that 1, 2 or 3 errors may occur in any set of 9 since the spacing of contours (though at 5 metres) are spatially spread across the terrain such that it is considered that at least 80% of the interpolated figures are good, and probably more so. Three errors is taken as a worst case condition with the greatest effect of 3 errors when all 3 occur along the same 'edge', thus having greatest effect on e or d. Errors are approximately constant for changing slopes and are summarized at Table 2.

TABLE 2 SLOPE ANGULAR ERROR DUE TO + 1M SPOT HEIGHT ERROR

	Max Angular Error (Deg)
Single Error in 'Corner'	$\pm$ 0.20
Single Error (Centre-side)	$\pm$ 0.19
Two Errors (same side)	$\pm$ 0.38
Three Errors (same side)	$\pm$ 0.56

24. <u>Aspect Errors</u>. Aspect $\theta = \text{Arctan} \frac{e}{d}$, hence the change in ratio is important, with an increase in e relative to d altering the aspect across boresight. The magnitude of aspect errors cannot be represented in simple form since a change in any of 9 positions affect both slope and aspect. At extreme cases a 1 metre change in one corner can swing the aspect angle from 14° to 8° but fortunately this has little overall effect on true grazing angle, as (slope (Cos θ)) does not change much for low angles of θ. Aspect angles reached a maximum of 54° during the experimental analysis for the terrain measured, and spot height errors could have produced this value with an error of 10°. Hence Cos θ would be represented as 0.58 where addition to the slope error of say 0.2°, described at Table 2, causes the multiplier Cos θ to be significantly in error.

25. <u>Combined Errors</u>. Assuming a boresight error of 0.01° (para 22), slope errors as shown (Table 2) and typical aspect errors as discussed (at para 24), the combined errors can be > 0.25° for a single error and exceed 0.5° for 3 errors. In practice errors may have occurred in various senses and combinations, however if they inevitably act in the same direction on some occasions the result could be as shown at Table 3.

<u>TABLE 3 COMBINED ERRORS</u>

	Correct	1 Error	2 Errors	3 Errors
Slope (Deg)	1.14	1.34	1.52	1.70
Boresight (Deg)	1.0	1.01	1.01	1.01
Aspect (Deg)	54°	44°	44°	40°
Overall ψ	1.67	1.97	2.10	2.31

26. <u>Other Errors - Refraction</u>. There is a slight change in refractive index between ground (radar) level and terrain surface levels which will give small angular pointing errors. As explained at Chap 8 the radar elevation angle is always slightly higher than the target at which it is aimed. However, for the purposes of clutter measurement here, elevation angle is not measured by the radar aerial position but by goemetry through radar range and terrain data base. Even though the radar energy is following a curved path the range measurement is assumed to be correct over such a short distance. Ray curvature will be slight and cause energy to impinge onto the surface at a slightly greater angle. The overall effect of refraction is taken to be negligible for the experimental readings.

27. <u>Other Effects - Diffraction.</u> Although the distributed clutter analysis was intended to be upon terrain backscatter from sloped and flat terrain, because of the extent of the area,flat terrain raised above sea level ie as small plateaus, appeared as a small negative slope during the analysis. On these occasions complete shadowing did not occur. They were detected by the program and flagged correctly on the data output. All fell in the range 0.0001° to 1.2° negative slope, but all produced backscatter, presumably due to diffraction effects. Backscatter values obtained did not indicate shadowing of the main lobe with residual side-lobe or wider beamwidth collection of back-scatter (>3dB), but remained substantially similar in value to the forward sloping terrain values which immediately preceeded and followed the negative slope values. Insufficient of these were available to carry out a full statistical and diffraction analysis, however, a rough check has shown changes in backscatter median of the order of 10-14 dB, and could reasonably correspond to the diffraction loss over the ridges.

VALIDITY OF BACKSCATTER POPULATION ANALYSED

28. Homogeneity of Terrain. It is reasonable to assume for rural terrain that a high spatial correlation value should be obtained from adjacent resolution cells (both in the range and azimuth directions). Spatial correlation was tested over a sample sector at azimuth increments of a beamwidth and in range for both 5 and 10 metre increments. Correlations were respectively 0.94 and 0.83, indicating also a consistency of measurement of backscatter since values were measured at different times in practice - less so in range but significantly so in azimuth.

29. It was not considered necessary to validate terrain homogeneity further, although even higher correlations would have been likely if adjacent cells with like grazing angle had been isolated and compared. As expected the terrain selected is truly representative of 'rural', with scattered isolated specular reflectors within a broadly representative backscatter range of -20 to -40 $dB.m^{-2}m^{2}$

30. The point should be made that sloping terrain does not necessarily imply a high grazing angle, since the actual arrival angle of the radar energy also depends on the relative radar transmitter height and elevation angle. Hence some of the lowest grazing angles are obtained at the crest of hills.

31. All radar measurements including calculated results for grazing angles, areas, ranges and aspect angles were thoroughly analysed in a number of ways:

a. As a total data base.

b. As a total package but rejecting outlying values.

c. By examination of means and medians at grazing angle class intervals.

d. By grazing angle steps by arbitrary division into 2^{o} and 3^{o} steps.

e. By contrasting data from different azimuth sectors.

f. By comparison of data from adjacent radar resolutions cells - as described above at para 28.

In each case standard statistical methods were applied, hypotheses tested, correlations made and distributions plotted. The aim was to deduce a backscatter-grazing angle relationship which can be applied in practice.

32. Regressions. Straight-line regressions, with grazing angle as the independent variable were interpreted with caution, since treatment of all results as an entity (for this purpose) could lead to major inaccuracies. The author was aware that some researchers had found the σ v ψ relationship to be a curve, at the lower values of ψ. One way to minimise this problem was to separate the data into sets based on grazing angle ie above and below say 2 or 3^{o}, and thus obtain separate regressions from the two parts of the plot.

33. It was decided to analyse the data, which covered grazing angles up to 12^{o}, as 4 sets of 3^{o} and also 6 sets of 2^{o}. Because the number of observations is less in each set, care must be taken to ensure that those outlying results do not have undue influence on the results of the smaller data set.

34. By comparison of scattergraphs, bargraphs and histograms several important factors were noted and plots of cumulative frequenices were then made against Weibull and Lognormal distributions while KOLMOROV-SMIRNOV tests were also made using a standard computer routine. A quantity of relevant data is included here for future reference purposes. It should of course be stated that although the terrain statistics are site specific - they may nevertheless be reasonably applied to any other similar terrain and radar conditions.

SECTOR RESULTS

35. Data was initially analysed in 5 azimuth sectors with statistical results shown at Table 4, and as an entity. Sections 1 to 4 each contain predominantly sloping, undulating or hilly backscatter measurements. Sector 5 is predominantly flat grassland at slightly less radar range. Table 5 summarises the regressions and correlations for Table 4. All results are commented upon at para 52 below, with reference to relevant plots.

36. Partition at 3° Steps. It was observed that the deduction of any significant relationship was being distorted by a scatter of extreme values, caused presumably by scattered specular reflectors; although not obvious from the maps, but probably sufficiently reflective rocks, boulders and fence posts etc - to act as K band reflectors. Although it is appreciated that these objects will occur in rural terrain in practice in a somewhat random way, it was thought prudent to filter these peak values to expose the underlying trend.

TABLE 4 SUMMARY OF ALL DATA (NO FILTERING)

PARAMETER	MEDIAN	MEAN	STD.DEV	MAX	MIN	STD.ERR
σ (dBs)	- 25.49	- 25.99	12.14	- 5.26	- 59.85	0.27
ψ (deg)	5.85	5.53	3.16	11.58	0.07	0.07
Area (m^2)	636	622	63.85	721	473	1.43
Aspect θ (deg)	23.25	24.06	12.85	59.79	0.09	0.29
Range (km)	6.03	5.98	0.59	6.88	4.52	13.63
Signal Received	0.28E - 2	0.28E - 1	0.05	0.29	0.1E - 5	0.1E - 2

TABLE 5 CORRELATIONS AND REGRESSIONS

	SECTORS					
	1	2	3	4	5	OVERALL
Correlation						
ψ v σ	0.18	0.05	0.08	0.4	0.15	0.12
θ v σ	0.18	0.06	0.37	0.67	0.39	0.35
Regression						
ψ v σ	− 38.06 + .52ψ	− 24.93 − 0.2ψ	− 27.79 + 0.35ψ	− 39.8 + 1.9ψ	− 18.89 + 1.9ψ	− 31.6 + 0.53ψ
R v σ						− 24.6 − 0.008R
θ v σ						− 36.4 + 0.15θ
Median σ	− 36.07	− 24.98	− 24.27	− 23.9	− 13.36	− 25.49
and s.d	9.1	9.8	12.2	12.9	10.18	12.14

37. At the other extreme a random scatter of very small values were present. These are attributed to sidelobe reception and small backscatter levels from partially shadowed areas, perhaps partly due to diffraction in a few cases or spurious propagation effects. Those cells which were shadowed were detected by the computer program and excluded from the working data.

38. Several options were considered; peak and trough values could be arbitrarily discarded by inspection or a cut off could be imposed to exclude all but the majority of the data.

39. Data Selection. Scatter plots indicated that it would be reasonable to exclude peaks and troughs by using only those values falling between - 20 and - 40 dB. Statistical values were then recalculated by taking results for each grazing angle. For example, the database was scanned for all like values of grazing angle and then relationships were considered by class interval, by reducing the data by taking the median and mean of each class. "Median filtering" (as suggested in some signal processing applications) could not be used since this would mean the imposition of an assumed rate of change in backscatter with grazing angle and thus defeat the objective of the analysis.

40. Reduction of the data in this way was justified for the following reasons:

a. Any particular backscatter value for a given grazing angle is the result of combining measurements (to get mean or median) taken at various azimuths, ranges and terrain heights. Since the terrain has been shown to be homogeneous, the individual values obtained should be more representative than an isolated backscatter value. It should also minimise signal measurement fluctuations and errors

TABLE 6 ANALYSIS BY 3° STEPS IN TRUE GRAZING ANGLE UNFILTERED DATA

			MEDIAN	MEAN	s.d	MAX	MIN	STD.ERR
0-3°	(a)	ψ (Deg)	0.70	1.34	1.00	2.86	0.07	0.45E - 1
	(b)	θ (Deg)	27.65	27.80	12.01	58.30	8.12	0.53
	(c)	σ ($m^2\ m^{-2}$)	0.87E - 2	0.49E - 1	0.61E - 1	0.24	0.15E - 4	0.27E - 2
	(d)	σ (dBs)	- 20.58	- 21.55	11.81	- 6.09	- 48 . 11	0.53
	(e)	Area (m^2)	509	559	85.12	721	473	3.82
3.6°	(a)	ψ (Deg)	4.54	4.52	0.89	5.93	3.07	0.40E - 1
	(b)	θ (Deg)	22.41	27.22	15.61	59.79	7.95	0.70
	(c)	σ ($m^2\ m^{-2}$)	0.17E - 2	0.14E - 1	0.30E - 1	0.20	0.12E - 4	0.14E - 2
	(d)	σ (dBs)	- 27.59	- 27.95	11.00	- 6.89	- 49.08	0.49
	(e)	Area (m^2)	652	651	33.79	720	523	1.52
6-9°	(a)	ψ (Deg)	7.03	7.4	0.87	8.73	6.15	0.03
	(b)	θ (Deg)	23.95	21.4	11.18	44.18	1.2	0.45
	(c)	σ ($m^2\ m^{-2}$)	0.11E - 2	0.2E - 1	0.4E - 1	0.19	0.1E - 5	0.17E - 2
	(d)	σ (dBs)	- 29.4	- 28.2	12.46	- 7.2	- 59.8	0.50
	(e)	Area (m^2)	645	651	31.6	706	581	1.27
9-12°	(a)	ψ (Deg)	9.55	9.9	0.77	11.57	9.17	0.04
	(b)	θ (Deg)	20.02	18.5	8.75	29.5	0.09	0.49
	(c)	σ ($m^2\ m^{-2}$)	0.3E - 2	0.27E - 1	0.46E - 1	0.29	0.01E - 4	0.02E - 2
	(d)	σ (dBs)	- 24.5	- 25.5	11.88	- 5.2	- 49.7	0.66
	(e)	Area (m^2)	617	618	21.5	679	560	1.20

TABLE 7 ANALYSIS BY 2° STEPS IN TRUE GRAZING ANGLE - UNFILTERED DATA

			MEDIAN	MEAN	s.d	MAX	MIN	STD.ERR
$0-2^{\circ}$	(a)	ψ (Deg)	0.65	0.64	0.38	1.5	0.7E - 1	0.21E - 1
	(b)	θ (Deg)	27.65	24.3	9.9	58.3	8.1	0.55
	(c)	σ ($m^2 m^{-2}$)	0.32E - 1	0.64E - 1	0.65E - 1	0.24	0.15E - 4	0.36E - 2
	(d)	σ (dBs)	- 14.9	- 18.57	11.06	- 6.09	- 48.11	0.61
	(e)	Area (m^2)	498	524	68.2	705	473	3.80
$2-4^{\circ}$	(a)	ψ (Deg)	2.84	3.00	0.47	3.97	2.26	0.26E - 1
	(b)	θ (Deg)	27.28	35.2	15.38	59.70	15.80	0.85
	(c)	σ ($m^2 m^{-2}$)	0.15E - 2	0.13E - 1	0.30E - 1	0.14	0.19E - 4	0.17E - 2
	(d)	σ (dBs)	- 28.21	- 28.25	10.4	- 8.42	- 47.05	0.57
	(e)	Area (m^2)	658	645	63.2	721	511	3.49
$4-6^{\circ}$	(a)	ψ (Deg)	4.87	4.97	0.57	5.93	4.27	0.31E - 1
	(b)	θ (Deg)	22.28	22.54	12.45	45.39	7.95	0.68
	(c)	σ ($m^2 m^{-2}$)	0.21E - 2	0.16E - 1	0.33E - 1	0.19	0.12E - 4	0.18E - 2
	(d)	σ (dBs)	- 26.61	- 27.69	11.46	- 7.21	- 49.08	0.63
	(e)	Area (m^2)	644	642	33.9	711	523	1.87

TABLE 7 CONT

			MEDIAN	MEAN	s.d	MAX	MIN	STD.ERR
6-8°	(a)	ψ (Deg)	6.74	6.66	0.26	7.06	6.15	0.14E - 1
	(b)	σ (Deg)	23.25	20.43	14.41	44.6	1.20	0.79
	(c)	σ ($m^2\ m^{-2}$)	0.65E - 3	0.43E - 2	0.10E - 1	0.08	0.16E - 4	0.57E - 3
	(d)	σ (dBs)	- 31.8	- 31.7	9.22	- 10.6	- 47.7	0.51
	(e)	Area (m^2)	672	669	23.69	706	630	1.31
8-10°	(a)	ψ (Deg)	8.70	8.88	0.49	9.79	8.02	0.24E - 1
	(b)	σ (Deg)	25.46	22.60	6.42	29.52	8.14	0.32
	(c)	σ ($m^2\ m^{-2}$)	0.62E - 2	0.41E - 1	0.53E - 1	0.29	0.10E - 5	0.26E - 2
	(d)	σ (dBs)	- 22.06	- 24.01	13.48	- 5.26	- 59.80	0.67
	(e)	Area (m^2)	624	622	19.12	680	560	0.95
10-12°	(a)	ψ (Deg)	10.55	10.77	0.51	11.57	10.24	0.43E - 1
	(b)	σ (Deg)	20.02	15.68	8.45	22.85	0.9E - 1	0.71
	(c)	σ ($m^2\ m^{-2}$)	0.51E - 2	0.35E - 1	0.5E - 1	0.20	0.14E - 4	0.42E - 2
	(d)	σ (dBs)	- 22.91	- 23.23	11.33	- 6.97	- 48.58	0.95
	(e)	Area (m^2)	606	609	16.22	655	588	1.37

by taking a sample which is statistically large.

b. Since data originates from a number of different surface textures and inaccuracies in terrain slope calculations, as explained previously; the use of a large number of readings at each grazing angle is likely to minimise error.

c. The method is likely to result in the most representative practical values for σ for all values of ψ.

RESULTS BY 2° AND 3° STEPS IN GRAZING ANGLE.

41. Tables 6 and 7 include as much statistical data as necessary for future reference. Figures 5 and 6 show other results graphically rather than as tables.

42. Observation. Parameters were tested for statistical distributions. For example, although aspect and grazing angle are site specific, these were tested in case of future cross reference of work in the same type of terrain. No recognisable distribution was found. This is to be expected since all negative slopes (shadowed terrain - as seen from the unique radar position) had been eliminated from the database. Therefore a general terrain analysis (as made by geographic surveyors) is not applicable, since here the terrain is viewed from a specific position.

43. Sample Spread of Grazing Angles, Areas and Aspect Angles. From the statistical viewpoint the author was well satisified by the spread of data in each parameter. The range of values was considered to well represent typical terrain. Although, as is expected, the data was not spread linearly, there were no significant gaps in the values or shortage of measurements at any particular point. In places a small spread of data did appear to be distributed normally, however, as seen below Weibull and Lognormal plots confirm the preference for using "Weibull" to represent this rural terrain.

44. Differences Between Means. It has been assumed that (although the ψ v σ gradient may be less at K Band than other frequency bands), the data would nevertheless exhibit an increase in backscatter for an increase in grazing angle. It was therefore necessary to test signal values obtained at different grazing angles to see if their differences could happen by statistical chance or whether differences could be attributed to a cause. An example comparison of means for 2-4° and 8-10°, respectively - 28.25 dB and - 24.01 dB with sd's of 10.4 and 13.4 dB's and 327, 404 samples, is shown:

$$\text{Hence} \quad \frac{10.4}{\sqrt{327}} = 0.575, \qquad \frac{13.4}{\sqrt{404}} = 0.666$$

$$\text{Then} \quad \sqrt{0.575^2 + 0.666^2} = 0.880$$

$$2 \times \pm 0.880 = \pm 1.76 \text{ dB}$$

$$28.25 - 24.01 = - 4.24 \text{ dB}$$

Since 4.24 is not less than 1.76, the difference has not happened by chance but is due to a definite cause. Similarly, a test between means for 0-2° with 8-10° also proved significant. However, taking two means (originating from 8-10° and 10-12°) from angles closer together the test failed - the difference in means could occur by chance. It is also observed that the difference in mean is likely to be less since the backscatter at 9° is not expected to be greatly different from that at 11°.

TOTAL DATA PACKAGE ANALYSIS

45. The results at Table 4 were obtained by taking all backscatter results (from all azimuths angles and grazing angles) and analysing as a complete data set, on the initial assumption that there were sufficient measurements to treat as a continuous result without significant gaps in the various parameters.
Distributions were plotted at Figures 7a and 7b to test for Weibull and Log Normal characteristics.

46. General Comments. Bargraphs produced by computer statistical package were used to examine the spread of data for each parameter. Observations are as follows:

a. Backscatter σ(dBs). An unusual number of readings occurred at about -9dBs. These were attributed to the rail-line or associated fencing, or both, as the obstacle could probably be seen at the lower grazing cycles (at the single range) over several azimuths. Backscatter plots well on Weibull paper, but a Kolmorov-Smirnov test gave a clearly negative result for all other distributions.

b. True Grazing Angle ψ (Deg). As expected, with the deliberate choice of low grazing angles, the histogram was strongly skewed towards the lower values. On examination the bargraph (not shown here) looks almost random. Indeed it would not be expected that the facets of a random piece of terrain, (illuminated by a radar operationally), should, for ψ, exhibit any particular distribution. For experimental purposes all shadowed terrain was excluded. Any distribution here would not be expected to accord with distributions made by geomorphological surveys, for example, for drainage purposes. On plotting the values, however, a good number of the data produced a log-normal distribution.

c. Illuminated 3dB Area (m^2). Area is a function of resolution cell parameters and terrain slope. The concept is nominal since, as explained previously it assumes a fairly sharp cut-off of energy at 3dB, whereas there will be backscatter also received from sidelobes or just outside the "footprint" area. With the tracking radar used here the sidelobe levels are extremely low. Further, any additional backscatter from the fringes of the nominal 3dB footprint will most probably be reflected from an adjacent facet which is likely to be at the same angle or nearly so. Area bargraphs show two distinct peaks in the general distribution; one centred on $498m^2$ and a second, more pronounced, centred on $640m^2$. There is no obvious reason for this, other than the likelihood of a fall-off in area due to the large number of measurements taken at both azimuth extremes of Challoch Hill, ie the occurence of high aspect angles becomes larger because of the geographical location. Thus no particular significance is attached the the Area distribution.

d. Aspect θ (deg). Aspect values are distributed lognormally for part of the spread but are not at all Weibull. They are slightly skewed to the left and relatively few values fall below 8°. It is pertinent to comment again that aspect is essential to calculate the true grazing angle. The spread of aspect was therefore considered important and an analysis at 0.3° class intervals showed that only a few intervals did not contain observations.

e. Range R (Km). Most measurements occurred at a range of 5 to 7 Km with a predominance around 6 Km, which is this radar's typical operational working range when acting as a low-level target tracker. The overall statistics do not give a strictly true picture here, since Sector 5 contributes about 20% of the readings taken mainly between 4.5 and 5 KM.

f. Backscatter Signal. An examination of the raw measurements before conversion to the decibel scale shows 80% to fall below 0.006 and a clear distribution of Weibull is even more strongly seen after the extreme values were removed as discussed. Because of the inclusion of the extremes observed on the scattergraph correlations can be significantly distorted. Correlation between ψ and backscatter was weakly negative (-0.11) and has little meaning when all data meaurements are lumped together.

FILTERED DATA

47. Data was next filtered to remove the outlying values < -20dB and< 40dB, and statistical tests repeated. Results and comments are as follows:

48. Effect of Reducing Data File. The complete backscatter measurements

TABLE 8a SUMMARY OF STATISTICAL RESULTS - WHOLE DATA-BASE (FILTERED)

	MEDIAN	MEAN	sd	MAX	MIN	STD.ERR
ψ (Deg)	5.90	5.57	3.02	11.54	0.07	0.10
σ $dBm^2.m^{-2}$	- 29.10	- 29.30	5.53	- 20.06	- 39.93	0.18
All Data no Filter σ (7)						
ψ	5.85	5.53	3.16	11.57	0.70E - 1	0.07
σ	0.28E - 2	0.28E - 1	0.48E - 1	0.29	0.10E - 5	0.11E - 2

TABLE 8b SUMMARY OF STATISTICAL RESULTS - UNFILTERED DATA-BASE

(WITH ALL RESULTS BELOW $\psi = 3^o$ REMOVED)

	MEDIAN	MEAN	sd	MAX	MIN	STD.ERR
ψ (Deg)	6.81	6.98	2.22	11.54	3.07	0.06
σ dBm^2 m^{-2}	- 27.63	- 27.53	11-89	- 5.26	- 59.85	0.31

CORRELATION + 0.15

TABLE 8c SUMMARY OF STATISTICAL RESULTS DATA-BASE (WITH FILTERED SIGNALS AND ALL BELOW $\psi = 3^{\circ}$ REMOVED)

	MEDIAN	MEAN	sd	MAX	MIN	STD.ERR
ψ Deg	6.74	6.76	2.27	11.54	3.07	0.08
σ dB m^2 m^{-2}	- 29.20	- 29.44	5.58	- 20.07	- 39.93	0.20

CORRELATION + .01

REGR $\sigma = -29.68 + .03\psi$

approximate roughly to both Weibull and Lognormal for much of the range of values. After excluding the extreme values the total data exhibits a closer Weibull distribution, and if the values for $\psi<3^{\circ}$ are eliminated an even stronger Weibull fit exists. These are plotted at Figure 7.

49. Results of the reduced data file are at Table 8. Under these conditions a check on the statistical distribution of ψ was also Weibull - although this may have no significance, being site-specific. Median and mean of each ψ class interval were also used, and these are plotted at figs 8a and 8b in comparison with the other results. In addition to the Weibull and Lognormal plots, the Kolmorov Smirnov Test indicated a strong normal tendency.

ANALYSIS IN 3° GRAZING ANGLE STEPS

50. Data in four sets enabled the 0- 3° values to be analysised separately to ensure that any reversal of characteristics would be isolated from any influence of backscatter values from the higher angles. Data was analysised in 2 ways:

a. All data included (Identified as 03C, 36C, 69C, 912C).

b. Data reduced in each set by a >-20 <-40dB filter (Identified as 03M, 36M etc) and means applied for each class set. Class sets were determined, not by arbitrary equal steps, but by grouping all backscatter readings from terrain of the same grazing angle. For example, the mean was found of all the backscatter readings at $\psi = 4.86^{\circ}$ and so on. Since $\psi = 4.86^{\circ}$ occurred a large number of times at different ranges and on different azimuths (and aspect is accounted for - since true grazing angle is used), the backscatter mean is taken to be the most

TABLE 9 STATISTICAL RESULTS - REDUCED DATA BY FILTER, MEANS AND MEDIANS OF CLASS INTERVALS

	MEDIAN	MEAN	s.d	MAX	MIN	STD.ERR
FILTERED DATA						
σ (dBs)	- 29.39	- 29.52	5.56	- 20.07	- 39.93	0.19
ψ (Deg)	6.52	6.12	2.73	11.57	0.07	0.09
Signal	0.12E - 2	0.22E - 2	0.24E - 2	0.98E - 2	0.10E - 3	0.86E - 4
MEANS OF CLASS INTERVALS						
σ (dBs)	- 29.72	- 29.77	3.37	- 21.91	- 36.54	0.54
ψ (Deg)	6.25	6.09	3.23	11.625	0.125	0.53
Signal	0.20E - 2	0.21E - 2	0.14E - 2	0.68E - 2	0.25E - 3	0.23E - 3
MEDIANS OF CLASS INTERVALS						
σ (dBs)	- 29.65	- 29.87	3.46	- 22.95	- 36.54	0.58
ψ (Deg)	6.125	6.00	3.21	11.875	0.25	0.54
FILTERED AND ALL BELOW ψ = 3° REMOVED						
σ (dBs)	- 29.20	- 29.44	5.58	- 20.07	- 39.93	0.20
ψ (Deg)	6.74	6.76	2.27	11.54	3.07	0.08
UNFILTERED AND ALL BELOW ψ = 3° REMOVED						
σ (dBs)	- 27.63	- 27.53	11.89	- 46.9	- 5.2	0.31
ψ (Deg)	6.81	6.98	2.27	11.57	3.07	0.06

TABLE 9b BY METHOD OF MEANS OF BACKSCATTER FOR LIKE ANGLES - FILTERED DATA

	MEDIAN	MEAN	s.d	MAX	MIN	STD.ERR
<u>0-3°</u>						
ψ (Deg)	0.25	0.47	0.50	2.61	0.07	0.08
σ (m^2m^{-2})	0.26E - 2	0.21E - 2	0.23E - 2	0.88E - 2	0.11E - 3	0.37E - 3
σ (dBs)	- 27.75	- 28.51	5.35	- 20.52	- 39.43	0.85
<u>3-6°</u>						
ψ (Deg)	3.95	3.85	1.00	5.79	2.26	0.06
σ (m^2m^{-2})	0.12E - 2	0.22E - 2	0.23E - 2	0.98E - 2	0.10E - 3	0.14E - 3
σ (dBs)	- 29.1	- 29.3	5.46	- 20.08	- 39.88	0.32
<u>6-9°</u>						
ψ (Deg)	6.79	6.71	0.88	0.98E - 2	0.10E - 3	0.05
σ (m^2m^{-2})	0.96E - 3	0.21E - 2	0.24E - 2	0.98E - 2	0.10E - 3	0.15E - 3
σ (dBs)	- 30.16	- 29.83	5.56	- 20.07	- 39.89	0.35

TABLE 9 CONT

	MEDIAN	MEAN	s.d	MAX	MIN	STD.ERR
$9\text{-}12^{\circ}$						
ψ (Deg)	9.44	9.31	1.39	11.57	6.76	0.09
σ (m^2m^{-2})	0.12E - 2	0.22E - 2	0.24E - 2	0.95E - 2	0.10E - 3	0.16E - 3
σ (dBs)	- 29.14	- 29.57	5.62	- 20.18	- 39.93	0.37

practical value to represent the particular grazing angle of interest on each occasion. Results using this method are at Table 9 and plotted at figures 9a, 9b and 10. The same process was applied for raw signal strength. Values obtained for the means of the total data file are included for comparison.

ANALYSIS IN 2° GRAZING ANGLE STEPS

51. Six data sets identified as 02, 24, 46 etc were analysed in the same way as the 3° sets.

COMMENTS ON TABULATED DATA - TABLES 4 TO 9

52. Within the overall data summarised at Table 4 considerable fluctuation occurred, not obvious until seen by sector at Table 5 and subsequent analysis in 2° and 3° steps. For example, the variation in regression models (ψ v σ) shows that quite different models are obtained from adjacent terrain sectors. These are inaccurate being distorted by extreme values and correlations are seen to vary widely.

53. Tables 6 and 7 reveal much more information about the general nature of the backscatter. The data in both tables is unfiltered, ie all measurements are included. Thus an examination and comparison of values (while showing trends as grazing angle varies) also highlights any unusual results due to extreme values falling within any particular step. The ratio of mean to median increased significantly as ψ decreased. This finding is in accord with observations in the USA (Report "Seek Igloo"). It is not clear why the standard error for aspect θ is significantly different for 8-10° at 0.32. Despite the various methods of data reduction, made to eliminate and

minimise undue influence of outlying values, it is of interest that σ_m remains at approximately - 29 dB; as seen in summary table 9b

COMMENTS ON PLOTTED DATA - FIGURES 5-9

54. It is assumed that a Weibull distribution exists if plotted values fit between the 10% and 90% levels. Several important facts are confirmed by the distributions at Figure 5(a). It is immediately apparent that a good Weibull fit exists, that the slope parameters are sensibly the same (slope parameter approx 2.57, shape parameter 0.39) for 5 of the 6 sets of data . The data set with a different slope (8-10°) warranted further investigation. Values were back plotted onto a large-scale map, since an unusually large number of high readings were found (- 8.5 to - 9.6 dB, at 56.4° to 56.7° azimuth and 5750 to 5800 metres range). These were found to come from a rail line, on an embankment, and rail bridge over the trunk road A75 between E and W Challoch. By removing these readings from an otherwise 'standard' set of results the distribution plot for 8-10° moves towards the slope of the other data sets. This confirmed the contamination in this case and it was thought reasonable to make this adjustment to the data. It should be noted that the median (50% Weibull) level fixes the position of the curves on the plot. These results most clearly demonstrate (confirmed again at figure 10) that backscatter values apparently increase at very low grazing angles - assuming of course that these angles are correctly measured (subject to terrain measurement errors discussed at para 25 above).

55. The lognormal plot at figure 5(b) shows that the LogN distribution could almost equally be used as a representative distribution. For 3° steps the mean slope parameter is approx 2.8. As before, these distributions clearly show an increase in signal strength at the lower grazing angles.

56. Results at figure 7 were commented upon at paras 45-46, however it is noted that introduction of the signal filter changes the slope (as expected), but does not change the excellent alignment of the plotted readings on Weibull paper. If all data for $\psi < 3^{\circ}$ is removed (postulating removal of data below the possible minimum in the σ v ψ curve). Figure 7 (Curve *) also shows a very good fit with a slope parameter identical to that at Figure 8 (means and medians).

57. The results at Figure 9 are for data taken in 4 sets with signal filter applied. Data was then separated into mean and median values by grazing angle class intervals. It is shown that a good Weibull fit exists (Figure 9(a)), for which the Weibull shape parameter is almost identical for the 4 sets (0.9 with slope parameter 1.1). Kolmorov-Smirnov tests indicated a strong tendency also to Lognormal, as seen at Figure 9(b).

SKEWNESS, VARIABILITY, REGRESSION AND CORRELATION

58. Data distribution were checked for skewness during the $\psi = 2^{\circ}$ intervals, where the σ (dB) skews were near zero on 2 occasions and negatively skewed on all others. A significantly higher coefficient of variation occurred below $\psi = 2^{\circ}$ and also between $8\text{-}10^{\circ}$. In the latter case this is probably due to the problem at this angle recognised at para 54 above. It was also noted that both true grazing angle and backscatter values became more variable as ψ reduced; markedly so for angles below 2°.

59. Regression. Regressions were made between σ and ψ, however once it became clear that σ increased for small values of ψ, it became clear that a straight line regression could not be used for the whole data base, but only to that portion to the right of the minimum. Reference to figure 10 shows that this minimum occurs at some point about $\psi = 2^{\circ}$. The best model for this section of the curve probably lies between $\sigma_{dB} = -29.6 + 0.05\,\psi$ and $-31.5 + 0.83\psi$ dBs.

60. Correlations. Correlations between σ and ψ is shown to be positive (for $\psi > 3^{\circ}$). The variability of data in some sets is such that without a greater number of samples a stronger correlation is unlikely.

61. General. Apart from the statistical values shown, a very large number of supporting calculations, computer file handling procedures an plots were made. It is not considered necessary to include bargraphs, scattergraphs, histograms or frequency tabulations, as this information appears on the various plots.

62. Weibull Relationships and Cell Size. Above $\psi = 3^{\circ}$, as also found {71} (see para 39 page 4-89), the s.d increased as pulse length effectively decreased (ie illuminated area reduced due to surface tilting effects), however the empirical relationships between τ and the Weibull shape parameter could not be established. As seen from the consistency of the curves at Figure 5(a) the shape parameter is approximately constant despite fluctuations in cell size by as much as 16% from the standardised value. Neither could the shape parameter found be fitted into the tables, curves or relationship given by {71} at $\lambda = 10$ cm.

CONCLUSIONS

63. It is proposed that the results here are statistically valid and that reasonable assumptions, with correct and careful procedures were used to expose the underlying trends in the backscatter data. More hypotheses were tested than have been shown; they are not included here if the results were inconclusive. For example a correlation matrix was made at each stage between all variables, together with all regressions and cumulative distributions; many were null or inadmissible relationships, or were site-specific.

64. The results compare well with other published findings as seen at Figure 5 Chapter 4, where the proposed model falls close to several others; although at a slightly shallower rate of change of σ for ψ at about 1.5 dB per deg; down to the minimum. Since there are few other published results at K Band, the results shown are inevitably contrasted with those from I or J Band, or with other models which take account of frequency by postulation rather than actual measurement.

65. A most difficult area to be sure about is that at very low grazing angles, where, as found by some other researchers, σ_c values inexplicably rise. It has already been postulated here that terrain slope angles are rarely what they appear to be, since even within a 50 or 100 metre square area terrain undulates appreciably. It may always be questioned as to the proportion of illumination actually impinging at the presumed mean angle. At shorter wavelengths this becomes even more relevant. A large part of a facet may be in shadow due to high frequency undulations of the surface eg in rows of crops, banks and hedegrows. In practice there will almost

always be a proportion of the cells containing (for the "rural" description), brick buildings, fences, metal farm buildings, vehicles and so on. Therefore the contamination these produce cannot be ignored. Production of a 2 part clutter model may be possible, ie under lying trend plus an allowance for peaking.

66. It may be questioned whether there is some unknown mechanism which applies only at very low grazing angles and causes σ_c to rise; or is the rise entirely due to inaccuracies in terrain angles? Consideration of this possibility commenced with a critical examination of possible terrain measurement errors. Correlation was definitely positive for $\psi > 3^o$ and reversed at some point $\psi < 3^o$. The variability of the data was such that a greater number of observations would be preferable to obtain stronger correlations. What errors were likely and where might the model fail? Every effort was made to minimise terrain errors and worst case errors would have to be present in large numbers to significantly change the underlying trend. Errors which did exist will have contributed to the fluctuations found.

67. It is suggested that the model is accurate within the constraints of such a study, especially at K Band wavelengths. There is a remarkable consistency in the culmulative distribution slopes when the data is analysed in arbitrary steps of 2 or 3^o. Further, if it is assumed that errors do exist in ψ, causing values to be misplaced on the curve at Figure 10, an angular error far larger than the worst case calculated above would have to be applied in order to correcting reposition the backscatter reading elsewhere on the curve. It is concluded therefore that a rise in backscatter level does occur at very low grazing angles. It is nevertheless re-iterated

that true grazing angle errors can also be included, and that these may not be obvious without careful consideration.

68. For "rural" terrain it is suggested that the proposed model shouldbe applicable to similar tracking radars in similar terrain conditions, in the context of detectability and tracking of LLSAM systems.

69. Returning finally to 2 aspects, those of useful $\tau\theta_A$ product relationships and the mechanism causing σ_c to rise at very low angles. First, a lot of effort was expended to try and apply Dodsworths proposal for scaling distributions to obtain new median values, and to compare shape parameters as suggested at Chapter 4 and Annex A, wothout success. It is clear that for meaningful Weibull conclusions a series of measurements must be made with a variable pulse duration radar at the same time and place for cell scaling relationships to be studied. In summary no conclusive evidence was found to link the shape parameter to the $\tau\theta_A$ product.

70. Secondly, the rise in σ_c definitely occurs at low grazing angles, as distinct from low terrain slopes. Calculated grazing angles were as much as 3.6° lower than slope angles, and many of the lower grazing angles were from terrain sloped at quite diverse angles. Above $\psi = 3^\circ$ the ratio of ψ to mean terrain slope increased almost linearly (from 0.78 at $\psi = 3^\circ$ to 0.98 at $\psi = 12^\circ$), but dropped abruptly to 0.63 at $\psi = 1^\circ$. The implication is that as terrain slope increases, low values of ψ are less likely. Greatest incident signal attenuation could be expected at the higher values of ψ, since the depth of penetration into surface cover is probably greater. It is proposed that below a critical angle (here about 2.5°), despite the fact that the rms surface roughness appears to be smoother in the general sense, ψ reaches a value where the signal finds it difficult to propagate into the culture; since the majority of reflectors in 'rural' terrain are seen increasingly as vertical structures

(grass blades as long cylinders), as ψ reduces. All other reflectivity factors, e.g. ground conductivity, relative dielectric constant, λ, etc. have not changed. Further, the mechinism would be more noticeable at higher frequencies, where absorption is higher. It is of interest that the experimental result here (Figure 10 and see Chapter 4, Figure 5) is generally below the other world-wide curves. Only Trebits at 95 GHz is lower.

71. <u>Reliance of Findings to Overall Tracking Predictions</u>: Irrespective of the terrain slope it is confirmed that any target flying at near grazing angles could enter a region (unless the underlying ground is shadowed) where a rise in clutter values may occur to a level which may compete with the target RCS. Targets should fly such that an angle of 1° or less occurs, typically 100 m altitude at 6 km range. This is easily achievable by manned aircraft and even more so by terrain following missiles with minimum RCS where grazing angles can be even lower.

72. <u>Compatibility With Other Models</u>: Within the past year Barton{234} has proposed a unified clutter model for flat or rolling terrain, at a number of RF's. Although ψ is implicit in his model out to $R_1 = 4\pi h_r^1 \sigma h_r^1 \lambda$, for both flat or rolling terrain, the model does not set out to relate σ with ψ in isolation. The short-range model, $\sigma = \gamma \sin \psi$ is plotted at Figure 10 in contrast to the K Band results obtained here. γ is a 'terrain constant' set at 0.04 for USA test-sites. It is observed that the K Band results here are not scaleable to meet Barton's proposals by simple adjustment of γ; since the σ V ψ gradient is shallower. Beyond R_1, out to the horizon, Barton used $\sigma = \gamma\, (h_r^1/R)F$, based on propagation factor $F = \frac{(R_1)}{R}4$, $h_r^1 = h_{t_x} + 2\sigma_h$ where σ_h is the terrain surface standard

deviation. It may be concluded that although the Barton unified model is a good assessment for flat or rolling terrain, it may not be as applicable when a target is being tracked against a background of gradually rising terrain, since the filtered model $(-29.6 + 0.05\psi)$ diverges significantly from Barton as ψ increased. However, the median model over comparable ranges $(-30.8 + 0.875\psi)$ confirms Barton's proposel within 1.5 dB or less, but it is only applicable for $\psi<3$. Below $\psi = 3°$ the values of σ rise at a rate which it would be inadvisable to quote as a general rule until more results become available to confirm the phenomenon and the mechanism becomes understood.

FI-43

FIG 1a VIEW FROM RADAR TOWARDS SLOPED TERRAIN USED FOR CORRELATION STUDIES

R H I N S
Fire Tower
148m
Challoch Hill
135m
DAT 44
DAT 54
DAT 64
DAT 53
DAT 63
DAT 43
DAT 42
DAT 52
DAT 62
TN
5 Km
7 Km
Glenwhan Moor
Castle Kennedy
Dunragit
Bareagle Forest
Glenluce
Torrs Warren
DANGER AREA
Luce Sands
West Freugh Airfield
Stoneykirk
Rifle Range

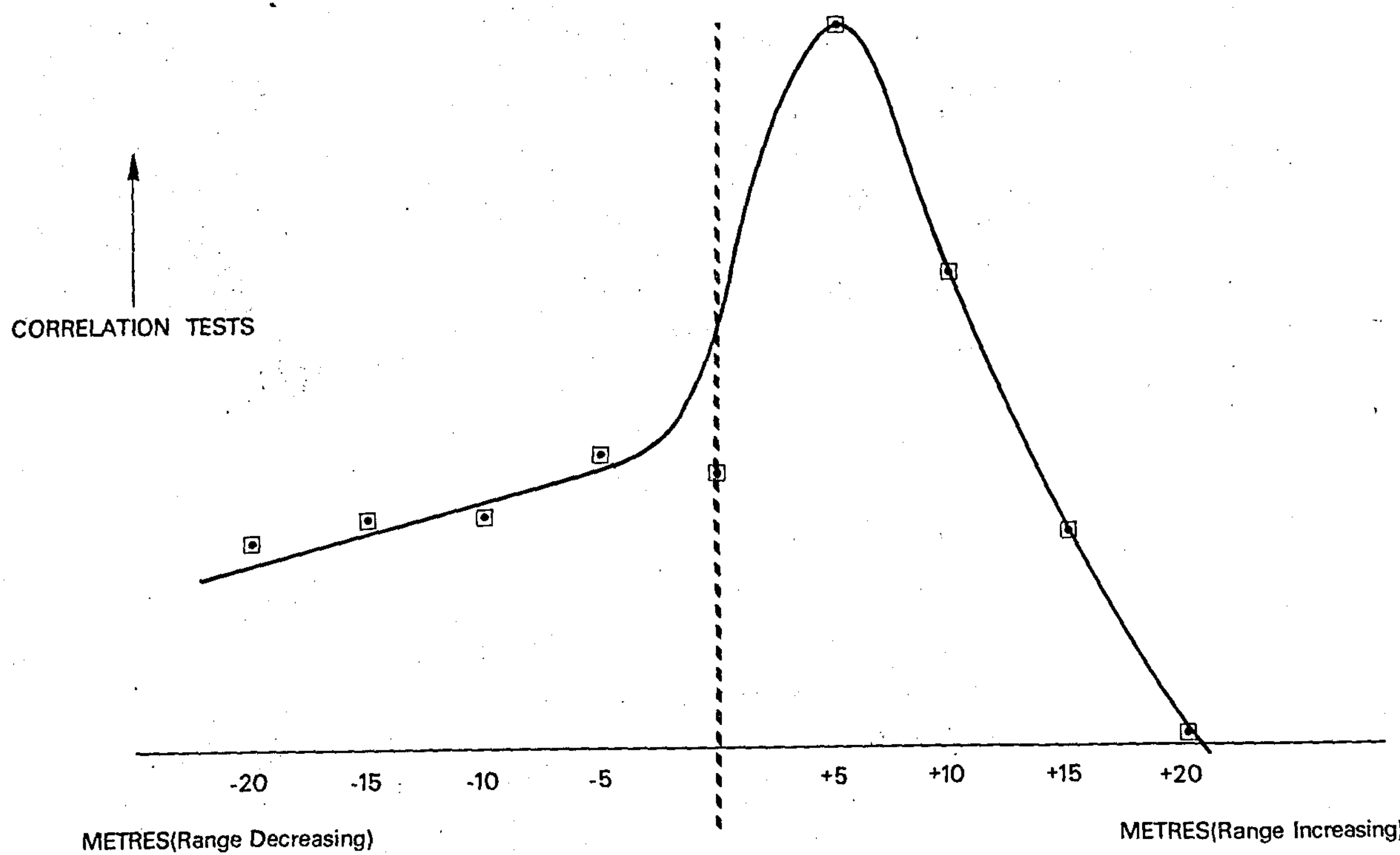

FIG 2 **OPTIMUM CORRELATION FOR ERROR CORRECTION**

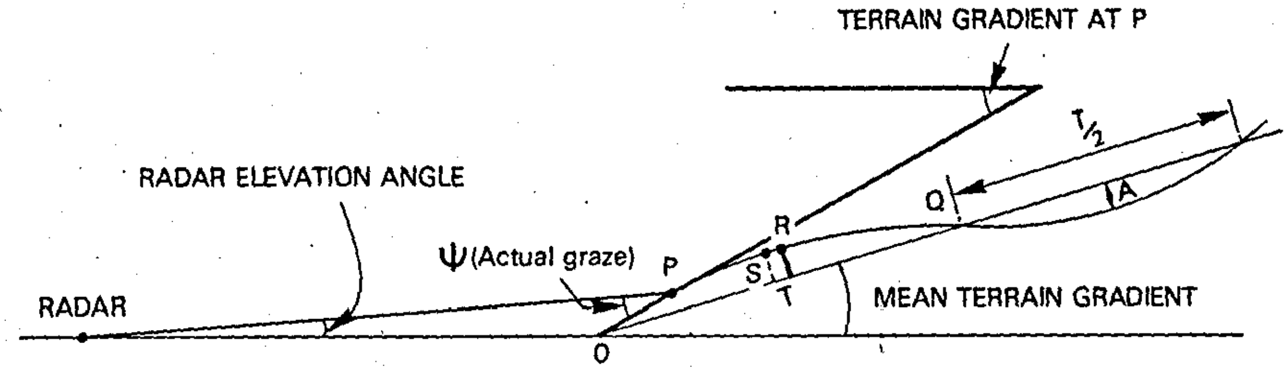

FIG 3 **UNDULATIONS ON SLOPED OR FLAT TERRAIN**

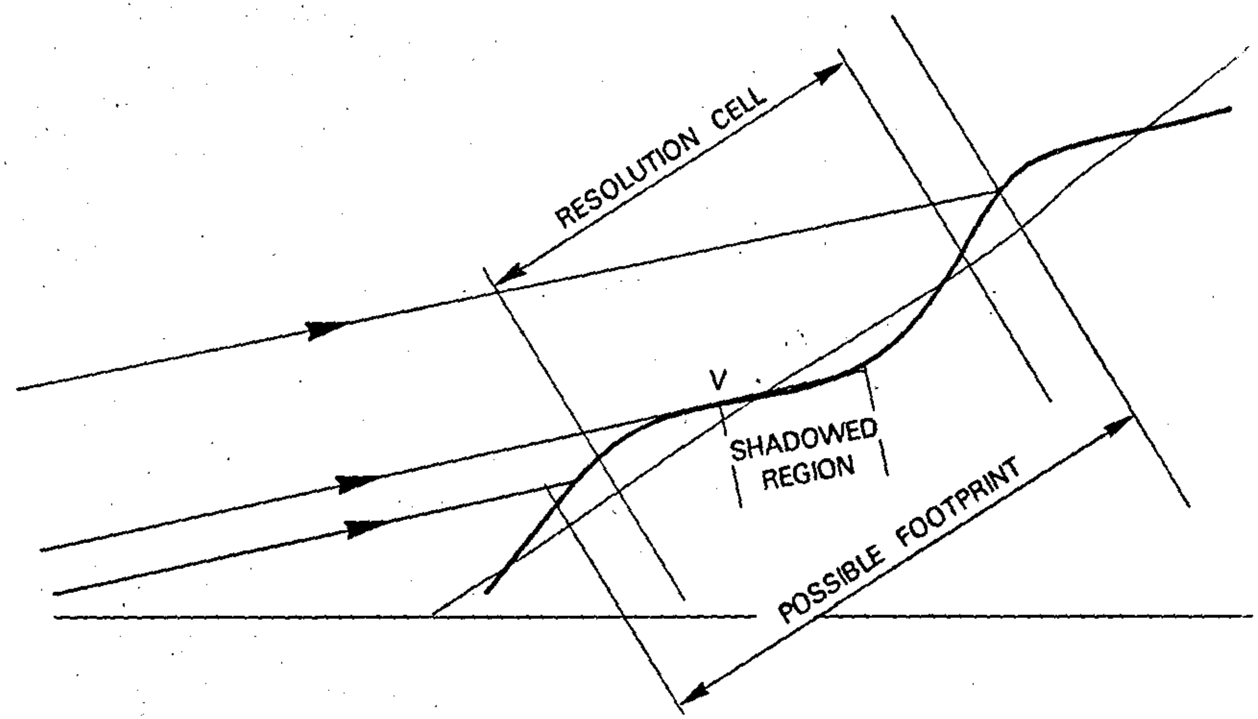

FIG 4. **EFFECT OF MOVING RESOLUTION CELL**

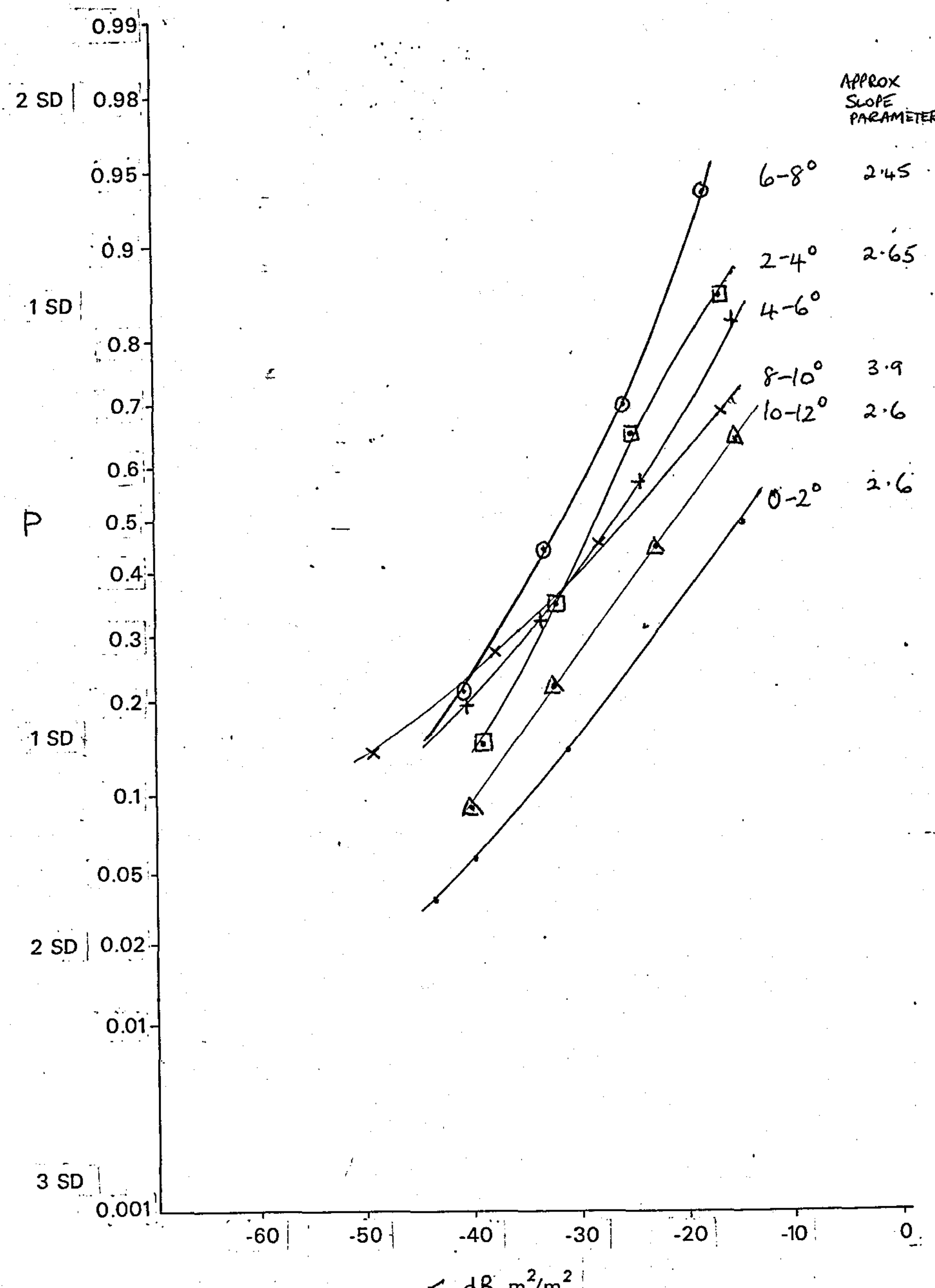

FIG 5(a) CUMULATIVE PROBABILITY THAT VALUE IS NOT EXCEEDED - 2° STEPS (WEIBULL SCALE)

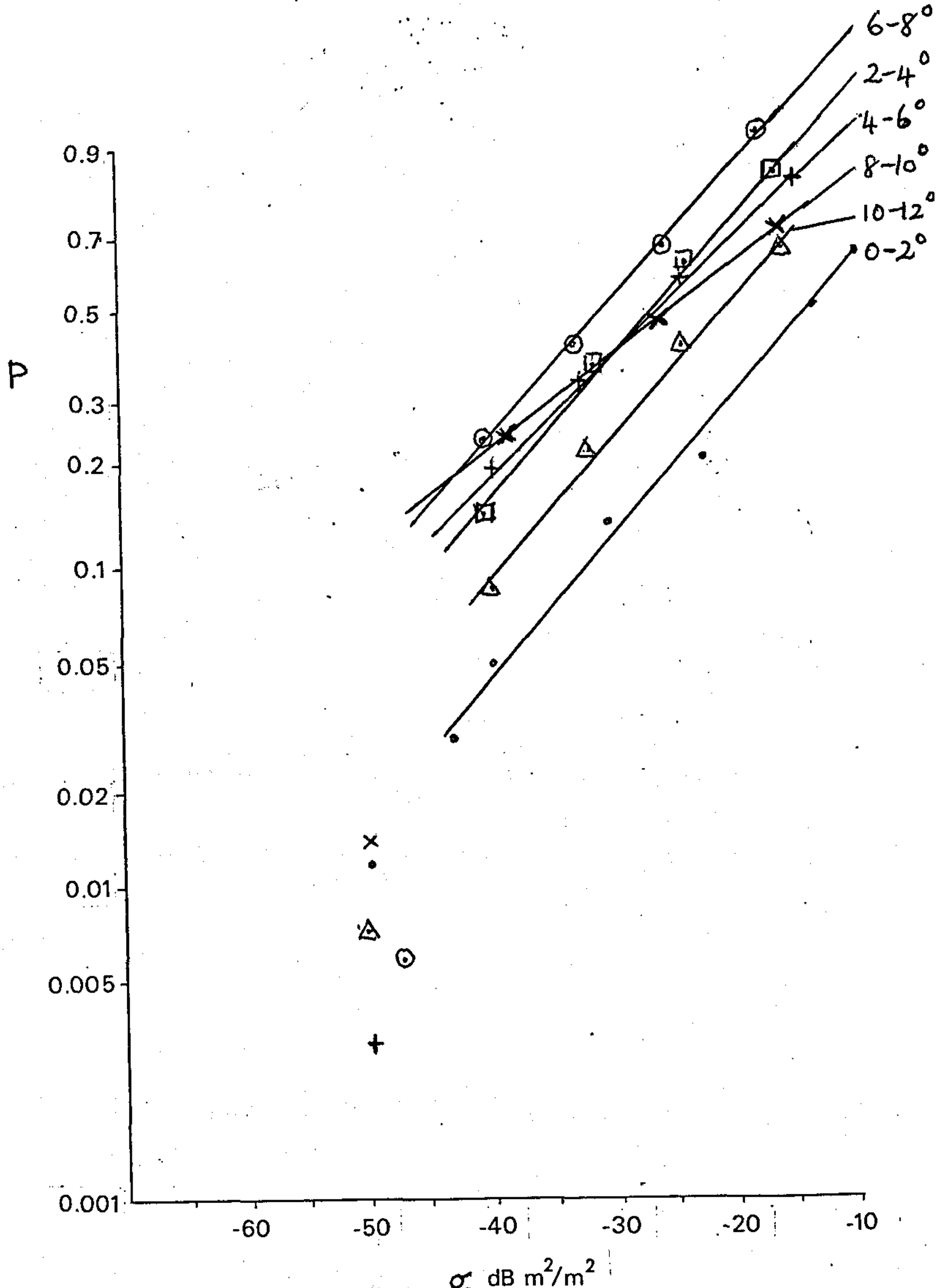

FIG 5(b) CUMULATIVE PROBABILITY THAT VALUE IS NOT EXCEEDED - 2° STEPS (LOGNORMAL SCALE)

APPROXIMATE SLOPE PARAMETERS IN BRACKETS

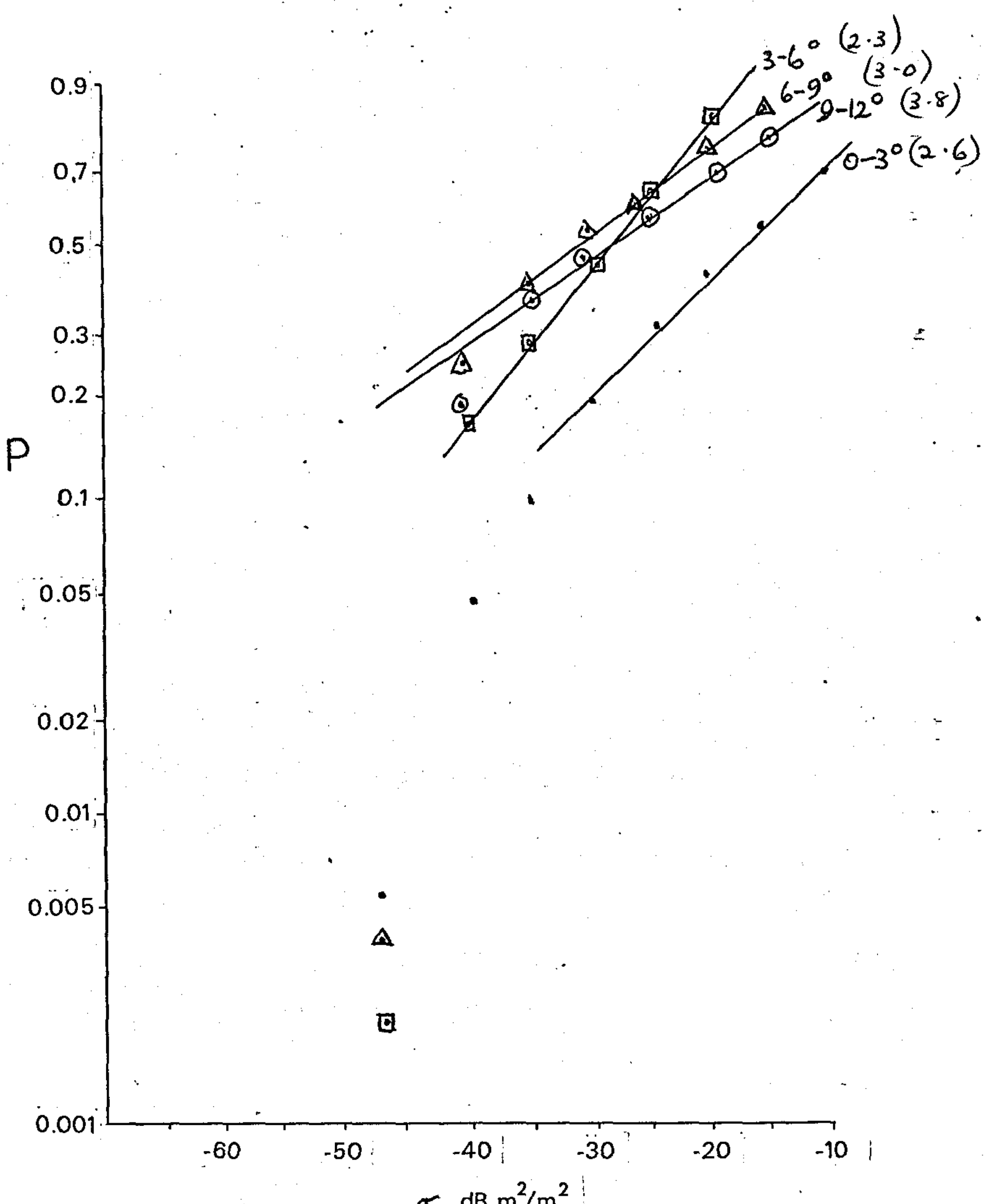

FIG 6(a) CUMULATIVE PROBABILITY THAT VALUE IS NOT EXCEEDED - 3° STEPS (WEIBULL SCALE)

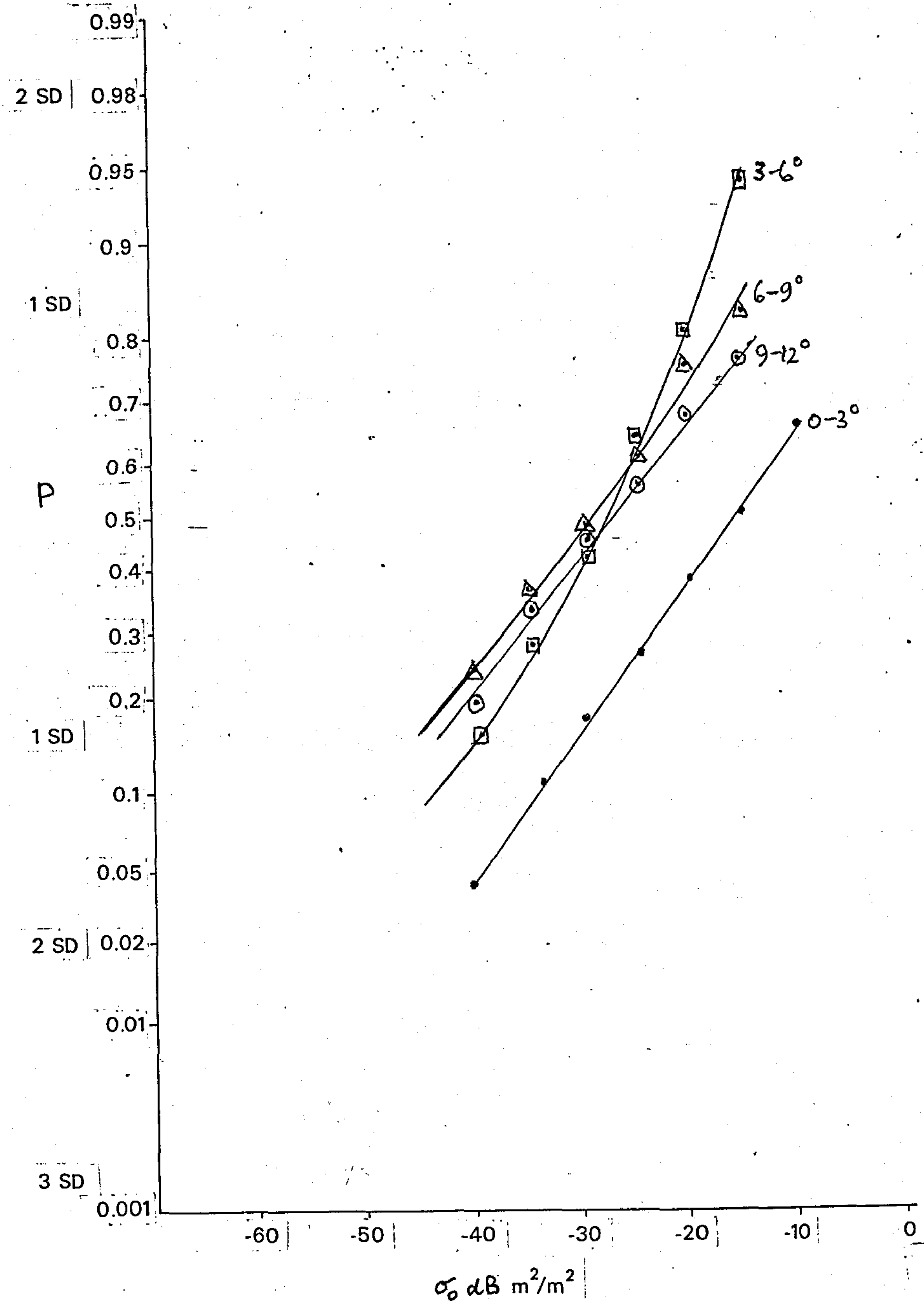

FIG 6(b) CUMULATIVE PROBABILITY THAT VALUE IS NOT EXCEEDED - 3° STEPS (LOGNORMAL SCALE)

F1-49

FIG 7(a) CUMULATIVE PROBABILITY THAT VALUE IS NOT EXCEEDED (WEIBULL SCALE) ALL PARAMETERS

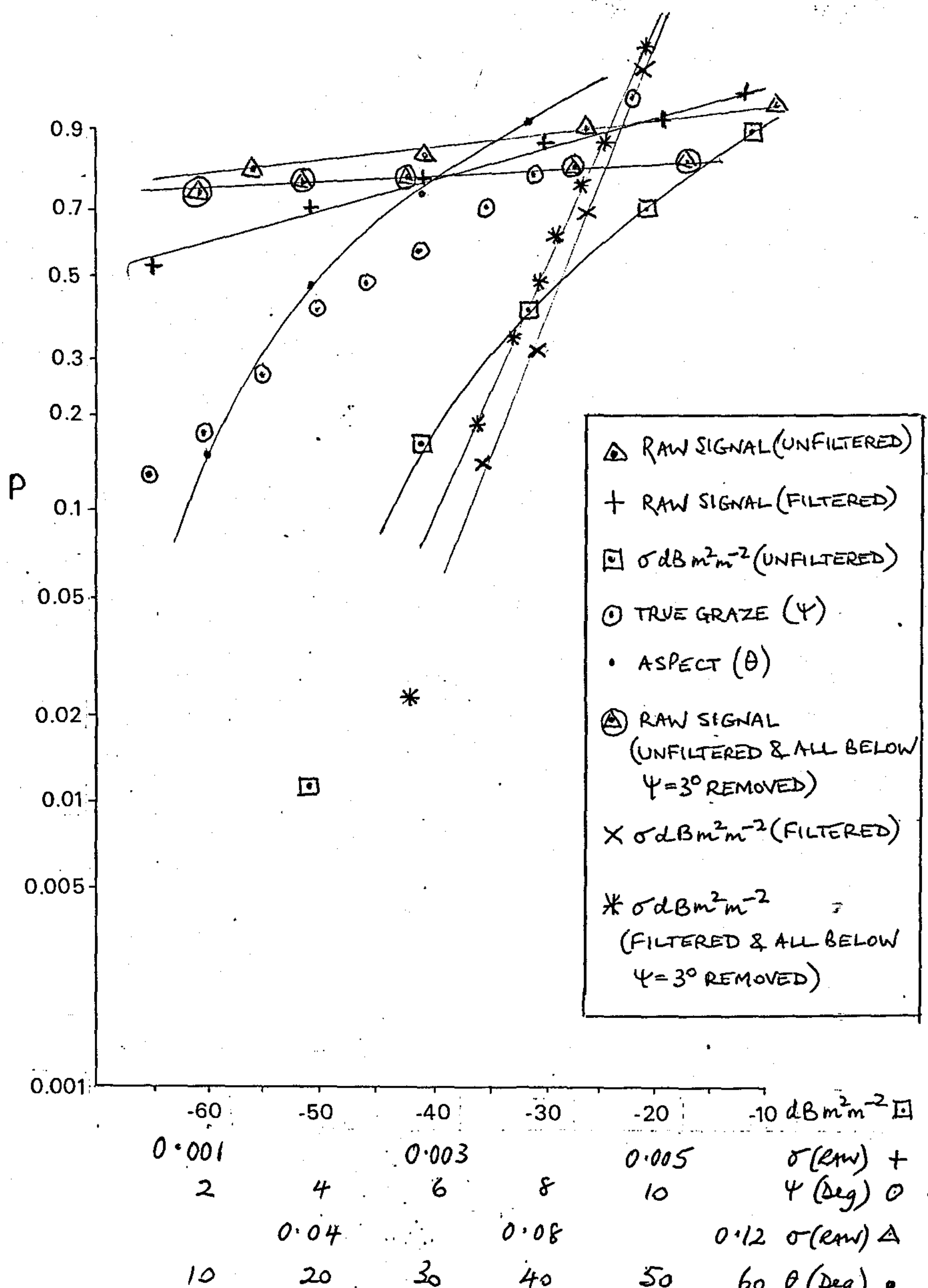

FIG 7(b) CUMULATIVE PROBABILITY THAT VALUE IS NOT EXCEEDED (LOGNORMAL SCALE) ALL PARAMETERS

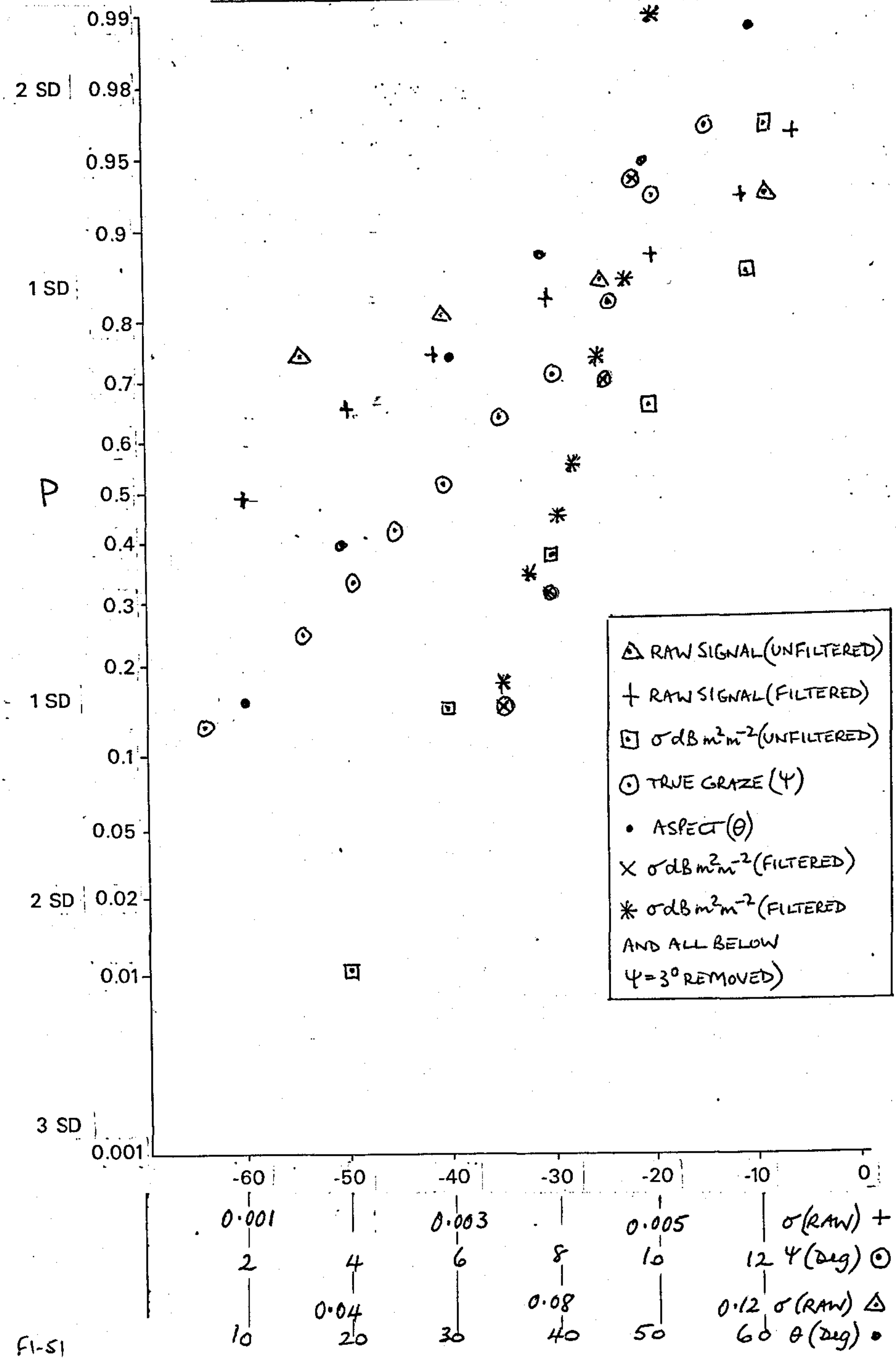

F1-51

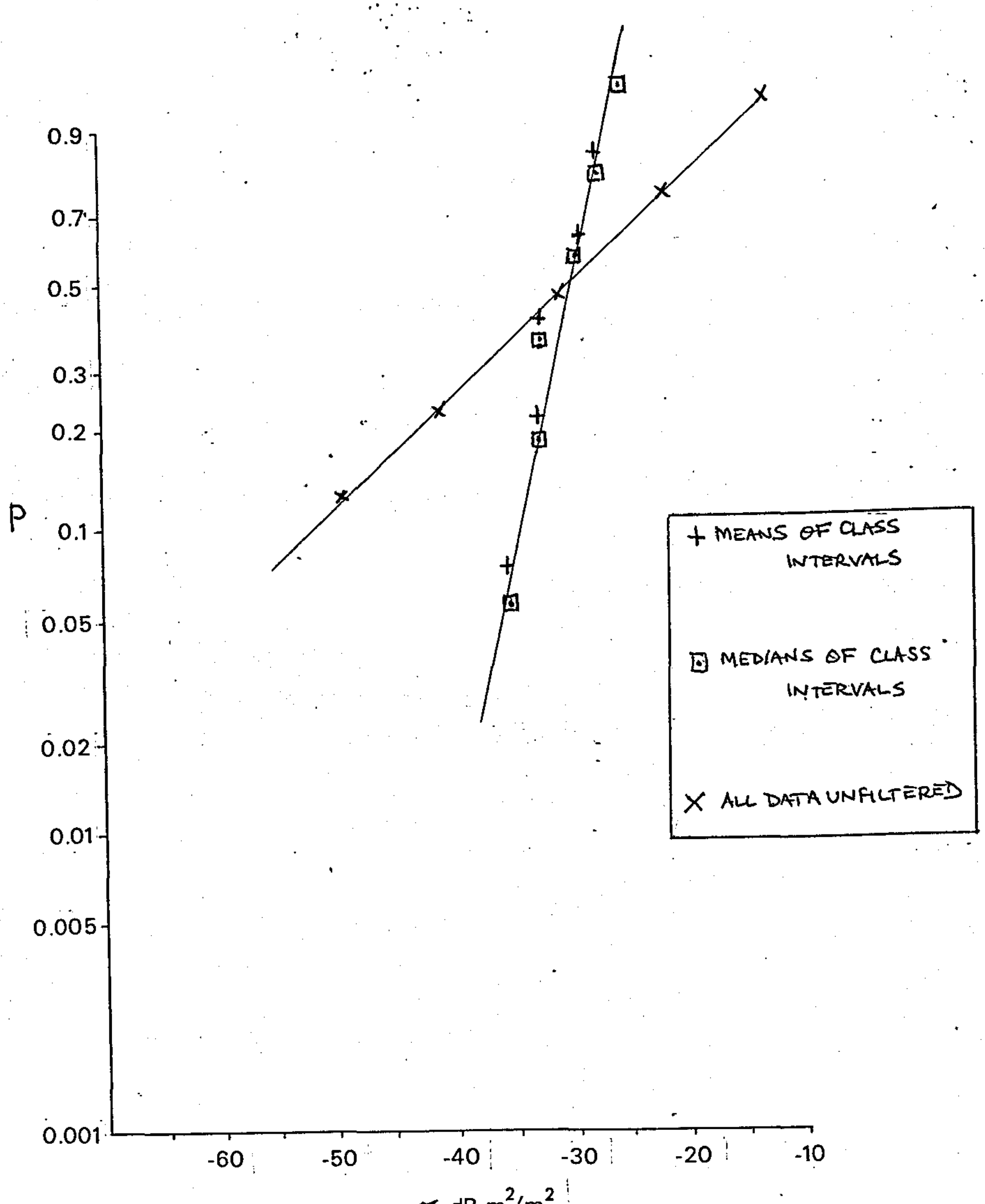

FIG 8(a) CUMULATIVE PROBABILITY THAT VALUE IS NOT EXCEEDED - MEANS AND MEDIANS (WEIBULL SCALE)

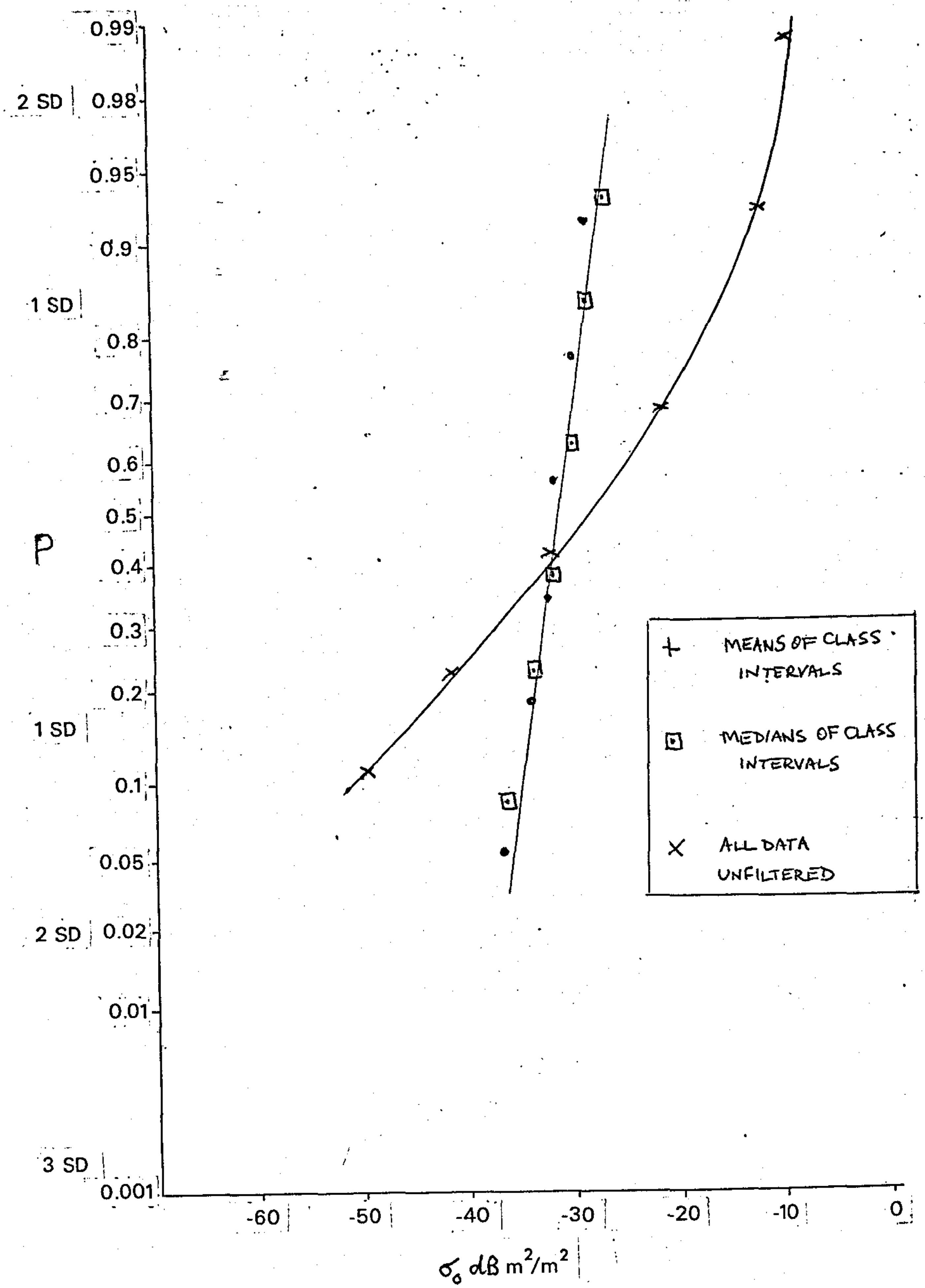

FIG 8(b) CUMULATIVE PROBABILITY THAT VALUE IS NOT EXCEEDED - MEANS AND MEDIANS (LOGNORMAL SCALE)

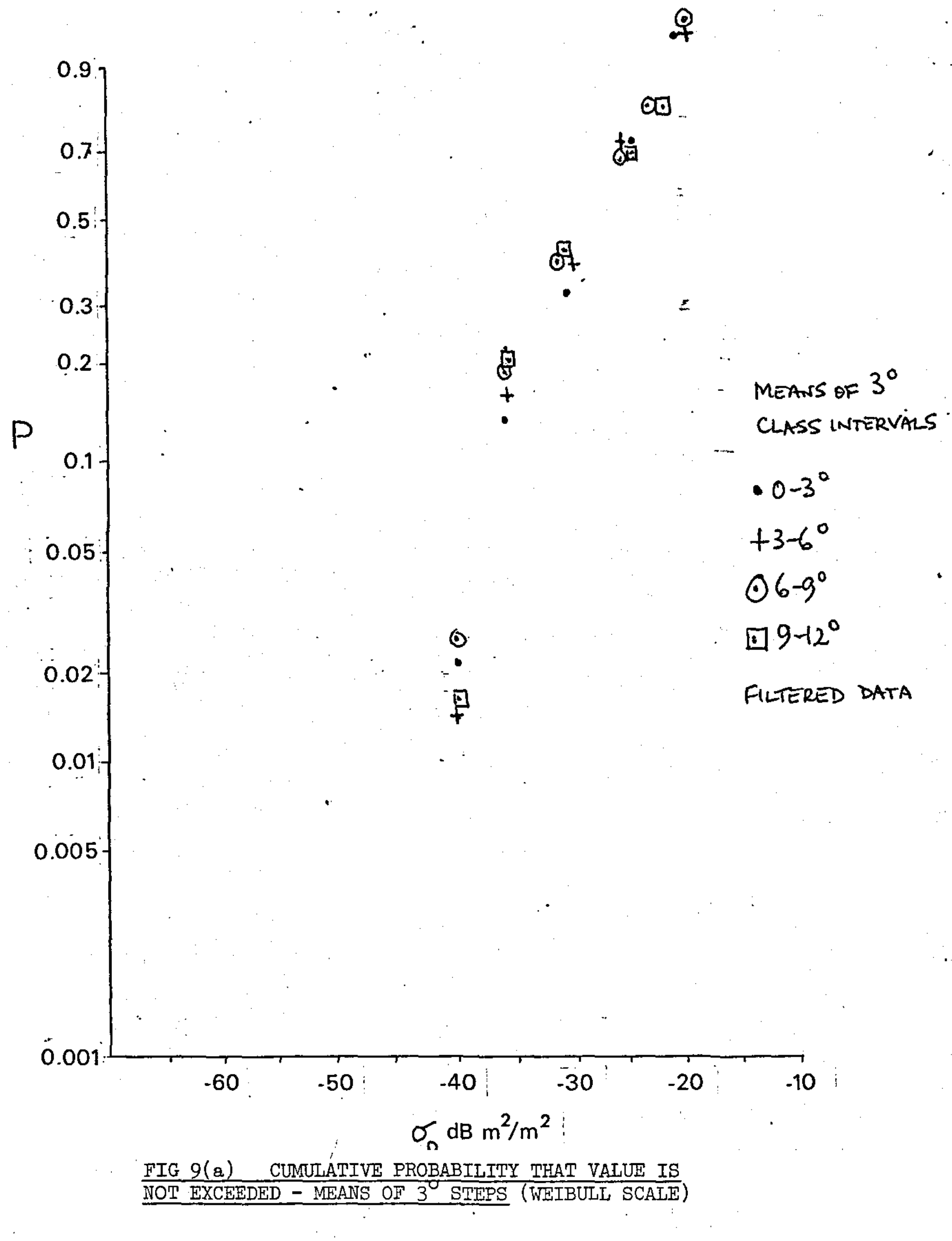

FIG 9(a) CUMULATIVE PROBABILITY THAT VALUE IS NOT EXCEEDED - MEANS OF 3° STEPS (WEIBULL SCALE)

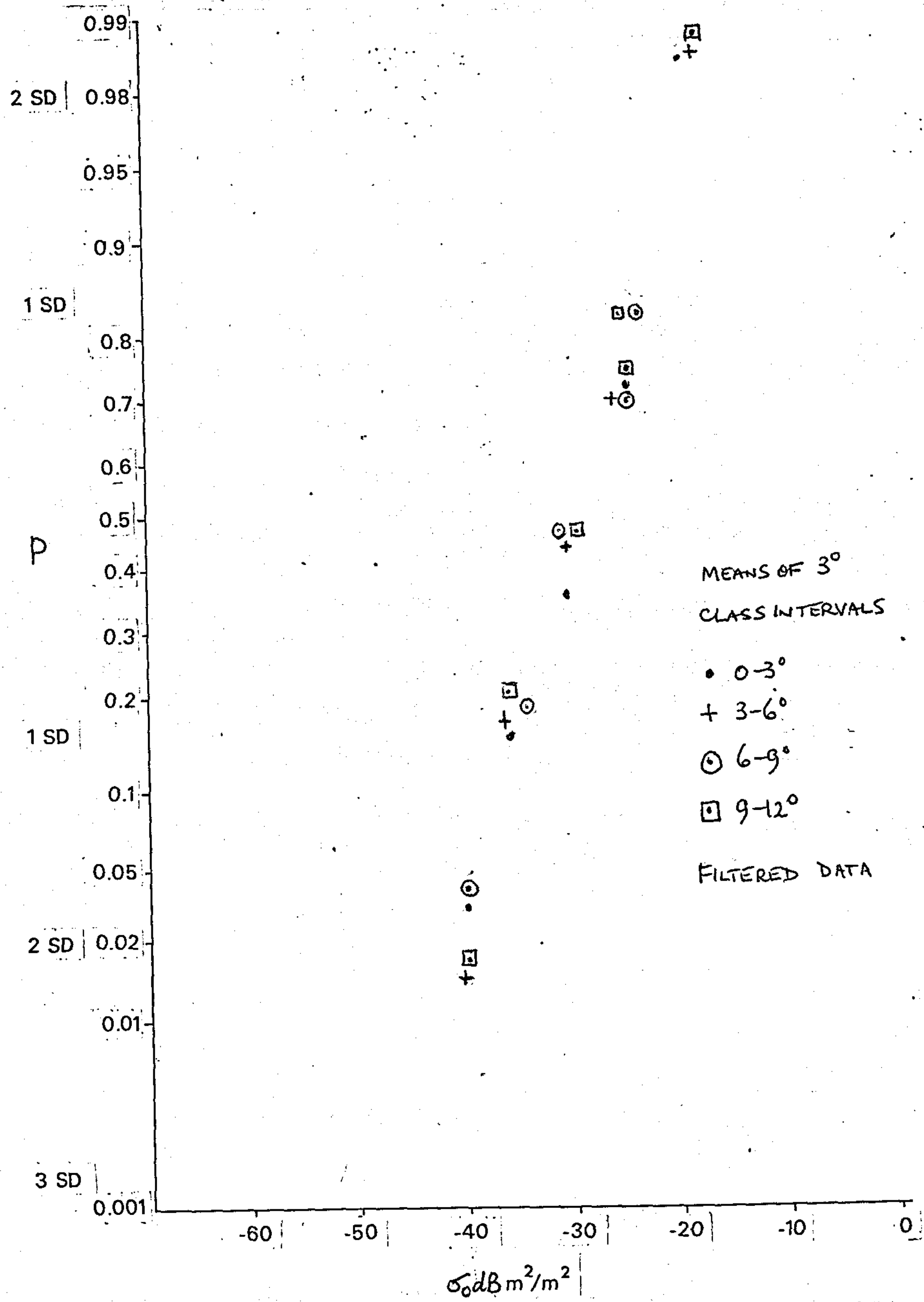

FIG 9(b) CULULATIVE PROBABILITY THAT VALUE IS NOT EXCEEDED - MEANS OF 3° STEPS (LOGNORMAL SCALE)

F1-55

FI-56

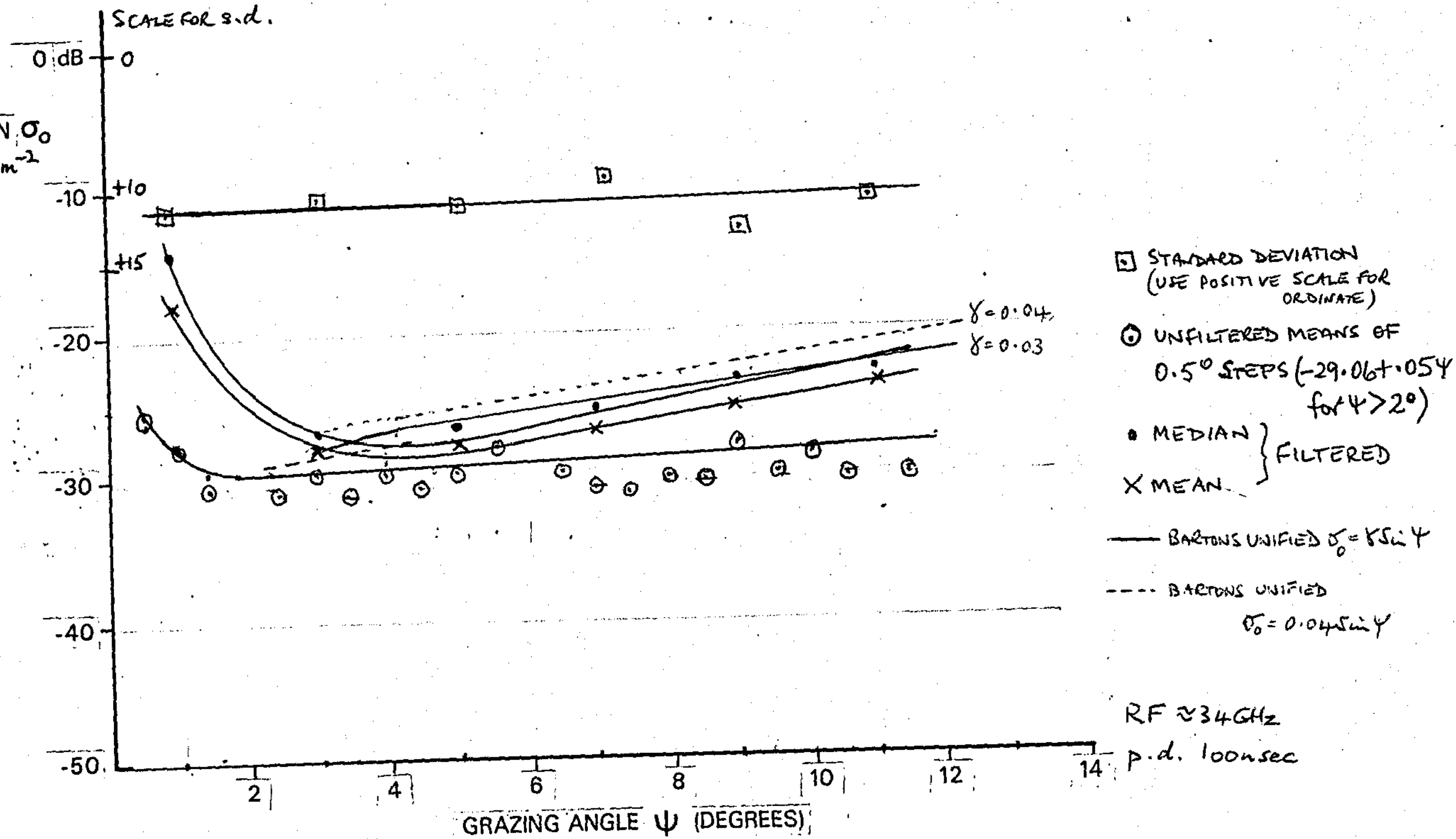

FIG 10 VARIATION IN σ_o WITH ψ FOR RURAL, FARMLAND & CULTIVATED TERRAIN

APPLICATION OF MODEL TO EXAMPLE SYSTEM AND LOCATION

1. It is assumed that clutter is present in the resolution cell for the entire observable track length, taking the worst-case condition; although there will be occasions when clutter is 'shadowed'. Certain other initial assumptions are necessary, either assessed or postulated according to the situation. For this example calculation the basic assumption are:-

(a) Terrain: Rural almost flat with vegetation and buildings giving a terrain sightline response as at Annex E, Figure 5a, page E-25. It is assumed that the mean terrain slope produces $\sigma_m = -28$ dBm^2.m^{-2} at 5 km range, and has a surface reflection coefficient of 0.3.

(b) Missile System Parameters: Considered next (since it dictates the required radar track length) a Reaction time of 10 seconds and $V_m = 600$ m.s^{-1}.

(c) Target Parameters: Transitting target at 300 ms^{-1}, and 60 m (200 ft) altitude and dimension maximum approximately 10 metres. RCS minimum 0.05 m^2 (see page E-22). Crossing the site at a range of 5 km.

(d) Tracking Algorithm: A tracking algorithm of the type described at Annex E (page E-12) is assumed.

(e) Radar Parameters: Radar parameters from the list at Chapter 6 (page 6-146) are used, but the aerial height is lowered to 4 m (i.e. not clear of obscuration). A diode mixer receiver is assumed on this occasion with a 1200 Hz filter bandwidth, 10 velocity gates and 90 range gates, i.e. 900 decisions per target pulse burst using a pulse-burst system of 4 bursts of 10 pulses, PRF's 12000 and 10750. For 60 rpm the dwell-time will be 5.5 msec.

2. Other assumptions on ECM degradation etc. are made later in the sequence which follows.

ASSESSED PROBABILITY VALUES

3. Track Length: A combination of parameters from paragraph 1(a), 1(b) and 1(c) above when applied to Table 1 and Figure 5a at Annex E gives

$P_{TL} = 0.22$

It is important to remember that this is the minimum tracklength necessary for an engagement (see also paragraph 4 below).

4. Tracking: It is assumed that the equipment under consideration was designed to give a probability of detection (given a sightline) of a 0.9 overall. Applying this to the tracking algorithm at page E-18, where 2 in any successive 3 looks must cross the threshold to delare a track (2 out of 3 sliding window algorithm) hence:

(a) Probability of declaring a new track $\overline{P_{TT}} = 0.57$

(b) Probability of maintaining track, once obtained $P_{TT} = 0.972$

Hence, (c) Probability of loosing track, once obtained $P_{\overline{TT}} = 0.028$

5. Detection: Time between false alarms is assessed as 900 secs (15 mins). Transmission time of each burst of pulses is 10 x 83.3 μs (for PRF 12000) and 10 x 93.02 μs (for PRF 10750); totalling 5.28 m.sec if 3 bursts of each are completed within the dwell time of 5.5 m.sec, i.e. at least 60 hits per antenna sweep. Probability of false alarm depends upon the number of decisions per second and the false alarm interval.

$$\text{No. of decisions} = \frac{900 \times 6}{5.28 \times 10^{-3}} \approx 1 \times 10^{6} \text{ and Pfa} \approx 1 \times 10^{-9}$$

The target is observed at least six times per antenna sweep, hence the probability of detection per burst for a P_D of 0.9 is given by $P = 1-(1-0.9)^{1/6} = 0.32$. Using the standard curves at Figure 3, the required S/N is 12.5 dB. Correcting for 10 pulses using Swerlings Integration Improvement factor adds 0.6 dB for the Swerling 3 Case.

6. Use of Clutter Model at Annex F: Using the standard equations, the total receiver clutter reduction for a target to be detected at 5 km, for q_m = -28 dB, is [-29.2 dB + (-12.5 - 0.6)] = -42.3 dB. Worst case rain conditions give -24.1 dB, well within the radar's capability. In practice the radar may have a far better performance in rain due to circular polarisation. If the target is reduced in altitude so that the radar grazing angle $\Psi = < 2°$ and the clutter level rises (as shown in the research at Appendix 1 to Annex F) to a level of -18 dB at $\Psi = 1°$, the values above become:-

[-39.2 dB + (-12.5 + 0.6)] = -52.3 dB

If a clutter rejection capability is postulated for a system it is thus possible, by the insertion of the clutter model, to reverse the calculation process to determine the detection performance, tracking performance and hence the total system prediction.

7. Area Assessment: For a particular terrain, given target size and full terrain data, for a given site position it is possible to assess a percentage of occasions when the target may be lost in clutter. Many modern radars can process clutter to a high standard. It is assumed that in the terrain

in question targets are lost in clutter for only 2% of the time a sightline exists.

Clutter Factor 0.98

8. Chaff, Noise and Deception ECM. Chaff may pose a detection problem unless filtered by MTI. In the basic detection mode, forward firing chaff from a radially approaching target can usually hide a target because of the large RCS produced. This would be a worst-case condition for a point defence tracking radar (failing MTI). 1 Kg of broadband chaff produces 660 m^2 (since $\sigma_{chaff} = 1365W/f_{GHz}$). The reader is referred to Haddow {137} and subsequent reports on the technique of radar tracker break-lock as a distinctly different use of chaff. For example purposes here it is postulated that system radar performance is degraded to 50% of its undergraded value by the use of ECM, ie tracking error is increased to an unacceptable level 50% of the time

$E_f = 0.5$

9. Tracking Errors. Para 4 above considers tracking probabilities given a sightline. Scanning radars will attract azimuth tracking errors ($\epsilon \propto \frac{1}{\sqrt{S/N}}$) Skolnik (p 1?8 Fig 5.16), while tracking radars will be subject to errors discussed at 9-187 and 9-193. Range, refraction and elevation errors should be applied as appropriate Pages 8-174 to 8-176. These are also calculated by reference to Annex E - probability of sightline falling on target. For this example it is taken (page E-23) that a target at 5 km can be tracked successfully when there is a surface reflection coefficient of 0.3. From Annex E (equations (4) and (5)) it is calculated that the probability of the sightline falling on the specified target is

$P_S = 0.24$

A ratio of 10 was assumed for q_s^2 giving ϕ (ε_1), (ε_2) as respectively 0.43 and 0.18.

10. Diffraction. The effect of diffraction, which could enhance track lengths, is more difficult to assess in the absence of site - specific data. A computer program was written by the author to produce the example plot at Annex F Fig 6. Page F10 together with Chap 7 provide the criteria. For this example a diffraction factor of 1 is used.

$D_f = 1$

(ie no enhancement).

11. Missile Performance. If an overall assessment of radar tracker system performance is to include a missile engagement, a lethality figure must be included. This will depend on many factors including trials results under idealised and possible under countermeasure conditions. A figure P_k = 60% is used here for example purposes.

$P_{MX} = 0.6$

12. Operator Performance. In those systems where an operator is used several sources of degradation may occur which can seriously affect overall system performance but which are often difficult to quantify. Conditions may also change day to day and reflect, for example, on morale, fear, training standards, coldness if exposed or lack of confidence in the system (following possible earlier failures). The operator may be using a system but forced into the optical mode by the enemy jamming of his associated tracking radar; the system is thus already in a degraded or reversionary mode of operation. He may of course be assisted if the system is semi-automatic (ie SACLOS compared with CLOS). For this example operator efficienty is taken to be 70% ie daylight with good visibility

$\therefore$

$P_{OE} = 0.7$

13. System Availability. If a system is mobile it may not be in an immediately operational condition, while others in a similar location may be able to partially defend the air space during its redeployment. System equipment availability is calculated from MTBF and MTTR (see Fig 2 page 11-226), taken to be 75 and 4 respectively. With redeployments and reload availability to account for, overall probability of readiness is taken here as 70%

$$\boxed{P_R = 0.7}$$

this may of course degrade after a redeployment due to vibration, weather etc.

14. Target Re-engagement. If an engagement fails for one reason or another it may be possible, depending on target speed, sightline and available time to re-acquire and refire. There will always be a low probability of obtaining a larger track length than the minimum, but the refire reaction time . is often much faster than the original reaction time. The re-establishment of tracking will naturally depend on clutter, operator skill or auto-system ability etc. To assist in the prediction process two nomograms are included at figs 1 and 2 (pages G 10 and G 11) Fig 2 is a standard multiple trial (engagement) nomogram to be used where required for salvo engagements. Fig 1 was deliberately produced as two 3rd order nomograms rather than a single (5th order Genus 1) nomogram so that either the track length covered by a target during missile flyout or tracklength flown during system reaction time can be read off a common scale. This means that the target velocity/reaction time grid on the nomogram can also be used to read off re-engagement track lengths.

OVERALL PREDICTION

15. Results can be easily read from the simple multiplying nomogram at figure 4.

a. Mobile System - Operator Controlled (No EOCM)

$P = P_{TL} \times P_{MX} \times P_{R} \times P_{OE}$

$P = 0.22 \times 0.7 \times 0.6 \times 0.7$

P = 0.06 (6%) this result is shown on the nomogram

b. Mobile System - Radar/Automatic Fire Control

$P = P_{TL} \times P_{MX} \times P_{R} \times P_{\bar{TT}} \times P_{S}$

additionally multiply by ECM, clutter and diffraction factors, as appropriate.

$P = 0.22 \times 0.6 \times 0.7 \times 0.57 \times 0.24$

P = 0.013 (1.3%) - this result is shown on the nomogram

16. This method assumes that tracking and hence engagement opportunities can always be used and that they apply to 360° azimuth cover. There will be cases where P_{TL} can be very much higher in value but only applicable to a limited sector in azimuth; advantage can, of course, only be taken from these sites if targets fly into the high P_{TL} sector. The probability of targets entering these sectors then also becomes of

interest. However such siting is usually deliberate in order to protect a sector along which targets may be constrained to fly due to type or alignment of the intended surface target. It is suggested that another factor P_E, ie probability of converting a detection to an engagement might be incorporated.

17. The importance of P_{TL} is re-iterated since in flat and gently undulating terrain it can be significantly improved by simply raising the tracker aerial clear of immediate obstructions. In the two cases at para 15 placing P_{TL} to 1 immediately changes the results to 29% and 6% respectively. Similarly on a fixed site P_R might be much better.

18. Interpretation. It is also necessary to remind the reader exactly what the results mean, since much misunderstanding of similar results has occurred in the past. The result (6%) at para 15a does not mean that 6% of all targets will be successfully engaged, however, 6% could ideally be engaged if every opportunity is taken since it is a statistical value. There may be slightly more - or far likely, less - opportunities in practice since it has been assumed that no target appears as a surprise and that targets are engaged (tracked) either approaching or crossing but not receding.

19. Further, improvements may occur in a radar tracked system if off-site assistance is given by other radars in the area; while on the other hand degradation will occur if electronic countermeasures or target manoeuvre is used to degrade the tracking function. Notice that with the tracking algorithm chosen there is a 3% probability of loosing a

successful track after obtaining it with a 90% detection probability once it became unmasked. Conversely there is a 97% probability that tracking will continue successfully subject to a sightline or diffraction path and no other degradation.

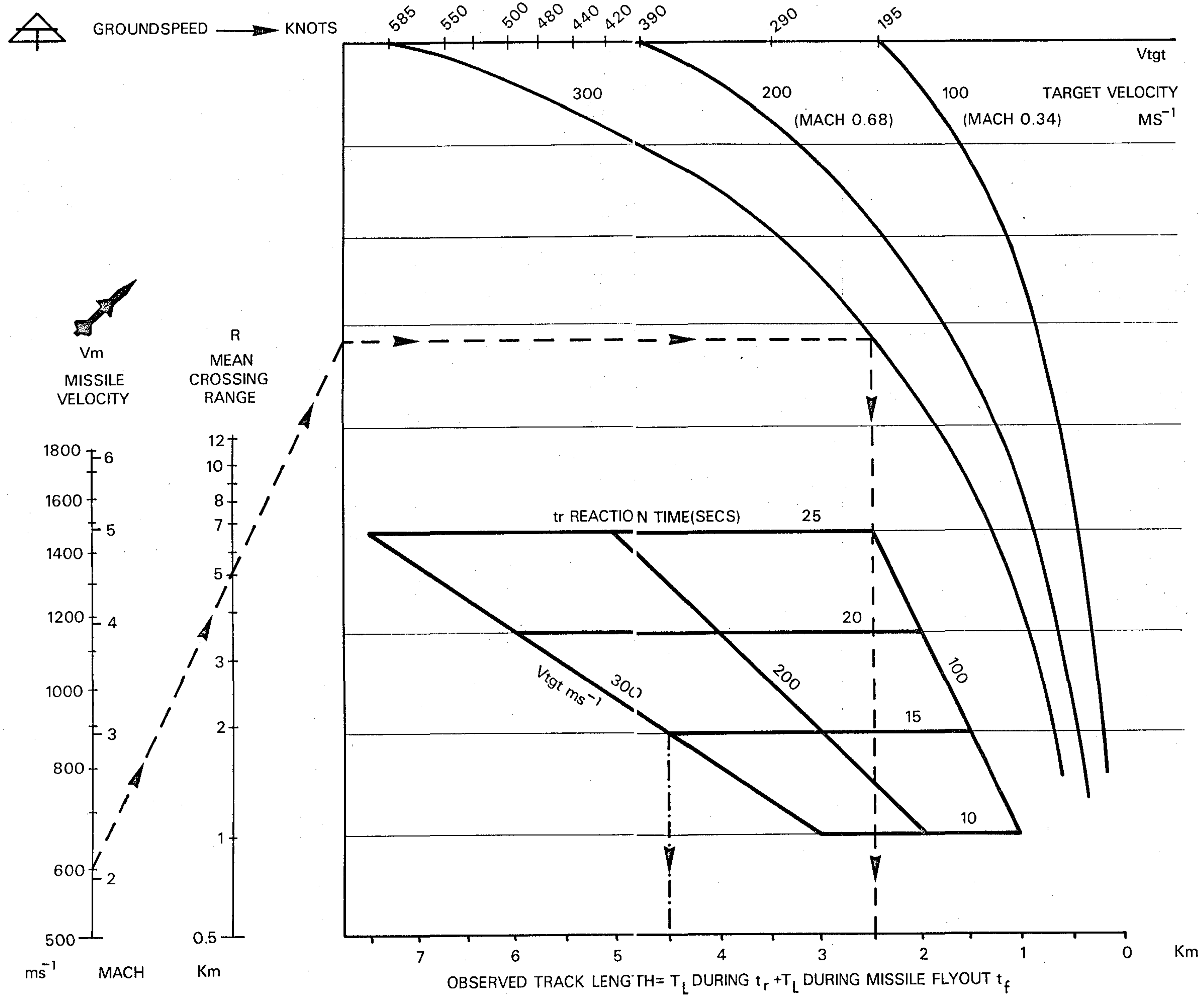

FIG 1 NOMOGRAM FOR CALCULATION OF MINIMUM OBSERVED TRACKLENGTH NECESSARY FOR AN ENGAGEMENT

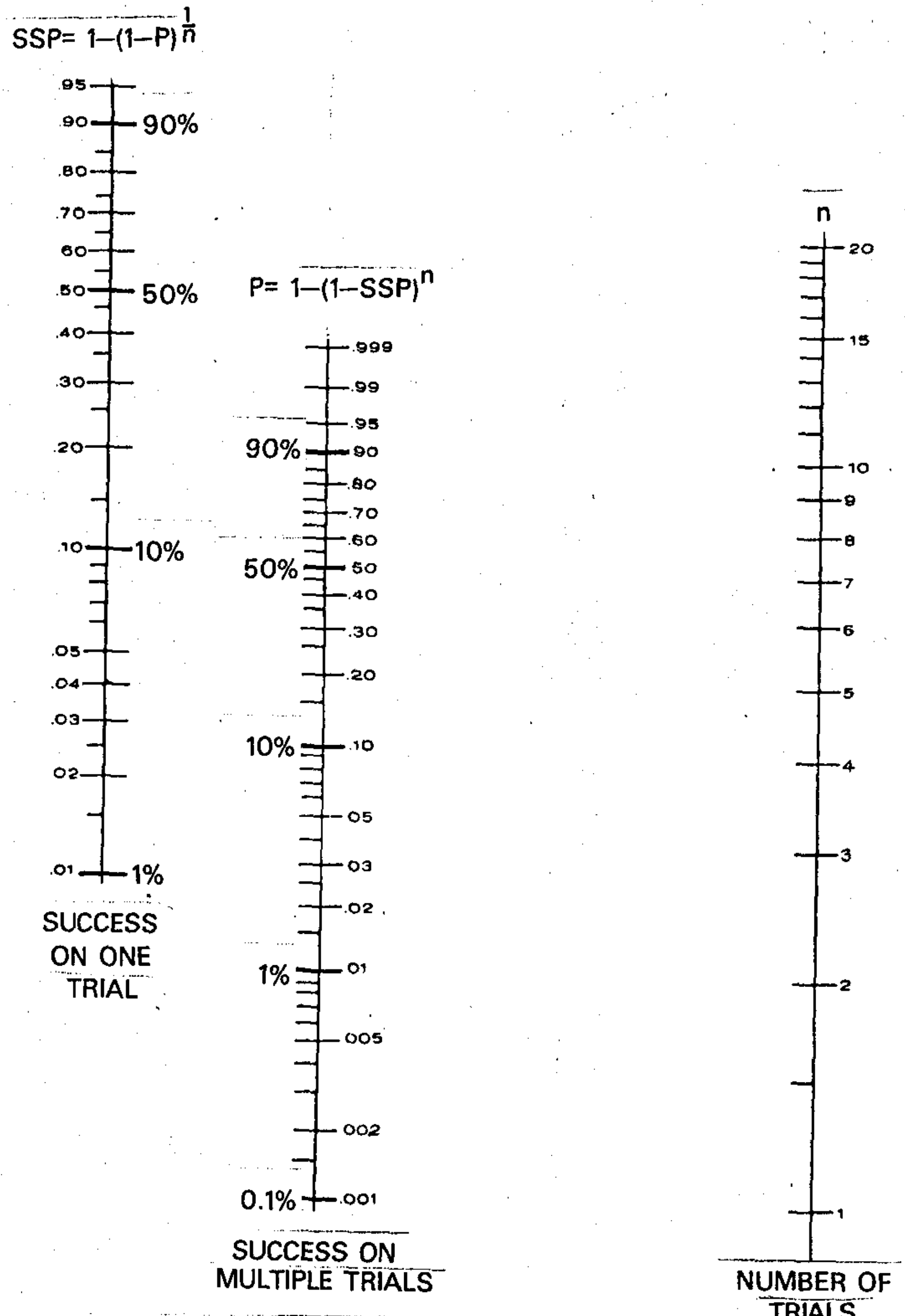

FIG 2 NOMOGRAM FOR MULTIPLE INDEPENDENT TRIALS

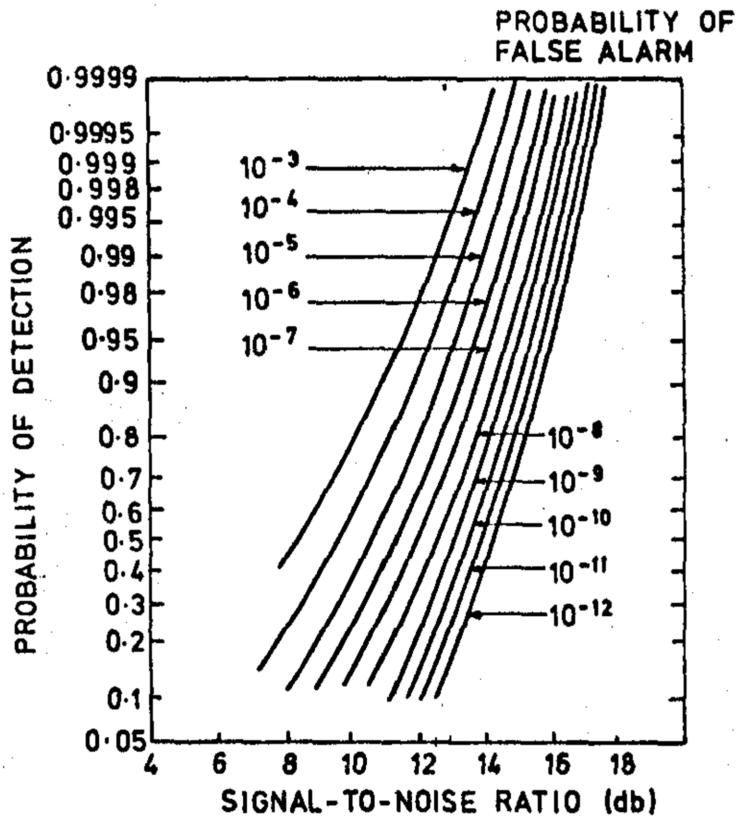

FIG 3a PROBABILITY OF DETECTION AS A FUNCTION OF THE SIGNAL-TO-NOISE RATIO AND THE PROBABILITY OF FALSE ALARM

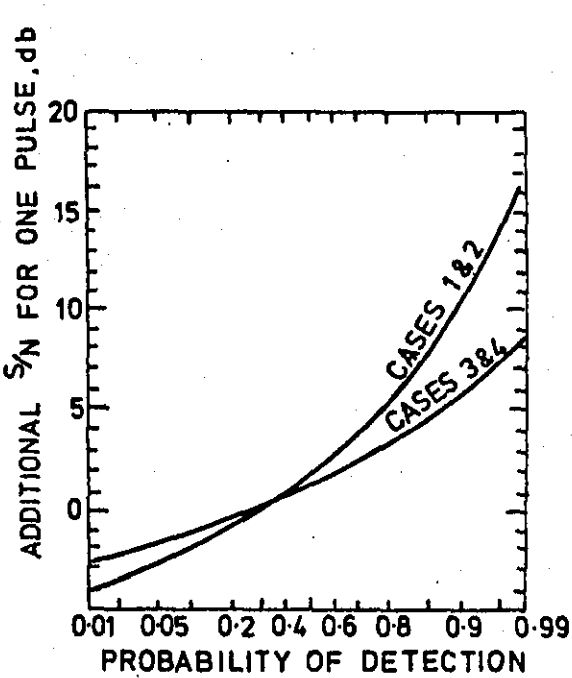

FIG 3b ADDITIONAL SIGNAL-TO-NOISE REQUIRED TO ACHEIVE A PARTICULAR PROBABILITY OF DETECTION WHEN THE TARGET CROSS SECTION FLUCTUATES

FIG 4 MULTIPLYING NOMOGRAM

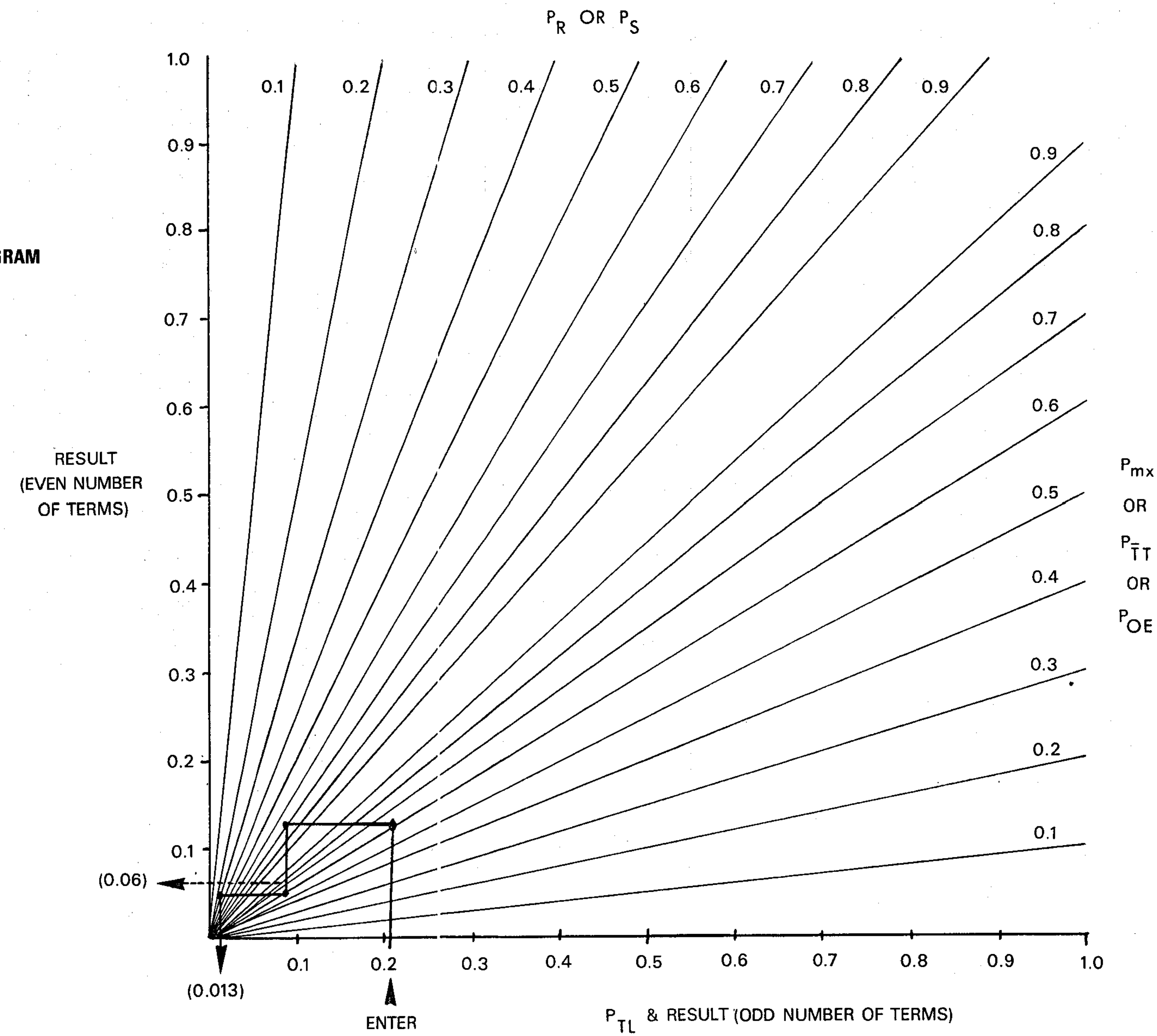

PART II

CLUTTER AND LOW-LEVEL TRACKING BIBLIOGRAPHY

Adgie R L	"The Effect of Terrain Screening on Clutter Visibility" RSRE Malvern Div Note 1/79 JUN 1979 (RESTD)
Allan D	"Predicting the Performance of Surface Radars in Land Clutter" Loughborough Univ of Technology and RAF College Cranwell dissertation AUG 1980
Ament W S	"Forward and Back Scattering from Certain Rough Surfaces" IRE Trans. Vol AP4 Jul 1956
Ament W S et al	"Radar Terrain Reflections from Several Polarisations and Frequencies" NRL Part 2 Trans 1959 Symposium on Radar Return (Unclass) AD 320 390 MAY 1959 (CONF)
Andre S N et al	"Radar Clutter Research" US Army Missile Cmd. Rep No RE TR-68-11 JUL 1968
Andrianov V A et al	"Scattering of Radio Waves by an Underlying Surface Covered with Vegetation" Radio Eng and Elect. Physics (USSR) Vol 21 SEP 1976
Antin J et al	"Low Angle Radar Tracking Phenomenology - a Data Compilation" USAF Contract F49-620-77-C-0025 (RESTD DISTR) DEC 1978
Arafiles V P	"Comparison of Radar Clutter Models" HQ FTD/SDER 1981
Armstrong and Cornwell	"Multipath Measurements" ER 74-4316 AD A001-064 AUG 1974
Attema E P W et al	"Short Range Vegetation Scatterometry" Proc URSI Conf Micro. Scatt. Berne SEP 1974
Baker C A	"Radar Terrain Return" AVCO Tech Memo RAD TM 62-103 AD 225-679 JAN 1963
Barnum J R	"High Frequency Backscatter from Terrain with Concrete Block Walls" Trans IEEE Ant and Prop MAY 1971
Barlow E J	"Doppler Radar" Proc IRE Vol 37 No 4 APR 1949
Barrick D E	"Radar Clutter in an Air Defence System" Battelle Memorial Inst. US Army Missile Cmd Redstone. AD 834-960L JAN 1968

Bechtel M E — "Diffraction Past Simple Buildings"
FAA/Calspan Rep. KH 5559-E-1 — DEC 1973

Beckmann P — "Shadowing of Random Rough Surfaces"
IEEE Trans. Vol AP 13 — MAY 1965

Beckmann P — "Scattering by Composite Rough Surfaces"
Proc IEEE Vol 53 — AUG 1965

Beckmann and Spizzichino — "The Scattering of Electromagnetic Waves from Rough Surfaces"
Macmillan NY — 1963

Becker and Surean — "Control of Radar site Environment by the use of Fences"
IEEE Trans. Ant and Prop Vol AF 14 — NOV 1966

Bianco D R and Morris C S — "Radar Terrain Cross-Section at Microwave Frequencies"
Joint URSI/IRE Conf. Pennsylvania Univ — OCT 1958

Billingsley J B and Briggs D L — "Survey of Terrain Reflectivity Measurements"
MIT CMT 8 Vol 2 Lincoln Labs — MAY 1980

Blau W and Farber J — "Radar Clutter Modelling"
Spectronics ONR. AD 868090 — NOV 1980

Blomfield D L H — "A Land Clutter Model which Includes the Effects of Dominant Scatterers"
ASWE. Tech Rep TR 74-11 AD 923-595 — JUL 1974

Bogush — "Correlated Clutter and Resultant Properties of Binary Signals"
IEEE Trans. Aerosp and Elect Syst — MAR 1973

Bond D S and Pidgeon R E — "Flight Tests of the Nighthawk Radar Systems"
RCA Advanced Techniques in Radar Components for Battlefield Surveillance. Project Michigan AD 101324 — FEB 1956

Bond R H — "A Summary of Measurements and Theories of Radar Ground Return"
Hughes Aircraft Co. Report TM 656 — SEP 1960

Boothe R R — "The Weibull Distribution Applied to the Ground Clutter Backscatter Coefficient"
US Army Redstone. Rep RE-TR-69-15 AD 691 109 — JUN 1969

Bradshaw S R et al — "Radar Backscatter as a Tool for Siting Communication Terminals"
Motorola Inc. Ad 244 937 — 1959

Bramley E N and Cherry S M — "Investigation of Microwave Scattering from Tall Buildings"
Proc IEEE Vol 120 — 1973

Campbell B D — "Preliminary Report on Results of AWACS Helicopter-based Discrete Clutter Measurement Program"
Mitre Corporation, Working Paper (RESTR DISTR)
No WP-4124 — DEC 1971

Campbell B D — "Discrete Clutter Models using Data from the AWACS Helicopter-based Discrete Clutter Measurement Program"
Mitre Corporation, Working Paper (RESTR DISTR)
No WP-5313 — APR 1973

Campbell B D et al — "Report on Second Phase AWACS Helicopter-based Discrete Clutter Measurement Program"
Mitre Wkg Paper WP-4443 (RESTR DISTR) — NOV 1972

Campbell J P — "Back-Scattering Characteristics of Land and Sea at X-Band"
Proc Nat Conf Aero. Elect. Dayton USA — MAY 1958

Campbell J P — "Back-scattering Characteristics of Land and Sea at X-Band"
AD 244937 — MAY 1959

Canning J W F — "Measurements at S-Band of the Doppler Spectrum and Amplitude of Echoes from Various Objects"
RRE Malvern RRE Report 3014 AS 116899 (SECRET)
OCT 1956

Carlson A B and Waterman J R — "Microwave Propagation over Mountain Diffraction Paths"
IEEE Trans Ant and Prop AP 14 No 4

Carlson and Sapp — "Azimuth Beamwidth Effect on Radar Sensed Terrain Horizon Profiles"
AGARD Conf Proc 269 — SEP 1979

Cassell P L et al — "Experimental Investigation of Mountain Obstacle Path Transmission at Microwave Frequencies"
Motorola Riverside Lab Report RL 3824-4 — AUG 1957

Charp S — "Research on Radar Returns Theory, Instrumentation and Techniques"
Wright Air Devel Centre AD 237-133 — JUN 1950 to JAN 1959

Childers D D — "Bistatic Scattering from Terrain"
Xonics Corporation, Technical Report No DCD-397,
AD B-016 870L — FEB 1977

Chudleigh W H et al — "Integrated Multifrequency radar (IMFRAD) Concealed Target Detection and Location System (U)"
Control Data Corporation; AF Avionics Laboratory
Tech Rep AFAL-TR-73-08 (CONFIDENTIAL) — MAY 1973

Cosgriff R L et al — "Terrain Scattering Properties for Sensor System Design (Terrain Handbook II)"
Ohio State University, Eng Station Bulletin No 181
May 1960; (reprinted in DK Barton "Rádar Clutter "
Artech House) 1975

Cost S T — "Measurements of the Bistatic Echo Area of Terrain at X-Band"
Ohio State University Rep No 1822-2 MAY 1965

Cottony and Wilson — "Spectral Characteristics of Radar Target Returns in Clutter"
Inst for Telecom Sciences AFCRL 71-0017/910-1462

Coulbourn D W — "Sea, Land and Rain Clutter Measurement II"
DRL Univ Texas Rep No DRL 548 for APL. AD 387 383
FEB 1967

Cross F R — "Scatterometer Data Analysis Operation Good Look"
Dep Comms Canada. CRC Tech Note 651 MAY 1973

Crysdale J H — "Comparison of some Practical Terrain Diffraction Losses with Predictions etc ....."
IRE Trans Ant and Prop JUL 1958

Currie N C et al — "Some Properties of Radar Returns from Rain at 9.375, 35, 70 and 95 GHz"
IEE 1975 Int. Radar Conf and Tech Rep. 3, ADA 012 709 APR 1975

Currie et al — "Radar Millimeter Backscatter Measurements from Snow"
Georgia Inst Tech Eng Exp Station AD B021 148
JAN 1977

Currie N C et al — "Radar Millimeter Backscatter Measurements Vol 1. Snow and Vegetation"
AD B030 190 JUL 1977

Daley J C — "NRL Interim Rep on Terrain Backscatter Measurements and Imagery"
Canadian Def Research Staff Rep 5270-79 (RESTR DISTR)
APR 1972

Dales J C — "NRL Terrain Clutter Study; Phase II"
NRL Rep 6749 OCT 1968

Dana R A et al — "Utilisation of Radar Clutter Correlation Characteristics for Automatic MTI Video Selection"
Hughes Aircraft Co. IEEE Int Rad Conf 1980

Dax P R — "Accurate Tracking for Low Elevation Targets over the Sea with a Monopulse Radar"
Int Conf Radar Present and Future OCT 1973

Dalaney and Meeks — "Prediction of Radar Coverage Against Very Low Altitude Aircraft"
AGARD Conf Proc 269 SEP 1979

Domille A R	"The Bistatic Reflection from Land and Sea of X-Band Radio Waves" Parts I, II and Supplement GEC Stanmore. Memos 1802 and 2116	JUL 1967, JUL 1968, and JUL 1969
Drake and Schuckman	"Feasibility of Using Multiplexed SLAR Imagery for Water Resources Management and Mapping Vegetation Communities" Proc Int Symp Renote Sens of Environ. Michigan Vol I	APR 1974
Doyle F J	"Digital Terrain Models: An Overview" Photo Eng and Remote Sens No 44	1978
Dougherty H T and Maloney L J	"Application of Diffractions by Convex Surfaces to Irregular Terrain Situations" Radio Sc NBS/USNC-URSI Vol 68D No 2	FEB 1964
Du L J and Peake W H	"Rayleigh Scattering from Leaves" IEEE Proc Vol 57	JUN 1959
Durlach N I	"Influence of the Earths Surface on Radar" MIT Lincoln Lab TR 373	JAN 1965
Earing D G and Smith J A	"Target Signatures Analysis Centre Data Compilation" AF Avionics Lab AD 489 968	JUL 1966
Easthaugh et al	"The Twin-Beam Solution to Ground and Angel Clutter" UK Symp Part 3 Elect for Civil Aviation London	SEP 1969
Edgar A K, Dodsworth E J and Warden M P	"The Design of a Modern Surveillance Radar" IEEE Conf Pub 105	OCT 1973
Edison et al	"Radar Terrain Measured at Near-Vertical Incidence" IEEE Trans Vol AP 8	MAY 1960
Edwards P N and Christie J M	"Yield Models for Forest Management" Booklet 48 Forestry Research Lab Bentley UK ISBN 0855-38 092-6	1981
Elderkin and Powell	"Measures of Time-Space Relationships in Atmospheric Turbulence" Battelle Pacific NW Labs Washington	(Pre 1974)
Emch G et al	"Assessment of Requirements for 1985-2000" ERA. US Navy Surface Ships Radar Inf Book II Vol II FS-79-144	

Fuller I W and Davis N L — "Some Results on Target Reflection Characteristics"
Naval Res Lab Symp Project Michigan AD 079 315
(CONFIDENTIAL) FEB 1955

Fung A K — "A Review of Rough Surface Scattering Theories"
Univ Kansas CRES Tech Rep 1971

Fung A K — "Mechanics of Polarized and Depolarized Scattering from a Rough Dielectric Surface"
J Franklin Inst Vol 2 FEB 1968

Furfine A L — "Measured Performance of an FM Altimeter Operating at X-Band Frequencies"
Trans 1959 Symp Radar Returns AD 320 390 (CONFIDENTIAL) 1959

Garlick J K — "A Survey of Low Reflection Co-efficients for Various Types of Land and Frozen Sea for Normal Incidence at 1600 MC/S"
RAE UK Tech Note RAD 536 AD 7-039 JAN 1953

GD/Convair — "SEV Feasibility Study RATSCAT, Radar Backscatter and Cross-Section Measurements of Snow and Ice"
AFSWC Tech Rep 71-19 AD 885 898 MAY 1971

Geale A — "Radar Refelctivity Vol 2"
Decca Radar Ltd UK Rep SRL 2973/15 AD 345 295
(SECRET) OCT 1963

Gent H et al — "Polarisation of Radar Echoes, Including Aircraft, Percipitation and Terrain"
Proc IEE Vol 110 No 12 DEC 1963

Georgia Inst Tech — "Low Altitude Clutter and Multipath Models fro TAC-ZINGER"
Georgia Inst Tech Radar and Instr Lab APR 1979

Ghose S C — "Radar Sea Clutter"
EMI Electronics UK Rep DP 1025 AD 328919 (CONFIDENTIAL) AUG 1961

Ginsberg M B — "Radar Modelling Study"
Harry Diamond Labs AD 009-055 DEC 1974

Gloerson et al — "Microwave Signatures of Snow, Ice and Soil at Several Wavelengths"
Proc URSI mtg Microwave Scatt and Emiss from the Earth Univ Berne Switz 1974

Goggins W B — "Foliage Penetration Radar"
Lincoln Lab Tech Note TN 1978-17 (SECRET) SEP 1978

Goggins W B et al — "New Concepts in AMTI Radar, Nulling Effects of Doppler"
AFCRL JAN 1974

Hall M P M et al	"Use of Dual Polarization Radar to Measure Rain Fall Rates and Distinguish Rain from Ice Particles" IEEE Int Radar Conf	MAY 1980
Hall S T et al	"Airborne Warning and Control System (AWACS) Radar Development Program Technical Support" AF Sus Cmd Rep ESD-TR-70-63 Vol 1 AD 379 357	MAY 1970
Harrold T W	"Estimation of Rainfall using Radar - A Critical Review" Meteorological Office Scientific Paper No 21 MET 0.767	1965
Harrold T W	"Ground Clutter Observed in the Dee Weather Radar Project" Met Mag Vol 103 No 1222	MAY 1974
Harrold T W et al	"The Dee Weather Project - Measurement of Area Precipitation Using Radar" Weather (UK) Vol 28 No 8	AUG 1973
Hartley-Smith A	"Ground and Angel Clutter in Radar Systems" GEC Journal of Sc and Tech UK Vol 39 No 4	1972
Hawkes C D and Haykin S S	"Modelling of Clutter for Coherent Pulsed Radar" IEEE Trans Vol IT 21	NOV 1975
Hayes et al	"Backscatter from Ground Vegetation at Frequencies between 10 and 100 GHz" AP-S Int Symp	1976
Hayes R D et al	"Study of Polarisation Characteristics of Radar Targets" GIT AD 304 957	OCT 1958
Hayes R D and Dyer F B	"Land Clutter Characteristics for Computer Modelling of Fire Control Radar Systems" GIT Tech Rep 1 AD 912 490	MAY 1973
Hayes R D	"Radar Clutter Models at 95 GHz" US Armament R & D Command Report ARSCD-MR 80001 A089986	
Hayes R D et al	"95 GHz Pulsed Radar Returns from Trees" EASCON	1979
Hayes R D et al	"Reflectivity and Emissivity of Snow and Ground at mm Waves" IEEE Int Rad Conf	1980
Hayes R D	"Clutter Returns from Ground Radars" Remote Sens Wkshp Rad Backscatter	JAN 1975
Heidbreder and Mitchell	"Detection Probability of Log-Normally Distributed Signals" IEEE Trans Aerosp	JAN 1967

Hunting Engineering — "Representation of Terrain in Combat Modelling" Hunting Engineering UK Doc TP 24283 (CONFIDENTIAL) OCT 1979

Hunting Engineering — "Model of Air-Ground Interactive Combat" Doc TP 24288 (CONFIDENTIAL) OCT 1979

Ishimaru A — "Wave Propogation and Scattering in Random Media" Academic Press NY 1978

Janse A R P — "Radar Reflections from Crops, Woods and Soil" Electrotech Elektron Netherlands Vol 30 No 2 JAN 1975

Jelantis J G — "The Ground Clutter Environment of the White Sands Missile Range Stallion Site L/UHF Radar" MIT Lincoln Lab Project PA 71 AUG 1975

John Hopkins Univ — "Quarterly APL Review of Bumblebee Activities I-Missile Programs" Bumblebee Rep 282A (SECRET) SEC 1958

John Hopkins Univ — "Radar Guided Land Attack Missile Study" Phase I Report Vol 1 FPI 066-1 SEP 1975

Kapitanov V A et al — "Spectra of Radar Signals Reflected from Forests at Centimeter Waves" Radio Teckhnika Electronika Vol 18 SEP 1973

Kapitanov V A et al — "Investigation of Radar Returns from Woods" Trans Tsen Aerol Obs Moscow No 110 1973

Katz I — "Radar Backscattering from Land at 'X' Band" APL REP CLO 4-002 JUN 1963

Katz I — "Wavelength Dependence of the Radar Reflectivity of the Earth and the Moon" J Geophys Res Vol 71 JAN 1966

Katz I and Spetner L M — "Polarization and Depression-Angle Dependence of Radar Terrain Return" J Res of Nat Bur Stds Vol 64D No 5 OCT 1960

Katzin M et al — "Investigations of Ground Clutter and Ground Scattering" Electromagnetic Research Corporation Report No CRC-5198-4; Air Force Cambridge Research Center AD 235 971 MAR 1960

Katzin M et al — "Evaluation of Airborne Overland Radar Techniques and Testing" Volume II Electromagnetic Research Corporation Airborne Instruments Laboratory AIL Report No 5057-1 Air Force Sys Cmd AD 487 604 SEP 1965

Larsen R S — "Measurement of the Backscattering Cross Section of anM4A2 Sherman Tank at X and K Bands" Canadian Armament R & D Estab CARDE Tech Memo 315/60 AD 31295 (SECRET) 1960

Larson R W and Carrara W — "Measurements of X-Band Clutter Statistics with Amplitude Calibrated Radar" AF Avionics Lab Tech Rep AFAL TR 74-44 AD 530 4921 JUN 1974
Supplement I JAN 1976

Larson R W et al — "Bistatic Clutter Measurements" IEEE Trans Vol AP 26 NOV 1978

Larson and Heimiller — "Bistatic Clutter Measurements Program" ERIM AD A049 037 NOV 1977

Larson, Smith and Fromm — "Measurements of Bistatic Clutter Cross-Section" ERIM 130300-15-F RADC TR 79-15 AD A071-193

Larson, Smith and Fromm — "Measurements of Bistatic Clutter Cross-Section" ERIM 118 200-14-F AD A049 037 NOV 1977

Laurie K A — "Microwave Reflection from Targets and Terrain - Literature Survey" Part 1 Canadian Armament R & D Estab CARDE Tech Memo 330/60 AD 321 924 MAY 1960

Laurie K A — "Microwave Reflection from Targets and Terrain" Part 2 Appendix CARDE Tech Memo 331/61 AD 321 925 (SECRET) NOV 1971

Leader J C — "The Relationship between the Kirchoff Approach and S Small Perturbation Analysis in Rough Surface Scattering Theory" IEEE Trans Vol AP 99 No 6 NOV 1971

Lekstrom J — "Detection of Steady Targets in Weibull Clutter" IEE Conf Pub 105 OCT 1973

Lewinski D J — "Characterisation of Non-Stationary Clutter" RADC TR 79-267 AD 079 655 NOV 1979

Lindquist T and Staleby G — "Ground Clutter Model for Radar Applications" Radar Present and Future IEE Conf Pub 105 OCT 1973

Linell T — "An Experimental Investigation of the Amplitude Distribution of Radar Terrain Returns" 6th Conf Swed Natl Comm Sci Radio Stockholm MAR 1963

Linlor W I et al — "Snow Wetness Measurements for Melt Forecasting" NASA Spec Pub SP 391 AUG 1975

Liskow C L — "Simultaneous Dual-Band Radar Development" Environmental Research Institute of Michigan NASA Contract NAS 9-12967 SEP 1974

McMullen C G — "Radar Return in Mountainous Areas"
Bendix Radio Symposium Record University of Michigan Project Michigan AD 101 324 — FEB 1956

McQueen J — "The Design and Operational Simulation of a 4 Pulse per Beamwidth MTI System"
IEE Conf Radar Past, Present and Future London — 1973

Mack R B et al — "Measured L-Band Radar Cross Sections of Ducks and Geese"
RADC Report RADC-TR-79-66 — MAR 1979

Meeks M L et al — "Bibliography of Radar Reflection Characteristics Volume 1"
GIT AD 13211 — 1952

Meeks M L et al — "Bibliography of Radar Reflection Characteristics Voll III"
GIT AD 8 866 — 1952

Meeks M L et al — "Reflection Properties of Radar Targets"
GIT AD 60211 (CONFIDENTIAL) — 1954
(SECRET SUPPLEMENT) — 1954

Meuche C E — "Moving Target Detector - An Improved Signal Processor"
MIT Report

Meyer E G et al — "Reflection and Doppler Characteristics of Targets and Clutter"
Report No 1 Vols I and II AD 358 264/AD 358 265
(CONFIDENTIAL) — JUL/DEC 1964

Miller C W and Johnson E M — "In Flight Measurements of Absolute Target Echoing Areas from Cultural Returns"
RADC AD 137 493 — NOV 1956

Michigan Univ — "Advanced Techniques in Radar"
Project Michigan AD 101-324 — FEB 1956

Michigan Univ — "Notes on Airborne Battlefield Surveillance Radar"
Project Michigan AD 079 315 (CONFIDENTIAL) — FEB 1955

Miller S J and Ward W W — "The Status of the AMRAD Facility WSMR Mid Oct 1965"
MIT Lincoln Lab Proj Rep RDT 10 — MAR 1968

Millington G et al — "Double Knife-Edge Diffraction in Field Strength Predictions"
IEE Monograph 507E — MAR 1962

Milne K — "Survey of Primary Radars for Air Traffic Systems"
Plessey Radar Research Centre Havant UK

Mullins W H — "An Experimental Study of Radar Terrain Returns Characteristics" Hughes Aircraft Co Proj Michigan AD 079 315 (CONFIDENTIAL) FEB 1955

Mullins B J and Feder A M — "Waterways Experimental Station Terrain Analysis Radar (PROJECT WESTAR)" Texas Instr Inc AD 465 403 JAN 1965

Nathanson F E — "Radar Design Principles" McGraw Hill NY 1969

Nathanson F E and Reilly J P — "Clutter Statistics which Affect Radar Performance Analysis" IEEE Trans Vol AES 3 EASCON NOV 1967

Neugabauer H E J and Bachynski M P — "Diffraction by Smooth Cylindrical Mountains" Proc IRE Vol 46 SEP 1958

Nichols A and Amble H — "Ku-Band Terrain Measurements at Grazing Incidence" Univ Michigan AD 138 911 (CONFIDENTIAL) JUN 1957

Norton K A et al — "The Probability Distribution of the Amplitude of a Constant Vector plus a Rayleigh-Distributed Vector" Proc IRE OCT 1955

Novak L M and Vote F W — "Millimeter Airborne Radar Target Detection and Selection Techniques" MIT Lincoln Lab NAECON MAY 1979

Oliver T L and Peake W H — "Radar Backscattering Data for Agricultrual Surfaces" Ohio State Univ Electroscience Rep 1903-9 AD 849 016 FEB 1969

Oxehufwud A — "Tests Conducted over Highly Reflective Terrain at 4000, 6000 and 11000 Megacycles" AIEE Trans Vol 78 JUL 1959

Parashar S K et al — "Investigation of Radar Discrimination of Sea Ice" Proc 9 Int Symp Rem Sens ENVIRON APR 1974

Parashar S K et al — "Radar Scatterometer Discrimination of Sea Ice Types" IEEE Trans Vol GE 15 No 2 APR 1977

Patriache M V — "Computer Simulation for Scan Modulated Radar Clutter" CRC Report 1238 Ottawa 1973

Peake W H — "Simple Models of Radar Return from Terrain" Ohio State Univ Rep No 694-3 AD 147 067 SEP 1957

Peake W H — "Theory of Radar Return from Terrain" IEEE Convention Record 1959

Peak W H — "Interaction of Electromagnetic Waves with Some Natural Surfaces" IRE Trans Vol AP7 DEC 1959

Raytheon Co — "Ground and Sea Returns" Sperry Rep No 5233-1366-3 AD 99816 NOV 1954

Reed H R and Russel C M — "Ultra High Frequency Propagation" Willy NY 1953

Rehkopf H Z — "Flight Test Data on Radar Reflectivity from Terrain" Boeing Co Doc D-16740 AD 093 657 MAR 1955

Reintjes J F et al — "X-Band Scattering Measurements of Earth Surfaces from an Aircraft" MIT Rep ESL R370 MIT DSR Project 76343 SEP 1968

Reiss et al — "Land and Precipitation Clutter Measurements at C-Band" ASWE UK AD 394083 (SECRET) OCT 1968

Reitz E A — "Radar Terrain Return Study" Goodyear Corp GERA 463 AD 229104 SEP 1959

Rice S O — "Reflection of EM Waves from Slightly Rough Surfaces" Bell Labs Symp Theory of EM Waves Washington JUN 1960

Rice S O — "Diffraction of Plane Waves by a Parabolic Cylinder" Bell Syst Tech J Vol 33 No 2 1954

Rice P L — "Transmission Loss Predictions for Tropospheric Communication Circuits" Nat Bur Stds Tech Note 101 AD 687 820/687 821 JAN 1967

Ridenour L N — "Radar Systems Engineering" McGraw Hill NY

Rider G C — "A Polarisation Approach to the Clutter Problem" IEEE Conf Proc Radar 1977

Rigden C J — "High Resolution Land Clutter Characterisitcs" IEE Conf Pub 105 London 1973

Riley J H — "An Investigation into the Spatial Characteristics of Land Clutter at C-Band" ASWE Tech Rep TR-71-6 FEB 1971

Ringwalt D and McDonald F C — "Terrain Clutter Measurements in the Far North" NRL Progress Rep DEC 1956

Rivers W K — "Shipboard Surveillance Radar Program Assessments 1985-2000 Vol II Radar Clutter" AD A061136 MAR 1978

Self A G — "The Prediction of Site Coverage at Radio and Radar Frequencies"
RSRE Malvern Memo 3339 — JAN 1981

Senior T B A — "The Elevation Errors Involved in the Radar Location of a Low Flying Target"
RRE Memo — MAR 1956

Semenor B — "Approximate Computations of Scattering EM Waves by Rough Surface Contours"
Radio Engr Elect Phys Vol II No 8 — 1966

Shapiro A — "Initial Results of Skylab Altimeter Observations over Terrain"
Proc URSI Berne Switz — SEP 1974

Shapiro A and Yaplee B S — "Anomalous Radar Backscattering from Terrain at High Altitudes"
Proc IEEE Vol 63 — APR 1975

Sharenson S — "Pulse Doppler Map Match Sensor"
AFAL Tech Rep TR-76-268 (SECRET) — NOV 1977

Shaw A H — "Land Clutter Levels for Elevation Angles of the Order of a Few Degrees"
RRE Malvern (SECRET) AD 373 456 — MAY 1966

Sherman — "Complex Indicated Angles Applied to Unresolved Radar Targets and Multipath"
IEEE Trans Aerosp and Elect Sys Vol AES 7 No 1 — JAN 1971

Sherwood E M and Ginzton E L — "Reflection Coefficients of Irregular Terrain at 10 cm"
Proc IEEE Vol 43 — JUL 1955

Simkins W L — "Key Vugraphs from First Clutter Meeting"
RADC — FEB 1978

Simkins W L et al — "Seek Igloo Radar Clutter Study"
RADC Tech Rep 77-338 — OCT 1977

Skolnik M — "Introduction to Radar Systems"
McGraw Hill NY — 1962

Smith B G — "Geometrical Shadowing of a Random Rough Surface"
IEEE Trans Vol AP-15 No 5 — SEP 1967

Smith J A — "Radar Detection of Ground Objects from the Ground"
MIT Radiation Laboratory Document 420 — SEP 1943

Smith J M — "Propagation Problems in Radar Systems Analysis"
Marconi Radar Syst Proc IEEE Int Radar Conf — 1980

Symonds
Smith — "Multi-Frequency Complex Angle Tracking of Low Level Targets"
IEE Int Conf Radar Present and Future. London
OCT 1973

Sun D F — "Experimental Measurements of Ground Reflection Elevation Multipath Effects on a Small Aperture Tracking Radar"
AD A077 915 — MAR 1979

Sunderan C S — "Expendables in Electronic Warfare"
IDR No 9 — DEC 1976

Theresby G B — "Some of the Problems in Digital Terrain Model Construction"
AGARD Conf Proc 269 — SEP 1979

Tolbert C W et al — "Radar Cross Sections at 4.3 mm of Ground Surfaces, Trees Vehicles and Man"
Univ Texas Elect Eng Rep 105 AD 304523 — NOV 1968

Tomlinson P G — "A Model for Space Radar Clutter"
RADC Final Tech Rep TR 336 — JUN 1979

Trebits R N et al — "Non-Wave Reflectivity of Land and Sea"
Microwave J — AUG 1978

Tsang L and
Kong J A — "Energy Conservation for Reflectivity and Transmissivity at a Very Rough Surface"
J Appl Phys Vol 51 No 1 — JAN 1980

Tsang L and
Kong J A — "Asymptotic Solution for the Reflectivity of a Very Rough Surface"
J Appl Physics Vol 51 No 1 — JAN 1980

Tsang L and
Kong J A — "Scattering of EM Waves from Random Media with Strong Permittivity Fluctuations"
Radio Sc (USA) Vol 16 No 3 — MAY/JUN 1981

Twerksy V — "On Scattering and Reflection of Electromagnetic Waves by Rough Surfaces"
IRE Trans Vol AP 5 No 1 — 1957

Ulaby F T — "Radar Measurement of Soil Moisture Content"
IEEE Trans Vol AP-22 — MAR 1974

Ulaby F T — "Vegetation and Soil Backscatter over the 4-18 GHz Region"
Proc URSI Comm II Specialist Meeting on Microwave Scattering and Emission from the Earth, Berne Switz
SEP 1974

Ulaby F T — "Radar Response to Vegetation"
IEEE Trans Vol 1 AP-23 — JAN 1975

Vander-Schuur and Tomlinson P G	"Bistatic Clutter Analysis" RADC TR 79-70 AD A069 385	APR 1979
Van Deusen R and Steckenreiter V	"Low Angle Target Tracking" RADC TR 73-212 AD 916 421	JUL 1973
Venier G O and Cross F R	"An Assessment of Canadian Forces Airborne Radars for Arctic Surveillance" CRC Rep 1270 Dept of Natul Def Canada TELS Rep No 39 (RESTR)	NOV 1976
Wagner R J	"Shadowing of Randomly Rough Surfaces" J Acoust Soc Amer Vol 41 No 1	1967
Wait J R and Conda A M	"Diffraction of EM Waves by Smooth Obstacles for Grazing Angles" J Res NBS 63D No 2	1959
Ward H R	" A Model Environment for Search Radar Evaluation" IEEE EASCON Record	1971
Ward R C and Powell D E	"Analysis of Clutter Data" US Army Missile Cmd RE-TR-66-13 AD 377 002 (CONFIDENTIAL)	MAY 1966
Warden M P	"An Experimental Study of Some Clutter Characteristics" RSRE Malvern AGARD Conf Proc 66	1970
Warden M P and Dodsworth E J	"A Review of Clutter" RRE Malvern UK Tech Note 783	SEP 1974
Warden M P and Wyndham B A	"A Study of Ground Clutter using a 10 cm Surveillance Radar" RRE Malvern UK Tech Note 745 AD 704 874	SEP 1969
Warden M P and Wyndham B A	"Ground Clutter Measurements at Staxton Wold" RRE Malvern UK Memo 2623	OCT 1969
Warden M P and Wyndham B A	"Ground Clutter Measurements at London Airport" RRE Malvern UK Memo 2606	MAY 1969
Waters W M	"On the Effect of Sampling Rate Upon Clutter Pattern Displays" NAECON Record	1974
Webb J A et al	"AW/TPQ 37 Clutter Analysis" Hughes Aircraft Corp MIT Lincoln Lab (CONFIDENTIAL)	AUG 1979
Wenisch G	"Prediction of Ground Clutter Echoes after Topography of the Terrain" L'Onde Electrique Vol 51	SEP 1971